JOURNAL OF
CHROMATOGRAPHY
INCLUDING ELECTROPHORESIS AND OTHER SEPARATION METHODS

ELSEVIER

JOURNAL OF CHROMATOGRAPHY

INCLUDING ELECTROPHORESIS AND OTHER SEPARATION METHODS

CONTENTS

REGULAR PAPERS

Contents (continued)

SHORT COMMUNICATIONS

Column Liquid Chromatography

Electrophoresis

BOOK REVIEW

Laser-based double beam absorption detector for high-performance liquid chromatography

Zeev Rosenzweig and Edward S. Yeung*

Ames Laboratory–US Department of Energy and Department of Chemistry, Iowa State University, Ames, IA 50011 (USA)

ABSTRACT

The performance of a new double-beam absorption detector based on an all-electronic noise canceler was tested under HPLC conditions. The test compounds were chosen to be 2'-Cl-4-dimethylaminoazobenzene and 4'-Cl-4-dimethylaminoazobenzene since they have absorption peaks in both the UV and the visible region. The major properties of the detector are discussed. The detector is linear through almost 4 orders of magnitude (10^{-5}–10^{-9} M). The deviation between consecutive measurements is about 3% and the absorption noise level is $2 \cdot 10^{-6}$ AU, which is lower by one order of magnitude compared to commercial absorption detectors.

INTRODUCTION

Liquid chromatography (HPLC) is already firmly established as a powerful technique for the separation, quantitation and identification of chemical components in liquid solutions. Much emphasis was put in developing new schemes for detection [1,2]. During the last decade mass spectrometry and Fourier transform infrared spectroscopy (FT-IR) coupled with HPLC have been perfected for qualitative analysis [3,4]. The use of laser excitation in fluorescence analysis has reduced the limit of detection (LOD) sometimes by 2–3 orders of magnitude compared to absorption detection and has opened up new possibilities for ultrasensitive measurements [5,6]. The major disadvantage of fluorescence detection is that not all compounds of interest fluoresce under HPLC conditions.

UV–visible absorption is by far the most widely used detection method. For conventional LC conditions typical detectability with commer-

cial absorption detectors is $1 \cdot 10^{-4}$ AU [7]. With the most modern state-of-the-art system the minimum noise level is about $2 \cdot 10^{-5}$ AU using a single wavelength [8,9]. The same equivalent noise level was obtained by using laser-induced photoacoustic spectroscopy (LIPAS) [10,11]. The LOD can be reduced even more by utilizing thermal lens calorimetry [12]. However, the thermal lens effect increases the observed signal but does not reduce the noise. In fact, because lasers are used and because of spatial filtering, noise is actually increased. So, thermal lens calorimetry can be enhanced further if intensity noise can be suppressed.

Utilizing a single laser beam as a light source in absorption detectors leads to limited performance because the intensity stability of a typical laser is barely above one part in 10^3 [13]. A typical approach to overcome this problem is to design a double-beam detector. In a conventional double-beam absorption detector, the beam is split into signal and reference beams. The two photocurrents or voltages are either subtracted from each other or divided. For subtraction an extremely fine adjustment is needed while divi-

---

* Corresponding author.

sion suffers from the poor performance of a typical analog divider [14]. Recently Haller and Hobbs [15,16] have proposed a new double-beam absorption detection scheme. It is based on an all-electronic noise canceler which theoretically can offer shot-noise-limited performance. The calculated noise equivalent absorption for 1 Hz bandwidth for their experimental conditions was $4.2 \cdot 10^{-8}$. However they did not demonstrate absorption measurements down to the detection limit. Based on averaging and filtering scans at 1000 Hz they determined the noise level of their system to be $3 \cdot 10^{-7}$ (equivalent absorption units). This technique was recently applied to sensitive absorption measurements in capillary electrophoresis (CE) [17], with a factor of 25 improvement in LOD compared to commercial detectors.

In the present paper the performance of the all-electronic noise canceler absorption detector under HPLC conditions is evaluated. We have tested the stability, linearity and LOD of the detector. Comparison is made with state-of-the-art commercial instruments. The two isomers of chloro-4-dimethylaminoazobenzene (DAAB) were chosen because they have absorption in both the UV and visible regions [10]. No attempt was made to optimize the chromatographic conditions. The main thrust is to demonstrate the performance of the new detector under HPLC conditions. The differences between the performance of the all-electronic noise canceler under CE and HPLC conditions are also discussed.

EXPERIMENTAL

Optical setup

The double-beam laser absorption detector for HPLC measurements is shown in Fig. 1. We have used an Ar ion laser (Cyonics 2211-30SL) as a light source operating at 488 nm. The 8-mW partially polarized laser beam was split using a broad-band (200–700 nm) beam splitter (Newport-BK7). The reflected beam was again reflected by a mirror (Newport), focused by a 300-mm focal length quartz lens (Melles-Griot) and directed to the reference photodiode. The
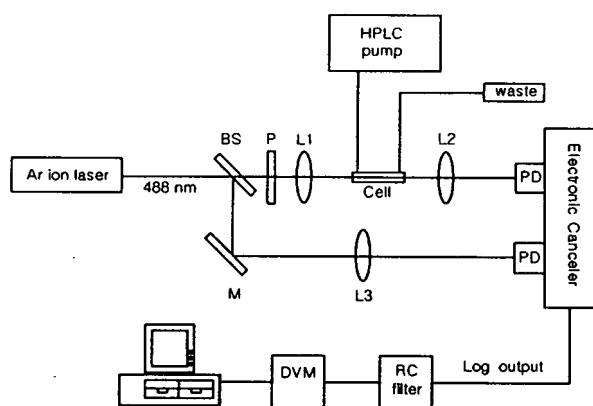
Fig. 1. Double-beam absorption detection system for HPLC. The instrument consists of three major components: a detection system (Ar ion laser and the all-electronic noise canceler), a separation system (HPLC pump and 1-cm length commercial absorption cell) and data acquisition system (A/D interface and computer). BS = Beam splitter; P = polarizer; L1 = 70-mm focal length lens; L2 = 50-mm focal length lens; M = mirror; L3 = 300-mm focal length lens; PD = photodiode; RC = resistor–capacitor; DVM = voltmeter. For details see text.

transmitted beam passed through a polarizer (Glan-Thompson) and was focused by a 70-mm focal length quartz lens (Melles-Griot) into the absorption cell. The flow cell is a commercial HPLC absorption cell taken directly from an Altex instrument (Model 153). After passing the cell the diverged beam was refocused by a 50-mm focal length quartz lens (Melles-Griot) and fell on the signal photodiode. The ratio between the reference and signal beam intensities was determined by the angle of rotation of the polarizer. For our experimental conditions a reference/signal ratio of 1.5 was maintained in order to minimize the log output to a typical offset voltage of 20 mV. The measurements were carried out in a dark box to prevent noise contributions due to the exposure to room light.

Electronic canceler and data acquisition

The double-beam absorption measurements were carried out utilizing the log output of the all-electronic noise canceler that was recently developed by Haller and Hobbs. A full description of the device is given in refs. 15 and 16. The

circuit of the noise canceler is shown in Fig. 2. Two photodiodes (BPW34, Siemens) were used as the signal and reference beam detectors. The bipolar junction transistor differential pair (Q1, Q2) (Analog Devices MAT-04) split the current. A PNP bipolar transistor (2N3906) was used to prevent the capacitance of the signal photodiode from loading the summing junction of the operational amplifier A1 (Motorola, Op-27) and causing instability. The operational amplifier converts the photocurrent to a voltage. The second operational amplifier A2 integrates the output voltage of A1 and adjusts the current splitting ratio of Q1/Q2 to keep that voltage at 0 V. The output voltage of A1 is the linear output of the circuit. The circuit has another output from A2 which is related to the log ratio of the signal and reference photocurrents and provides a straightforward method for absorption measurements. The circuit was driven by ±12 V batteries. The driving voltages were further
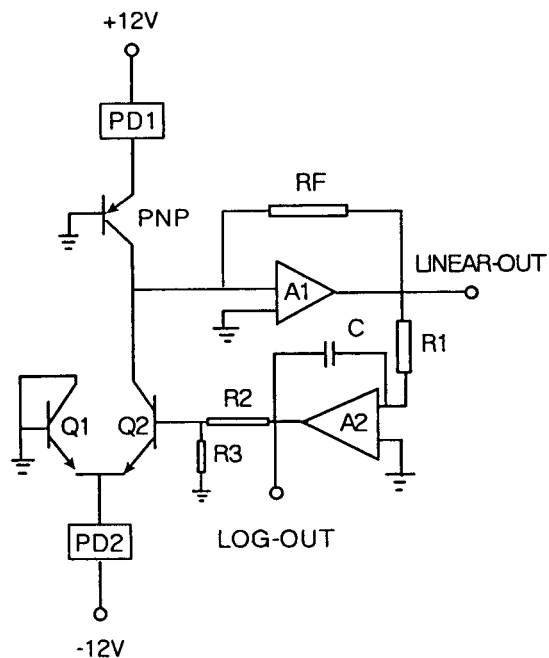
Fig. 2. Schematic diagram for an all-electronic noise canceler. PD1 = Signal photodiode; PD2 = reference photodiode; PNP = transistor; Q1, Q2 = differential pair of biopolar junction transistors; A1, A2 = operational amplifiers; R1 (1 kΩ), R2 (1 kΩ), R3 (24 Ω), RF (20 kΩ) resistors; C = 2.2 μF unpolarized capacitor.

stabilized by voltage regulators for the positive (LM7812, National Semiconductors) and for the negative (LM7912, National Semiconductors) voltages. The circuit was put in a metal box that was carefully grounded in order to shield the circuit from environmental noise. The log output voltage was passed through an RC filter which consists of a 10 kΩ resistor and a 10 μF unpolarized capacitor to increase the time constant of the circuit to 100 ms. The filtered output was connected to an analog voltmeter, DVM (Keithley 177), which was used to amplify the log output voltage. The amplified voltage was acquired at 5 Hz by an IBM-PC compatible computer equipped with an A/D board (Chromperfect, Justice Innovation).

The shot-noise limit measurements of the conventional absorption detectors were taken using a photodiode (Hamamatsu). The instruments were ISCO-3850, ISCO-3140, and Spectra-Physics SpectraPhoresis 1000TM. The three are CE absorption detectors that are based on deuterium and tungsten lamps as light sources.

Chromatography

An HPLC pump (LKB-2150) was operated at a pressure of 75 bar and delivered 1 ml/min with ±1% flow-rate accuracy. This pump has a pulsating flow of approximately 0.5 Hz. A 3-μm adsorbosphere column (100 mm × 4.6 mm I.D.) (Alltech) and an injection valve with a loop of 50 μl were used. The cell volume was 7.5 μl and the pathlength was 1 cm. All of the connections and tubing used in the HPLC system were stainless steel of 0.25 mm I.D. to minimize dead volume.

Reagents

HPLC-grade methanol (Fisher Scientific) was used as the eluting solvent without further purification. The solvent was degassed before use by a sonicator operated under vacuum·for 15 min. The two isomers of chloro-4-dimethylaminoazobenzene, 2′-Cl-DAAB and 4′-Cl-DAAB (Tokyo Kasei Co.) were used as received. The stock solutions of dyes were prepared and diluted just before use and were kept covered with Al-foil to prevent photodecomposition due to exposure to room light. The absorption spectra

of these dye solutions were measured with a photodiode array spectrometer (Hewlett-Packard HP8452A).

RESULTS AND DISCUSSION

UV–visible spectrum of Cl-4-DAAB

The absorption spectrum of 2'-Cl-4-DAAB in methanol is shown in Fig. 3. This spectrum is similar to that of 4'-Cl-4-DAAB. The molar absorptivities of 2'-Cl-4-DAAB were calculated (using Beer's law) and found to be 7575 1 mol^{-1} cm^{-1} at 488 nm and 9500 1 mol^{-1} cm^{-1} at 254 nm. These results deviate by less than 5% from the results obtained by Oda and Sawada [10] for the same compounds.

Separation of Cl-4-DAAB isomers

We were able to separate the two Cl-4-DAAB isomers following the procedure that was suggested by Oda and Sawada [10], which is based on using methanol as the solvent. The absorption peaks were detected by utilizing the all-electronic noise canceler double-beam system. A typical chromatogram of the Cl-4-DAAB isomer mixture is shown in Fig. 4. The retention times are 2.18 min for 2'-Cl-4-DAAB and 2.79 min for 4'-Cl-4-DAAB. The two peaks are clearly baseline separated.
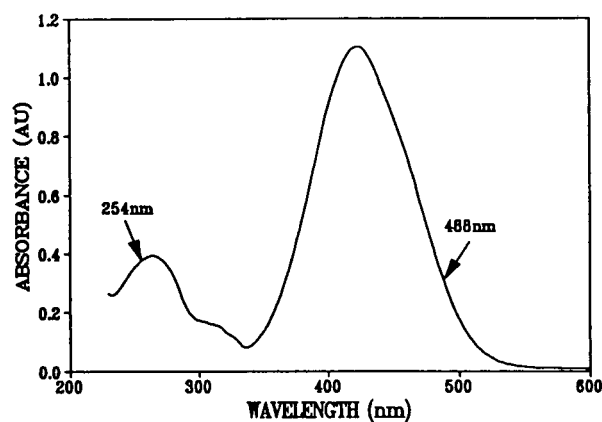
Fig. 3. Absorption spectrum of 2'-Cl-4-DAAB in methanol. The concentration is $4 \cdot 10^{-5}$ M and the cell pathlength is 1 cm. The molar absorptivities are found to be $7.575 \cdot 10^3$ 1 mol^{-1} cm^{-1} for 488 nm and $9.5 \cdot 10^3$ 1 mol^{-1} cm^{-1} for 254 nm.
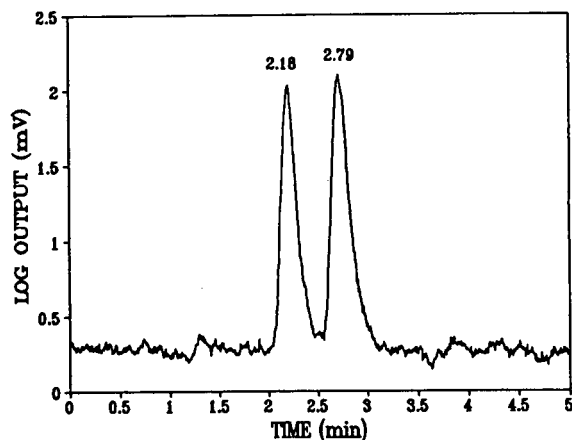
Fig. 4. Separation of a Cl-4-DAAB isomer mixture. The concentration of each isomer is $1 \cdot 10^{-7}$ M. A 3-μm adsorbosphere column (100 mm × 4.6 mm I.D.) and an injection valve with 50-μl loop were used. The cell volume is 7.5 μl and the pathlength is 1 cm.

Detection performance

The major advantage of the all-electronic canceler over a conventional double-beam detector is the ability to adjust the reference photocurrent so that an identical unmodulated copy of the signal photocurrent is subtracted. This unique property of the device led to perfect noise cancellation down to almost shot-noise limited performance. As was mentioned previously [15,16] the log output of the electronic canceler $V_{\log}$ was used to perform the absorption measurements. The dependence of the log output voltage on the ratio between the signal and reference photodiode currents is given in the following expression:

$$V_{\log} = -\ln \left(i_{\text{ref}}/i_{\text{sig}} - 1 \right) \qquad (1)$$

It is the maximum linear output voltage that was taken from operational amplifier A1 of the circuit when the reference beam is blocked. For 2 mW beam power at the signal photodiode $V_{\max}$ was measured to be 4.5 V. i_{ref} and i_{sig} are the photocurrents of the reference and signal photodiodes. The voltage difference $\Delta V_{\log}$ due to the presence of absorption is therefore:

$$\Delta V = (2 - V_0) \ln(i_0/i) \qquad (2)$$

where subscript 0 refers to the photocurrents in the absence of absorption. According to Beer's law:

$$\log (i_0/i) = \varepsilon bc \qquad (3)$$

where ε is the molar absorptivity of the sample, b is the pathlength and c is the sample concentration. The log output voltage difference can then be expressed as:

$$\Delta V = (2 - V_0) \ln 10\varepsilon^{bc} \qquad (4)$$

It can be seen that the concentration of the analyte can be directly evaluated from eqn. 4. In order to define the linear dynamic range of the double-beam absorption detector a concentration versus peak height calibration curve for 2'-Cl-4-DAAB in our HPLC system was constructed. The solution concentrations were from $5 \cdot 10^{-9}$ M to $5 \cdot 10^{-5}$ M. Each peak height was an average from three consecutive injections. The deviation from the average was about 3%. In order to confirm eqn. 4 a plot of log (peak height) as a function of log (concentration) is shown in Fig. 5. The slope of this curve is 0.94 with a correlation coefficient r^2 of 0.997. It can be seen that the deviations from the linear curve are larger at lower concentrations, where signal-to-noise ratios (S/N) are poorer.

Limit of detection

Due to optical losses caused by the optical components and the absorption cell the signal beam power at the detector was measured to be 2 mW. The photon flux of a 2-mW Ar ion laser beam that is operated at 488 nm is $N = 5 \cdot 10^{15}$ s^{-1}. For a measurement time of 1 s and a unit quantum efficiency the calculated S/N is $N^{1/2}/N = 1.4 \cdot 10^{-8}$. The noise-equivalent absorption should be $\sqrt{2}$ higher, i.e. $= 2 \cdot 10^{-8}$. The theoretical voltage noise level $\sigma V_{\log}$ for our HPLC system can be derived using the following expression:

$$\sigma V_{\log} = \sqrt{2}[\exp(V_{\log}/V_{\max}) + 1)](2e/i_{\mathrm{sig}})^{1/2} \qquad (5)$$

where e is the electron charge $(1.6 \cdot 10^{-19}$ Coulomb). Since $V_{\log}/V_{\max} \approx 0$, $\sigma V_{\log}$ is given as:

$$\sigma V_{\log} = 4(e/i_{\mathrm{sig}})^{1/2} \qquad (6)$$

For the measured 220 μA signal current $\sigma V_{\log} = 1.07 \cdot 10^{-7}$ V/$\sqrt{\mathrm{Hz}}$. With 5 Hz bandwidth the minimum noise level should be 0.24 μV. According to eqn. 4 and assuming a signal-to-noise ratio of 5 the theoretical limit of detection for 2'-Cl-4-DAAB ($\varepsilon = 7.575 \cdot 10^3$) is $1.5 \cdot 10^{-11}$ M (signal level of 1.2 μV).

A typical chromatogram of 2'-Cl-4-DAAB which demonstrates the performance of the all-electronic canceler at the detection limit is shown in Fig. 6. The peak height is about 100 μV and

Fig. 5. Plot of log (peak height) as a function of log (concentration) for 2'-Cl-4-DAAB. The concentration range is 10^{-5}–10^{-9} M. Each data point is an average of three consecutive measurements. The best-fit line has a slope of 0.94 and a correlation coefficient $r^2 = 0.997$.
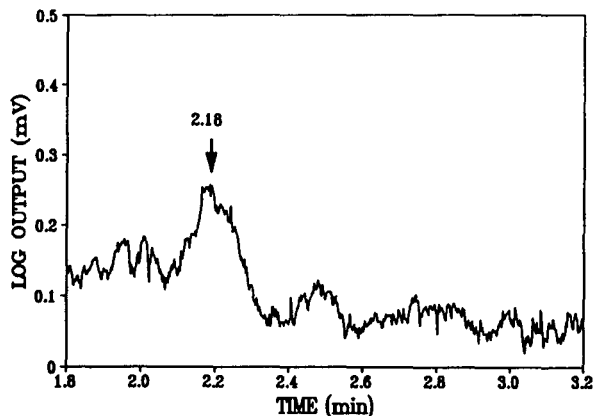
Fig. 6. Chromatogram of ultra-low concentration of 2'-Cl-4-DAAB. The peak height is 100 μV with a signal-to-noise ratio of 5. The concentration at the detector is $1.1 \cdot 10^{-9}$ M (50 pg injected).

the signal-to-noise ratio is 5. The concentration of the injected solution was $3.75 \cdot 10^{-9}$ M. The concentration at the detector was $1.1 \cdot 10^{-9}$ M due to a dilution factor of 3.3. This signal level deviates by less than 15% from the predicted concentration according to eqn. 4 which is $1.3 \cdot 10^{-9}$ M. The root mean square (rms) noise level is 20 μV. In terms of absolute absorption the 100 μV signal is related to an absorption peak height of $9 \cdot 10^{-6}$ AU while the 20 μV noise level is related to $2 \cdot 10^{-6}$ AU. This measurement implies that the sample mass detected is about 50 pg (injected). However, the LOD is still 100 times worse than the theoretical limit. This is partly due to the fact that the quantum efficiency of the photodiode is not unity. Also, theoretical performance is not achieved due to excess laser noise and environmental perturbations such as mechanic vibrations and flow disturbance.

In order to have a better comparison between our new detector and commercial systems we can use the predicted performance of commercial detectors based on the manufacturers' specifications. We also can estimate the shot-noise limit of commercial detectors that utilize a lamp as a light source. This estimation is based on actual measurements of the light power at the detector in several commercial instruments. The measurements were taken by placing a photodiode (Hamamatsu, S1227) into the pathlength of the detector. Based on the photodiode response curve and the wavelength dependence of the photodiode response the average power at the detector was found to be around $1 \cdot 10^{-4}$ mW for all three instruments tested. Assuming a measurement time of 1 s and a unit quantum efficiency this power corresponds to a photon flux of $1.25 \cdot 10^{11}$ s^{-1}. The shot-noise limit is thus $3 \cdot 10^{-6}$ and the equivalent absorption noise level is around $4.2 \cdot 10^{-6}$ AU. A typical state-of-the-art commercial detector is limited to a noise level of $2 \cdot 10^{-5}$ AU which is 5 times higher than the theoretical shot-noise limit of the lamp. The fact that the quantum efficiency is not unity and that there is a flow cell in the light path explains why commercial detectors do not approach the shot-noise limit. We were not able to replace the circuitry in a commercial detector with the all-electronic noise canceler because the beam size

there is substantially larger than the active area of the photodiodes. A major redesign of the optics would be necessary to allow a direct comparison.

Although the cost, fixed wavelength coverage and relatively short lifetimes of typical continuous wave (cw) lasers are disadvantages, when a lower noise level is needed, an absorption detector that utilizes a laser as a light source must be used. The equivalent absorption noise level of our detector is *ca.* $2 \cdot 10^{-6}$ AU, and it is still far from the full theoretical potential by almost two orders of magnitude. Further improvement can probably be achieved by using a low-pass narrow-band preamplifier between the log output and the input to the computer, by using more rigid mechanical mounts, by additional electronic shielding, and by narrowing the feedback bandwidth to 1 Hz. Even with the present performance we were able to decrease the minimum noise level and the detection limit to the 10^{-6} range. To the best of our knowledge this is an improvement by one order of magnitude compared to any commercial absorption detector. It should also be noted that since the molar absorptivity of DAAB at 254 nm is $9.5 \cdot 10^{3}$ l mol^{-1} cm^{-1} the detection limit of a commercial detector at a signal-to-noise ratio of 5 would be $1 \cdot 10^{-8}$ M, which is still poorer than in our detector. Other comparisons of LOD with those in the literature should always take into account the dilution factors on column and the molar absorptivities.

It is interesting to compare the performance of the all-electronic noise canceler in our HPLC system to its performance in a CE system [17]. While the HPLC system suffers from pump pulsation noise and from flow gradients due to the fact that a massive volume of liquid phases through the absorption cell, the CE system suffers from high voltage interference and from mechanic vibrations of the thin capillary. Although the two systems present different problems there are only minor differences in the detector performance, which amounts to a factor of 2 better (AU) under HPLC conditions. The CE detector however is 25 times better than the corresponding commercial system because the use of a laser increased the effective absorption

path there by a factor of 5. Our experiments under both CE [17] and HPLC conditions demonstrate that the all-electronic noise canceler is a powerful device that comes close to the performance of a fluorescence detector. This fact make the double-beam absorption detector suitable for a variety of future applications, particularly if UV lasers are used.

ACKNOWLEDGEMENT

REFERENCES

1 R.P.W. Scott, *Liquid Chromatography Detectors*, Elsevier, Amsterdam, 2nd ed., 1986.
2 T.M. Vickrey (Editor), *Liquid Chromatography Detectors*, Marcel Dekker, New York, 1983.
3 D.W. Virdine and D.R. Matson, *Appl. Spectrosc.*, 32 (1978) 502–507.
4 N. Teramae and S. Tanaka, *Spectrosc. Lett.*, 13 (1980) 117–125.
5 E.S. Yeung and M.J. Sepaniak, *Anal. Chem.*, 52 (1980) 1465A–1481A.
6 A.T.R. Williams, *Fluorescence Detection in Liquid Chromatography*, Perkin-Elmer, Beaconsfield, 1980.
7 J.J. Kirkland, *Anal. Chem.*, 40 (1968) 391.
8 *Life Science Research Products*, Bio-Rad Laboratories, Richmond, CA, 1992.
9 *Chromatography*, Catalog 250, Alltech, Deerfield, IL, 1991.
10 S. Oda and T. Sawada, *Anal. Chem.*, 53 (1981) 471.
11 S. Oda, T. Sawada, T. Moriguchi and H. Kamada, *Anal. Chem.*, 52 (1980) 650.
12 C.E. Buffett and M.D. Morris, *Anal. Chem.*, 54 (1982) 1824.
13 S.G. Burns and P.R. Bond, *Principles of Electronic Circuits*, West Publishing, St. Paul, MN, 1987, Ch. 4.
14 J.D. Ingle, Jr. and S.R. Crouch, *Spectrochemical Analysis*, Prentice-Hall, Englewood Cliffs, N.J., 1988, Ch. 4.
15 K.L. Haller and P.C.D. Hobbs, *Proc. SPIE–Int. Soc. Opt. Eng.*, 1435 (1991) 298.
16 P.C.D. Hobbs, *Optics Photonics*, April (1991) 17.
17 Y. Xue and E.S. Yeung, *Anal. Chem.*, 65 (1993) in press.

CHROM. 25 242

Computer simulation study of size-exclusion chromatography with simultaneous viscometry and light scattering measurements

C. Jackson* and W.W. Yau[☆]

E.I. du Pont de Nemours and Company, Central Research and Development, Experimental Station, P.O. Box 80228, Wilmington, DE 19880-0228 (USA)

ABSTRACT

The integration of an on-line viscosity or light scattering (LS) detector with size-exclusion chromatography (SEC) improves the accuracy with which polymer molecular mass distributions can be measured. The coupling of a viscometer and a light scattering detector in one SEC instrument potentially offers improved precision and dynamic range for SEC polymer conformation studies. However, the increased complexity of these experiments and the subsequent data handling introduce a number of problems not present in conventional SEC. A computer simulation of the multiple detector SEC experiment was developed in order to study these effects in detail. The computer model is described and preliminary data are presented to illustrate some of the additional features of SEC with multiple detectors.

INTRODUCTION

The addition of one or more molecular mass sensitive detectors to a size-exclusion chromatographic (SEC) system increases greatly the amount of information that can be determined in the analysis. Measurement of the light-scattering intensity and the sample concentration enables the molecular mass distribution to be determined directly [1,2] and measurement of the specific viscosity and sample concentration enables the intrinsic viscosity distribution (IVD) to be determined [3]. In both cases the measurement does not require column calibration. This information can be combined with the hydrodynamic volume derived from column calibration to provide measurements of a number of polymer properties. By using both molecular size and molecular mass, the accuracy of the distributions can be improved. In addition, polymer conformation and architecture can be studied across the molecular mass distribution. Several methods have been developed for combining molecular mass and molecular size information [4–7].

However, this wealth of information is obtained at the expense of the simplicity of conventional SEC, and complex computer-based algorithms often hide important features of the instrument signals. Each of the measured signals depends on different polymer solution properties, with different molecular mass sensitivity, and as a result has different measurement ranges. The combination of these signals in the

---

* Corresponding author.
[☆] Present address: Henkel Corporation, Research and Development, 300 Brookside Avenue, Ambler, PA 19002, USA.

final results can introduce errors in the final measurement [5,8–17].

In order to gain a clearer understanding of how the nature of the raw data affects the results we developed a computer simulation of the SEC experiment. The model is described and some of the preliminary results are discussed.

METHODOLOGY

SEC–light scattering computer model

We start by describing the mass fraction w_x, of x-mer, in a given polymer sample by the Wesslau distribution [18],

$$w_x = \frac{1}{\beta\pi^{1/2}} \cdot \frac{1}{x} \exp\left(-\frac{1}{\beta^2}\ln^2\frac{x}{x_0}\right) \qquad (1)$$

where $\beta^2 = \ln(x_w/x_n)^2$, x_w is the mass-average degree of polymerization, x_n is the number average, and the central value of the distribution, $x_0 = x_n \exp(\beta^2/4)$.

In SEC the mass fraction is measured as a function of the logarithm of molecular mass in which case the mass fraction w_x' is described by

$$w_x' = w_x \frac{dx}{d\ln x} = x w_x \qquad (2)$$

so,

$$w_x' = \frac{1}{\beta\pi^{1/2}} \exp\left(-\frac{1}{\beta^2}\ln^2\frac{x}{x_0}\right) \qquad (3)$$

It can be seen that w_x' is a symmetrical Gaussian with a variance given by

$$\sigma_x^2 = \frac{\beta^2}{2} \qquad (4)$$

which is related to the sample molecular mass polydispersity as

$$\frac{x_w}{x_n} = e^{\sigma_x^2} \qquad (5)$$

Fig. 1 shows the mass-fraction distribution plotted as a function of the logarithm of x.

In SEC the molecular mass is related to the column elution volume by a calibration curve of the form [19],

$$M_t(V) = xM_0 = D_1 e^{-D_2 V} \qquad (6)$$
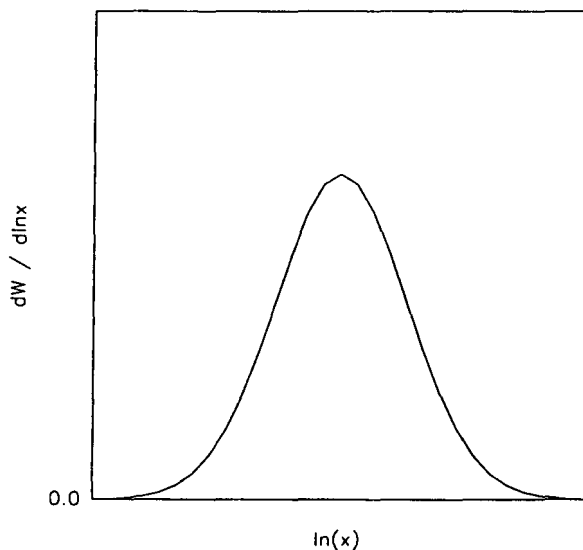
Fig. 1. Wesslau distribution for the mass-fraction molecular mass distribution plotted as a function of the logarithm of the degree of polymerization, x.

where M_0 is the repeat unit molecular mass and D_1 and D_2 describe the calibration curve for a given column set. D_2 is the slope in a plot of log molecular mass against elution volume. Eqn. 3 can then be rewritten in terms of elution volume using eqn. 6, as,

$$w_x'(V) = \frac{1}{\sigma_V\sqrt{2\pi}} \exp\left[\frac{-(V - V_R)^2}{2\sigma_V^2}\right] \qquad (7)$$

where the elution peak variance is related to the molecular mass variance by $\sigma_V = \sigma_x/D_2$, and V_R corresponds to the peak maximum in the concentration sensitive detector. Eqn. 7 describes the concentration detector elution profile for a sample with molecular mass distribution described by eqn. 1. Note that molecular mass decreases with increasing elution volume.

In the SEC–LS scattering experiment the sample can be considered to be at infinite dilution, in which case the intensity of scattered light at zero degrees from the incident beam is described by

$$I_{(\theta=0)}(V) = K^* M_t(V) w_x'(V) \qquad (8)$$

where K^* is an optical constant for the scattering system [20]. The molecular mass at each volume

is described by eqn. 6, and the mass fraction distribution by eqn. 7, thus

$$I_{(\theta=0)}(V)$$

$$= K^* D_1 e^{-D_2 V} \frac{1}{\sigma_V \sqrt{2\pi}} \exp\left[\frac{-(V - V_R)^2}{2\sigma_V^2}\right] \quad (9)$$

It can be shown that this is also Gaussian with the same variance as the concentration detector response, but with a peak maximum, V_L, shifted to lower elution volume by an amount depending on the sample polydispersity and the slope of the calibration curve,

$$V_L = V_R - \sigma_V^2 D_2$$

$$= V_R - \frac{\sigma_x^2}{D_2} \quad (10)$$

SEC–viscometry computer model

In SEC–viscometry the specific viscosity of the eluting sample is measured. At infinite dilution this is related to the intrinsic viscosity by

$$\eta_{sp}(V) = [\eta](V) w_x'(V) \quad (11)$$

The intrinsic viscosity at each elution volume is given by eqn. 11 and the Mark–Houwink coefficients, K and a, which describe the empirical relationship between intrinsic viscosity and molecular mass [21],

$$[\eta](V) = K[M_t(V)]^a \quad (12)$$

Eqn. 11 can then be rewritten

$$\eta_{sp}(V) = K D_1^a e^{a(-D_2 V)} w_x'(V) \quad (13)$$

This also describes a symmetrical Gaussian with the same variance as the concentration detector response, but this time the peak maximum, V_V, is shifted to a lower elution volume determined by the value of the Mark–Houwink exponent as well as the polydispersity and the calibration curve slope,

$$V_V = V_R - a\sigma_x^2/D_2 \quad (14)$$

Fig. 2 shows the three signal traces, excess light-scattering intensity, specific viscosity, and differential refractive index, for a sample with a polydispersity of 2 and a Mark–Houwink exponent of 0.725. For a monodisperse standard
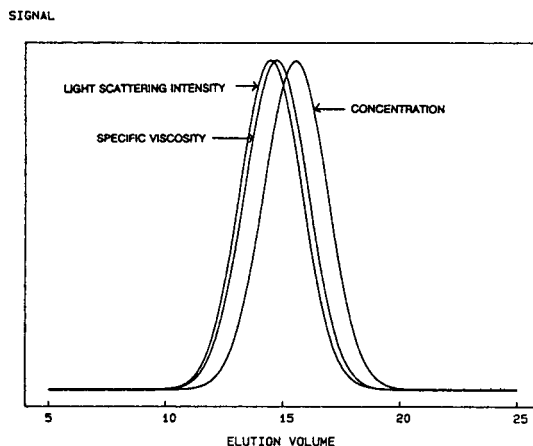
Fig. 2. Signal traces from the three detectors showing excess light-scattering intensity, specific viscosity, and differential refractive index, for a sample with a polydispersity of 2 and a Mark–Houwink exponent of 0.725. Elution volume in ml.

there is no volume shift between the three signal peaks and they all overlay. Fig. 3 illustrates an approximation to this situation with a nearly monodisperse sample of polydispersity 1.05

The universal calibration curve describes the hydrodynamic volume, HV, of the molecules at each elution volume [22],

$$HV_t(V) = [\eta]_t(V) \cdot M_t(V) = U_1 e^{-U_2 V} \quad (15)$$

where, from eqns. 6 and 13

$$U_1 = K D_1^{(a+1)} \quad (16)$$
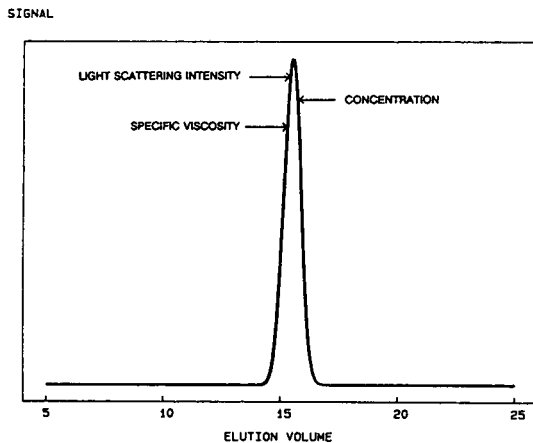
Fig. 3. Signal traces from the three detectors for a nearly monodisperse sample, polydispersity 1.05. Elution volume in ml.

$$U_2 = (1 + a)D_2 \tag{17}$$

The intrinsic viscosity distribution can be used to characterize a polymer sample in a way analogous to the molecular mass distribution, with various statistical averages defined by [3]:

$$[\eta]_0 = \sum_i \frac{c_i}{c_i/[\eta]_i} \tag{18}$$

$$[\eta]_{+1} = \sum_i \frac{c_i[\eta]_i}{c_i} \tag{19}$$

$$[\eta]_{+2} = \sum_i \frac{c_i[\eta]_i^2}{c_i[\eta]_i} \tag{20}$$

Band broadening computer model

Band broadening in the system is modelled by the convolution of a Gaussian band spreading function

$$G(V) = \frac{1}{\sigma_B\sqrt{2\pi}} e^{-V^2/2\sigma_B^2} \tag{21}$$

where σ_B^2 is the peak variance due to band broadening, with the elution profile derived in eqn. 7. The experimentally determined concentration elution profile is then described by

$$w_x'(V) = \frac{1}{\sigma_T\sqrt{2\pi}} e^{\frac{-(V-V_0)^2}{2\sigma_T^2}} \tag{22}$$

where the total peak variance is given by $\sigma_T^2 = \sigma_V^2 + \sigma_B^2$.

The true mass-average and number-average molecular mass of an infinitesimal fraction at retention volume V are now given by [23]:

$$\overline{M_w}(V) = \frac{f(V - D_2\sigma_B^2)}{f(V)} e^{1/2(D_2\sigma_B)^2} M_t(V) \tag{23}$$

$$\overline{M_n}(V) = \frac{F(V)}{F(V + D_2\sigma_B^2)} e^{-1/2(D_2\sigma_B)^2} M_t(V) \tag{24}$$

where $F(V)$ is the experimental chromatogram broadened by the column dispersion process described by eqn. 21, where $F(V) = w_x'(V)$.

The effect of this broadening of the elution peak is a rotation of the calibration curve around the first moment of the concentration distribution. This leads to an effective mass-average molecular mass calibration curve defined by

$$x = D_1' e^{D_2'V} \tag{25}$$

where

$$D_1' = D_1 \exp\left[\frac{D_2\sigma_B^2(D_2\sigma_V^2 - 2V_0)}{2\sigma_T^2}\right] \tag{26}$$

$$D_2' = D_2\left(1 - \frac{\sigma_B^2}{\sigma_T^2}\right) \tag{27}$$

These expressions can also be used to define an effective mass-average intrinsic viscosity calibration curve,

$$[\eta](V) = E_1' e^{E_2'V} \tag{28}$$

where

$$E_1' = KD_1'^a \tag{29}$$

$$E_2' = aD_2' \tag{30}$$

The model described can be used to generate light-scattering intensity, specific viscosity, and differential refractive index data for samples with different Mark–Houwink relationships and with different amounts of band broadening. Mixtures of up to three peaks with differing polydispersities can be generated. The raw signal tracings can then be used to calculate results using different detector combinations and interdetector delay volumes.

RESULTS AND DISCUSSION

Effect of detector alignment

It can be seen from eqns. 9 and 13 that the signals from the differential concentration detector, the viscometer and the light-scattering detector all have the same shape. When the sample is monodisperse the signals from all three detectors also have the same peak elution volume, and only differ in their relative areas which depends on the mass-average molecular mass. If there is any molecular mass polydispersity in the sample, eqns. 10 and 14 show that the light scattering and specific viscosity peaks are shifted to lower elution volumes although the overall shape is not changed. The amount of this shift in the light scattering signal, multiplied by the calibration curve slope, D_2, is the logarithm of the sample polydispersity.

$$\frac{M_w}{M_n} = e^{D_2(V_R - V_L)} \tag{31}$$

In the case of the viscometer the volume shift is multiplied by the Mark–Houwink exponent.

$$\frac{M_w}{M_n} = e^{aD_2(V_R - V_V)} \tag{32}$$

The difference between the viscometer volume shift and the light-scattering volume shift gives the Mark–Houwink exponent.

$$a = 1 - (V_\eta - V_l)D_2/\sigma_x^2 \tag{33}$$

If the Mark–Houwink exponent is greater than one, as is the case for rigid molecules, the viscometer will be shifted more than the light scattering signal. If the exponent is negative, as is the case in some star-shaped molecules, the viscometer signal will be shifted to a larger elution volume than the RI. If $a = 0$, as is the case for particles, $V_V = V_R$.

In the case of a linear polymer with a Wesslau molecular mass distribution, the main information obtained by using a molecular mass-sensitive detector is the mass average property: molecular mass or intrinsic viscosity, and the polydispersity of the sample as shown by the relative position of the two detector peaks (eqns. 31 and 32). Because of this it is critical that the actual physical volume difference that exists between detectors is correctly compensated before the data are analyzed. Any error in this correction produces a corresponding error in the measured polydispersity. If both viscosity and light scattering are measured there will be an additional error in the measured Mark–Houwink coefficients. Fig. 4 illustrates the sensitivity of these measurements to the interdetector volume difference. An error, $D_2\Delta V_{error}$, of 0.01 corresponds to about 1 s at a flow-rate of 1 ml/min.

Effect of band broadening on measured molecular mass distributions

Band broadening and the corresponding loss of resolution causes a rotation of the calibration curve about the first moment of the mass distribution of the eluting peak. This is because the molecular mass of each elution slice approaches
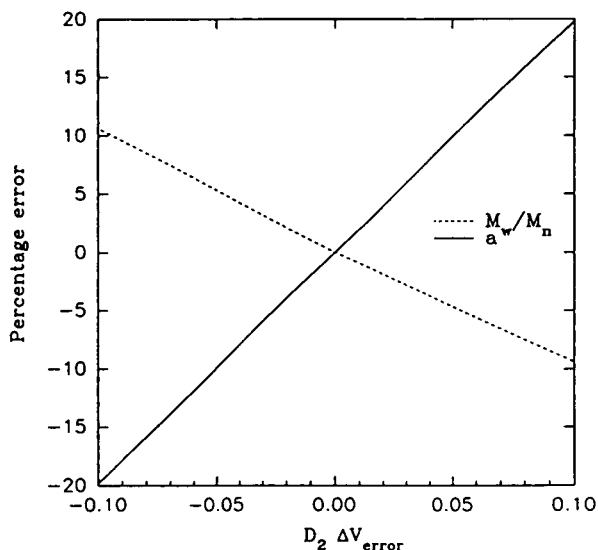
Fig. 4. Effect of errors in the determination of interdetector volume on SEC–viscometry–LS measurements of polydispersity and Mark–Houwink coefficients.

the average molecular mass of the sample. If there were no resolution, the calibration curve would be a straight line with zero slope. In practice the effect is much smaller but nevertheless it can have serious effects on the computed values. This situation is shown in Fig. 5 where the mass-average molecular mass, as measured by light-scattering, for a sample with polydispersity 2, is shown as a function of elution
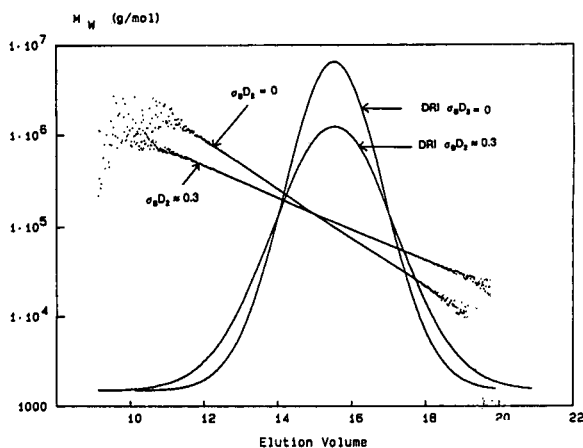
Fig. 5. Mass-average molecular mass at each elution volume, as measured by light-scattering, for a sample with polydispersity 2, for a perfectly resolved peak and for one with band broadening, $\sigma_B D_2 \approx 0.3$. Elution volume in ml. DRI = differential refractive index.

volume for a perfectly resolved peak and for one with band broadening. In the case of perfect resolution, the molecular mass measured *is* the calibration curve, with band broadening the line is less steep. Although not shown in this figure, band broadening does not alter the peak position on any of the detectors. One of the advantages of a molecular mass sensitive detector is that it

can distinguish between peak width due to polydispersity and that due to band broadening.

The effect of band broadening on the final results depends on the method of calculation used. If the molecular mass distribution is determined from the light scattering molecular mass, or from the intrinsic viscosity distribution by way of known Mark–Houwink coefficients then the effect is an apparent narrowing of the
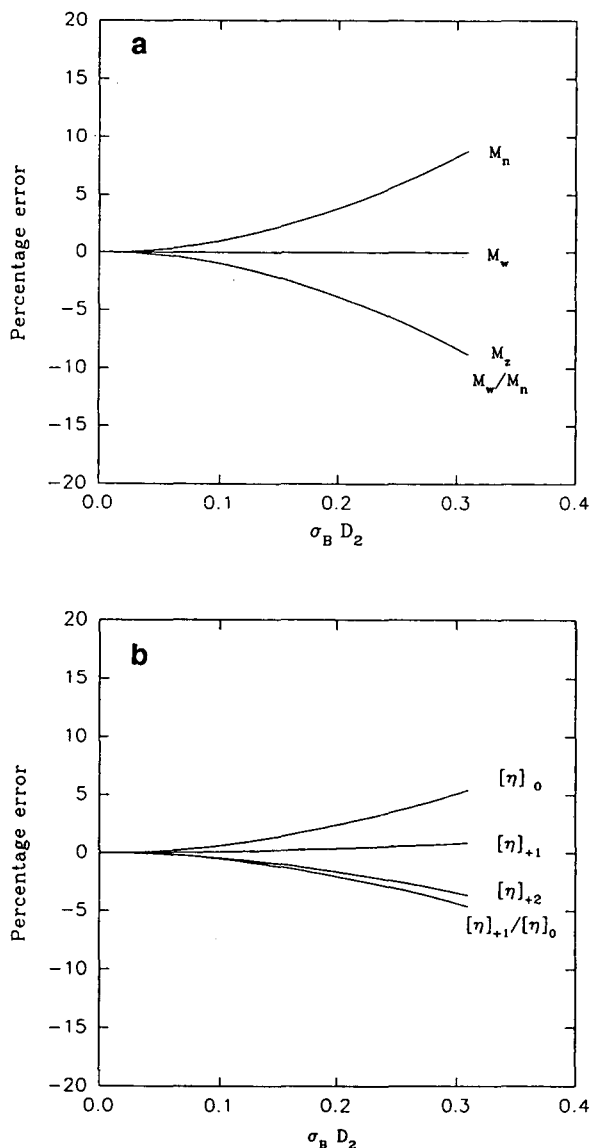
Fig. 6. Effect of band broadening for a polymer with polydispersity 2, on (a) measured moments of the molecular mass distribution by light scattering, and (b) moments of the intrinsic viscosity distribution measured by on-line viscometry.
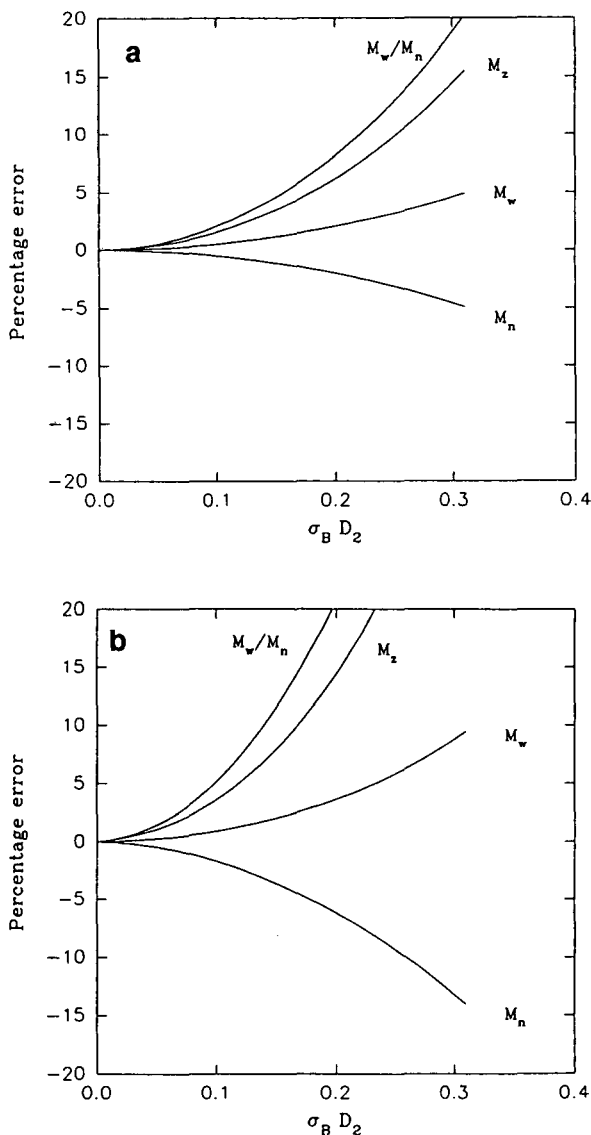
Fig. 7. Effect of band broadening for a polymer with polydispersity 2, on measured moments of the molecular mass distribution by (a) conventional SEC, and (b) universal calibration.

distribution (Fig. 6). This is because the system is losing resolution. However the mass-average molecular mass, or intrinsic viscosity are both unaffected.

By conventional SEC calibration the effect is the opposite, the peak broadening is interpreted as increased sample polydispersity (Fig. 7a). The same is true for universal calibration using on-line viscosity measurements (Fig. 7b). The relative errors caused by band broadening in this case are shown in Fig. 7. The averages determined by molecular mass sensitive detectors are less affected by band broadening than those obtained by calibration-based techniques. The measurement of molecular mass distribution by SEC–viscometry with universal calibration is the most sensitive to band broadening errors. However, if SEC–viscometry is used to measure the intrinsic viscosity distribution and then the Mark–Houwink coefficients are used to calculate the molecular mass distribution, the errors due to band broadening are the same as for SEC–LS.

Effect of band broadening on measurement of Mark–Houwink coefficients

Band broadening also has an effect on measurements of Mark–Houwink coefficients using universal calibration. When an on-line viscometer is used with universal calibration to determine the relationship between intrinsic viscosity and molecular mass, it can be shown, from eqns. 15 and 28–30 that the measured Mark–Houwink exponent, a', is given by,

$$a' = \left(\frac{1 - \sigma_B^2/\sigma_T^2}{1 + a\sigma_B^2/\sigma_T^2}\right)a \tag{34}$$

This results in an underestimate of the Mark–Houwink exponent and an overestimate of the prefactor, K.

If universal calibration is used in conjunction with light scattering, where the measured molecular mass is used with the universal calibration curve to calculate the intrinsic viscosity at each elution slice, then the situation is reversed and the Mark–Houwink exponent will be overestimated by,

$$a' = \left(\frac{a + \sigma_B^2/\sigma_T^2}{1 - \sigma_B^2/\sigma_T^2}\right) \tag{35}$$

Note that in Fig. 6 the mass-average molecular mass measured by light scattering and the mass-average intrinsic viscosity measured by on-line viscometry are unaffected by band broadening. As a result the Mark–Houwink coefficients and any determinations of molecular conformation, or branching based on them are similarly unaffected by band broadening. Fig. 8 shows the Mark–Houwink plot for a sample with polydispersity 2 with and without band broadening. In both cases, as expected, the calculated slope and intercept, a and K in eqn. 12 are the same.

Fig. 9 shows the effect of band broadening on measurements of Mark–Houwink coefficients by combined viscosity and light scattering detectors, universal calibration with a light scattering detec-
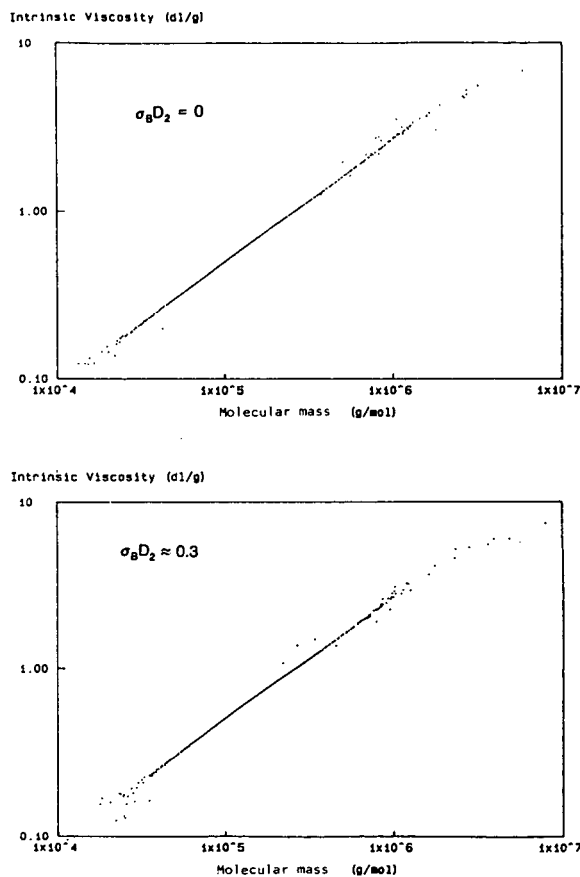
Fig. 8. Mark–Houwink plot by SEC with combined light scattering and viscometry for a sample with polydispersity 2 and $M_r \approx 150\,000$, (a) without band broadening, and (b) with band broadening, $\sigma_B D_2 \approx 0.3$. The calculated slope and intercept are the same in both cases.
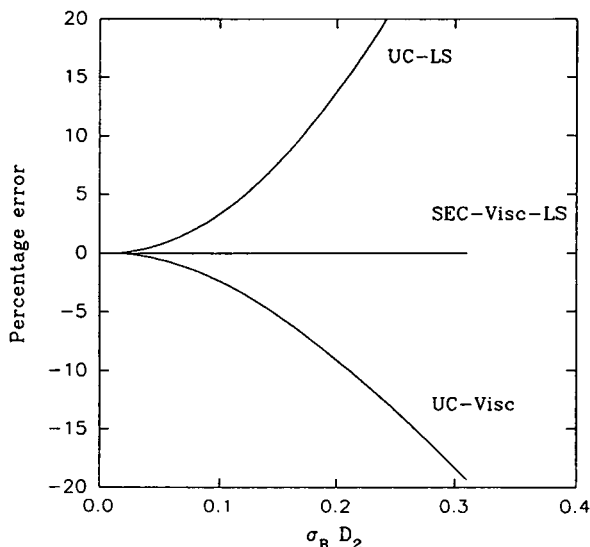
Fig. 9. Effect of band broadening on measurement of Mark–Houwink exponent, a, by different methods. UC = universal calibration.

tor, and universal calibration with a viscosity detector.

However, as mentioned above, the determination of the Mark–Houwink coefficients using on-line light scattering and viscosity detectors depends upon the volume delay between the three detectors being known accurately.

Effect of detector band broadening mismatch

An additional band broadening problem introduced by multiple detector systems is that the signals from different detectors are affected by differing amounts of post-column band broadening depending on the cell size and the order of detectors. When the ratio of these signals is taken to determine molecular mass and intrinsic viscosity the resultant values can be distorted. For example, if the concentration signal is the least broad, the calculated molecular masses or intrinsic viscosities for a near monodisperse sample will show a "U" shape rather than a straight line with the peak maximum molecular mass or intrinsic viscosity being underestimated (Fig. 10). Conversely if the concentration signal is the broadest the resultant values will show an "n" shape with the peak maximum molecular mass or intrinsic viscosity being overestimated (Fig. 11). This can be corrected by measuring
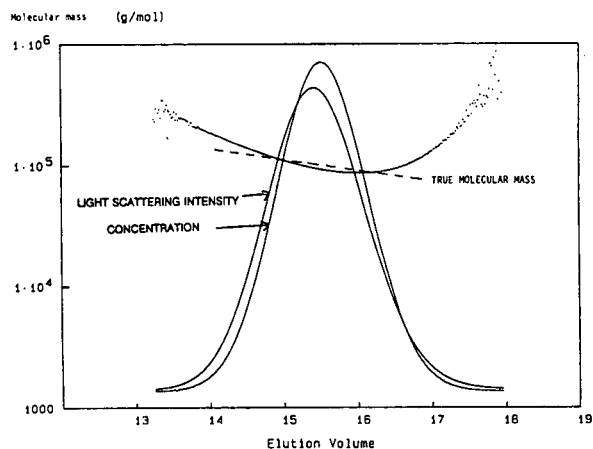
Fig. 10. Effect on the measured molecular mass at each slice of additional broadening on the light scattering detector signal, $\sigma_{add} \approx 0.06$. Elution volume in ml.
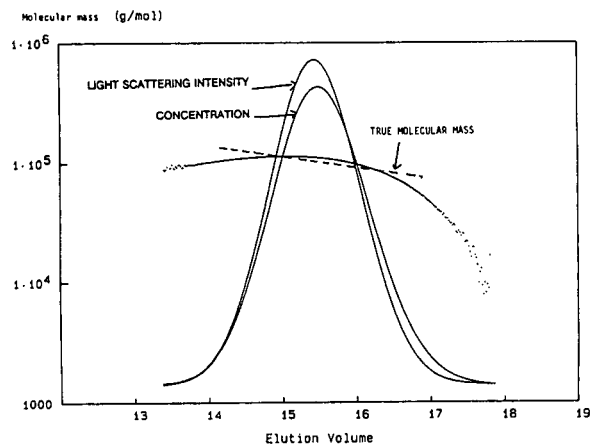
Fig. 11. Effect on the measured molecular mass at each slice of additional broadening on the concentration detector signal, $\sigma_{add} \approx 0.06$. Elution volume in ml.

the differences in band broadening in each signal, and then correcting the signals using eqn. 21 to make the narrower signal equivalent to the broader one.

CONCLUSIONS

The computer model described provides a functional simulation of SEC for linear polymers. Our findings emphasize the importance of determining the correct volume offset between the concentration detector and molecular mass sensitive detectors. The results also demonstrate

that molecular mass sensitive detectors are less sensitive to band-broadening errors than are column-calibration-based methods. In particular the Mark–Houwink coefficients, and resulting branching calculations, measured by combined light scattering and viscometry, are only slightly affected by band broadening. Future work will extend the model to incorporate peak skew and polymer branching.

REFERENCES

1 W. Kaye, *Anal. Chem.*, 45 (1973) 221A.
2 A.C. Ouano and W. Kaye, *J. Polym. Sci., Polym. Chem. Ed.*, 12 (1974) 1151.
3 J.J. Kirkland, S.W. Rementer and W.W. Yau, *J. Appl. Polym. Sci.*, 48 (1991) 39.
4 W.W. Yau, *Chemtracts*, 1 (1990) 1.
5 S.T. Balke, in H.G. Barth and J.W. Mays (Editors), *Modern Methods of Polymer Characterization*, Wiley, New York, 1991, Ch. 1.
6 W.W. Yau, C. Jackson and H.G. Barth, in *Proceedings International Gel Permeation Chromatography Symposium*, San Francisco, CA, 1991.
7 C. Jackson, H.G. Barth and W.W. Yau, in *Proceedings International Gel Permeation Chromatography Symposium*, San Francisco, CA, 1991.
8 O. Prochazka and P. Kratochvil, *J. Appl. Polym. Sci.*, 31 (1986) 919.
9 O. Prochazka and P. Kratochvil, *J. Appl. Polym. Sci.*, 34 (1987) 2325.
10 F.B. Malihi, C. Kuo, M.E. Koehler, T. Provder and A.F. Kah, *ACS Symp. Ser.*, 245 (1984) 281.
11 L. Letot, J. Lesec and C. Quivoron, *J. Liq. Chromatogr.*, 3 (1980) 427.
12 J. Lesec and G. Volet, *J. Liq. Chromatogr.*, 13 (1990) 831.
13 T.H. Mourey and S.M. Miller, *J. Liq. Chromatogr.*, 13 (1990) 693.
14 R. Lew, P. Cheung, S.T. Balke and T.H. Mourey, *J. Appl. Polym. Sci.*, 47 (1993) 1685.
15 P. Cheung, R. Lew, S.T. Balke and T.H. Mourey, *J. Appl. Polym. Sci.*, 47 (1993) 1701.
16 M. Guita and O. Chiantore, *J. Liq. Chromatogr.*, 16 (1993) 633.
17 S. Pang and A. Rudin, *J. Appl. Polym. Sci.*, 46 (1992) 763.
18 F. Rodriguez, *Principles of polymer systems*, McGraw-Hill, New York, 2nd ed., 1982, Ch. 6.
19 W.W. Yau, J.J. Kirkland and D.D. Bly, *Modern Size Exclusion Liquid Chromatography*, Wiley, New York, 1979, Ch. 9.
20 P. Kratochvil, *Classical Light Scattering from Polymer Solutions*, Elsevier, New York, 1987, Ch. 3.
21 M. Bohdanecky and J. Kovar, *Viscosity of Polymer Solutions*, Elsevier, New York, 1982, Ch. 2.
22 H. Benoit, Z. Grubisic, P. Rempp, D. Decker and J.G. Zilliox, *J. Chem. Phys.*, 63 (1963) 1507.
23 W.W. Yau, H.J. Stoklosa and D.D. Bly, *J. Appl. Polym. Sci.*, 21 (1977) 1911.

CHROM. 25 294

Binding characteristics of various neurochemicals to glassy carbon

Yasushi Ikarashi

Department of Neuropsychopharmacology (Tsumura), Gunma University School of Medicine, 3-39-22 Showa-machi, Maebashi, Gunma 371 (Japan)

C. LeRoy Blank*

Department of Chemistry and Biochemistry, University of Oklahoma, 620 Parrington Oval, Norman, OK 73019 (USA)

Yuji Maruyama

Department of Neuropsychopharmacology (Tsumura), Gunma University School of Medicine, 3-39-22 Showa-machi, Maebashi, Gunma 371 (Japan)

(First received May 27th, 1992; revised manuscript received April 19th, 1993)

ABSTRACT

The determination of acetylcholine and choline using liquid chromatography with electrochemical detection using the approach of Potter *et al.* [*J. Neurochem.*, 41 (1983) 188] normally requires isolation of the desired species before an analysis of tissue samples can be undertaken due to coeluting interferences afforded by other neutrochemicals. We have recently shown that this problem can be overcome by the use of a glassy carbon precolumn to effectively trap the interfering species [Ikarashi *et al.*, *J. Chromatogr.*, 575 (1992) 29]. We now report on the nature and mechanism of this adsorption onto glassy carbon for norepinephrine, dopamine, serotonin, 3,4-dihydroxyphenylacetic acid, homovanillic acid and 5-hydroxyindoleacetic acid. For both the acidic and basic compounds which comprise this group, distinct Langmuir adsorption processes appear to be involved for both the neutral and ionic forms of the individual compounds. Using various data fitting approaches, we have attempted to derive appropriate adsorption constants for the two forms of each compound. Theoretical predictions employing these derived constants provided results which match reasonably well with the observed adsorption data in most cases.

INTRODUCTION

We recently reported [1] that interfering species seen in the determination of acetylcholine and choline using liquid chromatography with electrochemical detection (LC–ED) [2–5] could be eliminated by utilization of a precolumn packed with glassy carbon particles. The precolumn selectively removed catecholamines, indoleamines and related metabolites while not adsorbing any of the quaternary amine species being analyzed. Further, the precolumn substantially decreased the solvent front peak associated with tissue homogenates. Thus, the precolumn allows direct injection of tissue homogenates, without the need for extensive isolation/purification, in the LC–ED determination of acetylcholine and choline.

Glassy carbon is a fairly well-characterized hard, char material which results from treatment of polymeric precursors at temperatures exceeding 1000°C. This material is well-known to exhibit considerable chemical inertness, a mirror-

---

* Corresponding author.

like finish, reasonable electrical conductivity, a hardness in the isotropic state, a relative impermeability to gases and liquids, an ability to withstand high temperatures in non-oxidizing atmospheres, and an ability to withstand considerable thermal shock. These characteristics of glassy carbon are generally attributed to its structure, which is fundamentally a variety of carbon ribbons forming a network of microfibrils [6,7]. Yet, little information exists concerning the mechanism of adsorption of species like the neurochemicals described onto this glassy carbon material [8].

In the current report, we examine the mechanism of adsorption onto glassy carbon particles for norepinephrine (NE), dopamine (DA), serotonin (5-HT), 3,4-dihydroxyphenylacetic acid (DOPAC), homovanillic acid (HVA) and 5-hydroxyindoleacetic acid (5-HIAA). The first three of these neurochemical species are notably basic compounds, while the latter three are acidic compounds. These fundamental acid–base properties are intimately related, as will be seen, to the adsorption characteristics of each compound.

MATERIALS AND METHODS

Reagents

The chemical reagents employed in this investigation were all obtained from commercial suppliers at the highest available purity and used without further purification. The only exception to this involves N,N-dimethyl-N-ethyl-3-amino-1-propanol, more commonly known as ethylhomocholine (EHC), which was prepared according to a previously described procedure [2,3]. The particular neurochemicals of concern were all purchased from Sigma (St. Louis, MO, USA). These included NE hydrochloride, DA hydrobromide, 5-HT creatinine sulfate monohydrate, HVA, DOPAC, 5-HIAA, acetylcholine (ACh) chloride and choline (Ch) chloride.

Glassy carbon particles

Glassy carbon particles used in these experiments were obtained from the Analytical Laboratories of IRICA Instruments (Kyoto, Japan). They are listed as IRICA type CP-2250. Physical

investigations showed that the particles were of a glass-like, vitreous, hard carbon material [1]. They had an electrical resistivity of $4.5 \cdot 10^{-3}$ Ω/cm, a specific gravity of 1.52, a thermal expansion coefficient of $2.2 \cdot 10^{-6}$, and impurities totalling less than 0.008%. The particles were irregular, with typical dimensions on the order of 70 μm [1].

LC–ED system for determination of catecholamines, indoleamines and related metabolites

The liquid chromatographic system employed for the determination of NE, DA, 5-HT and the three related acid metabolites primarily employed components from Bioanalytical Systems (BAS, West Lafayette, IN, USA). These included a PM-60 pump, a CC-4 injector, a BioPhase ODS IV (3μm, 110 × 4.6 mm) analytical column, a dual glassy carbon electrode, and an LC-4B amperometric potentiostat. Temperature in the column was maintained by an LC-22 temperature controller to be 35 ± 1°C. The potential of the working electrode was set at +0.70 V vs. the Ag/AgCl reference electrode. The mobile phase was a 0.050 M citrate buffer of pH 3.2, containing 0.80 mM sodium 1-octanesulfonate and 0.50 mM disodium EDTA. The flow-rate was typically 0.80 ml/min. Data collection and processing were accomplished with the aid of an SIC Chromatocorder from Yokogawa (Tokyo, Japan). A typical chromatogram observed for the six components of interest is shown in Fig. 1A. Retention times observed, in order of elution, were: NE, 3.1 min; DOPAC, 4.3 min; DA, 6.2 min; 5-HIAA, 7.2 min; HVA, 10.2 min; and 5-HT, 15.3 min. Detection limits were 0.3–1.0 pmol for the species of concern when operating at the usual 20 nA full scale setting.

LC–ED system for determination of ACh, EHC and Ch

The liquid chromatographic system employed for the determination of these three quaternary amines employed at LC100P pump and an LC100S injector from Yokogawa, an LC-4A amperometric detector with a dual platinum
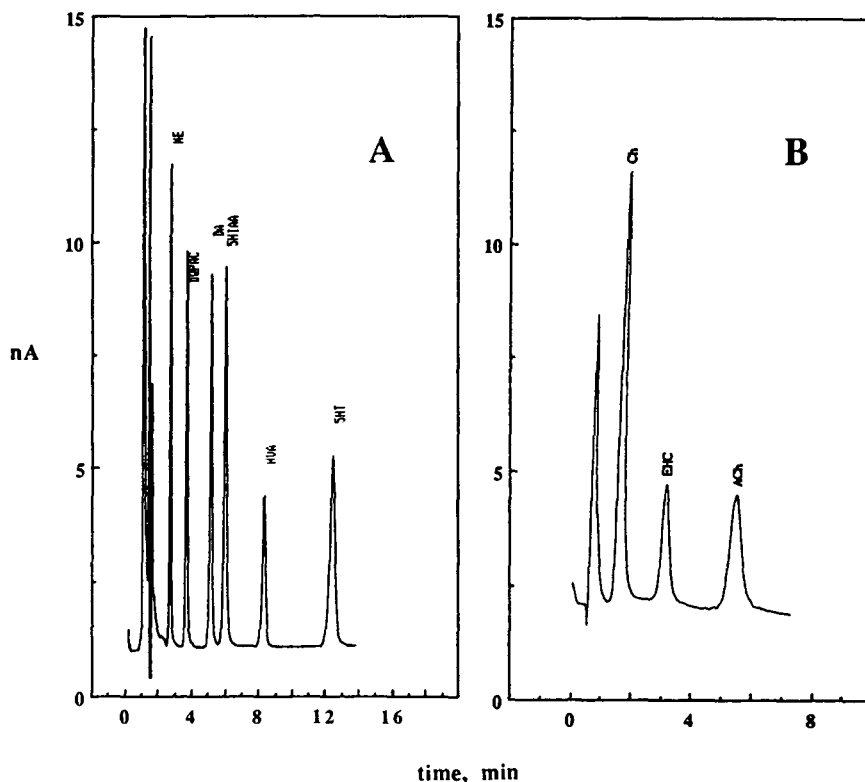
Fig. 1. Typical chromatograms obtained from mixture of (A) indoles/catechols and (b) quaternary amines. Injection of 4.0 μl of sample containing 2.00 nmol/ml of each substance identified.

working electrode from BAS, an Acetylcholine Separation analytical column (3 μm, 60 × 4 mm, polymeric styrene based packing material) from BAS, and an immobilized post-column enzyme reactor (5 × 4 mm) containing acetylcholinesterase and choline oxidase from BAS. Data collection and processing employed an LC100W/F work station from Yokogawa. The mobile phase for this system was a 0.050 M phosphate buffer, pH 8.4, containing 1.0 mM disodium EDTA and 0.40 mM sodium 1-octanesulfonate. The flow-rate was typically 0.80 ml/min, and the working electrode potential was set to 0.50 V vs. Ag/AgCl. Temperature of the column and post-column were maintained at 35 ± 1°C by a BAS Model LC-22 temperature controller. A typical chromatogram obtained for the compounds of concern is presented in Fig. 1B. Pertinent retention times, in order of elution, were: Ch, 2.2 min; EHC, 4.5 min; and ACh, 8.4 min. Detec-

tion limits were 2–5 pmol at the usual setting of 20 nA full scale.

Adsorption of neurochemicals onto glassy carbon

Three separate sets of experiments were performed to determine the binding characteristics of the neurochemicals of concern. In all three, a mixture of indoles/catechols and a mixture of quaternary amines were separately exposed to glassy carbon particles. For the indoles/catechols, each sample incorporated a pre-determined amount of glassy carbon and a 1.00-ml aliquot of 0.100 M phosphate buffer containing 2.00 nmol each of NE, DA, 5-HT, HVA, DOPAC and 5-HIAA. For the quaternary amines, each sample incorporated the glassy carbon and a 1.00-ml aliquot of 0.100 M phosphate buffer containing 2.00 nmol each of ACh, Ch and EHC. After the

described agitation, the glassy carbon particles with the adsorbed species were separated by filtration through a 0.45-μm Millipore filter, and a 4.00-μl aliquot of the filtrate was injected into the appropriate LC–ED system for quantitation. The results for each substance were compared to the LC–ED results obtained from equivalent mixtures which had not been exposed to any glassy carbon particles. This procedure yielded a percent adsorbed for each species, calculated as:

$$\% \text{ Adsorbed} = \frac{(\text{PH}_{\text{no GC}} - \text{PH}_{\text{GC}})}{\text{PH}_{\text{no GC}}} \times 100$$

where $\text{PH}_{\text{no GC}}$ = LC–ED peak height observed for the species of concern when no glassy carbon particles were included

$\quad\quad\quad \text{PH}_{\text{GC}}$ = LC–ED peak height observed for the species of concern when glassy carbon particles were included.

The fraction adsorbed, f, is simply equal to the percent adsorbed divided by 100. All results were calculated and reported as the mean ± S.D. for at least 3 separate determinations.

The first set of experiments was designed to examine the importance of the time of exposure on the amount of adsorption. In both groups associated with these experiments, a 1.00-ml pipet of the compounds, in a pH 8.40 phosphate buffer, was added to 100 mg of the glassy carbon particles. In the first group, the samples were shaken on a vortex mixer for a few (≤5) seconds prior to filtration. In the second group, the samples were shaken on a mechanical shaker for 10 min prior to filtration.

The second set of experiments was designed to determine the effect of the amount of glassy carbon on the adsorption observed. In this case, a 1.00-ml pipet of the compounds, again contained in a pH 8.40 phosphate buffer, was added to 0, 10, 20, 50, 100 or 200 mg of the glassy carbon particles. After shaking on a vortex mixer for a few (≤5) seconds, the samples were filtered, and the filtrate was subjected to LC–ED analysis.

The third set of experiments was designed to examine the effect of pH on the adsorption

process. In this case, a 1.00-ml pipet of the compounds was added to 100 mg of the glassy carbon particles, the mixture was shaken on a vortex mixer for a few (≤5) seconds, the samples were filtered, and the resultant filtrate was subjected to LC–ED analysis. The pH values employed for these experiments were 1.00, 3.00, 5.00, 7.00 and 9.00.

Calculations

Cursory examination of the data from the second and third sets of experiments indicated a Langmuir adsorption type behavior for the six indoles/catechols, while no adsorption was observed for any of the quaternary amines under any of the conditions investigated. The attempted fitting of the empirical data to simple and multiple versions of Langmuir adsorption involved two basic approaches. In the first, the non-linear least squares (NLLSQ) method of Christian and Tucker [9], based on the original strategy of Marquardt [10], was employed. In the second, a successive approximation was employed, in which sum of the squares of the deviations of the calculated values from the experimental values, Σd_i^2, was directly minimized. In both approaches, we sometimes considered only one and sometimes considered two separate adsorption processes to be concurrently active. Only the approaches which provided the final reported results are given immediately below. Alternative attempts are briefly covered in the text.

Method 1. This calculation used the non-linear least squares approach and assumed that, at the pH value of 8.40, only one adsorption process was significant for the compound under the conditions utilized. The one adsorption process involved the neutral form of the compound for the basic compounds and the ionic form of the compound for the acidic compounds. For the bases, the equation of concern, derived below, can be expressed as:

$$f = \frac{m}{C_{\text{init}}} \left(\frac{K_{\text{ads,neut}} C_{\text{neut}}^* C_{\text{neut}}}{1 + K_{\text{ads,neut}} C_{\text{neut}}} \right) \quad (1)$$

where f is the fraction of the compound adsorbed, m is the number of milligrams of carbon

used per ml of solution, $K_{ads,neut}$ (ml/nmol or μM^{-1}) is the adsorption constant for the neutral species, C^*_{neut} is the number of available adsorption sites (nmol/mg carbon), C_{neut} is the concentration of the unbound neutral species in solution (nmol/ml), and C_{init} is the initial total concentration (ionic + neutral forms) of the compound (nmol/ml). For the acids, a completely analogous equation was employed in which the terms given above for the neutral form of the compound were replaced by those representative of the ionic form of the compound.

Method 2. Having obtained values of $K_{ads,ion}$ and C^*_{ion} for the acidic species at pH 8.40 using method 1, we were able to simultaneously consider the more complex adsorption situation involving both the ionic and neutral species at lower pH values. Using the empirical data for the fraction adsorbed at pH values of 3.00 and 5.00 along with the previously derived values of $K_{ads,ion}$ and C^*_{ion} provided two equations containing two unknowns ($K_{ads,neut}$ and C^*_{neut}), which were readily solved for the latter constants. A similar approach was not successful in an attempted determination of the constants for the ionic form of the basic compounds.

Method 3. Calculation of the theoretical values for the percent adsorbed was accomplished for the acids using the derived values for $K_{ads,neut}$, C^*_{neut}, K_{ion} and C^*_{ion} and using a successive approximations technique. In this case, we started by assuming that the concentration of unbound compound, representing the sum of the neutral and ionic forms of the compound, was initially equal to the value present in the absence of any adsorbent, *i.e.*, C_{init}. In the first step, we calculated the fraction adsorbed considering only the adsorption of the ionic form and the appropriate form of the quadratic expression for f (see below); this yielded a modified value for the total concentration of unbound compound. In the second step, the modified value of the unbound compound was used with a second form of the quadratic expression considering adsorption of the neutral form of the compound only, yielding a further modified value for the unbound concentration of the compound. If the further modified value was within 0.001% of the initial value for the unbound concentration, the iteration was

considered complete; if not, the initial value was set equal to the further modified value, and the process was repeated. Since we did not determine the values of K_{ion} and C^*_{ion} for the basic compounds, this process involved only a simple and single solution of the appropriate quadratic expression.

RESULTS AND DISCUSSION

Initial experiments focused on the time required to achieve equilibration in the adsorption of various neurochemicals onto glassy carbon particles. The amount of glassy carbon employed was a constant 100 mg. This and the following set of experiments notably employed a pH 8.40 phosphate buffer as the solvent for the neurochemicals, since this solution is identical to the eluting solvent employed in the LC–ED determination of ACh and Ch using the glassy carbon precolumn [1]. The time allowed for contact between the glassy carbon particles and the solutions was either a few ($\leqslant 5$) seconds or 10 min, respectively.

The results for the indoles/catechols, as shown in Fig. 2, indicate a convenient subdivision of these species into acids (HVA, DOPAC and 5-HIAA) and bases (NE, DA and 5-HT). The bases were adsorbed in amounts exceeding 90%, while the acids showed adsorption varying between 25 and 80%. However, for each compound investigated, there was no significant difference between the results obtained for the percent adsorbed when comparing the brief shaking with a vortex mixer ($\leqslant 5$ s) to the extended shaking period of 10 min (two-tailed *t*-test, $P > 0.05$). Thus, the shorter time was used for all subsequent investigations. The comparable experiments for the quaternary amines (ACh, Ch and EHC) showed no significant adsorption onto the glassy carbon particles using either the short or long shaking times.

A second set of experiments was intended to investigate the effect of varying amounts of glassy carbon particles on the adsorption phenomena. While investigating Langmuir type adsorption phenomena as a function of adsorbent is a bit unusual (one would normally examine adsorption as a function of the solution concen-
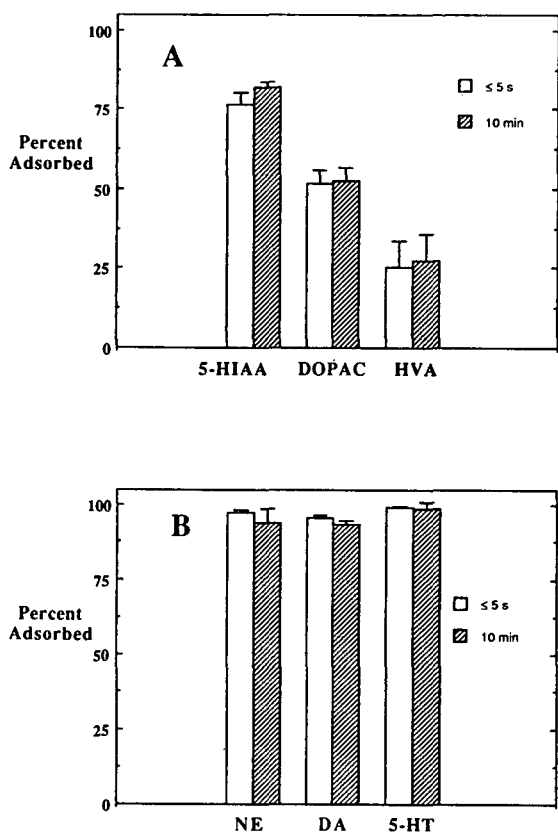
Fig. 2. Effect of adsorption time on percent adsorbed onto glassy carbon for various neurochemicals. Compounds are grouped as acids (A) and bases (B).

tration of the adsorbed species), we felt this approach was more relevant to the intended use of these materials; users of the mentioned precolumns [1] have some control over the amount of carbon employed but virtually no control over the concentration of the adsorbing species. Thus, in this second set of experiments, 1.00 ml of the test solution of indoles/catechols or quaternary amines, in a pH 8.40 phosphate buffer, was briefly shaken with 0 to 200 mg of the particles prior to filtration and analysis of the filtrate. The results, as presented in Table I, again indicate that there was no significant adsorption for the quaternary amines, even at the highest amounts of glassy carbon employed. With the indoles/catechols, the three bases (NE, DA and 5-HT) show a rapid rise in the percent adsorbed with increasing amounts of glassy carbon at small amounts of glassy carbon used, followed by an

asymptotic approach to 100% adsorbed at the higher values of glassy carbon used. The three acids (DOPAC, HVA and 5-HIAA) exhibit a more moderate rise in percent adsorbed with increasing amounts of glassy carbon at the small amounts of carbon used; the results at the higher amounts of carbon, however, indicate an eventual asymptotic approach to 100% adsorbed. Thus, for both the acids and bases at pH 8.40, we observe a Langmuir type of adsorption curve for each of the indole/catechol species involved.

In the third set of experiments, we briefly examined the effect of the pH on the adsorption process. As seen in Table II, no significant adsorption was again observed for any of the three quaternary amines at any pH value between 1.0 and 9.0. For the indoles/catechols, however, there was a marked pH dependence observed. For the bases, the largest amounts of adsorption were observed at pH 9.0, with substantially greater amounts being adsorbed at this value than the low pH values. The adsorption of the bases decreased with decreasing pH, although the decrease observed was not linear and not reminiscent of a classic pH titration curve. In the case of the acids, the percent adsorbed appears to be fairly constant for each compound in the pH range of 1.0 to 3.0; the percent adsorbed then modestly declines in the pH range of 3.0 to 7.0 and becomes relatively constant, although slightly lower, in the pH range of 7.0 to 9.0. These results for the acids are reminiscent of classic pH titration curves.

In examining the results obtained in Tables I and II, we can initially and unequivocally state that adsorption of ACh, Ch and EHC was not significant for any of the pH values or amounts of carbon investigated. This means that the glassy carbon precolumn previously described [1] will in no way impede the determination of these three targeted compounds.

However, understanding the results of Tables I and II with respect to the behavior of the indoles/catechols turned out to be somewhat more difficult. Preliminary observation of the results for, particularly, Table II indicates that there is clearly some effect(s) associated with the individual forms, neutral or ionic, of the compound of concern. For the bases, the deproto-

TABLE I

PERCENT OF COMPOUND ACTUALLY ADSORBED (AND THEORETICALLY CALCULATED) AS A FUNCTION OF THE AMOUNT OF GLASSY CARBON EMPLOYED

Each experimental value represents the mean ± S.D. derived from three determinations. See text for calculation of theoretical values.

Compound	Percent adsorbed (calculated)					
	Amount of carbon (mg)					
	0	10	20	50	100	200
NE	0.0 ± 3.3(0)	25.8 ± 0.6(17.3)	32.8 ± 1.9(34.2)	83.6 ± 0.7(76.6)	94.5 ± 0.5(95.1)	98.4 ± 0.5(98.3)
DA	0.0 ± 0.7(0)	51.6 ± 2.5(24.9)	51.9 ± 0.8(48.8)	93.7 ± 1.0(91.8)	96.9 ± 1.1(97.9)	99.2 ± 0.2(99.2)
5-HT	0.0 ± 2.7(0)	78.5 ± 0.8(65.2)	90.8 ± 1.3(93.9)	98.5 ± 0.7(98.8)	99.5 ± 0.4(99.5)	100.0 ± 0.0(99.8)
DOPAC	0.0 ± 1.6(0)	13.1 ± 1.3(7.0)	15.1 ± 0.9(13.8)	30.5 ± 1.4(32.5)	54.2 ± 1.5(56.8)	80.2 ± 0.6(80.2)
HVA	0.0 ± 2.1(0)	18.4 ± 2.7(5.1)	21.5 ± 3.2(9.8)	29.3 ± 2.9(21.3)	36.7 ± 2.2(35.1)	49.8 ± 2.3(52.0)
5-HIAA	0.0 ± 1.3(0)	18.8 ± 1.7(17.4)	23.8 ± 1.5(31.7)	60.4 ± 1.2(58.8)	78.2 ± 1.7(77.2)	88.4 ± 0.7(88.4)
ACh	0.0 ± 1.5	−0.9 ± 5.0	−3.4 ± 2.2	−0.3 ± 1.5	1.8 ± 3.5	1.2 ± 1.6
Ch	0.0 ± 1.7	−0.1 ± 1.2	−0.6 ± 1.4	1.2 ± 1.7	2.5 ± 2.2	−2.0 ± 1.2
EHC	0.0 ± 4.1	−1.0 ± 0.9	−3.3 ± 2.9	−0.7 ± 3.0	−2.0 ± 3.1	−4.0 ± 3.5

nated form appears to have a much stronger attraction for the glassy carbon than the protonated form, while for the acids, the protonated form appears to have a much stronger attraction for the glassy carbon than the deprotonated form. One could alternatively say that, in both cases, the neutral form has a stronger attraction for the glassy carbon than does the ionic form. Thus, we clearly must consider the deprotonation constants for these compounds. These

TABLE II

PERCENT OF COMPOUND ACTUALLY ADSORBED (AND THEORETICALLY CALCULATED) AS A FUNCTION OF pH EMPLOYED

Each experimental value represents the mean ± S.D. derived from three determinations. Theoretical values only calculated for the acids (see text).

Compound	Percent adsorbed (calculated)					
	pH					
	1.0	3.0	5.0	7.0	8.4	9.0
NE	6.7 ± 2.1	25.7 ± 0.9	35.9 ± 1.7	58.1 ± 1.7	94.5 ± 0.5	97.3 ± 0.6
DA	32.8 ± 1.4	56.0 ± 1.4	69.6 ± 2.0	76.1 ± 2.0	96.9 ± 1.1	98.8 ± 0.5
5-HT	95.0 ± 0.9	97.2 ± 0.5	98.3 ± 0.4	98.6 ± 0.3	99.5 ± 0.4	99.5 ± 0.2
DOPAC	90.0 ± 8.9(85.1)	84.8 ± 7.8(84.8)	69.0 ± 1.9(69.0)	49.9 ± 0.9(57.0)	54.2 ± 1.5(56.8)	44.3 ± 1.9(56.8)
HVA	82.2 ± 0.5(79.7)	79.1 ± 1.5(79.1)	55.1 ± 3.5(55.1)	28.0 ± 3.3(35.3)	36.7 ± 2.2(35.1)	26.8 ± 4.5(35.1)
5-HIAA	96.8 ± 0.4(96.8)	96.7 ± 1.0(96.7)	92.2 ± 1.8(92.2)	74.6 ± 1.7(78.3)	78.2 ± 1.7(77.2)	76.4 ± 1.9(77.2)
ACh	−4.9 ± 4.1	1.0 ± 0.9	−4.6 ± 7.5	0.6 ± 1.0	1.8 ± 3.5	3.6 ± 4.9
Ch	−2.4 ± 2.9	1.0 ± 1.6	3.3 ± 3.1	−2.8 ± 5.0	2.5 ± 2.2	−4.9 ± 4.4
EHC	−6.4 ± 6.7	1.5 ± 3.4	−5.3 ± 4.8	−8.7 ± 7.4	−2.0 ± 3.1	−5.9 ± 3.5

TABLE III

ACID DISSOCIATION CONSTANTS

For the first three compounds (NE, DA and 5-HT), the pK_a refers to deprotonation of the ammonium ion, while for the last three compounds (DOPAC, HVA, 5-HIAA), the pK_a refers to deprotonation of the neutral acid.

Compound	pK_a
NE	8.61
DA	8.88
5-HT	9.85
DOPAC	4.14
HVA	4.31
5-HIAA	4.14

constants are presented in logarithmic form in Table III. These values were all obtained from the reference work by Smith and Martell [11–13], with the exception of that for 5-HIAA. Since no pK_a value could be found for 5-HIAA, we assumed a value of 4.14 to be reasonable after examining a number of different carboxylic acids in which the acid functionality was located one methylene group away from an aromatic structure; we estimate that this pK_a value for 5-HIAA is accurate within ± 0.5, which is more than sufficient for the current discussion. For the remainder of the species, the reported pK_a values were determined at ionic strengths between 0.1 and 0.37 and at temperatures of 20–30°C, both of which are entirely appropriate to the current investigation.

Initial attempts to fit the indoles/catechols data to a Langmuirian conceptual framework considered both the neutral and ionic forms of the compound of concern. The adsorption process for the neutral species, neut or N, is given as:

$$N + A \rightleftharpoons NA \qquad (2)$$

where A represents an unoccupied adsorption site on the glassy carbon particle and NA represents an adsorption site occupied by the neutral species. The associated adsorption constant is given as

$$K_{ads,neut} = \frac{C_{NA}}{C_{neut} C_A} \qquad (3)$$

and has the units of $(nmol/ml)^{-1}$ or μM^{-1}. The total number of available adsorption sites for the neutral species, given in units of nmols per milligram of glassy carbon adsorbent, is correspondingly labeled as C^*_{neut}. Thus,

$$mC^*_{neut} = C_{NA} + C_A \qquad (4)$$

where m is the number of milligrams of carbon per ml of solution used in the experiment. The fraction adsorbed is simply

$$f = \frac{C_{NA}}{C_{init}} \qquad (5)$$

where $C_{init} = 2\ \mu M$ is the initial concentration, prior to adsorption, employed for all the compounds of concern. Rearrangement of eqns. 3–5 provides the originally presented eqn. 1, which may be directly fitted to the observed data (see below). For the determination of the C_{neut} term in eqn. 1, we define the fraction of the total amount of unbound compound which is in the neutral form as

$$g_{neut,base} = \frac{C_{neut}}{C_{neut} + C_{ion}} = \frac{1}{1 + 10^{pK_a - pH}} \qquad (6)$$

for the basic compounds investigated. Then,

$$C_{neut} = g_{neut,base} C_{unbound} \qquad (7)$$

where $C_{unbound}$ is the measured, total concentration of unbound species ($=C_{neut} + C_{ion}$).

By analogy to that given above, adsorption of the ionic form of the compound, represented as I or ion, to a second adsorption site, B, is

$$I + B \rightleftharpoons IB \qquad (8)$$

$$K_{ads,ion} = \frac{C_{IB}}{C_{ion} C_B} \qquad (9)$$

$$mC^*_{ion} = C_{IB} + C_B \qquad (10)$$

with the corresponding fractional concentrations for a basic compound being

$$g_{ion,base} = \frac{C_{ion}}{C_{neut} + C_{ion}} = \frac{1}{1 + 10^{pH - pK_a}} \qquad (11)$$

$$C_{ion} = g_{ion,base} C_{unbound} \qquad (12)$$

Consideration of simultaneous adsorption of both the neutral and ionic forms of the compound requires modification of the fraction adsorbed in eqn. 5 to

$$f = \frac{C_{NA} + C_{IB}}{C_{init}} \qquad (13)$$

Then, utilization of eqns. 3, 4, 9 and 10 leads to

$$f = \frac{m}{C_{init}} \left(\frac{K_{ads,neut}C^*_{neut}C_{neut}}{1 + K_{ads,neut}C_{neut}} + \frac{K_{ads,ion}C^*_{ion}C_{ion}}{1 + K_{ads,ion}C_{ion}} \right) \qquad (14)$$

which is a comprehensive expression for the fraction adsorbed for basic compounds incorporating both neutral and ionic adsorption sites. Eqn. 1 is simply a shortened version of this in which the right-hand expression inside the parentheses of eqn. 14, corresponding to adsorption of the ionic species, is eliminated.

Consideration of the acidic compounds likewise leads to an expression for f which is identical to eqn. 14. However, in this case, the corresponding fractional concentrations of unbound species are

$$g_{neut,acid} = \frac{C_{neut}}{C_{neut} + C_{ion}} = \frac{1}{1 + 10^{pH-pK_a}} \qquad (15)$$

and

$$g_{ion,acid} = \frac{C_{ion}}{C_{neut} + C_{ion}} = \frac{1}{1 + 10^{pK_a-pH}} \qquad (16)$$

which are employed as above with the $C_{unbound}$ to yield the values of C_{neut} and C_{ion} to be used in eqn. 14. We will return to these comprehensive results shortly.

For both the acids and the bases, one may, in an alternative approach, note that the values of C_{neut} and C_{ion} can be expressed in terms of the fraction adsorbed. For the basic compounds, these values would be given as

$$C_{neut} = g_{neut,base}C_{unbound} = g_{neut,base}(1-f)C_{init} \qquad (17)$$

and

$$C_{ion} = g_{ion,base}C_{unbound} = g_{ion,base}(1-f)C_{init} \qquad (18)$$

Utilization of these equations, along with

eqns. 3, 4, 9, 10 and 13, leads to a cubic equation in f when one considers simultaneous adsorption of both the neutral and ionic forms of the compound at two separate sites. The only other parameters appearing in this cubic expression are the two unknown K_{ads} values, the two unknown C^* values, the known pK_a value, and the pH. A comparable cubic equation also results for the acidic compounds. Since these cubic equations are intractable (see below) and since our primary focus was on the adsorption processes occurring at the pH of 8.40 [1], we also proceeded along this same general path but considered adsorption of only the prominent species at this important pH. For both the basic and acidic compounds, this results in a quadratic equation for f, the solution for which is the usual

$$f = \frac{-b \pm \sqrt{b^2 - 4ac}}{2a} \qquad (19)$$

where, for the basic compounds, focussing on the neutral form,

$$a = K_{ads,neut}C_{init}g_{neut,base} \qquad (20)$$

$$b = -(C_{init} + mC^*_{neut})(g_{neut,base}K_{ads,neut}) - 1 \qquad (21)$$

$$c = g_{neut,base}K_{ads,neut}mC^*_{neut} \qquad (22)$$

and, for the acidic compounds, focussing on the ionic form,

$$a = K_{ads,ion}C_{init}g_{ion,acid} \qquad (23)$$

$$b = -(C_{init} + mC^*_{ion})(g_{ion,acid}K_{ads,ion}) - 1 \qquad (24)$$

$$c = g_{ion,acid}K_{ads,ion}mC^*_{ion} \qquad (25)$$

Armed with theoretical frameworks to attack the data in a number of appropriate ways, we began by trying to fit all the data of Tables I and II simultaneously. Using NLLSQ or successive approximations along with the two adsorption sites outlined above yielded non-convergence for all of the six compounds attempted. The corresponding cubic equation mentioned was solved, in both of these attempts, through the use of the Newton–Gauss method. Trying either NLLSQ or successive approximations with eqn. 14 also failed to yield convergence for any of the compounds. Similar attempts were undertaken by assuming two different adsorption sites for the

neutral species and none for the ionic species; these attempts were also unsuccessful.

Having obtained unacceptable results using the comprehensive considerations of two adsorption processes simultaneously, we narrowed our efforts to the most important pH 8.40 data presented in Table I considering only the adsorption of a single form of the compound in question, the species of interest being the neutral compound for the bases and the anion for the acids. Starting with the appropriate form of the quadratic eqn. 19, the NLLSQ approach failed to converge for any of the compounds. On the other hand, the successive approximations approach did converge for all the compounds of concern. Comparing the theoretical data using the obtained constants to the actual data of Table I graphically seemed to show reasonable results for most of the compounds. However, there is no estimation of the precision with which the derived adsorption constants are known when using this approach. At this point, we moved to the single adsorption process represented by eqn. 1 for the neutral form of the bases and the corresponding equation for the anionic form of the acids. Again, restricting ourselves to the data of Table I, we were successful in obtaining convergence for all of the

compounds as well as estimates of the precision associated with the constants. Further calculations, using data for the selected pH values of 3.0 and 5.0 for the acids, yielded two equations with two unknowns (method 2) allowing the determination of both $K_{ads,neut}$ and C^*_{neut} for the three acidic compounds. Unfortunately, efforts to obtain the $K_{ads,ion}$ and C^*_{ion} values for the basic compounds did not yield satisfactory results.

The values of the derived constants are presented in Table IV. Graphical comparisons of theoretical curves obtained using these constants are shown in Fig. 3 along with the experimental points. As can be seen, the theoretical curves fit the empirical data reasonably well for all the compounds of concern, except in the case of HVA. For HVA, the fit is quite poor, and, as noted in the footnote to Table IV, we seriously doubt the reliability of the numerical constants derived for this compound. The reasonably good fit for the other five compounds shown in Fig. 3 are particularly pertinent when one considers that the primary use of the glassy carbon in the determination of ACh and Ch employs a completely comparable phosphate buffer at the identical pH of 8.40. Thus, the theoretical approach described should be useful in predicting

TABLE IV

ADSORPTION CONSTANTS AND NUMBER OF ADSORPTION SITES FOR ADSORPTION OF NEUROCHEMICALS ONTO GLASSY CARBON

Values derived from NLLSQ are presented as the converged result ± the standard error estimate. Values for the neutral form of the acids determined using method 2. N.D. = Values not determined.

Compound	Neutral form		Ionic form	
	$K_{ads,neut}$ (μM^{-1})	C^*_{neut} (nmol/mg)	$K_{ads,ion}$ (μM^{-1})	C^*_{ion} (nmol/mg)
NE	29.0 ± 6.0	0.036 ± 0.005	N.D.	N.D.
DA	59.0 ± 10.0	0.052 ± 0.007	N.D.	N.D.
5-HT	466.0 ± 138.0	0.14 ± 0.03	N.D.	N.D.
DOPAC	0.093	0.63	2.13 ± 0.53	0.0175 ± 0.0024
HVA	0.74^a	0.069^a	^{a}	^{a}
5-HIAA	59.0	0.024	0.66 ± 0.16	0.066 ± 0.014

[a] The values obtained for HVA are highly questionable and considered generally unreliable, since the standard error estimates resulting from the NLLSQ fitting are 5–6 orders of magnitude greater than the values. The values obtained were: $K_{ads,ion} = 1.6 \cdot 10^{-5} \pm 0.79$ and $C^*_{ion} = 334 \pm 1.6 \cdot 10^7$.
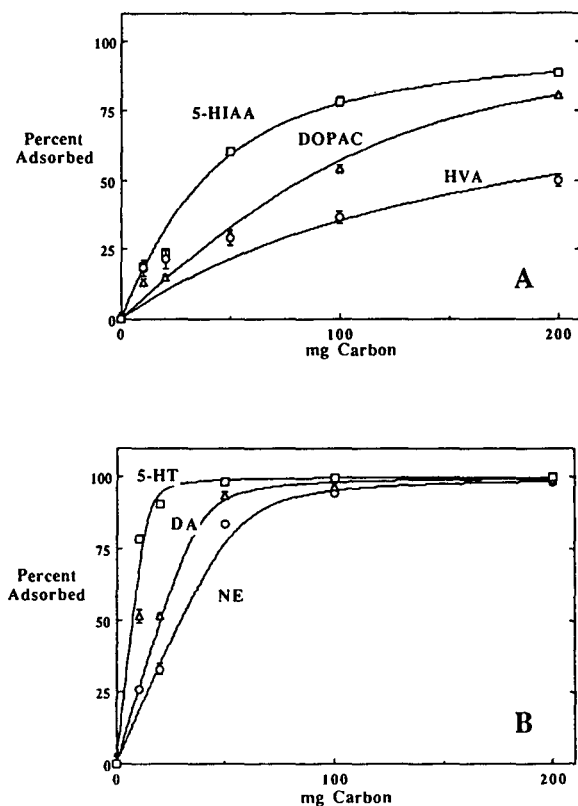
Fig. 3. Effect of amount of glassy carbon on percent adsorbed for various neurochemicals. The theoretical lines shown were derived using the constants listed in Table IV. For the bases (B), quadratic eqn. 19 was used for the theoretical curve, while for the acids (A) method 3 described in the text was employed. Empirical values are shown as mean ± S.D. for NE (○), DA (△), 5-HT (□), HVA (○), DOPAC (△) and 5-HIAA (□).

the adsorption behaviour of the six indoles/ catechols and the useful lifetime of glassy carbon precolumns in such applications.

As an example of the use of adsorption constants derived in connection with Fig. 3, one might make a crude approximation of the capacity of a precolumn packed with 1 g of such carbon materials in the determination of ACh and Ch in whole mouse brains. A typical whole mouse brain weighs ca. 0.5 g and contains approximately 1.5 nmol NE, 3.0 nmol DA, 2.5 nmol 5-HT, 1.5 nmol 5-HIAA, 0.5 nmol HVA and 0.5 nmol DOPAC. Simply considering the C^* values to represent the maximal capacity of the 1-g carbon column for each of these compounds yields

individual capacities of 36 nmol NE, 52 nmol DA, 140 nmol 5-HT, 18 nmol DOPAC, >1000 nmol HVA and 66 nmol of 5-HIAA. We can further reasonably assume that each whole mouse brain is homogenized in 1.0 ml of solution, and the normal injection volume is 5 μl per sample. Then, the precolumn thus considered would have a capacity for ca. 3500 injections with the first predicted break-through occurring for DA. Of course, this is an overly optimistic estimation of the column lifetime, since it ignores adsorption equilibrium with the moving mobile phase.

For the remaining pH data, a theoretical curve (calculated with method 3) is shown along with the experimental data for each of the three acids in Fig. 4A, while a graphical presentation of the empirical data only for the bases is given for reference in Fig. 4B. As can be seen, the data for the acids is moderately well described by the four adsorption related constants form Table IV. In the case of the bases, however, the adsorption observed as a function of pH is even more complex. Simple consideration of two adsorption processes for the bases, independent of the values of the constants involved, would lead to an S-shaped theoretical curve similar to an acid/ base titration of pH vs. ml. Indeed, the empirical data of Fig. 4B seems to indicate some of this character, with strong adsorption of the neutral species at pH values of 9.0, and, after the percent adsorbed drops off as the pH is lowered, the three bases each seem to indicate the beginnings of an expected leveling associated with the predominance of the cationic species at a pH value of approximately 5.0. But, as the pH falls below 5.0 toward 1.0, the adsorption for each of the three compounds falls substantially instead of remaining level in this range. This deviation at pH values below 5.0, seen with the bases only, is ascribed to probable surface structural features of the glassy carbon and/or simple competitive displacement. It is likely that the glassy carbon contains adsorption sites for the protonated forms of the bases which consist of oxidized forms of carbon [14–17]. Such oxygenated forms of carbon would include aldehyde, ketone, quinone, or carboxylic functionalities which could exhibit protonation at lower pH leading to less
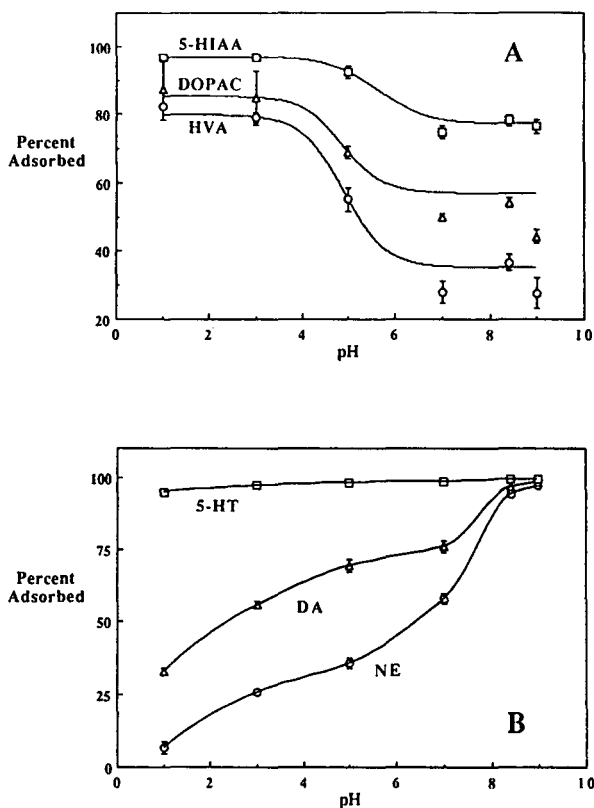
Fig. 4. Effect of pH on percent adsorbed for various neuro-chemicals. The theoretical lines shown for the acids (A) were derived using the constants listed in Table IV and calculation method 3 The empirical results are simply connected for the bases (B); no theoretical fit was obtained for the three basic compounds. Empirical values are shown as mean ± S.D. for NE (O), DA (△), 5-HT (□), HVA (O), DOPAC (△) and 5-HIAA (□).

phenomena which were not further investigated. But, the adsorption data for the acids at low and high pH and the data for the bases at high pH are at least adequately explained by the approach given. While there is almost certainly competition between the neurochemicals investigated for adsorption sites, this concept notably did not need to be invoked to fit the data. Finally, while most of the efforts in this paper were concerned with determination of the binding characteristics of the indoles/catechols, it should be emphasized that no adsorption of the quaternary amines onto the glassy carbon occurred under any of the conditions examined. Thus, the glassy carbon material is entirely appropriate to be used as a precolumn in the determination of acetylcholine and choline.

ACKNOWLEDGEMENTS

adsorption of the protonated amines. But, perhaps a more feasible explanation simply concerns competition for the cationic binding sites by the increasing concentration of H^+ ions which exists at lower pH [16,17]. In any case, this low pH adsorption phenomena for the basic compounds was not pursued any further.

In short, however, the Langmuir adsorption framework incorporating consideration of separate adsorption of both the neutral and ionic forms of the indoles/catechols provides a reasonable theoretical approach by which the adsorption of these species onto glassy carbon may be understood. The low pH data for the bases indicate the existence of one or more adsorption

REFERENCES

1 Y. Ikarashi, H. Iwatsuki, C.L. Blank and Y. Maruyama, J. Chromatogr., 575 (1992) 29.
2 P.E. Potter, J.L. Meek and N.H. Neff, J. Neurochem., 41 (1983) 188.
3 C. Eva, M. Hadjiconstantou, N.H. Neff and J.L. Meek, Anal. Biochem., 143 (1984) 320.
4 Y. Ikarashi, T. Sasahara and Y. Maruyama, J. Chromatogr., 322 (1985) 191.
5 H. Parvez, M. Bastart-Malsot, S. Parvez, T. Nagatsu and G. Carpenter, Electrochemical Detection in Medicine and Chemistry, VNU Science Press, Utrecht, Netherlands, 1987.
6 S. Yamada, A Review of Glass-Like Carbons, Defense Ceramic Center, Battelle Memorial Institute, Columbus, OH, 1968.

7 G.M. Jenkins and K. Kawamura, *Polymeric Carbons*, Cambridge University Press, London, 1976.

8 H. Jaegfeldt, T. Kuwana and G. Johansson, *J. Am. Chem. Soc.*, 105 (1983) 1805.

9 S.D. Christian and E.E. Tucker, *Am. Lab.*, 14 (1982) 31.

10 D.W. Marquardt, *J. Soc. Ind. Appl. Math.*, 11 (1963) 431.

11 R.M. Smith and A.E. Martell, *Critical Stability Constants, Vol. 2: Amines*, Plenum Press, New York, 1975, p. 142.

12 A.E. Martell and R.M. Smith, *Critical Stability Constants, Vol. 5: First Supplement*, Plenum Press, New York, 1982, pp. 347, 448.

13 R.M. Smith and A.E. Martell, *Critical Stability Constants, Vol. 6: Second Supplement*, Plenum Press, New York, 1989, p. 171.

14 R.J. Rice, N.M. Pontikas and R.L. McCreery, *J. Am. Chem. Soc.*, 112 (1990) 4617.

15 G.E. Cabaniss, A.A. Diamantis, W.R. Murphy, Jr., R.W. Linton and T.J. Meyer, *J. Am. Chem. Soc.*, 107 (1985) 1845.

16 T. Nagaoka and T. Yoshino, *Anal. Chem.*, 58 (1986) 1037.

17 T. Nagaoka, T. Fukunaga, T. Yoshino, I. Watanabe, T. Nakayama and S. Okazaki, *Anal. Chem.*, 60 (1988) 2766.

Some aspects of the enantiorecognition of derivatized primary amines on a Pirkle-type chiral stationary phase utilizing tocainide and mexiletine as model compounds

D. Uzunov and G. Stoev*

Institute of Organic Chemistry with Centre of Phytochemistry, Bulgarian Academy of Sciences, Sofia 1113 (Bulgaria)

ABSTRACT

The principles of chiral recognition responsible for the operation of the Pirkle (*R*)-N-(3,5-dinitrobenzoyl)phenylglycine chiral stationary phase (CSP) were employed for generating complementary functionality by achiral derivatization of chiral amines. The model amines chosen were tocainide and mexiletine considering their common structural features. The chromatographic behaviour of four types of derivatives was studied on the covalent and ionic versions of the CSP. Chiral discrimination mechanisms are proposed to expain the results obtained and to account for the observed elution orders.

INTRODUCTION

Since the preparation and evaluation of the Pirkle chiral stationary phase (CSP) based on the immobilization of (*R*)-N-(3,5-dinitrobenzoyl)-phenylglycine (DNBPG) on aminopropyl functionalized silica [1], this unique CSP has received considerable attention in terms of its areas of applications and principles of operation [2].

The relative contributions to the chiral recognition mechanism(s) of donor-acceptor interactions, dipole stacking of amide dipoles, hydrogen bonding and steric repulsive forces arising between the CSP and the chiral solute have been discussed by many workers. Interesting research has been carried out on the role of the amide group in the formation of the diastereomeric complexes between the CSP and the solute's antipodes [3–12]. Dipole stacking and hydrogen

bonding of amides together with the $\pi-\pi$ donor–acceptor interactions have been considered as being the major associative interactions responsible for the formation of the diastereomeric adsorbates [9]. The successful operation of the CSP is a result of the joint action of groups of factors, one of which in some specific instances could attain a predominant position over the others, whereas in other instances they would contribute equally to the overall performance of the CSP.

A good understanding of what kinds of interactions are necessary for chiral recognition on this Pirkle-type CSP is essential in the derivatization of a chiral molecule to introduce functionalities complementary to those which the CSP utilizes for its operation. Derivatization is carried out with chiral or achiral reagents. The latter may serve to block polar functional groups that cause excessive band broadening or to introduce groups that interact favourably with the CSP [3]. Chiral derivatizing agents (CDA) suffer several drawbacks, such as different reaction rates of the analyte's enantiomers with the CDA, the fact

---

* Corresponding author. Present address; National Doping Laboratory, 1 N. Gabrovski Street, Diana-2, 1172 Sofia, Bulgaria.

that the CDA could be contaminated with its antipode and racemization.

Generally, primary chiral amines require derivatization prior to chromatography on a DNBPG CSP because the highly polar amine functionality gives rise to superfluous achiral interactions with the CSP [13]. Amines can undergo reactions with various achiral acylating agents to produce amides (–NHCO– group). Ureas and thioureas are provided easily by isocyanates and thioisocyanates, respectively, creating a urea (–NHCONH–) linkage. Hence, by modifying a chiral amine first with an acylating agent and then with the corresponding isocyanate (bearing the same alkyl or aryl substituent), one could visualize the effec of the additional –NH– group of the urea on the chiral recognition mechanism.

The aim of this study was to elucidate some principles for the modification of chiral compounds bearing an amine group on their stereogenic centre and possessing a π-basic aromatic moiety not linked to the latter. The purpose of this modification is to enhance the selectivity of the DNBPG CSP towards the chiral analyte and to provide resolvable derivatives.

As model compounds we chose the antiarrhythmic agents tocainide (Toc) and mexiletine (Mex) (Fig. 1). They both possess an amine group on the stereogenic centre and have a xylyl moiety exhibiting π-basic properties. Considering the structural difference between Toc and Mex, we could assess the role of the amide group on the chiral recognition mechanism by reacting the model analytes with the same derivatizing agent. Gal *et al.* [14] have reported on the resulation of Toc and Mex ($R = 1.5$) via derivatization with homochiral derivatizing agents (thioisocyanates) on a reversed-phase column. Another RP-HPLC method of separating and determining Toc enantiomers employs an α-1
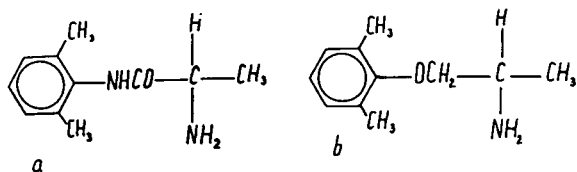
acid glycoprotein CSP [15]. Derivatization of Mex with an achiral acylating agent, 2-naphthoyl chloride, and subsequent separation on ionic DNDPG CSP has been reported by McErlane *et al.* [16].

EXPERIMENTAL

Column preparation

Two laboratory-made columns (250 mm × 4.5 mm I.D.) were employed: (1) DNBPG covalently bound to aminopropyl silica, 5 μm (CSP I) and (2) DNBPG ionically bound to aminopropyl silica, 5 μm (CSP 2).

The silica, silanized with γ-aminopropyltriethoxysilane, and the chiral selector (DNBPG) were synthesized according to Pirkle *et al.* [1]. CSP 1 was prepared and filled in the column as described [1] and CPS 2 was generated *in situ* by the procedure of Pirkle *et al.* [17].

Derivatives

The 3,5-dinitrophenyl urea derivatives were prepared starting from 3,5-dinitrobenzoyl chloride according to Pirkle *et al.* [18]. The other ureas were synthesized by mixing 2 mg of the free base with a 5 molar excess of the corresponding isocyanate in 1 ml of dry acetonitrile. After shaking vigorously for 5 min, the reaction mixture was allowed to stand for 30 min at room temperature, then 10-μl aliquots of the sample were injected on to the column immediately after filtration and dilution with acetonitrile. The same procedure was carried out in pyridine. After the reaction had taken place, the mixture was evaporated to dryness and the residue was taken up in chloroform and again evaporated to dryness. After dissolving the derivative in 2 ml of acetonitrile, 10-μl aliquots were analysed after filtration.

The 3,5-dinitrobenzoyl derivatives of Toc and Mex were prepared by the action of a 2 molar excess of the reagent on the respective free base in dry acetonitrile. The reaction mixture was stirred for 1 h at room temperature. All derivatization reactions were controlled by thin-layer chromatography [mobile phase toluene–ethanol–acetonitrile (7:2:1), silica gel plate; Merck, Darmstadt, Germany]. Elution orders were es-

Fig. 1. Structures of the model compounds: (a) tocainide; (b) mexiletine.

tablished by injecting an excess of one of the enantiomer derivatives.

All derivatives, unless specified otherwise, were analysed using a mobile phase consisting of 2-propanol–n-hexane (5:95). Fig. 2 shows the structures of the derivatives prepared and their abbreviations.

Equipment

A Perkin-Elmer (Norwalk, CT, USA) Series 2 liquid chromatograph with a Rheodyne Model 7105 injector and an LC-75 UV detector operating at 254 nm were used.

Reagents and materials

All solvents were of analytical-reagent or HPLC grade (Merck). The mobile phase was degassed and filtered through a 0.5 μm Millipore membrane filter. Triethylamine and pyridine of purities over 99% were supplied by Merck.

The derivatizing agents 3,5-dinitrobenzoyl chloride, 1-naphthyl isocyanate and methyl isocyanate (Fluka, Buchs, Switzerland) were of

Fig. 2. Structures of the 3,5-dinitrobenzoyl (DNB), 3,5-dinitrophenylurea (DNPU), 1-naphthylurea (NU) and methylurea (MU) derivatives.

purities better than 99%. The silica gel Nucleosil 100-5 was obtained from Macherey–Nagel (Düren, Germany). 3–Aminopropyltriethoxysilane (99%) was purchased from Janssen Chimica (Beerse, Belgium).

(±)-, (−)- and (+)-Mex and (±)-, (−)- and (+)-Toc were kindly donated by Boehringer (Ingelheim, Germany) and Astra Hässle (Mölndal, Sweden), respectively.

RESULTS AND DISCUSSION

The results of the initial testing of the two columns for efficiency (number of theoretical plates, N) and enantiocelectivity (α) are given in Table I. We used substance with 1 to compare the efficiencies of the two CSPs, because it was similar to the derivatives of Tox and Mex. Using substance 2 we wanted to see the influence of the silonol groups. The ionic column provides a resolution R twice as large as that given by the covalent column because the efficiency of the former is higher. Taking into account their application for enantioseparation, howerer, we could qualify them as comparable because the values of the selectivity are similar. Considering the reported resolution of the enantiomers of Mex as their 2-naphthoyl derivatives on an ionic DNBPG CSP [16], we decided to prepare a derivative possessing a urea (–NHCONH–) functionality (Table II). Thus, an additional amido group was introduced (as compared with the amide bond).

Whereas no resolution was observed for the 1-naphthylurea derivative of Toc, the corresponding Mex derivative was resolved. As indicated in Table II, the covalent CSP provides a greater enantiomeric separation than the ionic CSP of the 3,5-dinitrobenzoyl derivative of Toc. This is seen also on the chromatograms in Fig. 3.

It is of interest to elucidate the mechanism underlying this different operation of the two CSPs. Despite its higher efficiency, the ionic column affords $R = 1.15$ for DNB-Toc whereas on the covalent CSP $R = 3.42$, because of the greater selectivity. The chiral recognition mechanism that we suggest is shown in Fig. 4. Three simultaneous interactions take place: an interaction between the π-basic 2,6-dimethylphenyl
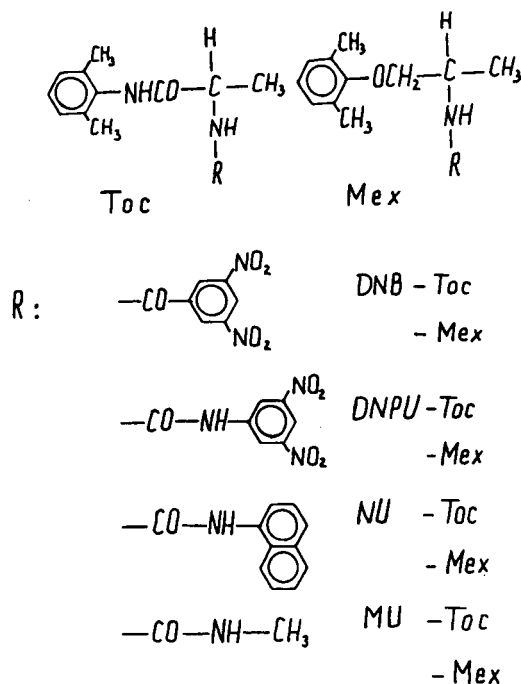
TABLE I

EFFICIENCY AND ENANTIOSELECTIVITY OF THE COVALENT AND IONIC DNBPG COLUMNS

Test compound	Type[a]	$k'^{[b]}$	α	R	$N^{[c]}$
(1) CH$_3$CO–D,L-alanine- β-naphthylamine	C	8.6	1.52	4.32	5900
CH$_3$CHCONHC$_{10}$N$_8$ | HNCOCH$_3$	I	5.3	1.60	6.23	10 800
(2) 2,2,2-Trifluoro-9- anthrylethanol	C	3.1	1.40	2.71	12 000
HOCHC$_{14}$H$_9$ | CF$_3$	I	5.0	1.44	5.35	19 000

[a] C = Covalent column; I = ionic column.
[b] Capacity factor of the more retained enantiomer.
[c] Number of theoretical plates.

moiety of the derivative and the CSP's π-acidic 3,5-dinitrobenzoyl group; a "head-to-tail" amide dipole stacking between the analyte's amide bonded to the 2,6-dimethylphenyl group and the amide dipole of the 3,5-dinitrobenzoyl moiety; and a "head-to-tail" alignment of the amide group introduced by the derivatization with the amide linkage of the chiral selector to the silica support. The latter interaction does not take place on the ionic CSP. The enantiodifferentiation is achieved by the spatial position of the methyl group on the stereogenic centre of the derivative. The S-configuration offers an orientation of the methyl group such that it remains in

TABLE II

CHROMATOGRAPHIC BEHAVIOUR OF THE STUDIED DERIVATIVES OF TOCAINIDE AND MEXILETINE

Derivative[a]	Type[b]	Tocainide					Mexiletine				
		$k'^{[c]}_1$	$k'^{[d]}_2$	$\alpha^{[e]}$	$R^{[f]}$	Elution order	$k'^{[c]}_1$	$k'^{[d]}_2$	$\alpha^{[e]}$	$R^{[f]}$	Elution order
DNB	C	8.4	11.0	1.31	3.42	R, S	6.6				
	I	7.8	8.5	1.06	1.15	R, S	8.2				
DNBU	C	7.4					7.2				
	I	7.0					6.3				
MU	C	9.4	11.6	1.23	2.88	R, S	7.0				
	I	8.2	11.5	1.02	1.11	R, S	8.2				
NU	C	9.5					11.0	12.2	1.15	1.05	R, S
	I	8.6					12.0	13.2	1.15	1.05	R, S

[a] For derivative abbreviations, see caption to Fig. 2.
[b] C = Covalent chiral stationary phase; I = ionic chiral stationary phase.
[c] k'_1 = Capacity factor of the first-eluted enantiomer in case of chiral recognition. If no resolution occurs, $k'_1 = k'$, where k' = capacity factor of racemic analyte; $k = (t_R - t_0)/t_0$, t_R = retention time of the solute, t_0 = retention time of a non-retained solute.
[d] k'_2 = Capacity factor of the more retained enantiomer.
[e] α = Enantioseparation factor (selectivity).
[f] Resolution factor, $R = 2\Delta t/w_1 + w_2$, where w = peak width at peak half-height.
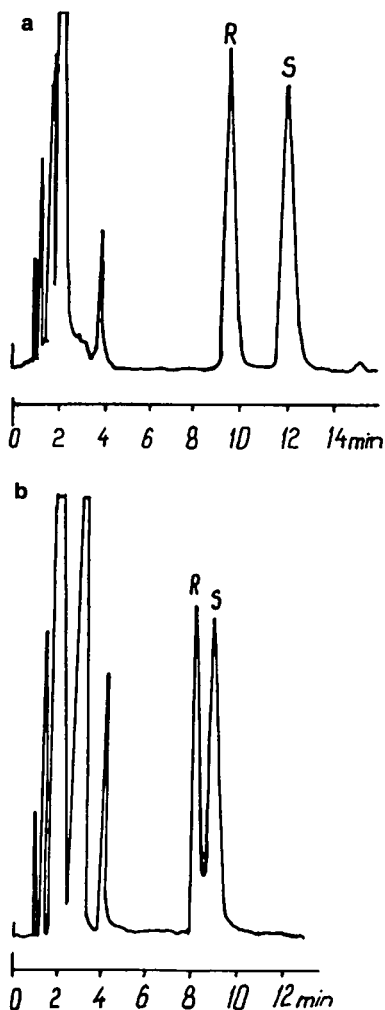
Fig. 3. Chromatograms of the 3,5-dinitrobenzoyl derivative of tocainide obtained on (a) the covalent column and (b) the ionic column. Mobile phase, 2-propanol–n-hexane (5:95); detection wavelength, 254 nm; temperature, 25°C; flow-rate, 2 ml/min.

Fig. 4. Proposed chiral recognition mechanism of the 3,5-dinitrobenzoyl derivative of tocainide on the covalent DNBPG CSP.

the plane of the neighbouring carbonyl group, thus not causing any steric interference with the CSP's interaction face. The R-enantiomer has its methyl group positioned towards the "free" face of the CSP and the phenyl ring of the chiral selector. Hence the corresponding diastereomeric complex is not as stable as that formed by the S-antipode.

The contribution of the "head-to-tail" stacking of amide dipoles to the separation of the enantiomers of DNB-Toc is demonstrated by the lack of resolution of DNB-Mex. The only differ-

ence between the DNB derivatives of Toc and Mex is one amide (–NHCO–) functionality.

The proposed interaction mechanism between the 1-naphthylurea (NU) derivative of Toc and the covalent CSP is presented in Fig. 5. No separation occurs with the 1-naphthylurea (NU)
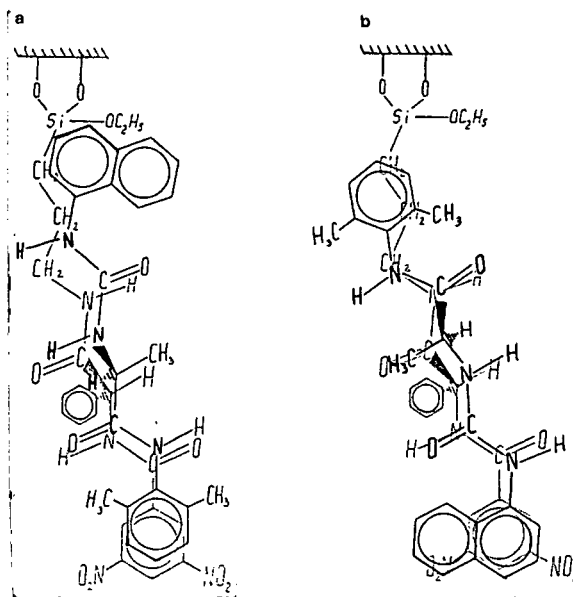
Fig. 5. Proposed solute–CSP interaction mechanism of tocainide 1-naphthylurea on the covalent DNBPG CSP.

derivative of Toc despite the presence of such a valuable site to chiral recognition as the naphthylurea moiety.

We suggest the existence of two solute–CSP interaction mechanisms, both being unable to resolve the analyte. The urea's additional amido group (Fig. 5a) moves the naphthyl moiety, intercalated between neighbouring strands of the bonded phase, further towards the silica support. This bulky aromatic system tends to interfere with the connecting aminopropyl arm, thus displacing the analyte's molecule from the interaction sites. As a result, the seemingly more stable diastereomeric complex cannot be formed, as the corresponding enantiomer is pushed "downwards'. The other possible mechanism of chiral recognition is shown in Fig. 5b. It is most unlikely, however, that this mechanism is responsible for any chiral recognition, as the additional amido group of the urea functionality displaces the chiral centres from their former position (Fig. 5a), and it turns out that the configuration about the stereogenic centre of the analyte has little or no effect on the stability of the represented associative interactions.

Support for the role of the naphthyl moiety in destroying the diastereomeric complex in Fig. 5a is provided by the observed chiral resolution when the aromatic moiety is replaced with a methyl group. This is achieved by derivatizing Toc with methyl isocyanate (Fig. 6). We advance the same chiral recognition mechanism as the interaction mechanism depicted in Fig. 5a, with the only difference that a methyl group has replaced the bulky naphthyl system. The proposed chiral discrimination mechanism is consistent with the observed elution order. Again, the results obtained with the covalent column are superior to those with the ionic version. The same explanation could be put forward as for DNB-Toc.

By comparing the chromatographic behaviour of the 3,5-dinitrophenylurea derivative of Toc with that of the 3,5-dinitrobenzoyl derivative we could assess the role in chiral recognition of the additional amido group introduced by the urea linkage when the initial isocyanate bears a bulky aromatic substituent. This role is simply mechanistic, because owing to the amido group the
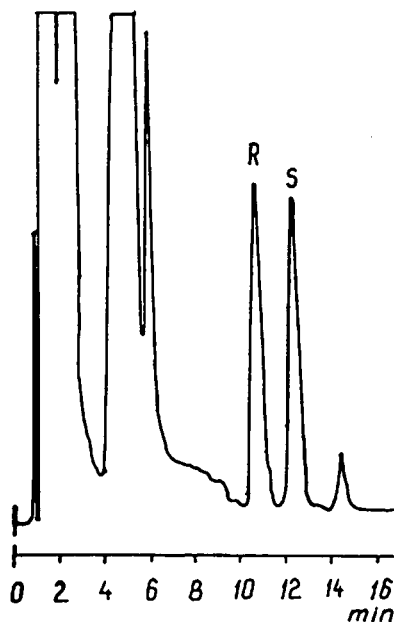
Fig. 6. Separation of the enantiomers of the methylurea derivative of tocainide on the covalent column. Experimental conditions as in Fig. 3.

aromatic moiety is moved "a step" further to the surface of the silica support.

The corresponding urea derivate of Mex (DNPU-Mex) affords a measure of the valuable contribution to chiral recognition of the "head-to-tail" amide dipole stacking between the chiral
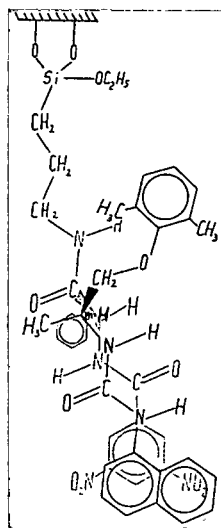
Fig. 7. Proposed chiral recognition mechanism of mexiletine 1-naphthylurea on the covalent DNBG CSP.

analyte and the CSP. The presence of an O-methylene linkage instead of an amide functionality in the molecule of DNPU-Mex is responsible for the lack of resolution. The 1-naphthylurea derivative of Mex is being resolved, however, with an enantiomeric separation of 1.15. Actually this is the only derivative of Mex to be resolved in this study. Obviously, this is due to the presence of a π-basic moiety introduced through the derivatization with 1-naphthyl isocyanate (Fig. 7). We assume that in order for the enantiomeric species to be differentiated by the CSP, their chiral centres should be in close proximity to each other. In this way the spatial arrangement about the analyte's stereogenic centre would give rise to a sterically dependent destabilization of one of the diastereomeric solute–CSP complexes. This enantiodifferentiating role is played by the methyl group on the asymmetric chiral carbon of the derivative. On carrying out the separation at 0°C, no change in the elution order of NU-Mex enantiomers was observed. This means that the π–π interaction is a more important factor than the conformational mobility of the moieties with regard to the stabilization of the complex.

Finally, we present a rapid method for the separation of the enantiomers of Toc derivatized with 3,5-dinitrobenzoyl chloride. With a mobile phase consisting of 2-propanol–ethanol–*n*-hexane (10:3:87) we achieved a selectivity $\alpha = 1.21$ and a resolution $R = 1.00$ in less than 3 min on the covalent column. An eluent of 2-propanol–*n*-hexane (10:90) with no addition of ethanol afforded on the same column a better resolution ($R = 2.44$) and a greater selectivity ($\alpha = 1.30$) The analysis time was 6 min.

CONCLUSIONS

We propose that the additional amide functionality introduced in the molecule of tocainide by achiral derivatization is capable of becoming involved in a "head-to-tail" dipole-dipole stacking with the covalent amide linkage between the DNBPG chiral selector and the silica support. This interaction has proved to be of significant

value in the chiral recognition process. The additional amide bond can be generated by the action of an acylating agent or an isocyanate. The achiral derivatizing agent employed for this purpose should not possess a bulky substituent, as it would otherwise sterically interfere with the underlying support, resulting in loss of resolution.

Chiral compounds resembling mexiletine in structure require the introduction of a π-base along with the necessary amide functionality. This aromatic moiety is expected to interact with the π-acidic 3,5-dinitrobenzoyl moiety of the CSP.

REFERENCES

1 W.H. Pirkle, D.W. House and J.M. Finn, *J. Chromatogr.*, 192 (1980) 143.
2 W.H. Pirkle, and T.C. Pochapsky, *Chem. Rev.*, 89 (1989) 347.
3 W.J. Lough (Editor), *Chiral Liquid Chromatography*, Blackie, Glasgow and London, printed by Chapman and Hall, New York, 1989. p. 39
4 I.W. Wainer and T.D. Doyle, *J. Chromatogr.*, 284 (1984) 117.
5 I.W. Wainer and M.C. Alembik, *J. Chromatogr.*, 367 (1986) 59.
6 I.W. Wainer, T.D. Doyle, F.S. Fry and Z. Hamidzadeh, *J. Chromatogr.*, 355 (1986) 149.
7 D.M. McDaniel and B.G. Snider, *J. Chromatogr.*, 404 (1987) 123.
8 D.A. Nicoll-Griffith, *J. Chromatogr.*, 402 (1987) 179.
9 W.H. Pirkle and C.J. Welch, *J. Org. Chem.*, 49 (1984) 138.
10 W.H. Pirkle and J.E. McCune, *J. Chromatogr.*, 469 (1989) 67.
11 W.H. Pirkle, *Tetrahedron Lett.*, 24 (1983) 5707.
12 A. Dobashi and S. Hara, *Tetrahedron Lett.*, 12 (1983) 1509.
13 W.H. Pirkle and C.J. Welch, *J. Chromatogr.*, 589 (1992) 45.
14 J. Gal, D.M. Desai and S. Meyer-Lehnert, *Chirality*, 2 (1990) 43.
15 S.R. Wirebaugh and D.R. Geraets, *J. Liq. Chromatogr.*, 415 (1987) 335.
16 K.M. McErlane, L. Igwemezie and C.R. Kerr, *J. Chromatogr.*, 415 (1987) 335.
17 W.H. Pirkle, J.M. Finn, B.C. Hamper and J.L. Schreiner, *J. Am. Chem. Soc.*, 103 (1981) 3964.
18 W.H. Pirkle, G. Mahler and M.H. Hyun, *J. Liq. Chromatogr.*, 9 (1986) 443.

Characterization of the binding and chiral separation of D- and L-tryptophan on a high-performance immobilized human serum albumin column

Ju Yang[☆] and David S. Hage[*]

Department of Chemistry, University of Nebraska–Lincoln, 738 Hamilton Hall, Lincoln, NE 68588-0304 (USA)

ABSTRACT

High-performance affinity chromatography was used to study the separation and binding of D- and L-tryptophan on an immobilized human serum albumin (HSA) column. Frontal analysis and zonal elution studies indicated that both D- and L-tryptophan were binding to single but distinct sites on HSA. L-Tryptophan bound to the indole site of HSA. D-Tryptophan had indirect interactions with the warfarin site of HSA but no interactions with the indole site. The association constants for the binding of D- and L-tryptophan at pH 7.4 and 25°C were $0.4 \cdot 10^4$ and $2.7 \cdot 10^4 \, M^{-1}$, respectively. The value of ΔG for these sites ranged from −5.2 to −5.7 kcal/mol (1 cal = 4.184 J) and had a significant entropy component. The effects of varying the pH, phosphate concentration, temperature and polarity of the mobile phase on the binding of D- and L-tryptophan to HSA were examined. The role of sample size in determining peak shape and retention was also considered. From these data, general guidelines were developed for the separation of D- and L-tryptophan on immobilized HSA. Under optimized conditions the enantiomers were separated in less than 2 min with baseline resolution.

INTRODUCTION

The separation of chiral molecules is an area of increasing importance in pharmaceutical and biochemical testing. However, this also represents one of the most difficult challenges in separation science. To meet this challenge, a number of techniques have been developed for the analysis and purification of chiral compounds. Examples include liquid chromatographic methods based on chiral derivatives, complexing agents, ion-pairing agents, and chemically bonded chiral stationary phases [1]. This study will examine the use of high-performance affinity columns using immobilized human serum albumin for the separation of D- and L-tryptophan.

Human serum albumin (HSA) is the most abundant protein in blood [2]. HSA is useful as an affinity ligand since it is known to bind to a variety of biological and pharmaceutical compounds [3]. It is believed that this binding occurs at a number of relatively well-defined sites or regions on HSA. The two most important of these regions are the warfarin–azapropazone and indole–benzodiazepine binding sites [4–6]. These two sites are believed to be involved in the interactions of most compounds with HSA [7]. As its name suggests, the warfarin site is characterized by its binding to warfarin and related substances [4,8–10]. This site is known to show stereoselectivity in binding such compounds as *R*- and *S*-warfarin or *R*- and *S*-phenprocoumon [11]. The indole site binds to a number of indole-

---

* Corresponding author.
[☆] Present address: Analytical Service Division, Harris Laboratories, 624 Peach Street, P.O. Box 80837, Lincoln, NE 68501, USA.

containing compounds, including L-tryptophan [12,13]. Binding at this site is highly specific and can also be stereoselective in nature [11,14].

L-Tryptophan is one of the essential amino acids and is used as a pharmaceutical antidepressant agent [15]. D-Tryptophan has no known significant biological effects [16,17] but can appear as a contaminant in L-tryptophan samples. In view of recent US Food and Drug Administration (FDA) guidelines regarding chiral drugs [18], this makes the determination of D- and L-tryptophan in pharmaceuticals an area of great potential importance. One way of separating and analyzing D- and L-tryptophan is through the use of immobilized albumin columns [19]. However, baseline resolution of tryptophan enantiomers in a reasonable amount of time (*i.e.*, less than 10 min) has not yet been achieved by this approach.

The aim of this work is to obtain a better understanding of how D- and L-tryptophan bind to immobilized HSA, allowing the development of more rapid separation techniques for these enantiomers. In previous work with HSA immobilized to diol-bonded silica by the Schiff base method, it has been shown that L-tryptophan binds to a single type of site on the immobilized HSA [20]. Data indicated that L-tryptophan was binding to the indole site of HSA, in agreement with solution studies [20]. However, little or no specific information is yet available regarding the binding of D-tryptophan to immobilized HSA.

The first part of this study will use frontal analysis to determine the number of binding sites and the association constants for the interactions of D- and L-tryptophan with the immobilized HSA. Thermodynamic constants for these interactions, such as their changes in enthalpy and entropy, will also be evaluated. The binding of D-tryptophan will be further characterized by examining its competition with *R*-warfarin and L-tryptophan for the warfarin and indole sites of HSA. Changes in the retention and binding of D- and L-tryptophan with pH, phosphate concentration, column temperature, mobile phase polarity and sample size will then be studied. From this data, optimum conditions for the rapid separation of D- and L-tryptophan on the immobilized HSA column will be determined.

THEORY

Frontal analysis

For the continuous application of solute (E) to a column containing a single type of immobilized ligand site (L), the apparent moles of E required to reach the mean point of the resulting breakthrough curve (m_{Lapp}) is given by the following equation [20,21]:

$$\frac{1}{m_{Lapp}} = \frac{1}{K_a m_L [E]} + \frac{1}{m_L} \tag{1}$$

where K_a is the association constant for the binding of E to L, [E] is the concentration of solute applied to the column and m_L is the true number of moles of binding sites on the column. Eqn. 1 predicts that a plot of $1/m_{Lapp}$ vs. $1/[E]$ for this type of system will give a straight line with a slope of $1/K_a m_L$ and an intercept of $1/m_L$. The association constant K_a can be determined directly from this plot by calculating the ratio of the intercept to the slope. The true number of binding sites for solute on the column (m_L) can be determined from the inverse of the intercept [20].

Temperature studies

In the injection of a small amount of solute onto a column with a single type of binding site, the capacity factor of the solute (k') can be related to the solute's association constant by the equation [21]:

$$k' = K_a m_L / V_m \tag{2}$$

where V_m is the column void volume and all other terms are the same as defined previously. The association constant for this system can also be related to the absolute temperature (T) by:

$$\ln K_a = -\Delta H / RT + \Delta S / R \tag{3}$$

where ΔH and ΔS are the changes in the enthalpy and entropy of the reaction and R is the ideal gas law constant. By combining eqns. 2 and 3, the following expression can be derived:

$$\ln k' = -\Delta H / RT + \Delta S / R + \ln (m_L / V_m) \tag{4}$$

Eqn. 4 predicts that a plot of ln k' *vs.* $1/T$ will yield a linear relationship with a slope of $-\Delta H/R$ and an intercept of $[\Delta S/R + \ln (m_L/V_m)]$ for a system with single site binding. Using the values of ΔH and ΔS obtained from this plot, the change in the total free energy of the system (ΔG) can also be calculated [20,22].

EXPERIMENTAL

Reagents

The D- and L-tryptophan, HSA (Cohn fraction V, 99% globulin-free), bovine serum albumin (BSA) and R-/S-warfarin racemic mixture were purchased from Sigma (St. Louis, MO, USA). The Nucleosil Si-300 (4 μm particle diameter, 300 Å pore size) was from Alltech (Deerfield, IL, USA). The reagents for the bicinchoninic acid (BCA) protein assay were purchased from Pierce (Rockford, IL, USA). The HPLC-grade 1-propanol and uracil were from Aldrich (Milwaukee, WI, USA). All other chemicals used were of purest grade available. All solutions were prepared with water from a NANOpure water system (Barnstead, Dubuque, IA, USA).

Apparatus

The chromatographic system consisted of one CM3000 isocratic pump, one CM4000 gradient pump, and one SM3100 UV–Vis variable-wavelength absorbance detector (Milton Roy, Riviera Beach, FL, USA). Samples were injected using a Rheodyne 7012 valve (Cotati, CA, USA) equipped with a PhaseSep event marker (Phase Separations, Queensferry, UK) and a 20-μl injection loop. A Milton Roy Chromlink interface and LCAdvantage software were used for data collection. Chromatographic data were processed using programs written in QuickBASIC (Redmond, WA, USA) with double-precision logic. An Isotemp 9100 circulating water bath (Fisher Scientific, Pittsburgh, PA, USA) was used for temperature control of both the column and mobile phases. All columns were packed using an Alltech HPLC column slurry packer (Deerfield, IL, USA).

Methods

The Nucleosil Si-300 silica was converted to a diol-bonded form using a previously-published method [23]. The diol coverage of the Nucleosil prior to activation was 25 ± 4 μmol (±1 standard error of the mean, S.E.M.) per gram of silica, as determined in duplicate by the periodate oxidation method [24,25]. HSA was immobilized onto the diol-bonded Nucleosil using the Schiff base method [23]. After the immobilization step, the silica was centrifuged, washed three times with 0.10 M phosphate buffer (pH 7.0) containing 2.0 M NaCl, and rinsed three times with 0.10 M phosphate buffer (pH 7.0). The silica was then stored at 4°C prior to column packing. A small portion of the HSA–silica was further washed with deionized water and dried under reduced pressure for use in the BCA protein assay [26]. The BCA assay was performed using BSA as the standard and diol-bonded silica as the blank.

Chromatography

The HSA-silica and diol-bonded silica were downward slurry-packed into two separate 100.0 mm × 4.1 mm I.D. stainless steel columns at a pressure of 400 bar using 0.10 M phosphate buffer (pH 7.0) as the packing solvent. Both columns were enclosed in water jackets for temperature control. All studies, except those examining the temperature dependence of tryptophan–HSA binding, were performed at 25 ± 0.1°C. The mobile phases were filtered prior to use by passing them through 0.45-μm cellulose acetate or 0.45-μm nylon filters. All mobile phases were degassed under vacuum for at least 10 min before use on the HPLC system. Elution of the D- and L-tryptophan was monitored at 290 nm.

Frontal analysis was performed by continuously applying 0.05 M phosphate buffer (pH 7.4) containing D- or L-tryptophan to the HSA column at a flow-rate of 0.20 ml/min. The analyte solutions were applied using the same valve configuration as reported in ref. 20. The concentrations of D- and L-tryptophan used in this experiment ranged from $6.0 \cdot 10^{-6}$ to $1.0 \cdot 10^{-4}$ M. The retained D- and L-tryptophan were eluted by applying 0.05 M phosphate buffer (pH

7.4) to the column. The amount of D- or L-tryptophan required to saturate the HSA column was determined by integration of the resulting breakthrough curves [27]. Corrections for the system void volume and non-specific binding were made by subtracting the amount of D- or L-tryptophan needed to saturate the diol-bonded column under identical chromatographic conditions. This correction was within 20% of the system void volume, as measured by injecting uracil or sodium nitrate onto the column.

Zonal elution studies with the D- and L-tryptophan were performed at flow-rates ranging from 0.50 to 1.50 ml/min. The D- and L-tryptophan solutions injected were freshly prepared for each experiment by dissolving up to $1 \cdot 10^{-5}$ *M* of the appropriate enantiomer into the buffer being used as the mobile phase. Three injections of sample were made under each set of mobile phase conditions. The retention times and peak widths of the D- and L-tryptophan peaks were calculated by moments analysis and the $B/A_{0.1}$ method [28]. The void volume was determined by injecting uracil or sodium nitrate under the same chromatographic conditions. The retention times and column void time were corrected for the extra-column volume of the system by making injections of D- or L-tryptophan onto the system with no HSA column present.

Competition between D- and L-tryptophan for HSA binding sites was studied at a flow-rate of 1.00 ml/min by making 20-μl injections of $1 \cdot 10^{-5}$ *M* D-tryptophan in the presence of 0.05 *M* phosphate buffer (pH 7.0) containing $1 \cdot 10^{-4}$ to $1 \cdot 10^{-6}$ *M* L-tryptophan. Competition between D-tryptophan and *R*-warfarin for HSA binding sites was similarly examined by making 20-μl injections of $1 \cdot 10^{-5}$ *M* racemic warfarin in the presence of 0.05 *M* phosphate buffer (pH 7.0) containing $1 \cdot 10^{-4}$ to $1 \cdot 10^{-6}$ *M* D-tryptophan and determining the retention time of the first eluting peak (*i.e.*, *R*-warfarin).

RESULTS AND DISCUSSION

Binding of D- and L-tryptophan to immobilized HSA

The initial properties of the immobilized HSA matrix used in this study are listed in Table I.

TABLE I

INITIAL PROPERTIES OF THE IMMOBILIZED HSA MATRIX

Property	Value (± 1 S.D.)
HSA immobilized (nmol/g silica)	500 (± 7)
Binding capacity (nmol/g silica)	
L-Tryptophan	170 (± 10)
D-Tryptophan	80 (± 10)
Specific activity (mol/mol HSA)	
L-Tryptophan	0.34 (± 0.02)
D-Tryptophan	0.16 (± 0.02)

The coverage of HSA on the matrix, as determined by protein assay, was approximately 0.2 monolayers. This coverage is similar to that obtained in previous work using the same immobilization method for HSA on diol-bonded Nucleosil Si-1000 silica [20]. By assuming 1:1 binding for both the D-tryptophan and L-tryptophan with the immobilized HSA, 16% of the D-tryptophan binding sites and 34% of L-tryptophan binding sites (or indole sites) were determined to be active on this matrix. This relatively low activity has been reported previously for immobilized HSA [20] and is probably the result of such factors as steric hindrance, denaturation, or improper orientation of protein attached to the matrix [29]. The lower specific activity for D-tryptophan may reflect a greater sensitivity of its binding sites to these immobilization effects.

Fig. 1. Frontal analysis results for D- (■) and L- (●) tryptophan on the immobilized HSA column. The chromatographic conditions are given in the text.

The frontal analysis results obtained for D- and L-tryptophan on the immobilized HSA column are given in Fig. 1. As shown in this figure, plots of $1/m_{\text{Lapp}}$ versus both 1/[L-tryptophan] and 1/[D-tryptophan] gave linear relationships over the entire concentration range studied. The correlation coefficients for these plots were 0.9980 and 0.9997, respectively, over the 6 points shown in each graph. According to eqn. 1, this linear behavior indicated that both D- and L-tryptophan were binding to a single type of site on the immobilized HSA matrix. Single-site binding for L-tryptophan to HSA has been previously reported in work with HSA in solution [30] and with HSA immobilized onto high-performance affinity columns [20].

Based on eqn. 1, the plots in Fig. 1 were used to determine the binding capacities (m_L) and association constants (K_a) for D- and L-tryptophan on the immobilized HSA matrix. The resulting values are shown in Tables I and II, respectively. The association constant for L-tryptophan at 25°C was almost an order of magnitude larger than that for the D-tryptophan. This agrees with earlier results reported at 37°C [31]. D- and L-tryptophan also differed in that L-tryptophan had over 2-fold more binding sites on the HSA column. This difference in capacity indicated that D- and L-tryptophan were binding to separate regions on the immobilized HSA.

An experiment examining competitive binding between D- and L-tryptophan was used to confirm that these enantiomers were binding to different regions on HSA. This was done by injecting small amounts of D-tryptophan onto an immobilized HSA column in the presence of mobile phases containing various concentrations

of L-tryptophan. No change in the retention of D-tryptophan (i.e., less than 1% variation in k') was noted over the concentration range of 0 to $4 \cdot 10^{-5}$ M L-tryptophan. These results indicated that D- and L-tryptophan had no competition (either direct or indirect) in their binding to HSA. This confirmed that the enantiomers were interacting at separate binding sites.

A similar competition study was performed between D-tryptophan and R-warfarin to determine if D-tryptophan was binding to the warfarin site of HSA. The results are shown in Fig. 2. It was found that the retention of R-warfarin changed as different concentrations of D-tryptophan were applied to the column. However, a plot of $1/k'_{R\text{-warfarin}}$ versus [D-tryptophan] did not give the linear relationship expected for direct competition at a single site [20]. Instead, the retention of R-warfarin initially increased in going from 0 to $0.33 \cdot 10^{-5}$ M D-tryptophan, followed by a gradual decrease in retention at higher D-tryptophan concentrations. These results suggest that the binding sites for D-tryptophan and R-warfarin are related through allosteric interactions or some other type of indirect competition.

Effect of mobile phase composition on the retention of D- and L-tryptophan

After it was determined that D- and L-tryptophan bound to two distinct sites on the immobilized HSA, work was performed to see how

TABLE II

ASSOCIATION CONSTANTS FOR THE BINDING OF D- AND L-TRYPTOPHAN TO IMMOBILIZED HSA AT 25°C

Compound	Association constant $(M^{-1})^a$
L-Tryptophan	$2.7 \cdot 10^4$ ($\pm 0.3 \cdot 10^4$)
D-Tryptophan	$0.4 \cdot 10^4$ ($\pm 0.1 \cdot 10^4$)

^{a} Values in parentheses represent ± 1 S.D.
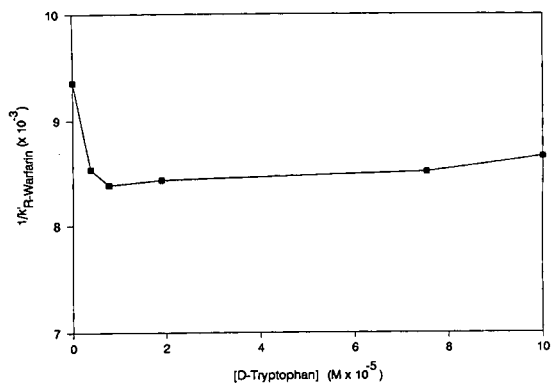
Fig. 2. Competitive binding of R-warfarin with D-tryptophan on the immobilized HSA column. The chromatographic conditions are given in the text.

changing the pH, phosphate concentration, temperature, and organic modifier content of the mobile phase would affect the interactions of D- and L-tryptophan at these sites. The effect of varying pH on the retention (k') of both compounds is shown in Fig. 3.

The results in Fig. 3 were obtained by injecting tryptophan samples onto the HSA column using a 0.10 M phosphate buffer at pH values ranging from 4.0 to 7.4. As the pH decreased, the capacity factors for both D- and L-tryptophan decreased. The retention of both compounds on the diol-bonded column was negligible (*i.e.*, $k' \leqslant$ 0.05) throughout this entire pH range. In going from pH 7.4 to 4.0, the capacity factor for D-tryptophan dropped from 0.52 to 0.25 (52%), while the capacity factor for L-tryptophan decreased from 1.43 to 0.23 (84%). The fact that these changes were not of the same relative size indicates that the binding sites of the L- and D-tryptophan were subjected to different local ionic interactions. This supports the model proposed earlier in which the two enantiomers bind to two distinct sites. As the pH was decreased from 7.4 to 4.0, the separation factor for D- and L-tryptophan (α, where $\alpha = k'_{\text{L-Trp}}/k'_{\text{D-Trp}}$) decreased from 2.75 to 1. The best separation of the enantiomers was obtained at pH 7.4. This was the pH used in the remainder of the study.

The ionic strength of the mobile phase is another parameter which can affect the stereoselectivity of an immobilized protein. In this study, this parameter was examined by maintaining the mobile phase at pH 7.4 while varying the concentration of the phosphate buffer from 0.010 to 0.250 M. As shown in Fig. 4, the capacity factors of both D- and L-tryptophan on the HSA column decreased with increasing phosphate buffer concentration. Binding to the diol–silica column was again negligible under these conditions (*i.e.*, $k' < 0.05$). The changes observed on the HSA column are consistent with previous work performed with oxazepam hemisuccinate on immobilized HSA–silica [32] and chiral separations performed on immobilized BSA–silica [33,34].

In this study, the capacity factor for L-tryptophan decreased much faster with increasing phosphate concentration than the capacity factor for D-tryptophan (*i.e.*, 72% *versus* 12% change, respectively). This suggested that the binding site for L-tryptophan was more sensitive to changes in the mobile phase ionic strength. This agrees with the results noted earlier in the pH studies. One result of this difference in sensitivity to changes in the ionic strength was that the value of α for D- and L-tryptophan dropped from 7.62 to 2.44 over the range of phosphate concentrations studied. Optimum separation of the two enantiomers was obtained at phosphate concentrations of 0.05 M or less. This concentration range was used in all later work.

Temperature is a third parameter which can be varied to adjust the resolution of an enantio-

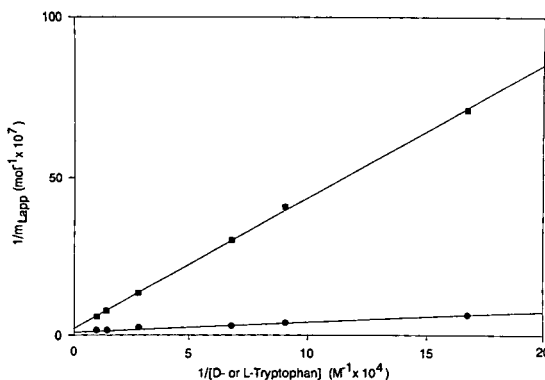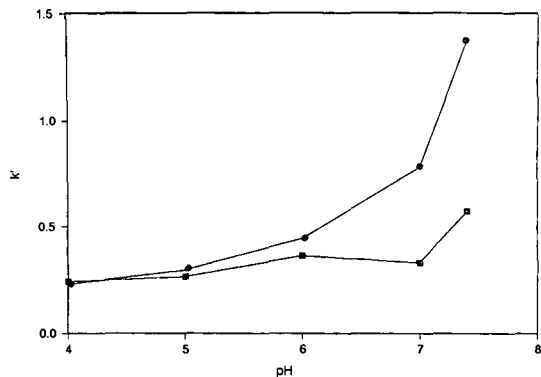Fig. 3. Effect of mobile phase pH on the retention of D- (■) and L- (●) tryptophan on the immobilized HSA column. The chromatographic conditions are given in the text.
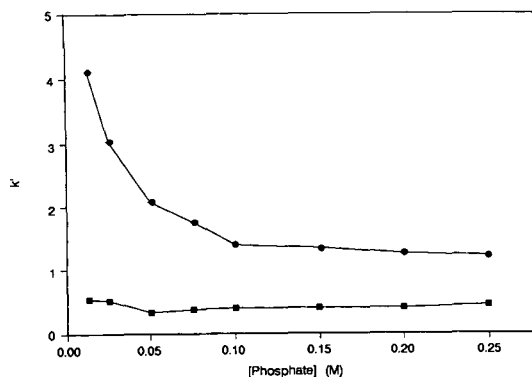
Fig. 4. Effect of phosphate concentration on the retention of D- (■) and L- (●) tryptophan on the immobilized HSA column. The chromatographic conditions are given in the text.
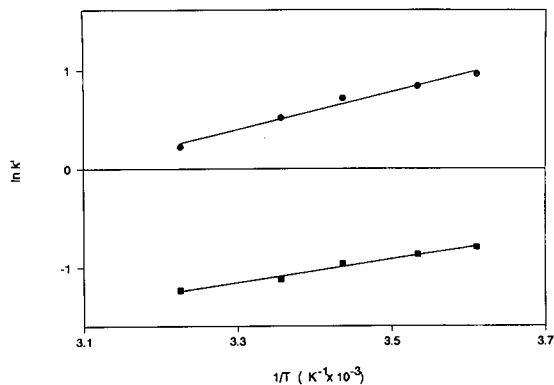
Fig. 5. Temperature dependence of D- (■) and L- (●) tryptophan binding to the immobilized HSA column. The chromatographic conditions are given in the text.

meric separation. The effect of temperature on the binding of D- and L-tryptophan to the immobilized HSA column was examined using a mobile phase containing 0.05 M phosphate buffer (pH 7.4). The resulting plots of ln k' versus $1/T$ are shown in Fig. 5. Both D- and L-tryptophan gave linear relationships over the temperature range of 4 to 37°C. The correlation coefficients for these plots were 0.9922 and 0.9925, respectively, over the 5 points shown in each graph. According to eqn. 4, these linear relationships confirmed that both the D- and L-tryptophan had single-site interactions with the immobilized HSA.

From the slopes and intercepts of these plots and the data in Table I, it was possible to calculate the change in enthalpy, entropy, and total free energy for the binding of each of these enantiomers. The results are given in Table III. The change in total free energy (ΔG) for these sites ranged from −5.2 to −5.7 kcal/mol (1

cal = 4.184 J) at 25°C. These values agree with those calculated using the association constants from Table II. For both the D- and L-tryptophan, a significant portion of the total free energy change (i.e., 33–54%) was due to the entropy term ($-T \Delta S$). This significant entropy contribution has been previously observed in the binding of L-thyroxine to a similar immobilized HSA column [20].

In Fig. 5 it was found that the capacity factors for both the D- and L-tryptophan decreased proportionately as the temperature increased. For example, the value of k' for L-tryptophan decreased from 2.62 to 1.26 (48%) in going from 4 to 37°C while the k' value for D-tryptophan decreased from 0.45 to 0.29 (64%). The result was that the separation factor α changed only slightly over this temperature range. This indicated that adjusting the temperature was not particularly useful as a means for obtaining optimum resolution in this separation. In further work, a temperature of 25°C was used for the sake of convenience.

The use of small amounts of mobile phase modifiers, such as 1-propanol, is yet another technique which has commonly been reported as a way of decreasing retention on protein columns while maintaining or improving stereoselectivity. The effect of using 1-propanol as an organic modifier in the separation of D- and L-tryptophan was examined by using a mobile phase containing 0.05 M phosphate buffer (pH 7.4) with 1-propanol levels of 0 to 5% (v/v). The effects of adding 1-propanol on the k' values for the D- and L-tryptophan are shown in Fig. 6. In this figure, increasing the concentration of 1-propanol from 0 to 5% caused the capacity factor for L-trypto-

TABLE III

THERMODYNAMICS FOR THE BINDING OF D- AND L-TRYPTOPHAN TO IMMOBILIZED HSA

Values in parentheses represent ±1 S.D.

Compound	ΔG at 25°C (kcal/mol)	ΔH (kcal/mol)	ΔS (cal/mol K)
L-Tryptophan	−5.7 (±0.4)	−3.8 (±0.3)	6.3 (±0.7)
D-Tryptophan	−5.2 (±0.4)	−2.4 (±0.2)	9.4 (±1.3)
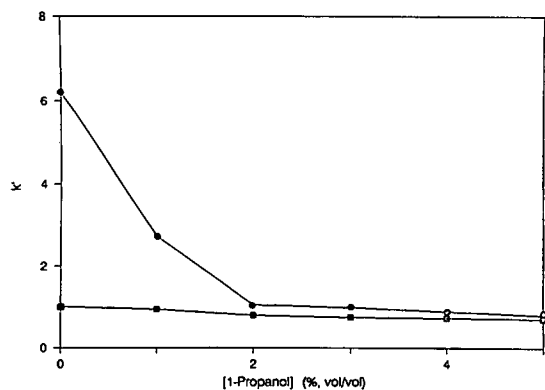
Fig. 6. Effect of mobile phase 1-propanol content on the retention of D- (■) and L- (●) tryptophan on the immobilized HSA column. The chromatographic conditions are given in the text.

Fig. 7. Effect of sample size on the retention of D- (■) and L- (●) tryptophan on the immobilized HSA column. Chromatographic conditions: mobile phase, 0.015 M phosphate buffer (pH 7.4); 20-μl injection loop; flow-rate, 1.00 ml/min.

phan to decrease from 1.98 to 0.24 (88%) while the capacity factor for D-tryptophan changed only from 0.32 to 0.24 (25%) under the same conditions. The binding of both compounds to the diol-silica column was negligible ($k' < 0.05$) under these conditions.

The effect of 1-propanol noted in Fig. 6 agrees with that observed by Allenmark and Bomgren [33,34] on a BSA-silica column and that seen by Dominici *et al.* [32] for the separation of hemisuccinate enantiomers on an HSA-silica column. In our study, the separation factor for D- and L-tryptophan fell from 6.2 to 1.16 in going from 0 to 5% 1-propanol. This decrease reflects the greater sensitivity of the L-tryptophan site to the organic modifier. Since the separation factor decreased by adding 1-propanol, and both D- and L-tryptophan were already separated in a reasonable amount of time when no 1-propanol was added, 1-propanol was not used in the remainder of this study.

Effect of sample size on peak retention and symmetry

The effect of sample size on the separation of D- and L-tryptophan was investigated by determining the values of k' for D- and L-tryptophan as different amounts of each solute were loaded onto the HSA column. As shown in Fig. 7, the capacity factor for D-tryptophan remained relatively stable (*i.e.*, less than 2% change) throughout the entire range of solute concentrations

studied while the capacity factor for L-tryptophan decreased by over 32% over the same concentration range. These results are consistent with effects observed by Gilpin *et al.* [19] for the separation of D- and L-tryptophan on a BSA column. This supports the model in which the D- and L-tryptophan are binding to two distinct regions on the immobilized HSA. The greater sensitivity of the L-tryptophan site to sample size is somewhat surprising since there were almost two-fold more binding sites for L-tryptophan than for D-tryptophan present on the HSA column. However, these results may reflect differences in the kinetics or binding mechanisms of D- and L-tryptophan with the immobilized HSA.
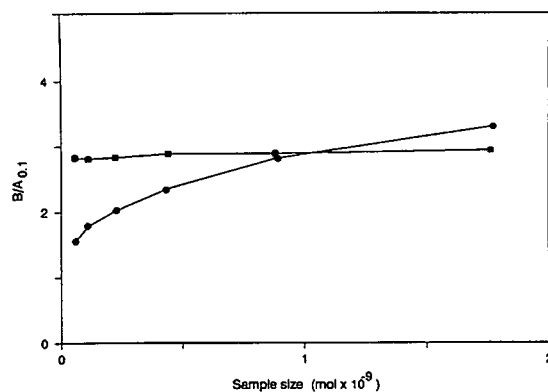
Fig. 8. Effect of sample size on the peak symmetry ($B/A_{0.1}$) of D- (■) and L- (●) tryptophan on the immobilized HSA column. The chromatographic conditions were the same as in Fig. 7.

The effect of sample size on peak shape was examined by using the tenth height B/A ratio ($B/A_{0.1}$) as a measure of peak symmetry. Changes observed in the $B/A_{0.1}$ ratio with sample size are shown in Fig. 8. For D-tryptophan, the $B/A_{0.1}$ ratio varied by only 20% over the range of sample loads studied. But for L-tryptophan, this ratio varied by 54% over the same sample load range and became stable only at very small sample sizes (*i.e.*, $<10^{-10}$ mol per injection). These results are consistent with the observed changes in the capacity factor with sample size. From the data in Fig. 8 it was determined that relatively small sample sizes (*i.e.*, 10^{-11} to 10^{-10} mol per injection) are needed for the optimum resolution of D- and L-tryptophan on this type of immobilized HSA column.

Optimized separation of D- and L-tryptophan

From the previous studies examining the effects of various mobile phase compositions on the separation of D- and L-tryptophan, the optimum chromatographic conditions for this separation were determined. These conditions included using a neutral mobile phase (pH 7.4) with a low-ionic-strength phosphate buffer (<0.05 M), 0% 1-propanol, and a sample size of 10^{-10} to 10^{-11} mol injected at room temperature. An example of a separation obtained under these conditions is shown in Fig. 9. At a flow-

rate of 3.0 ml/min, the D- and L-tryptophan were completely resolved ($R_s = 1.72$, $\alpha = 2.56$) in less than 2 min. It is expected that D- and L-tryptophan could be separated in an even shorter period of time if higher flow-rates were used.

The HSA columns used in this study were found to be quite stable under the optimum mobile phase conditions given. No significant change in column behavior was noted over the course of 500 injections and over the range of pH, temperature, and 1-propanol conditions used in this study. The only item noted to give a permanent decrease in HSA activity and tryptophan retention was the use of phosphate buffers with concentrations greater than 0.10 M. The mechanism for the loss in tryptophan retention at high phosphate buffer concentrations is currently under investigation.

CONCLUSIONS

In this study high-performance affinity chromatography was used to study the separation and binding of D- and L-tryptophan on an immobilized HSA column. From frontal analysis and zonal elution studies it was found that both D- and L-tryptophan were binding to single but distinct sites on HSA. In earlier work, it has been shown that L-tryptophan binds to the indole site of the immobilized HSA [20]; however, little information has previously been reported on the binding of D-tryptophan to this protein. In competition studies with L-tryptophan and *R*-warfarin, it was determined that the D-tryptophan had indirect interactions with the warfarin site of HSA but no interactions with the indole site. Although the exact location of the D-tryptophan site is still not known, these results are of interest since they definitely show that the two enantiomers are binding to totally different regions on HSA.

More detailed information on the interactions of D- and L-tryptophan with HSA was obtained by measuring the association constants and thermodynamic parameters for these binding processes. The L-tryptophan bound to HSA more strongly than D-tryptophan, with association constants of $2.7 \cdot 10^4$ and $0.4 \cdot 10^4$ M^{-1}, respectively, at pH 7.4 and 25°C. The value of
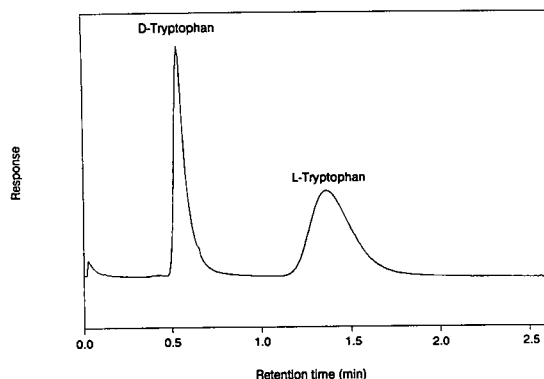
Fig. 9. Separation of D- and L-tryptophan on an immobilized HSA–silica column. Chromatographic conditions: mobile phase, 0.015 M phosphate buffer (pH 7.4); sample, $2.75 \cdot 10^{-6}$ M D-/L-tryptophan, 20-μl injection loop; flow-rate, 3.00 ml/min. The void time of this separation was at 0.31 min.

ΔG for the binding of D- and L-tryptophan to HSA was in the range of -5.2 to -5.7 kcal/mol at 25°C and had a significant contribution due to entropy.

This work also examined the effects of pH, phosphate concentration, temperature and 1-propanol content of the mobile phase on the binding of D- and L-tryptophan to HSA. In each case the retention of L-tryptophan was affected to a greater extent than that of the D-tryptophan. These differences in behavior agree with a model in which the enantiomers are binding to two distinct regions on HSA. Another parameter considered was the role of sample size in determining the retention and peak shape for each enantiomer. It was found that L-tryptophan had a greater sample size dependence in its chromatographic behavior than was noted for D-tryptophan.

Based on these studies, several guidelines were developed for the separation of D- and L-tryptophan on immobilized HSA. The strongest binding and best separation factor for these enantiomers was obtained when working with a neutral pH, low ionic strength phosphate buffer containing no organic modifier (i.e., 1-propanol). Temperature was found to have only a small effect on the separation of D- and L-tryptophan. Under the optimized conditions, D- and L-tryptophan were separated in less than 2 min with baseline resolution. This method is much faster than current separation techniques and should prove useful in the analysis of these compounds in food or pharmaceutical preparations.

ACKNOWLEDGEMENT

REFERENCES

1 D.W. Armstrong, Anal. Chem., 59 (1987) 84A.
2 A. Kaplan and L.L. Szabo, Clinical Chemistry, Lea & Febiger, Philadelphia, 1979, Ch. 5.
3 C.F. Chignell, in G.D. Fasman (Editor), Handbook of Biochemistry and Molecular Biology, Vol. 2, CRC Press, Cleveland, OH, 3rd ed., 1976, pp. 554–582.
4 I. Sjöholm, in M.M. Reidenberg and S. Erill (Editors), Drug–Protein Binding, Praeger Publishers, New York, 1986, Ch. 4 and 36.
5 J.-P. Tillement, G. Houin, R. Zini, S. Urien, E. Albengres, J. Barre, M. Lecomte, P. D'Athis and B. Sebille, Adv. Drug Res., 13 (1984) 59.
6 W.E. Müller and U. Wollert, Nauyn-Schmiedeberg's Arch. Pharmacol., 288 (1975) 17.
7 W.E. Müller, K.J. Fehske and S.A.C. Schlafer, in M.M. Reidenberg and S. Erill (Editors), Drug–Protein Binding, Praeger Publishers, New York, 1986, Ch. 2.
8 I. Sjöholm, Proc. FEBS Meeting, 50 (1978) 71.
9 G. Sudlow, D.J. Birkett and D.N. Wade, Molec. Pharmacol., 11 (1975) 824.
10 G. Sudlow, D.J. Birkett and D.N. Wade, Molec. Pharmacol., 12 (1976) 1052.
11 W.E. Müller and U. Wollert, Pharmacology, 19 (1979) 59.
12 R.H. McMenamy, J. Biol. Chem., 240 (1965) 4235.
13 H. Bruderlein and J. Bernstein, J. Biol. Chem., 254 (1979) 11570.
14 C. Lagercrantz, T. Larsson and H. Karlsson, Anal. Biochem., 99 (1979) 352.
15 P. Newton, LC·GC, 9 (1991) 208.
16 R.R. Langner and C.P. Berg, J. Biol. Chem., 214 (1955) 699.
17 W.C. Rose, G.F. Lambert and M.J. Coon, J. Biol. Chem., 211 (1954) 815.
18 S.C. Stinson, Chem. Eng. News, 70(39) (1992) 46.
19 R.K. Gilpin, S.E. Ehtesham, R.B. Gregory, Anal. Chem., 63 (1991) 2825.
20 B. Loun and D.S. Hage, J. Chromatogr., 579 (1992) 225.
21 R.R. Walters, in I.M. Chaiken (Editor), Analytical Affinity Chromatography, CRC Press, Boca Raton, FL, 1987, Ch. 3.
22 J.G. Kirkwood and I. Oppenheim, Chemical Thermodynamics, McGraw-Hill, New York, 1961.
23 P.-O. Larsson, Methods Enzymol., 104 (1984) 212.
24 S. Siggia and J.G. Hanna, Quantitative Organic Analysis, Wiley, New York, 1979, pp. 42–43.
25 A.A. Woolf, Anal. Chem., 54 (1982) 2134.
26 P.K. Smith, R.I. Krohn, G.T. Hermanson, A.K. Mallia, F.H. Gartner, M.D. Provenzano, E.K. Fujimoto, N.M. Goeke, B.J. Olson and D.C. Klenk, Anal. Biochem., 150 (1985) 76.
27 U. Lund, J. Liq. Chromatogr., 4 (1981) 1933.
28 D.J. Anderson and R.R. Walters, J. Chromatogr. Sci., 22 (1984) 353.
29 J. Tuková, Affinity Chromatography, Elsevier, Amsterdam, 1978.
30 R.H. McMenamy and R.H. Seder, J. Biol. Chem., 238 (1963) 3241.
31 C. Lagercrantz, T. Larsson and I. Denfors, Comp. Biochem. Physiol., 69C (1981) 375.
32 E. Domenici, C. Bertucci, P. Salvadori, G. Félix, I. Cahagne, S. Motellier and I.W. Wainer, Chromatographia, 29 (1990) 170.
33 S. Allenmark, J. Liq. Chromatogr., 9 (1986) 425.
34 S. Allenmark and B. Bomgren, J. Chromatogr., 264 (1983) 63.

Evaluation of deactivated reversed phases for the analysis of an N,N,N-trimethylethanaminium analogue of α-tocopherol

Application to its purity control and determination in biological samples

J. Verne-Mismer*, M. Lamard and J. Wagner

Department of Analytical Chemistry, Marion Merrell Dow Research Institute, 16 Rue d'Ankara, B.P. 067, 67046 Strasbourg Cedex (France)

ABSTRACT

Several non-deactivated and deactivated reversed-phase columns were evaluated for the determination of the quaternary ammonium analogue of α-tocopherol, 3,4-dihydro-6-hydroxy-N,N,N,2,5,7,8-heptamethyl-2H-1-benzopyran-2-ethanaminium 4-methylbenzenesulphonate, which is being developed as a cardioselective antioxidant. The retention characteristics of the compound, its corresponding quinone and their tertiary amine analogues were studied using UV detection at 280 nm. The effect of pH, ionic strength of the sodium phosphate buffer and nature of the organic solvent (methanol, acetonitrile) on the retention times and peak symmetry of the different compounds studied was evaluated. The effect of the addition of a basic modifier, N,N-dimethyloctylamine, was also investigated. The best results were obtained with deactivated C$_8$ and C$_{18}$ phases and with a mixture of methanol and sodium phosphate buffer. The method was applied to the purity control of the title compound and is compatible with electrochemical detection, which allows the determination of this α-tocopherol analogue and its corresponding amine in the sub-picomolar range.

INTRODUCTION

The α-tocopherol analogue 3,4-dihydro-6-hydroxy-N,N,N,2,5,7,8-heptamethyl-2H-1-benzopyran-2-ethanaminium 4-methylbenzenesulphonate [chromanol, code No. MDL 73404; **1** (Fig. 1)] has been shown to be a potent cardioselective antioxidant [1]. The aim of this study was the development of HPLC procedures for the determination of this quaternary ammonium derivative of α-tocopherol. The method
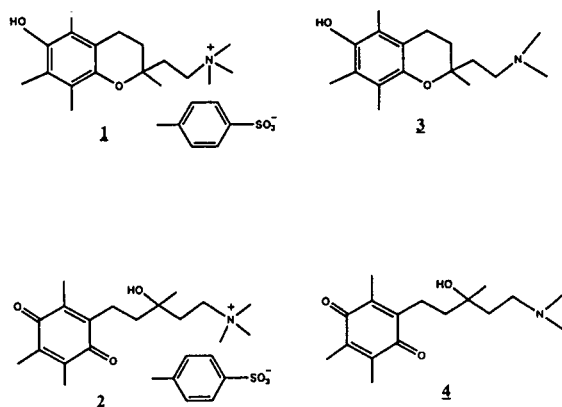
Fig. 1. Structures of the compounds studied.

---

* Corresponding author.

should allow the separation of **1** from its quinone **2**, which occurs as an oxidation product, and from the corresponding tertiary amines **3** and **4**, which may arise as potential by-products of the synthesis or decomposition. In recent years, numerous HPLC procedures have been developed for the determination of α-tocopherol and model compounds in biological samples, foods and pharmaceuticals [2–6] and for the study of their oxidation pathways [7–11]. These methods are based on either normal- or reversed-phase HPLC, depending on the lipophilicity and charges of the compounds to be analysed. The present compounds are quaternary ammonium and tertiary amine analogues of 2,2,5,7,8-pentamethyl-6-chromanol, **1** and **3**, and their corresponding quinones, **2** and **4**. Tertiary amine and quarternary ammonium groups are well known to interact with residual silanol functions present in most reversed-phase packings, giving strongly tailing peaks [12–15]. These peak broadening problems are usually overcome by the addition of tertiary alkylamines to the eluent [12,16,17] or by masking the residual silanol groups by chemical derivatization and coating. Recently, so-called deactivated reversed-phase packings have been developed and have been shown to give excellent results with strongly basic analytes [14,18,19].

The peak shapes (as measured by the asymmetry factor) and separation efficiencies of compounds **1–4** were studied using conventional and deactivated C_8 and C_{18} reversed-phase columns. The following parameters were studied: effect of addition of a lipophilic amine (N,N-dimethyloctylamine), effect of the nature and strength of the buffer salt, effect of pH and the influence of the nature of the organic solvent. It was found that the best results were obtained with deactivated phases, which allowed an efficient separation of **1** from its potential by-products **2–4**. The method, using UV detection, was applied to the purity control of **1** and can be used for stability studies. The use of an electrochemical detector gives a marked increase in sensitivity for the oxidizable compound, *i.e.*, **1** and **3**.

EXPERIMENTAL

Chemicals

3,4-Dihydro - 6 - hydroxy-N,N,N,2,5,7,8-heptamethyl-2H-1-benzopyran-2-ethanaminium 4-methylbenzenesulphonate (**1**) and the amine 3,4-dihydro-2-[2-(dimethylamino)ethyl]-2,5,7,8-tetramethyl-2H-1-benzopyran-6-ol (**3**) were synthesized as described previously [1]. The quinones 3 - hydroxy - N,N,N,3 - tetramethyl - 5 - (2,4,5-trimethyl-3,6-dioxo-1,4-cyclohexadien-1-yl)pentanaminium, 4-methylbenzene sulfonate (**2**) and 1 - (3-hydroxy-3-methyl-5-dimethylaminopentyl)-2,4,5 - trimethyl - 1,4 - cyclohexadien-3,6-dione (**4**) were obtained by established procedures [20]. N,N-Dimethyloctylamine (DMOA) was obtained from ICN Pharmaceuticals (Plainview, NY, USA), ammonium acetate from Prolabo (Paris, France) and trifluoroacetic acid from Janssen (Beerse, Belgium). Acetonitrile (LiChrosolv), methanol (Uvasol) and all other chemicals (analytical-reagent grade) were purchased from Merck (Darmstadt, Germany).

Liquid chromatographic system

A modular HPLC system was used, consisting of a Model 9010 solvent delivery system from Varian (Palo Alto, CA, USA), a WISP 715 automatic injector with thermostating from Waters (Milford, MA, USA) and a Model 486 UV detector from Waters. An HP 1049A electrochemical detector from Hewlett-Packard (Palo Alto, CA, USA) with a glassy carbon electrode whose potential was maintained at 0.6 V *versus* a silver–silver chloride reference electrode was used for electrochemical detection. The chromatograms were recorded and integrated with a Nelson 6000 data acquisition system. The columns were thermostated at 40°C with a Croco-cil from Interchim (Montluçon, France). The flow-rate was usually 1 ml/min.

Columns

The following columns were used: LiChroCART Superspher 60 RP-8e and 100 RP-18e (4 μm) (250 × 4.0 mm I.D.) from Merck, Ultrabase

C_8 and C_{18} (5 μm) (250 × 4.6 mm I.D.) from Shandon-SFCC (Eragny, France), Zorbax Rx-C_8 (5 μm) (250 × 4.6 mm I.D.) from Rockland Technologies (supplied by Shandon-SFCC) and Nucleosil 100-5 C_{18}AB (5 μm) (250 × 4.0 mm I.D.) from Macherey–Nagel (Düren, Germany).

Mobile phases

Different mobile phases were used under isocratic conditions. For the Superspher RP-8e and RP-18e columns, the following eluents were prepared: 0.15 *M* NaH$_2$PO$_4$ buffer–methanol (65:35, v/v) with apparent pH 5.2; and the same eluent but with addition of 0.02% (v/v) of DMOA and with the pH adjusted to 5.2 with 1 *M* H$_3$PO$_4$. For the studies with the other columns, the mobile phases were 0.12 *M* NaH$_2$PO$_4$–acetonitrile (80:20, v/v) or 0.15 *M* NaH$_2$PO$_4$–methanol (65:35, v/v). The pH was adjusted to lower values, *e.g.*, 3 and 4, by addition of H$_3$PO$_4$ and to higher values, *e.g.*, 6, 7 and 8, with 4 *M* NaOH. For LC–MS studies, the mobile phase was 0.15 *M* ammonium acetate buffer–methanol (65:35, v/v) with an apparent pH adjusted to 5.2 with concentrated acetic acid. For semi-preparative HPLC, the eluent was water–methanol–concentrated trifluoroacetic acid (65:35:1, v/v/v) with an apparent pH of 2.00.

All the eluents were filtered under vacuum with a 0.45-μm Millipore HV filter.

Solutions

Standard solutions of compounds 1–4 were prepared by dissolving 0.5–3 mg (standard 1) or 0.2–0.8 mg (standard 2) of the different compounds in 10 ml of water. Solutions were stored at 0–5°C under nitrogen to prevent oxidation. Aliquots of 50 μl of the standard solutions were usually injected, corresponding to 3–9 μg (10–35 nmol) or 1–3 μg (2–12 nmol), respectively, of the different compounds. The automatic injector was thermostated at 4°C to limit thermal degradation of the compounds.

Calculations

The following factors were used for the column evaluation. The capacity factor was measured using the relationship $(t_r - t_0)/t_0$, where t_r is the retention time of the compound and t_0 that of a non-retained compound measured by using the solvent disturbance peak [21]. The peak asymmetry factor *B/A* was measured at 10% of the peak height using the ratio of the widths of the rear and front sides of the peak [21,22]. The Foley–Dorsey method [22] was used to measure the column efficiency as skewed peaks were often involved. The method uses the equation

$$N = \frac{41.7(t_R/w_{0.1})^2}{B/A + 1.25}$$

were *N* is the efficiency (plates per column) and $w_{0.1}$ the peak width at 10% height.

RESULTS AND DISCUSSION

Use of conventional reversed-phase columns and effect of amine modifier

The first studies with the quaternary ammonium compound 1 and its analogues 2–4 were done by using the classical end-capped Superspher RP-18e and RP-8e stationary phases. With mixtures of 0.15 *M* sodium phosphate buffer and methanol at an apparent pH of 5.2, separation of the four compounds was obtained with badly tailing peaks, the separation being only partial for 2 and 3 with the RP-8e column, as illustrated in Fig. 2a and c. The addition of a small amount of DMOA, *i.e.*, 0.02% (v/v), to the mobile phase at the same pH greatly improved the peak shapes, with a slight decrease in retention times. Satisfactory separation of the four compounds was obtained with the RP-18e column, whereas with the RP-8e column 2 and 3 co-eluted (see Fig. 2b and d). Under these conditions, 1 was always eluted first, followed by 3, 2 and 4. This is in agreement with the differences in lipophilicity, log *P* being −0.60 for 1 and 1.15 for 3 [1]. The chromatographic characteristics for 1 are summarized in Table I. For the injection of smaller amounts, *eg.*, 1.6 μg (5 nmol) of 1, no change in *k'*, a marked

x = 0   x = 0.02
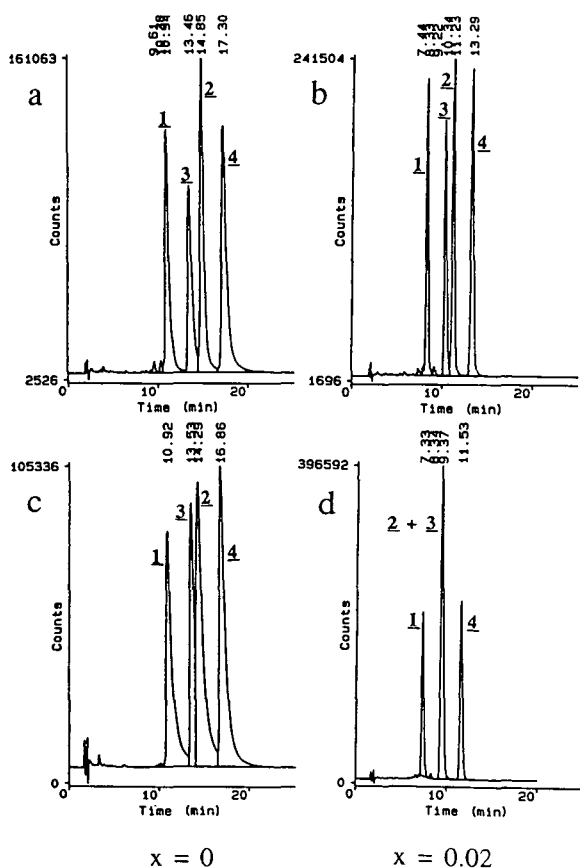
Fig. 2. Effect of DMOA on the separation of compounds 1–4. Column: (a,b) Superspher RP-18e; (c,d) Superspher RP-8e. Conditions as defined in Table I. x = % of DMOA.

decrease in the asymmetry factor, e.g., 1.6 for the RP-18e column with DMOA instead of 2.6, and nearly a doubling of the plate number, e.g.,

6700 for the RP-18e column with DMOA instead of 3500, were observed.

Use of deactivated C_8 and C_{18} phases

In order to improve the separation between the amine 3 and the quinone 2, which corresponds to the first and major oxidation product formed, and to apply the HPLC method to coupled LC–MS or semi-preparative chromatography using simplified mobile phases without addition of an amine modifier, several deactivated C_8 and C_{18} phases were tested (a complete stability study with isolation and characterization of the major oxidation compounds formed has been carried out and will be described elsewhere). These deactivated supports have been shown to improve greatly the separation and peak shapes of basic analytes without addition of basic modifiers such as triethylamine or DMOA [14,18,19].

Method development: effect of ionic strength, DMOA addition, pH and nature of the organic solvent. The optimization of the mobile phase conditions was done with the Ultrabase C_8 column. In fact, the conditions giving the best results with the Superspher columns without DMOA addition, i.e., 0.15 M NaH_2PO_4 buffer–methanol (65:35, v/v) at an apparent pH of 5.2, gave a very good separation of 1–4 with the Ultrabase C_8 column.

As expected, an increase of the ionic strength from 0.038 to 0.15 M NaH_2PO_4 clearly improved the efficiency of the column and the asymmetry factors of the peaks. For an amount of ca. 9 μg

TABLE I

EFFECT OF DMOA ON THE CHROMATOGRAPHIC CHARACTERISTICS OF COMPOUND 1 WITH THE SUPERSPHER RP-8E AND RP-18E COLUMNS

Conditions: mobile phase, 0.15 M NaH_2PO_4–methanol (65:35, v/v) with or without 0.02% of DMOA, apparent pH = 5.2; flow-rate, 1 ml/min; temperature, 40°C; detection, UV at 280 nm; sample, 50 μl of standard 1 corresponding to amounts of ca. 9 μg of 1 and 3 and ca. 3 μg of 2 and 4; k', B/A and N as defined in the text.

Eluent	k'		B/A		N	
	RP-8e	RP-18e	RP-8e	RP-18e	RP-8e	RP-18e
Without DMOA	4.20	3.68	6.37	4.82	250	850
With DMOA	2.49	2.56	2.45	2.58	2400	3500

(30 nmol) of **1** injected, the plate number N increased from 1300 to 2800 and the asymmetry factor decreased from 3.2 to 2.7. Addition of 0.02% (v/v) of DMOA to the eluent containing 0.15 M NaH$_2$PO$_4$ buffer further improved the plate number and asymmetry factor to 6000 and 1.9, respectively. Further addition of up to 0.1% of DMOA led only to a slight additional improvement. A typical chromatogram obtained for **1–4** on the Ultrabase C$_8$ column under the above-described conditions, without addition of DMOA, is given in Fig. 3a.

Variation of the pH between 3 and 6 with the 0.15 M NaH$_2$PO$_4$ buffer–methanol (65:35, v/v) eluent had no effect on the capacity factors for the four compounds. Above pH 6 the capacity factors of the amines **3** and **4** rapidly increased, as expected, owing to the deprotonation of the amino function. An apparent pH of 5.2 was adopted for all further studies. No systematic study of the effect of temperature was made, but a temperature of 40°C was found to provide a good compromise between reduced pressure and column lifetime.

The use of acetonitrile instead of methanol as an organic modifier, i.e., 0.12 M NaH$_2$PO$_4$–acetonitrile mixture (80:20, v/v) at an apparent pH of 5.2, which gave similar capacity factors, led to large and unresolved peaks for **1** and its analogues **2–4**. The addition of 0.02% (v/v) of DMOA restored satisfactory peak shapes, but with incomplete resolution of the four compounds. In particular, the quinone **2** was eluted very close to **1**.

This is a further example of a specific solvent interaction with analytes and reversed-phase packings, especially with quaternary ammonium and tertiary amine analogues [12,13–15]. It is noteworthy that the four compounds here have significantly lower solubilities in acetonitrile than in methanol.

These different trials led us to adopt 0.15 M sodium phosphate buffer–methanol (65:35, v/v) at an apparent pH of 5.2 for the remainder of the experiments.

Comparison of different deactivated phases. Considering the remarkable peak-shape improvements observed with the Ultrabase C$_8$ column without addition of DMOA, it was of obvious interest to study some other commercially available deactivated phases. Three of them were tested, Zorbax Rx-C$_8$, Ultrabase C$_{18}$ and Nucleosil C$_{18}$ AB.

The same amount of the standard solution of the four compounds was injected, using the chromatographic conditions that gave the best separation with the Ultrabase C$_8$ column, i.e., 0.15 M NaH$_2$PO$_4$ buffer–methanol (65:35, v/v) at an apparent pH of 5.2 at 40°C and a flow-rate of 1 ml/min. The general elution patterns shown in Fig. 3b–d are similar although the separation of **2** and **3** with the Zorbax Rx-C$_8$ column is clearly less effective. The retention times for the C$_8$ and C$_{18}$ columns, except for the Nucleosil C$_{18}$ phase, are nearly the same.

The chromatographic characteristics of **1** (k', B/A and N) are summarized in Table II. The best peak shapes and efficiencies were obtained with the Ultrabase C$_8$ and C$_{18}$ and the Nucleosil
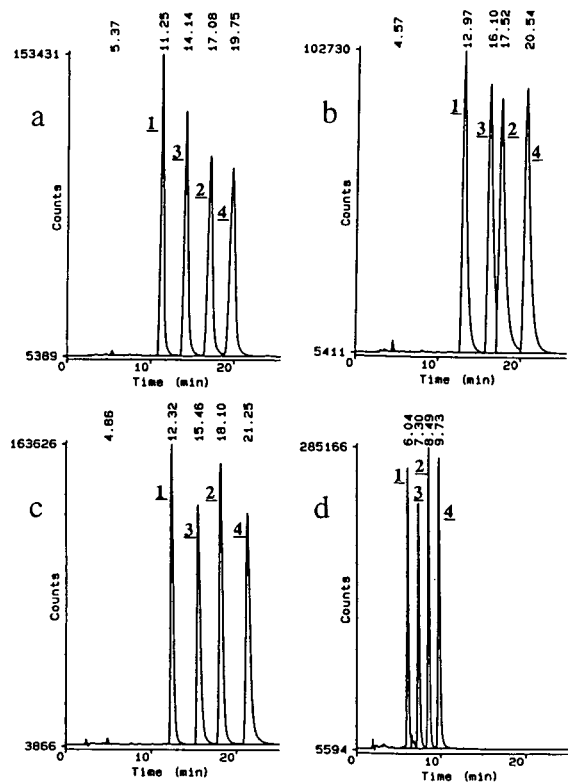
Fig. 3. Separation of compounds 1–4. Column: (a) Ultrabase C$_8$; (b) Zorbax Rx-C$_8$; (c) Ultrabase C$_{18}$; (d) Nucleosil C$_{18}$ AB. Conditions as defined in Table II.

TABLE II

CHROMATOGRAPHIC CHARACTERISTICS FOR COMPOUND 1 WITH THE DIFFERENT DEACTIVATED COLUMNS

Conditions: mobile phase, 0.15 M NaH_2PO_4–methanol (65:35, v/v), apparent pH = 5.2; other conditions as in Table I: k', B/A and N as defined in the text.

Column	k'	B/A	N
Superspher RP-8e	4.20	6.37	250
Superspher RP-18e	3.68	4.82	850
Ultrabase C_8	2.97	2.67	3500
Ultrabase C_{18}	3.79	2.79	3400
Zorbax Rx-C_8	3.67	4:23	800
Nucleosil C_{18}AB	1.88	2.54	2450

C_{18} columns. The results are similar to those obtained with the RP-8e and RP-18e columns but in the presence of DMOA. These results show that the Ultrabase and Nucleosil phases tested present less residual silanol activity than the Superspher phases and that the end-capping as done with the Superspher phases is not sufficient to minimize silanol interactions with these quaternary ammonium and tertiary amine analogues.

Extension to other buffers. Most of the studies were done with the Ultrabase C_8 column, al-

though the results obtained with the Ultrabase C_{18} and Nucleosil C_{18} are nearly equivalent in terms of asymmetry factor and separation efficiency for the four compounds of interest. Sodium phosphate can be replaced with ammonium acetate for coupled LC–MS studies. The separation obtained with the Ultrabase C_8 column with ammonium acetate buffer–methanol (65:35, v/v) is shown in Fig. 4a.

The use of 0.1% trifluoroacetic acid also gives a satisfactory separation (see Fig. 4b) and allows an easy scale-up to the semi-preparative HPLC separation of 1 from its decomposition products.

Applications

Purity control of compound 1. The method using the Ultrabase C_8 column and 0.15 M NaH_2PO_4–methanol (65:35, v/v) at an apparent pH of 5.2 has been routinely applied for the purity control of 1. Addition of DMOA to the mobile phase to improve the peak shape of the compounds was not used for the final purity control conditions. Indeed, 1 is determined as a *p*-toluenesulphonate salt and with DMOA addition the retention time of the *p*-toluenesulphonate group is increased, *e.g.*, addition of 0.02% (v/v) of DMOA increases its retention time from 5 to 7 min, and it will interfere with one of the oxidation products of 1. A typical chromatogram
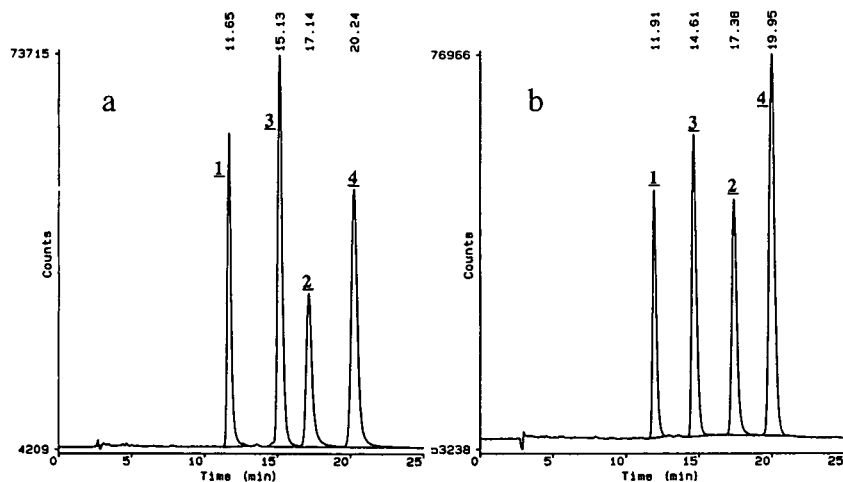
Fig. 4. Separation of compounds 1–4 with the Ultrabase C_8 column. Conditions: mobile phase, (a) 0.15 M ammonium acetate–methanol (65:35, v/v), apparent pH = 5.2 and (b) water–methanol–concentrated trifluoroacetic acid (65:35:1, v/v/v), apparent pH = 2.00; sample, 50 μl of standard 2 corresponding to amounts of *ca.* 3 μg of 1 and 3 and *ca.* 1 μg of 2 and 4; other conditions as defined in Table I.
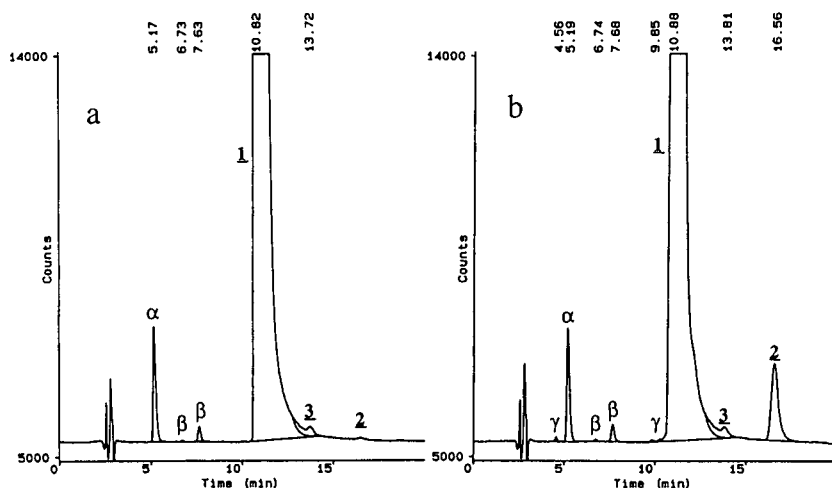
Fig. 5. Purity control of compound 1. Conditions: column, Ultrabase C_8; mobile phase, 0.15 M NaH_2PO_4–methanol (65:35, v/v), apparent pH = 5.2; flow-rate, 1 ml/min; temperature, 40°C; detection, UV at 280 nm; sample, 50 μl of solution of 1 corresponding to 15 μg. (a) At time zero; (b) after 1 day. $\alpha = p$-Toluenesulphonate; β = impurities; γ = oxidation compounds.

obtained with UV detection at 280 nm for the injection of 50 μl of a 5 mg per 10 ml aqueous solution of 1 is given in Fig. 5a. No detectable quinone 2 at a level of 0.05% by area was observed. The sensitivity of the procedure is illustrated by the chromatogram in Fig. 5b, which corresponds to the same solution of 1 left in presence of air for 1 day. The quinone 2 is now clearly observed and corresponds to 0.67% by area or 0.16 mol%.

Use of electrochemical detection. Vitamin E analogues are easily oxidizable compounds and therefore electrochemical detection has been a method of choice for the determination of these analogues in various media [4–6]. Using an electrochemical detector, the sensitivity of detection was markedly increased for 1 and 3. Compounds 2 and 4 were no longer detected. The chromatogram obtained with UV detection at 280 nm with injection of amounts ranging from
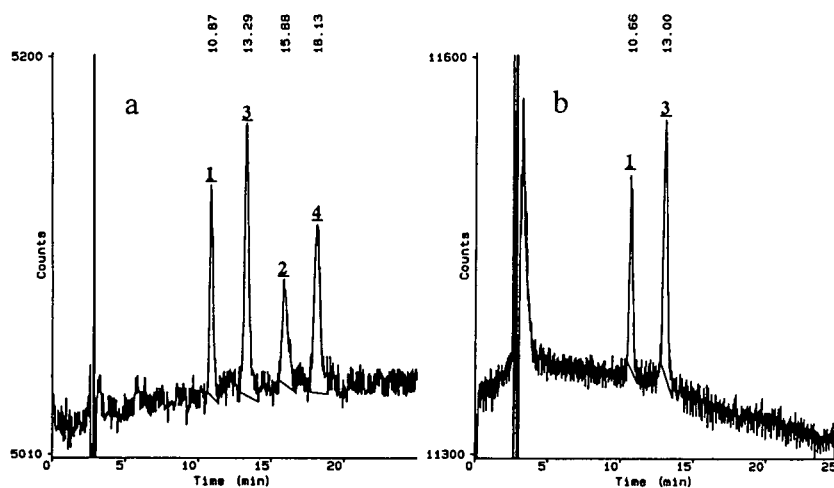
Fig. 6. Detection limits obtained for compounds 1–4 with the Ultrabase C_8 column, with conditions as defined in Fig. 5. (a) UV detection at 280 nm; amounts injected, *ca.* 5 ng of 1 and 3 and 1.5 ng of 2 and 4. (b) Electrochemical detection; electrode potential, 0.6 V *versus* Ag/AgCl reference electrode; amounts injected, *ca.* 100 pg of 1 and 3 and 30 pg of 2 and 4.

1.5 to 5 ng (from 4 to 24 pmol) of **1–4** is shown in Fig. 6a; the detection limit corresponds to *ca.* 2 ng (7 pmol) injected for **1** and **3** and *ca.* 1 ng (3.5 pmol) for the corresponding quinones **2** and **4** at a signal-to-noise ratio of 3. Fig. 6b illustrates the gain in sensitivity obtained for **1** and **3** with the electrochemical detector by applying a working potential of 0.6 V. The detection limits are *ca.* 40 pg (0.15 pmol) for both compounds, which corresponds to a gain in sensitivity by a factor of 50 compared with UV detection at 280 nm. This method is now routinely applied to the determination of **1** and analogues in biological samples such as brain and heart homogenates of mice and rats [23].

CONCLUSIONS

The best results for the separation of **1** from its potential impurities **2–4** were obtained on deactivated phases, *i.e.*, Ultrabase C_8 and C_{18} and the Nucleosil $C_{18}AB$ columns, with addition of DMOA to the eluent. The purity control of **1** was developed on an Ultrabase C_8 column with sodium phosphate buffer–methanol as eluent, but without DMOA addition. These conditions gave the best compromise between good peak shapes and separation of all the potential impurities considered. The method was easily adapted to coupled LC–MS studies and to semi-preparative chromatography by replacing sodium phosphate with ammonium acetate or trifluoroacetic acid. The method was also applied to the determination of **1** in biological samples by using electrochemical detection, allowing a great enhancement of sensitivity.

REFERENCES

1 J.M. Grisar, M.A. Petty, F.N. Bolkenius, J. Dow, J. Wagner, E.R. Wagner, K.D. Haegele and W. De Jong, *J. Med. Chem.*, 34 (1991) 257.

2 A. Deschuytere and H. Deelstra, *Fresenius' Z. Anal. Chem.*, 324 (1986) 1; and references cited therein.

3 M. Balz, E. Schulte and H.P. Thier, *Fett Wiss. Technol.*, 94 (1992) 209.

4 J.K. Lang, K. Gohil and L. Packer, *Anal. Biochem.*, 157 (1986) 106.

5 M.E. Murphy and J.P. Kehrer, *J. Chromatogr.*, 421 (1987) 71.

6 G.A. Pascoe, C.T. Duda and D.J. Reed, *J. Chromatogr.*, 414 (1987) 440.

7 M. Matsuo, S. Matsumoto, Y. Iiataka and E. Niki, *J. Am. Chem. Soc.*, 111 (1989) 7179.

8 D.C. Liebler, P.F. Baker and K.L. Kaysen, *J. Am. Chem. Soc.*, 112 (1990) 6995.

9 D.C. Liebler and J.A. Burr, *Biochemistry*, 31 (1992) 8278.

10 M. Baca, C. Suarna and P.T. Southwell-Keely, *J. Liq. Chromatogr.*, 14 (1991) 1957.

11 I. Molnar and S. Koswig, *J. Chromatogr.*, 605 (1992) 49.

12 E. Bayer and A. Paulus, *J. Chromatogr.*, 400 (1987) 1.

13 M.A. Stadalius, J.S. Berus and L.R. Snyder, *LC · GC*, 6 (1988) 494.

14 R.J.M. Vervoort, F.A. Maris and H. Hindriks, *J. Chromatogr.*, 623 (1992) 207.

15 B. Buszewski, J. Schmid, K. Albert and E. Bayer, *J. Chromatogr.*, 552 (1991) 415.

16 J.S. Kiel, S.L. Morgan and R.K. Abramson, *J. Chromatogr.*, 320 (1985) 313.

17 K.-G. Wahlund and A. Sokolowski, *J. Chromatogr.*, 151 (1978) 299.

18 T.L. Ascah and B. Feibush, *J. Chromatogr.*, 506 (1990) 357.

19 J. Coene, M. Ghijs, E. Van Den Eeckhout, W. Van Den Bossche and P. Sandra, *J. Chromatogr.*, 553 (1991) 285.

20 J.M. Grisar, unpublished work.

21 L.R. Snyder and J.J. Kirkland (Editors), *Introduction to Modern Liquid Chromatography*, Wiley, New York, 1979, 2nd ed., Ch. 5.

22 J.P. Foley and J.G. Dorsey, *Anal. Chem.*, 55 (1983) 730.

23 F. Bolkenius and J. Verne, unpublished work.

Preparation and determination of zinc(II) chlorophylls by reversed-phase high-performance liquid chromatography

Hidenari Inoue*, Miki Imai, Takashi Naemura, Kenji Furuya and Yoshikazu Shizuri

Faculty of Science and Technology, Keio University, 3-14-1 Hiyoshi, Kohoku-ku, Yokohama 223 (Japan)

ABSTRACT

A preparative method for zinc(II) chlorophyll *a* and *b* [Zn(II)-chl-a and -b] was developed on the basis of their purification by semi-preparative high-performance liquid chromatography. Zn(II)-chl-a and -b and the corresponding epimers were separated and determined with an ODS (C_{18} chemically bonded silica gel) column using methanol–acetone (75:25, v/v) as mobile phase. Linear calibration graphs were obtained over the concentration range 0–50 μg cm^{-3} of each zinc(II) chlorophyll with photometric detection at 425 nm. The present HPLC determination provides an accurate and conventional method with a detection limit of 3.5 ng cm^{-3} for Zn(II)-chl-a, 2.5 ng cm^{-3} for Zn(II)-chl-a' and 3.0 ng cm^{-3} for Zn(II)-chl-b with a relative standard deviation of less than 2.3% ($n = 10$). The analytical values obtained for synthetic samples by a spectrophotometric method were confirmed to be high compared with those determined by the proposed HPLC method.

INTRODUCTION

A variety of metal-substituted chlorophylls, *i.e.*, metallochlorophylls in which the central magnesium ion of chlorophylls is replaced with other metal ions such as iron(III) and copper(II), are used for colouring materials of foods and some kinds of medicines [1,2]. In recent years a diverse group of metallochlorophylls, including iron(III) and copper(II) chlorophylls, has also received a great deal of attention because of their potential use for electrode materials for photoelectron conversion [3]. This continuing interest in metallochlorophylls re-

quires a conventional method for their preparation and determination. The development of methods suitable for the determination of chlorophylls and metallochlorophylls has been the subject of intense research for many years. In fact, there have been many reports on the chromatographic determination of chlorophylls themselves, *i.e.*, the parent compounds of metallochlorophylls [4–6]. The determination of iron(III), nickel(II) and copper(II) chlorophylls by high-performance liquid chromatography (HPLC) has been reported in previous papers [7–9]. In this paper we propose a semi-preparative HPLC method for purifying zinc(II) chlorophyll *a* and *b* [Zn(II)-chl-a and -b] and also a rapid and accurate HPLC method for their determination. In addition, the liquid chromato-

---

* Corresponding author.

graphic behaviour of zinc(II) chlorophylls is described in comparison with that of chlorophylls because Zn(II)-chl-a may serve as an internal standard in the HPLC determination of native chlorophylls.

EXPERIMENTAL

Preparation of zinc(II) chlorophylls

Chlorophylls were extracted from fresh spinach as described [10–12] and purified by reprecipitation from a water–dioxane solution of crude chlorphylls [13]. The chlorophylls thus obtained were pheophytinized by adding 10 cm^3 of dilute hydrochloric acid (0.1 M) to 150 cm^3 of an acetone solution of chlorophylls (200 mg) and keeping the mixed solution at 40°C for 30 min. Pheophytins were extracted from this acetone–water solution with hexane and evaporated to dryness on a rotary evaporator. A 20-cm^3 volume of a chloroform solution of 20 mg of pheophytins was added to 40 cm^3 of a methanol solution of 21 mg of zinc(II) acetate dihydrate and the mixture was stirred at 40°C in an argon atmosphere for 1 h. After evaporation of the chloroform–methanol solution, the residue was extracted with hexane and the extract was washed twice with distilled water. The hexane solution was rotary evaporated at 40°C to obtain zinc(II) chlorophylls. Zn(II)-chl-a and -b were separated with a semi-preparative Develosil ODS column (10-μm spherical octadecyl silica, 25 cm × 3 cm I.D.) (Nomura Chemical, Aichi, Japan) equipped with a Kusano–Kagaku loop injector (0.59 cm^3). The flow-rate of the mobile phase of methanol–acetone (75:25, v/v) was 7.4 cm^3 min^{-1}. Each fraction from semi-preparative HPLC was evaporated to dryness on a rotary evaporator at 40°C to obtain Zn(II)-chl-a and -b in pure form.

Apparatus and measurement method

The analytical HPLC system consisted of a JASCO BIP-1 pump, a Unisilpak 5C$_{18}$ column (10-μm spherical ODS, 250 mm × 4.6 I.D.) or an Inertsil ODS-2 column (5-μm spherical ODS, 250 mm × 4.6 mm I.D.), a Rheodyne Model 7125 injector with a 100-mm^3 injection loop and a Shimadzu C-R3A Chromatopac integrator. The detector used for this system was a Uvidec-1000 variable-wavelength UV–Vis detector or a Shimadzu SPD-MIA photodiode-array detector. Each HPLC solvent or solvent mixture was filtered through a fresh 0.45-μm hydrophilic Millipore filter and degassed every time before use by ultrasonically vibrating the solvent container. The mobile phase was methanol–acetone (75:25, v/v), the flow-rate was 0.5–1.0 cm^3 min^{-1}, the inlet pressure was 4.9–9.8 MPa and the analytes were usually detected at 425 nm. The ^{1}H NMR spectra at 270 MHz of samples in C^{2}HCl$_3$ solution containing tetramethylsilane were recorded with a JEOL JNM-GX 270 FT-NMR spectrometer. The chemical shifts are reported in ppm relative to CHCl$_3$ (δ = 7.23). The electronic absorption spectra were recorded with a Hitachi U-2000 spectrophotometer using 1-cm quartz cells. Every product container was wrapped with aluminium foil and stored under an argon atmosphere to prevent photo-decomposition from exposure to light.

Analytical procedure

A 100 μg cm^{-3} stock solution of Zn(II)-chl-a and -b was prepared in glass-stoppered volumetric flasks, which were then sealed and stored at 5°C in the dark. Standard solutions for calibration graphs were prepared with a solvent composition as near to the sample as possible, by diluting the appropriate volume of the stock solution with a mixture of methanol and acetone (75:25, v/v). All sample solutions were filtered (0.2 μm) prior to injection into the chromatograph. The mobile phase was an isocratic mixture of HPLC-grade methanol and acetone (75:25, v/v). The analytical columns used were operated at ambient temperature with a flow-rate of 1.0 cm^3 min^{-1}.

RESULTS AND DISCUSSION

Identification of zinc(II) chlorophylls

Zinc(II) chlorophylls consist of a relatively hydrophilic zinc(II)–chlorin complex and a lipophilic phytyl group. Zn(II)-chl-a has a methyl group on the chlorin ring, whereas Zn(II)-chl-b
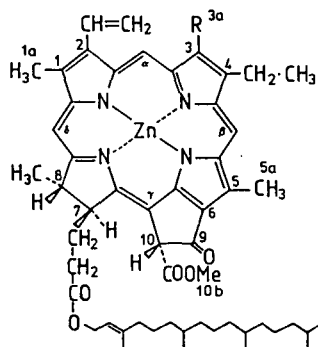
Fig. 1. Structure of zinc(II) chlorophylls. R = CH$_3$, Zn(II)-chl-a; R = CHO, Zn(II)-chl-b.

Fig. 3. Absorption spectra of zinc(II) chlorophylls. 1 = Zn(II)-chl-a; 2 = Zn(II)-chl-b.

has an aldehyde group (Fig. 1). This difference in the substituent attached to the chlorin ring causes a dramatic change in their spectroscopic properties and chromatographic behaviour.

The three-dimensional chromatogram of a mixture of zinc(II) chlorophylls is shown in Fig. 2. The absorption spectra of Zn(II)-chl-a and -b are very similar to those of the corresponding epimers, i.e., Zn(II)-chl-a' and Zn(II)-chl-b'. Further detailed observation revealed that the absorption spectra of the epimers are identical with those of their parent compounds. The absorption spectra give rise to only small red shifts of the Soret band on going from pheophytins to the corresponding zinc(II) chlorophylls. Typical absorption spectra of Zn(II)-chl-a and -b are presented in Fig. 3. The absorption maxima and molar absorptivities of these compounds have been given in a previous paper [14]. These spectroscopic characteristics were useful in the present HPLC and absorption spectrophotometric determination.
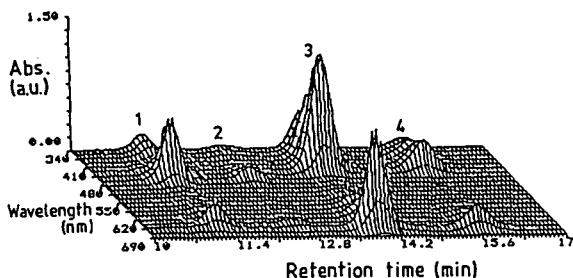
Fig. 2. Three-dimensional chromatogram of zinc(II) chlorophylls. 1 = Zn(II)-chl-b; 2 = Zn(II)-chl-b'; 3 = Zn(II)-chl-a; 4 = Zn(II)-chl-a'.

^{1}H NMR spectroscopy provides a good opportunity to identify each derivative of zinc(II) chlorophylls because their central zinc(II) ion is diamagnetic. The ^{1}H NMR spectra of zinc(II) chlorophylls and their epimers fractionated by semi-preparative HPLC were measured to confirm the identification of each peak component on the chromatogram. The proton resonance signals observed were assigned in analogy with those for pheophytins and chlorophylls [15] and the partial results of the assignments are summarized in Table I. It is noteworthy that the diamagnetic ring-current shifts of the meso-protons are accompanied by the formation of zinc(II) chlorophylls from pheophytins.

Chromatographic separation

Taking into account previous studies of chlorophylls [16,17] and metallochlorophylls [14], a reversed-phase ODS column in combination with a methanol–acetone mobile phase was chosen for zinc(II) chlorophylls. A good separation of Zn(II)-chl-a and -b and of their corresponding epimers was achieved on an ODS column with methanol–acetone (75:25, v/v) as the mobile phase (Fig. 2). The chromatogram of zinc(II) chlorophylls prepared under the present experimental conditions illustrates the appearance of Zn(II)-chl-a' and -b', i.e., the C-10 epimers of Zn(II)-chl-a and -b, respectively. As expected, Zn(II)-chl-b and -b' are eluted earlier than Zn(II)-chl-a and -a' because there is less interaction of the former with the non-polar ODS stationary phase. This elution order agrees with the general tendency that the aldehyde

TABLE I

^{1}H NMR CHEMICAL SHIFTS OF ZINC(II) CHLOROPHYLL a AND b

Zn(II)-chl-a			Zn(II)-chl-b		
δ (ppm)	Multiplicity	Proton	δ (ppm)	Multiplicity	Proton
9.52	s	β-H	9.16	s	β-H
9.29	s	α-H	9.41	s	α-H
8.45	s	δ-H	8.24	s	δ-H
6.11	s	10-H	6.04	s	10-H
3.88	s	10b-CH$_3$	3.99	s	10b-CH$_3$
3.64	s	5a-CH$_3$	3.57	s	5a-CH$_3$
3.33	s	1a-CH$_3$	3.42	s	1a-CH$_3$
3.21	s	3a-CH$_3$	10.20	s	3a-CHO

group attached to the chlorin ring is more polar than the methyl group. Hence the retention behaviour of zinc(II) chlorophylls is interpreted on the basis of both hydrophobic interactions between the phytyl group and the octadecyl chain of the ODS stationary phase and hydrophilic interactions between the chlorin ring including the aldehyde group and the mobile phase.

It is of interest to compare the retention behaviour of the Zn(II)-chls with that of normal chlorophylls [Mg(II)-chls] because the skeletal structures are very similar except for the central metal ion. A typical chromatogram obtained for a mixture of Zn(II)-chls and Mg(II)-chls with photometric detection at 425 nm, using an Inertsil ODS-2 column and a flow-rate of 1.4 cm^3 min^{-1}, is shown in Fig. 4. The peak of Zn(II)-chl-b overlaps partially with that of Mg(II)-chl-a,
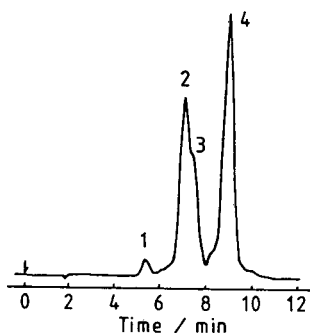
Fig. 4. Typical chromatogram of a mixture of Zn(II)-chls and Mg(II)-chls. 1 = Mg(II)-chl-b; 2 = Mg(II)-chl-a; 3 = Zn(II)-chl-b; 4 = Zn(II)-chl-a.

but the peak of Zn(II)-chl-a is well resolved from those of Mg(II)-chl-a and -b. Therefore, Zn(II)-chl-a in pure form can be used as an internal standard in the HPLC determination of native chlorophylls. Advantages are that Zn(II)-chl-a is relatively stable and can be easily prepared by the proposed method.

Determination of zinc(II) chlorophylls

Four kinds of zinc(II) chlorophylls, *i.e.*, Zn(II)-chl-a, -a', -b and -b', were fractionated on a semi-preparative ODS column with methanol–acetone (75:25, v/v) as the eluent. The calibration graphs for zinc(II) chlorophylls fractionated in pure form were constructed by analytical HPLC with a Uvidec-1000 variable-wavelength UV–Vis detector. The amounts of Zn(II)-chl-a, -a' and -b fractionated were sufficient to construct their calibration graphs, but the amount of Zn(II)-chl-b' was not. The linear range of the calibration graphs was 0–50 μg cm^{-3} for the three zinc(II) chlorophylls.

The detection limits of the HPLC method with visible detection at 425 nm were calculated from the amount of each zinc(II) chlorophyll which yielded a signal-to-noise ratio of 2. The minimum detectable concentrations were 3.5, 2.5 and 3.0 ng cm^{-3} for Zn(II)-chl-a, -a' and -b, respectively, with relative standard deviations ($n = 10$) of 1.92%, 2.19% and 1.49%, respectively.

For comparison purposes, calibration graphs for spectrophotometry with a Hitachi U-2000 spectrophotometer were constructed for Zn(II)-

chl-a, -a' and -b at 427, 427 and 455 nm, respectively. The detection limits calculated from the standard deviation at the lowest concentration level of the standard solution were 15, 14 and 16 ng cm^{-3} for Zn(II)-chl-a, -a' and -b, respectively. Hence the spectrophotometric method seems to be less sensitive to the determination of Zn(II)-chls than the proposed HPLC method, probably because of the differences in the analytical procedure and/or handling of the standard solutions. However, the detection limits of these two methods cannot be directly compared because the detector used and the definition of detection limit are different in each method.

Evaluation of analytical results

The RP-HPLC method proposed here was evaluated in comparison with the spectrophotometric method because the latter has been used as a conventional method for determination of chlorophylls [18] and metallochlorophylls [1]. The analytical HPLC method was applied to artificial samples prepared by mixing Zn(II)-chl-a and -b obtained by the semipreparative HPLC method. These artificial samples prepared using pure Zn(II)-chls were also analysed spectrophotometrically for comparison purposes. The analytical values obtained by the spectrophotometric method are plotted against those determined by the HPLC method in Fig. 5, where the concentrations of the artificial samples, *i.e.*, the mixtures of Zn(II)-chl-a and -b, are employed as analytical values instead of the content of each component. The slope of the regression line calculated for Zn(II)-chl-a was greater than unity: $y = 1.07x + 0.045$, with a correlation coefficient $r = 0.997$. The slope calculated for Zn(II)-chl-b was clearly larger than unity: $y = 1.32x + 0.085$ with $r = 0.999$. These results suggest that the spectrophotometric method overestimates the contents of Zn(II)-chl-a and -b at least under the present analytical conditions. This overestimation is ascribed to the partial overlapping of the absorption bands of Zn(II)-chl-a and -b (*cf.*, Fig. 3). In other words, the spectrophotometric determination of Zn(II)-chl-a could be subject to interference to some extent in the presence of Zn(II)-chl-b, although
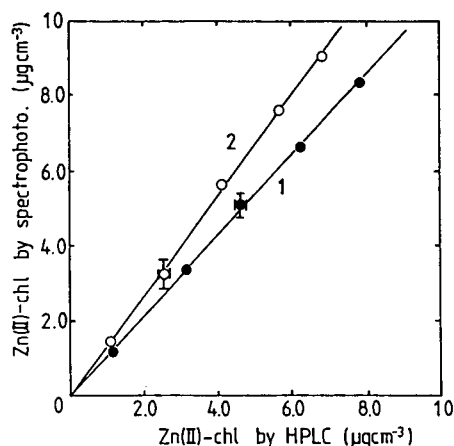
Fig. 5. Comparison of analytical results obtained by the HPLC method with those by the spectrophotometric method. The errors are expressed as bars on the plot of the averages for at least three independent determinations. 1 = Zn(II)-chl-a; 2 = Zn(II)-chl-b.

the exact composition of the mixture of Zn(II)-chl-a and -b can be calculated from the absorbances at the λ_{max} of each Zn(II)-chl using multiple-component software.

A typical plot of the analytical results obtained by the spectrophotometric method against those by the HPLC method is shown only for Zn(II)-chl-a and -b in Fig. 5, but a similar plot with a slope larger than unity was also obtained for Zn(II)-chl-a'. The comparison of the HPLC and spectrophotometric methods demonstrated that the RP-HPLC method developed here is an accurate and conventional method for the determination of zinc(II) chlorophylls.

ACKNOWLEDGEMENTS

REFERENCES

1 M. Ishidate and A. Tanimura, *Shokuhintenkabutsu-Kouteisho-Kaisetsusho*, Hirokawa Shoten, Tokyo, 1979, pp. B-655, B-678.
2 M. Sato, I. Fujimoto, T. Sakai, R. Kimura and T. Murata, *Yakugaku Zasshi*, 99 (1979) 1055.
3 M. Aizawa, H. Shinohara and S. Watanabe, *Denki Kagaku*, 50 (1982) 854.

4 T. Braumann and L.H. Grimme, *Biochim. Biophys. Acta*, 637 (1981) 8.

5 L.M. Brown, B.T. Hargrave and M.D. Mackinnon, *Can. J. Fish. Aquat. Sci.*, 38 (1981) 205.

6 T. Watanabe, A. Hongu, K. Honda, M. Nakazato, M. Konno and S. Saitoh, *Anal. Chem.*, 56 (1984) 251.

7 K. Furuya, H. Inoue and T. Shirai, *Anal. Sci.*, 3 (1987) 353.

8 K. Furuya, N. Ohki, H. Inoue and T. Shirai, *Chromatographia*, 25 (1988) 319.

9 H. Inoue, K. Furuya, K. Watanabe, K. Tanaka, T. Shirai and E. Miyoshi, *Anal. Sci.*, 4 (1988) 599.

10 P.H. Hynninen and S. Assandri, *Acta Chem. Scand.*, 27 (1973) 1473.

11 P.H. Hynninen, *Acta Chem. Scand.*, 27 (1973) 1487.

12 P.H. Hynninen, *Acta Chem. Scand., Ser. B*, 31 (1973) 829.

13 K. Iriyama, M. Shiraki and M. Yoshiura, *J. Liq. Chromatogr.*, 2 (1979) 255.

14 H. Yamashita and H. Inoue, *Anal. Sci.*, 7, Suppl. (1991) 1371.

15 P.H. Hynninen and S. Lotjonen, *Synthesis*, (1983) 705.

16 K. Iriyama and A. Yoshiura, *Tanpakushitsu Kakusan Kouso*, 24 (1979) 612.

17 L. Goeyens, E. Post, F. Dehairs, A. Vandenhoudt and W. Baeyens, *Int. J. Environ. Anal. Chem.*, 12 (1982) 51.

18 S.W. Jeffrey and G.F. Humphrey, *Biochem. Physiol. Pflanz.*, 167 (1975) 191.

Development of high-performance liquid chromatographic systems for the separation of radiolabelled carotenes and precursors formed in specific enzymatic reactions

Paul D. Fraser[*], Manuela Albrecht and Gerhard Sandmann[*]

Lehrstuhl für Physiologie und Biochemie der Pflanzen, Universität Konstanz, P.O. Box 5560, W-7750 Konstanz (Germany)

ABSTRACT

High-performance liquid chromatographic (HPLC) systems were developed to separate radiolabelled carotenes and precursors formed in the following carotenogenic enzyme reactions: geranylgeranyl pyrophosphate synthase, phytoene synthase, phytoene desaturase(s), lycopene cyclase and β-carotene hydroxylase. Separations were carried out on reversed- (C_{18}) and normal-phase columns, using mobile phase mixtures of acetonitrile, methanol and hexane with appropriate modifiers. An isocratic mode of elution was employed throughout, although in several instances isocratic steps were necessary to achieve the desired resolution. The methods developed are specific for each enzyme reaction, resolving substrate from its reaction products and any interfering radiolabelled compounds, thus permitting reliable and accurate determination of enzyme activities. The new separation systems will facilitate further studies on the characterization of these proteins.

INTRODUCTION

Carotenoids are naturally occurring pigments responsible for many of the yellow, red and orange colours distributed throughout nature [1]. Commercially they have found uses as natural colourants [2] and medically their antioxidant properties have been exploited in the treatment of certain cancers [3]. Inhibition of carotenoid biosynthesis in plants is also an important target of bleaching herbicides [4].

The biosynthesis and properties of carotenoids have been studied extensively over the past decade and general aspects of their formation are now well elucidated [5]. More recently, carotenoid genes from a variety of carotenogenic organisms have been isolated and characterized (see ref. 6 for a review). However, despite these notable advances in the field, our understanding of the biosynthetic enzymes and their regulation has not progressed with the same moment. A contributing factor to this void in our knowledge is the difficulties associated with assaying the enzymes involved. For example, their substrates are not available commercially and they are also unstable and insoluble in water, complicating their effective use in aqueous solution. One approach that circumvents some of these difficulties is the use of common isoprenoid substrates directly or provided by a coupled assay system [7,8] which typically exploits the ability of a cell extract usually from a carotenoid biosynthetic fungal mutant to produce the desired carotenoid *in situ*. This experimental approach has over-

---

* Corresponding author.
[*] Present address: Department of Biochemistry, Royal Holloway and Bedford New College, University of London, Egham, Surrey TW20 0EX, UK.

come many practical difficulties but is not ideal and necessitates rigorous purification of the reaction products and substrates to ensure radiochemical purity from radiolabelled compounds formed as a consequence of the initial heterogeneous substrate.

HPLC has become the analytical procedure of choice in the separation of carotenoid mixtures, although TLC separations must not be ignored. Papers describing such separations are relatively common and have recently been reviewed [9–11]. However, the problems associated with the separation of radiolabelled carotenes from their precursors have not been addressed to the same degree. When separating labelled carotenes formed in enzyme reactions, the routine separations typically used in analysis rarely fulfil the rigorous requirements necessary for the purification of radiolabelled reaction products. This paper describes HPLC systems developed for the separation of reaction products formed in specific carotenoid enzyme assays, permitting the reliable determination of different reaction products as a measure of specific enzyme activity.

EXPERIMENTAL

Carotenogenic enzyme assays

(R)-[2-^{14}C]Mevalonic acid lactone was converted into sodium mevalonate [8] and used as the initial substrate from which specific carotenogenic substrates were formed in situ using cell extracts prepared from a variety of fungal mutants. These mutants and their respective coupled substrates included the Neurospora crassa al-3 forming FPP, Gibberella fujikuroi SG4 producing GGPP and the Phycomyces blakesleeanus C5 carB10(−), C9 carR21(−) and C115 carS42mad-107(−) mutants yielding radiolabelled phytoene, lycopene and β-carotene, respectively. The precise experimental details concerning these assays have been extensively described [7,8,12].

Extraction of radiolabelled isoprenoids

Incubations were terminated with 6% KOH–methanol (1.5 ml) and heating for 20 min. The radiolabelled isoprenoids formed were then partitioned into 10% diethyl ether in light pe-

troleum (b.p. 35–80°C) (3 × 2.5 ml). To the pooled epiphases authentic unlabelled carotene standards were added in amounts ranging between 0.1 to 1 μg and the extract was evaporated to dryness under a stream of nitrogen. The residue was dissolved in acetone (20 μl) and any particulate material removed by centrifugation (2000 g for 3 min).

HPLC

An LKB Model 2150 HPLC pump (Pharmacia Biosystem, Freiburg, Germany) was used to pump the mobile phase at a constant flow-rate of 1.0 ml/min. Mobile phases were premixed to alleviate any problems resulting from irregularities in the pump mixing and degassed extensively by sonication prior to use.

The HPLC columns used to perform the separations included a normal-phase 3-μm Spherisorb silica column (250 × 4.5 mm I.D.), reversed-phase 5-μm ODS-1 and ODS-2 columns (250 × 4.6 mm I.D.), all obtained from Gynkotek (Germering, Germany), and a 3-μm Nucleosil C_{18} reversed-phase column (250 × 4.6 mm I.D.) from Macherey–Nagel (Düren, Germany). After prolonged use the columns were routinely washed with methanol. Further details of the specific separation systems used are provided under Results and Discussion.

Identification and determination of the radiolabelled carotenes separated by HPLC

An on-line radiodetector (Ramona LS, Raytest, Straubenhardt, Germany) was connected to detect radioactivity eluted from the column. A 1.5-ml flow cell together with Flo Scint A from Packard (Frankfurt, Germany) was used as a liquid scintillator. Integration of the peak areas and calibration by simultaneous collection of several eluted fractions and their counting in a liquid scintillation spectrometer permitted direct determination. Radiolabelled carotenes were identified by co-chromatography with authentic carotenes prepared using methods described previously [13]. The characteristic absorbance of the standards in the column eluate was monitored continuously with a Jasco Model 8201 programmable UV–visible spectrophotometer (Biotronik, Maintal, Germany). The spectral

properties and relative polarities were also used to aid the identification of carotenoid isomers [14]. The radiochemical purity of the eluted compounds was determined by separation using several HPLC and TLC systems as described previously [15].

Chemicals

(*R*)-[2-^{14}C]Mevalonic acid lactone was purchased from Amersham Buchler (Braunschweig, Germany) and farnesol from Sigma (Munich, Germany). The following HPLC-grade solvents were used: acetonitrile (from Lab-Scan, Stillorgan, Ireland), methanol, 2-propanol, ethyl acetate and hexane (all from Merck, Darmstadt, Germany) and water. Carotenes were isolated from natural sources as described [13].

RESULTS AND DISCUSSION

The water-soluble substrates mevalonic acid and isopentyl pyrophosphate can be metabolized to a wide range of isoprenoids [16]. As a consequence, numerous isoprenoids in addition to the specific substrates used in the carotenogenic assays are formed. Typically sterols and their precursors, a range of prenyl alcohols and carotenoid oxidative products are formed by the fungal extracts used in coupled assays. Such compounds share similar physical chemical properties with the carotenoids of interest and are therefore partitioned into the crude lipid extract and possess similar chromatographic properties. In this paper we focus on the HPLC systems developed during our studies on carotenogenic enzymes that can be utilized to achieve radiochemical purity of the substrates and their products formed. For convenience the chromatographic conditions of these systems are comprehensively summarized in Table I and are arranged and described below according to the reactions of the biosynthetic pathway.

TABLE I

HPLC SEPARATION OF RADIOLABELLED CAROTENES FORMED IN CAROTENOGENIC ENZYME ASSAYS

Abbreviations: RP = reversed phase; NP = normal phase; ACN = acetonitrile; EA = ethyl acetate; MeOH = methanol; 2-PrOH- = 2-propanol; Bdh-Lycop. = bisdehydrolycopene; Car. = carotene; Lycop. = lycopene; Neurosp. = neurosporene; Phyt. = phytoene; Phytofl. = phytofluene; Zeax. = zeaxanthin; *t-* = *trans-*; *c-* = *cis-*.

Enzymatic assay	Separation system		Substrate	Retention time (min)	Products	Retention time (min)
	Mobile phase	Support				
(A) GGPP synthase	Isocratic: MeOH–H$_2$O (90:10)	5-μm Spherisorb ODS-1 (RP)	FPP[a]	6.5	GGPP[b]	11.0
(B) Phytoene synthase	Isocratic + solvent change: (A) ACN–MeOH (98:2), 10 min; (B) ACN–MeOH– 2-PrOH (85:10:5)	5-μm Spherisorb ODS-1 (RP)	GGPP[b]	4.5	*c*-Phyt. *t*-Phyt.	28.5 30.0
(C) Phytoene desaturase(s)						
(I) Phyt. to ζ-Car.	Isocratic: ACN–MeOH– 2-PrOH (85:10:5)	3-μm Nucleosil C$_{18}$ (RP)	*c*-Phyt.	40	*t*-ζ-Car. *c*-ζ-Car. *c*-ζ-Car. *t*-Phytofl. *c*-Phytofl.	27.5 28.0 30.0 36.0 37.5

TABLE I *(continued)*

Enzymatic assay	Separation system		Substrate	Retention time (min)	Products	Retention time (min)
	Mobile phase	Support				
(II) Phyt. to Lycop.	Isocratic: EA–ACN–H$_2$O (35:60:5)	3-μm Nucleosil C$_{18}$ (RP)	c-Phyt.	32	Bdh-Lycop.	13.0
					t-Lycop.	15.5
					t-ζ-Car.	21.0
					c-ζ-Car.	22.0
					c-ζ-Car.	23.0
					t-Phytofl.	25.5
					c-Phytofl.	26.5
	Isocratic + solvent change: (A) ACN–MeOH (98:2) 0–10 min; (B) EA–ACN–H$_2$O (25:70:5), 10–20 min; (C) MeOH	3-μm Nucleosil C$_{18}$ (RP)	c-Phyt.	55	Lycop.	25.0
					ζ-Car.	35.0
(III) Phyt. to Neurosp.	Isocratic + solvent change: (A) ACN–MeOH–H$_2$O (94:2:4), 0–20 min; (B) ACN–MeOH–2-PrOH (85:10:5), 20–40 min; (C) MeOH	3-μm Nucleosil C$_{18}$ (RP)	c-Phyt.	72	t-Neurosp.	50.0
					c-Neurosp.	52.0
					t-ζ-Car.	57.0
					c-ζ-Car.	59.0
					t-Phytofl.	66.0
					c-Phytofl.	68.0
(D) Lycopene cyclase	Isocratic: ACN–MeOH–2-PrOH (85:10:5),	5-μm Spherisorb ODS-2 (RP)	t-Lyc.	21	t-β-Car.	37.0
					c-β-Car.	40.0
	Isocratic: EA–ACN–H$_2$O (35:60:5)	3-μm Nucleosil C$_{18}$ (RP)	Lycop.	17	γ-Car.	22.0
					t-β-Car.	28.0
					c-β-Car.	30.0
(E) β-Carotene hydroxylase	Isocratic + solvent change: (A) hexane, 0–14 min; (B) EA–hexane (20:80), 14–34 min; (C) EA–hexane (50:50)	3-μm silica (NP)	β-Car.	4	Monohydrox. products	32–38
					t-Zeax.	48.0
					c-Zeax.	52.0

[a] Farnesyl pyrophosphate (FPP) determined as alcohol.
[b] Geranylgeranyl pyrophosphate (GGPP) determined as alcohol.

Geranylgeranyl pyrophosphate synthesis

The enzyme geranylgeranyl pyrophosphate (GGPP) synthase condenses isopentenyl pyrophosphate (IPP) to farnesyl pyrophosphate (FPP) (C_{15}) yielding the C_{20} product GGPP. The substrates for the reaction can be supplied by the al-3 *Neurospora crassa* mutant [12]. These diphosphate compounds can be converted into their alcohol derivatives by acid hydrolysis or naturally as a consequence of inherent phosphatase activity. The principle compounds posing interference to the purification of FOH and GGOH are other prenyl alcohols and their respective isomers of differing chain lengths. To separate such compounds, a methanol-based mobile phase containing 10% of water to alter the polarity was employed [Table I (A)]. Development on a reversed-phase 5-μm ODS-1 column separates these compounds on the basis of their aliphatic chain length, with increases in chain length prolonging their retention on the column. Such a system has proved ideal in the determination of GGPP synthase activity in chloroplast stromal extracts and more recently in an *Escherichia coli* strain expressing the *Erwinia uredovora crtE* gene [17].

Phytoene synthesis

Phytoene synthesis is the first specific reaction in the carotenoid biosynthetic pathway and the enzyme is a characteristic marker of the chloroplast stroma. A typical trace of a chloroplastic phytoene synthase assay is illustrated in Fig. 1A. In this instance the *Gibberella fujikuroi* SG4 mutant was used to provide the substrate GGPP and the solvents consisted of two acetonitrile-based mixtures. After good separation of the prenyl alcohols from each other, a switch from the first to the second solvent was carried out in order to obtain a good and fast resolution of the two phytoene isomers. When the assay mixture is separated on a 5-μm C_{18} reversed-phase column the alcohol derivative of the substrate is detected at a retention time of 4.5 min. The products 15-*cis*-phytoene and all-*trans*-phytoene eluted at 28.5 and 30 min, respectively [Table I (B)]. These compounds of interest are clearly separated from interfering radiolabelled compounds
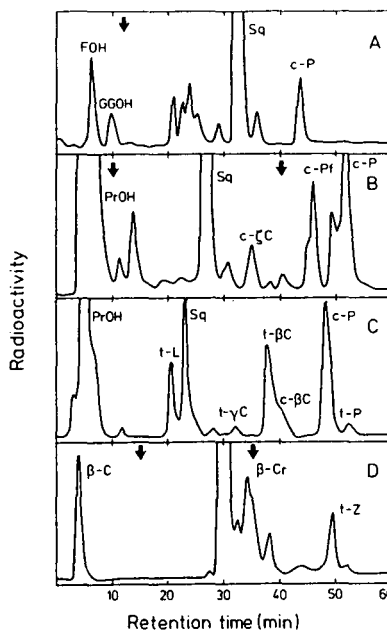
Fig. 1. Selected HPLC traces of radiolabelled carotenoids formed *in vitro* along the biosynthetic pathway. (A) Conversion of FPP to phytoene (chloroplast extract); (B) conversion of phytoene to ζ-carotene (*E. coli*/pds); (C) conversion of lycopene to β-carotene (*Synechococcus*); (D) conversion of β-carotene to zeaxanthin (*Synechococcus*). The HPLC systems used were as follows: (A) 5-μm Spherisorb ODS-1 with methanol–water (90:10) for 12 min, then acetonitrile–methanol-2-propanol (85:10:5); (B) 3-μm Nucleosil C_{18} with acetonitrile–methanol (98:2) for 10 min, then ethyl acetate–acetonitrile–water (25:70:5) until 40 min, then methanol; (C) 5-μm Spherisorb ODS-2 with acetonitrile–methanol-2-propanol (85:10:5); (D) 3-μm Spherisorb silica with hexane for 14 min, then ethyl acetate–hexane until 34 min, then methanol.

derived from the biosynthetic capabilities of the fungal extract.

Phytoene desaturation reactions

During carotenoid biosynthesis, phytoene undergoes a series of desaturations, the enzyme or enzymes responsible for this conversion being phytoene desaturase. Several functionally diverse desaturases form different reaction products and intermediates [18]. The complete resolution of all carotenes formed, including their isomers, is difficult to achieve with a single system. Therefore, it has been necessary to develop specific separation methods based on the

characteristic reaction products formed by each desaturase. One of the principal problems in such separations is the presence of squalene, a sterol precursor. This compound is an example of a molecule whose behaviour in numerous chromatographic systems does not adhere to that predicted for its relative polarity. As a consequence, it co-migrates with desaturase products on many typical carotenoid-separating systems. The incorporation of radioactivity by the fungal coupling extract into squalene is relatively substantial (Fig. 1). This has a secondary effect of masking any adjacent compounds poorly resolved which are present at low levels.

The numerous systems that have been developed for specific desaturase types are listed in Table I (C). For example, the products of a desaturase-converting phytoene (supplied by the C5 *Phycomyces* mutant) to ζ-carotene can be resolved on a 3-μm Nucleosil column using the mobile phase of Märki-Fischer *et al.* [19], *i.e.*, acetonitrile–methanol–2-propanol (85:10:5, v/v/v), as indicated in section I in Table I (C). This separation has been illustrated in a recent publication [20] and is ideal for analysing the typical desaturases from photosynthetic organisms such as the pds of *Synechococcus*. An even better separation of all the reaction products and their isomers as well as the substrate can be obtained in a more complicated system which involves three different solvents which are changed after a certain period as indicated in Fig. 1B. With this procedure the setting up of a gradient system can be avoided. This technique of changing solvents during the HPLC separation of carotenoids has already been successfully employed [21]. The 3-μm Nucleosil C_{18} column used in this and in the following desaturase assays gave good separations of *cis–trans* carotene isomers in shorter runs than described for HPLC separations on Zorbax ODS columns [22].

The *Erwinia uredovora* desaturase is typical of a desaturase that converts phytoene into lycopene (*i.e.*, the introduction of four double bonds). To achieve the effective separation of the reaction products the inclusion of ethyl acetate and water as modifiers of an acetonitrile-based solvent and the use of a 3-μm support

were necessary [Table I (C), section II]. Such a system permits the separation of lycopene from squalene, which is an important achievement in the accurate determination of such desaturase activity; this system has been illustrated recently [23]. The migration of the products in this system can be altered slightly to suit more specific requirements by keeping the water content constant and altering the level of ethyl acetate. Another advantageous feature of the system is the speed of the separation, *ca.* 35 min, in which excellent resolution is achieved. One disadvantage of this system, however, is the presence of an unknown compound, believed to be an epoxide from its chromatographic behaviour, whose presence in close proximity to the lycopene can mask low lycopene levels. To overcome this problem, the absence of water from the initial acetonitrile-based mixture can alleviate such an occurrence and the three-phase system described in section II in Table I (C) has to be used. This particular system is also suited to the separation of the ζ-carotene desaturase reaction where only small amounts of lycopene are found owing to the limiting ζ-carotene level. An example of such a system is shown in Fig. 1B where the *Synechococcus* pds was assayed.

The final type of desaturase found in some photosynthetic bacteria such as *Rhodobacter* is one responsible for the desaturation of phytoene to neurosporene. As discussed previously, the main prerequisite in achieving an effective system is the resolution of neurosporene, the principal desaturase product from squalene. Using a system described in Table I (C), section III, this has been achieved and recently illustrated [24].

Lycopene cyclization

The cyclization of lycopene to β-carotene can be assayed using the C9 *Phycomyces* mutant to prepare [^{14}C]lycopene *in situ*. In general, HPLC systems that separate desaturase products are also applicable to the cylase [*e.g.*, the three-step system described in section II in Table I (C)]. However, two less complicated isocratic HPLC systems which basically differ in the stationary phase material and the particle size [Table I (D)] are more convenient for lycopene cyclase assays.

Both systems give a good example of how diverse reversed-phase supports can also be used to attain an efficient system. A very detailed study of the chromatographic behaviour of carotenoids on different reversed-phase columns has recently been published [25].

A typical trace of a cyclase assay developed on an ODS-2 column with an acetonitrile mixture is illustrated in Fig. 1C. The substrate lycopene (21 min) is resolved adequately from squalene (25 min), with the monocyclic products of the reaction eluting at 33 min and the bicyclic β-carotene at 38 min. Also illustrated clearly is the resolution of *cis*-phytoene (48 min) from *trans*-phytoene (53 min).

β-Carotene hydroxylation

The final enzyme-catalysed reaction in most carotenogenic organisms is the hydroxylase. This enzyme introduces two hydroxy moieties into the β-carotene molecule, forming zeaxanthin, thus altering the polarity of the carotene considerably. Xanthophylls such as zeaxanthin are very weakly adsorbed on reversed-phase columns in the typical solvents used for carotenoid separations. Hence, in order to separate the radiolabelled products and substrates formed in the hydroxylase reaction, it is necessary to use a normal-phase silica column. An example of a typical trace is illustrated in Fig. 1D and the chromatographic conditions are defined in Table I (E). It can be seen that the substrate elutes from the column initially at the start and then after a progressive stepwise gradient the zeaxanthin (49 min) is eluted with ethyl acetate–hexane (50:50).

CONCLUSIONS

This paper has described the separation of radiolabelled carotenes formed in specific carotenogenic enzyme assays by HPLC. It is worth addressing as a separate entity to traditional analyses of carotenoids by HPLC as such systems rarely fulfil the rigorous purification requirements. The systems described for GGPP synthase, phytoene synthase, phytoene desaturase, lycopene cyclase and β-carotene hydroxylase are reproducible and can be used in a routine mode. In addition, they can be used for the separation of the intermediates and products formed by the *Synechococcus in vitro* carotenogic enzyme system in the presence of bleaching herbicides, which provides an excellent insight into their mode of action [26]. Some of the HPLC separation systems described have already been successfully employed for assays of carotenogenic enzymes which have been purified very recently [20,23] and the others will be needed in the near future when more enzymes of this pathway will be functionally characterized after purification.

REFERENCES

1 T.W. Goodwin, *Annu. Rev. Nutr.*, 6 (1986) 273–298.
2 R.F. Taylor, in *Spectrum Food Industry*, Decision Resources, MA, 1990, pp. 12.1–12.11.
3 M.M. Matthews-Roth, in *New Protective Notes for Selected Nutrients*, Alan R. Liss, New York, 1989, pp. 17–38.
4 G. Sandmann and P. Böger, in P. Böger and G. Sandmann (Editors), *Target Sites of Herbicide Action*, CRC Press, Boca Raton, FL, 1989, pp. 25–44.
5 P.M. Bramley, *Methods Plant Biochem.*, 9 (1993) 281–297.
6 G. Sandmann, *Physiol. Plant.*, 83 (1991) 186–193.
7 G. Sandmann and P.M. Bramley, *Planta*, 164 (1985) 259–263.
8 P.D. Fraser and G. Sandmann, *Biochem. Biophys. Res. Commun.*, 185 (1992) 9–15.
9 P.M. Bramley, *Phytochem. Anal.*, 3 (1992) 97–104.
10 G. Britton, *Methods Plant Biochem.*, 7 (1991) 473–518.
11 C.A. O'Neil and S.J. Schwartz, *J. Chromatogr.*, 624 (1992) 235–252.
12 G. Sandmann, N. Misawa, M. Wiedemann, P. Vittorioso, A. Carattoli, G. Morelli and G. Macino, *J. Photochem. Photobiol. B*, 18 (1993) 245–251.
13 S. Ernst and G. Sandmann, *Arch. Microbiol.*, 150 (1988) 590–594.
14 B.H. Davies, in T.W. Goodwin (Editor), *Chemistry and Biochemistry of Plant Pigments*, Vol. 2, Academic Press, New York, 2nd ed., 1976, pp. 38–165.
15 A. Schmidt and G. Sandmann, *J. Bacteriol.*, 172 (1990) 4103–4105.
16 P.M. Bramley and A. Mackenzie, *Curr. Top. Cell Regul.*, 29 (1988) 291–343.

17 G. Sandmann and N. Misawa, *FEMS Microbiol. Lett.*, 90 (1992) 253–258.

18 H. Linden, N. Misawa, D. Chamovitz, I. Pecker, J. Hirschberg and G. Sandmann, *Z. Naturforsch., Teil C*, 46 (1991) 1045–1051.

19 E. Märki-Fischer, U. Marti, R. Buchecker, C.H. Eugster, *Helv. Chim. Acta*, 66 (1983) 494–513.

20 P.D. Fraser, H. Linden and G. Sandmann, *Biochem. J.*, 291 (1993) 687–692.

21 J. De Las Rivas, J.C.G. Milicua and R. Gomez, *J. Chromatogr.*, 585 (1991) 168–172.

22 M.H. Saleh and B. Tan, *J. Agric. Food Chem.*, 39 (1991) 1438–1443.

23 P.D. Fraser, N. Misawa, H. Linden, S. Yamano, K. Kobayashi and G. Sandmann, *J. Biol. Chem.*, 267 (1992) 19891–19895.

24 G. Sandmann, P.D. Fraser and H. Linden, in N. Murata (Editor), *Research in Photosynthesis*, Vol. III, Kluwer, 1992, pp. 51–54.

25 K.S. Epler, L.C. Sander and R.G. Ziegler, *J. Chromatogr.*, 595 (1992) 89–101.

26 G. Sandmann and P. Böger, in P. Böger and G. Sandmann (Editors), *Target Sites of Herbicide Action*, CRC Press, Boca Raton, FL, 1989, pp. 25–44.

Sensitive detection of nicotine after its novel perfluoroacylation and analysis using capillary gas chromatography–electron-capture detection

James M. Moore*, Donald A. Cooper, Theodore C. Kram and Robert F.X. Klein

Special Testing and Research Laboratory, US Drug Enforcement Administration, 7704 Old Springhouse Road, McLean, VA 22102-3494 (USA)

ABSTRACT

The on-column chromatographic detection of nicotine at low picogram levels is described. Nicotine is first subjected to chemical derivatization with heptafluorobutyric anhydride in the presence of pyridine. In the absence of pyridine, the derivatization reaction is markedly retarded. This high-yield reaction results in the opening of the N-methylpyrrolidine ring of nicotine with concomitant formation of a highly electrophilic N,O-diheptafluorobutyryl derivative. After extraction of the nicotine derivative into isooctane, it is subjected to splitless capillary gas chromatographic analysis using a ^{63}Ni electron-capture detector and a moderately polar fused-silica capillary column. The nicotine derivative can be detected on-column at levels below 5 pg.

INTRODUCTION

Nicotine, **1**, an N-methylpyrrolidine-substituted pyridine alkaloid of *Nicotiana Tabacum*, has been the subject of numerous studies. We have reviewed 36 selected references that describe the analyses of **1** in a variety of matrices [1–36]; most address the detection of **1** and/or its metabolites in biological specimens, including plasma [4,6–13,16,17,20,23,24,26,28,30,35,36], blood [1,3,13], urine [5,7,13,16,19–21,24–27, 29,30,32,34], saliva [7,11] and tissue [15]. Similar methods have been applied for the detection of **1** in tobacco [14], allergenic extracts of tobacco [18], environmental samples [9,31,33] and neat [2,22]. Due to recent concerns over the passive inhalation of tobacco smoke, detection of environmental contamination by **1** has come into sharp focus [31,33]. Of the various methods reviewed, all but one [25] were chromatographic,

with twenty-one utilizing gas chromatography (GC) [1–4,6–13,15–17,20,23,24,30,31,35,36] and thirteen employing high-performance liquid chromatography (HPLC) [5,14,18,19,21,22,26–29,32–34]. Of the GC methods reviewed, twelve utilized nitrogen–phosphorous detection [4,7,9–13,15,17,23,30,31], six employed mass spectrometry (MS) [6,15,20,30,35,36], three utilized flame ionization detection [1,3,16] and three employed electron-capture detection (ECD) [2,8,24]. Six of the HPLC procedures relied upon UV detection [5,14,18,19,21,33], while radiometric detection [26], electrochemical detection [22,28] and MS [34] were used in four methods. Finally, in three instances HPLC analyses were preceded by chemical derivatization (ChD) to give colored products which were subsequently measured in the visible range [27,29,32].

In general, GC analysis of **1** and its congeners was superior to HPLC in terms of on-column detectability and specificity. Typical GC on-column minimum detectable quantity (OC-

---

* Corresponding author.

MDQ) levels were usually in the 50–100 pg range, with a few methods reporting lower than 10 pg [8,9,13,17] and one method below 100 fg [36]. The highest specificities were observed with high-resolution capillary columns and element-specific or, especially, MS detectors. In contrast to GC, typical OC-MDQs for HPLC ranged from 100 pg to over 10 ng. However, the overall methodology MDQ (MTH-MDQ) was still reasonably sensitive due to the much larger HPLC injection volumes. In addition, HPLC was better suited for the analysis of certain highly polar metabolites of 1 (e.g., nicotine N-oxide), which either do not chromatograph or exhibit poor chromatographic behavior using GC.

Our interest in 1 has been peripheral and evolved during investigations into the detection of coca alkaloids in refined, illicit cocaine samples, in particular the N-methylpyrrolidine alkaloids hygrine and cuscohygrine. Specifically, we were interested in determining whether either alkaloid underwent high-yield heptafluoro-butyrylation at a carbon site for subsequent analysis using capillary gas chromatography-electron-capture detection (cGC–ECD). We have previously reported such unusual acylation/derivatization reactions for the cGC–ECD analyses of fentanyl [37], morphine N-oxide and didehydroheroin [38]. Since hygrine and cuscohygrine were not commercially available, the N-methylpyrrolidine-substituted alkaloid nicotine, 1, was utilized as a model compound.

Herein, we report the successful derivatization of 1 with heptafluorobutyric anhydride (HFBA) in the presence of pyridine. The resultant derivative exhibited excellent chromatographic behavior and was extremely sensitive towards cGC–ECD analysis, with an OC-MDQ below 5 pg. The overall methodology represented a significant improvement over most existing procedures in terms of on-column detectability.

EXPERIMENTAL

Standards, solvents and chemicals

Nicotine, 1 (98%), was obtained from the Aldrich (Milwaukee, WI, USA). Other drug standards were acquired from the standards collection of the Special Testing and Research Laboratory, US Drug Enforcement Administration (McLean, VA, USA). All solvents except water were distilled-in-glass products of Burdick and Jackson (Muskegon, MI, USA). Aldrin (utilized as an internal standard) was obtained from Supelco (Bellefonte, PA, USA). HFBA, supplied in 1-ml ampules, was obtained from Pierce (Rockford, IL, USA). All other chemicals were reagent grade.

Glassware

All derivatization reactions and extractions were performed in either 5- or 15-ml glass-stoppered centrifuge tubes. Prior to use, the tubes were treated with hot Nochromix (commercial oxidant)–sulfuric acid solution, rinsed with water, methanol and acetone and dried under vacuum.

Capillary gas chromatography–electron-capture detection

All chromatograms were generated in the splitless mode using two Hewlett-Packard Model 5880 gas chromatographs interfaced with Hewlett-Packard Level IV data processors; both were equipped with ^{63}Ni electron-capture detectors (15 mCi). For the initial phase of this study, gas chromatograph No. 1 was fitted with a 15 m × 0.25 mm I.D. fused-silica capillary column coated with DB-5 + (0.25 μm) (J&W Scientific, Rancho Cordova, CA, USA). The oven temperature was multilevel programmed as follows: (level 1) initial temperature, 90°C, initial hold, 1.0 min; temperature program rate, 25°C/min; final temperature, 200°C; final hold, 1.0 min; (level 2) temperature program rate, 4.0°C/min; final temperature, 275°C; final hold, 10 min. In the latter part of this investigation, the 15-m DB-5 + column was replaced by a 30 m × 0.25 mm I.D. column coated with DB-5 (0.25 μm). Gas chromatograph No. 2 was fitted with two separate 30 m × 0.25 mm I.D. fused-silica capillary columns coated with DB-1 (0.25 μm) and DB-1701 (0.25 μm), respectively. For all three 30-m columns, the oven temperatures were multilevel programmed as follows: (level 1) initial temperature, 90°C, initial hold, 1.5 min; temperature program rate, 25°C/min; final tem-

perature, 170°C; final hold, 1.0 min; (level 2) temperature program rate, 4.0°C/min; final temperature, 275°C; final hold, 30 min. Injector and detector temperatures were maintained at 200 and 300°C, respectively. Hydrogen (Zero Grade, Roberts Oxygen, Merrifield, VA, USA) was used as the carrier gas at a linear velocity of between 35–45 cm/s and measured for isooctane at an oven temperature of 90°C. An argon–methane (95:5) mixture (Roberts Oxygen) was the make-up gas at a flow-rate of between 30 and 40 ml/min. During the splitless injection, the solvent was vented after a 1.0-min hold. Chart speeds and attenuation settings are given in the appropriate figures.

Capillary gas chromatography–mass spectrometry

Low-resolution electron ionization (EI) and negative chemical ionization (NCI) mass spectra were acquired on a Finnigan-MAT Model 4630 (San Jose, CA, USA) quadrupole mass spectrometer. In the initial phase of this study, the cGC–MS was fitted with a 15 m × 0.25 mm I.D. fused-silica capillary column coated with either 0.25 μm DB-1 or DB-5. In the latter part of this investigation, a 15 m × 0.25 mm I.D. fused-silica capillary column coated with 0.25 μm RT$_x$-200-Methyl Trifluoropropyl (Restek, Bellefonte, PA, USA) was used. Sample injection was accomplished with an on-column injector (J&W Scientific) at a helium carrier velocity of 60 cm/s for methane. All EI data were acquired at an ionization potential of 60 eV at a source temperature of 120°C (uncorrected). All NCI data were acquired via cGC introduction of the sample; methane was utilized as the reagent gas. The source temperature was 80°C (uncorrected).

^{1}H and ^{13}C nuclear magnetic resonance (NMR) spectroscopy

All NMR spectra were obtained in deuterated chloroform on a Bruker AM-30 WB NMR spectrometer operating at 300.1 MHz for ^{1}H and 75.5 MHz for ^{13}C. Tetramethylsilane was utilized as an internal calibration standard. Gated decoupled ^{13}C, ^{1}H–^{1}H COSY and ^{1}H–^{13}C HETERO-COSY experiments were run using standard Bruker software.

Infrared spectroscopy

A Beckman 4240 infrared spectrometer and KBr plates were used in the recording of all infrared (IR) spectra.

Standard solutions

Solution A. An anhydrous acetonitrile solution of **1** at a concentration of 0.10 mg/ml.

Solution B. An aliquot of solution A diluted with anhydrous acetonitrile to a concentration for **1** of 25 ng/ml.

Solution C. An anhydrous acetonitrile solution of **1** (0.10 mg/ml), ephedrine (0.10 mg/ml), methamphetamine (0.20 mg/ml), and tetracaine (0.20 mg/ml).

Derivatization procedures

Microgram level. To 1.0 ml of standard solution A or C in a 15-ml glass-stoppered centrifuge tube was added 50 μl of HFBA. After vortexing, 100 μl of pyridine was added. After again vortexing, the solution was heated at 75°C for 15 min. After cooling, 8.0 ml of isooctane (containing aldrin at 100 pg/μl) and 5 ml of saturated aqueous sodium bicarbonate were added. The tube was immediately shaken vigorously for 5–10 s and then centrifuged at 2000 rpm (796 g) for 5 min. The isooctane extract was isolated and dried over anhydrous sodium sulfate. A 1.0 ml aliquot of the isooctane extract was diluted to an appropriate volume with additional isooctane (containing aldrin internal standard at 100 pg/ μl). About 2 μl of the final isooctane extract was injected into the cGC–ECD under conditions described under Experimental.

Nanogram level. For determination of MTH-MDQ, 200 μl of standard solution B was dispensed into a 5-ml glass-stoppered centrifuge tube. To the tube was added 10 μl of a solution containing 10% (v/v) HFBA in anhydrous acetonitrile followed by 10 μl of a solution containing 20% (v/v) pyridine in acetonitrile. After vortexing, the solution was heated at 75°C for 75 min. After cooling, 2–3 ml of petroleum ether (containing aldrin internal standard at 100 pg/μl) and 1 ml of saturated aqueous sodium bicarbonate were added. The tube was immediately shaken vigorously for 5–10 s and then centrifuged. The petroleum ether extract was passed

through anhydrous sodium sulfate into another tube and evaporated just to dryness (55–65°C/ N_2). The residue was reconstituted in 100 μl of ethyl acetate at about 75°C for 2 min, and about 2 μl of the resulting solution was injected into the cGC–ECD under the conditions described in the Experimental section.

RESULTS AND DISCUSSION

Nicotine derivatization reaction and structural elucidation of product

Reaction of **1** with HFBA in the presence of pyridine resulted in scission of the C2'–N bond and addition of heptafluorobutyryl (HFB) and heptafluorobutyryloxy [HFB(O)] moieties to the molecule, giving **2**. This reaction is illustrated in Fig. 1. The ring cleavage was highly unusual and in sharp contrast with our previously reported HFBA derivatization of nitrogen heterocycles, wherein the nitrogen-containing ring remained intact and the reaction resulted in formation of a ring-substituted HFB-vinylogous amide with HFB attachment at a carbon site [37,38]. We have additionally observed that when the N-

methylpyrrolidine-containing compound hygrinol, obtained by lithium aluminum hydride reduction of hygrine, was subjected to similar HFBA derivatization, the N-methylpyrrolidine ring also remained unopened, with HFB attachment at a carbon site [39]. These results strongly suggested that the presence of the aromatic ring at the α carbon in nicotine directed the HFBA derivatization reaction towards an alternate, previously unknown reaction pathway (Fig. 1).

Structural confirmation of the nicotine derivatization product was accomplished as follows. Milligram quantities of **2** were prepared and subjected to cGC–MS, ^{1}H and ^{13}C NMR and IR analyses.

GC–MS. The mass spectrum of the perfluorinated nicotine derivative, illustrated in Fig. 2, was acquired using three different capillary columns, coated with DB-1, DB-5 and RT_x-200; all were found to be similar. The EI spectrum of **2** displayed an $M^{+\cdot}$ at $m/z = 572$, which was confirmed by an intense $M^{-\cdot}$ at $m/z = 572$ under negative chemical ionization conditions. This molecular mass corresponds to incorporation of an HFB and an HFB(O) group into **1** with concomitant opening of the N-methylpyrrolidine ring. Fragment ions in the EI spectrum occurring at $m/z = 553$, 375 (base peak) and 359 are probably due to losses of F, HFB and HFB(O), respectively. Cleavage at C2'–C3' and C3'–C4' is believed to give rise to ions at $m/z = 304$ and 318, respectively, with charge retention on the pyridinyl-containing moiety. An intense fragment ion at $m/z = 240$ is probably due to fission of the C4'–C5' bond with charge retention on the HFB-amide moiety.

In order to confirm the presence of an HFB(O) substituent, **2** was subjected to hydrolysis with warm methanol. After removal of the solvent, the residue was divided into two equal aliquots, with one-half being treated with N,O-bis(trimethylsilyl)acetamide (BSA) and the other half treated with [2H₉]BSA, the deuterated analogue of BSA. The EI-MS spectrum of the resultant trimethylsilyl (TMS) derivative yielded the expected molecule ion at $m/z = 448$, which shifted to $m/z = 457$ as the [2H₉]TMS derivative, suggesting the new derivative to be N-HFB-O-TMS-nicotine. The base peak fragment ion at
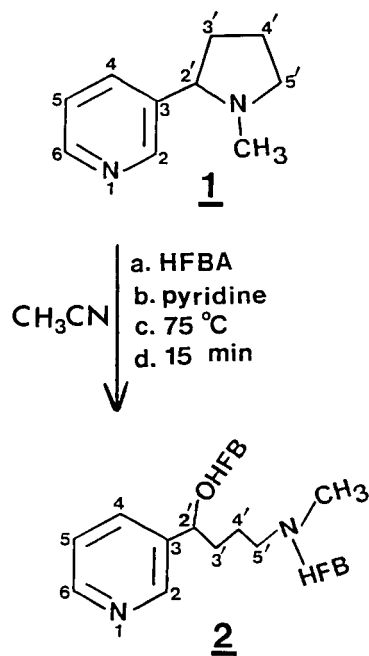

Fig. 1. Derivatization of nicotine with heptafluorobutyric anhydride in the presence of pyridine.
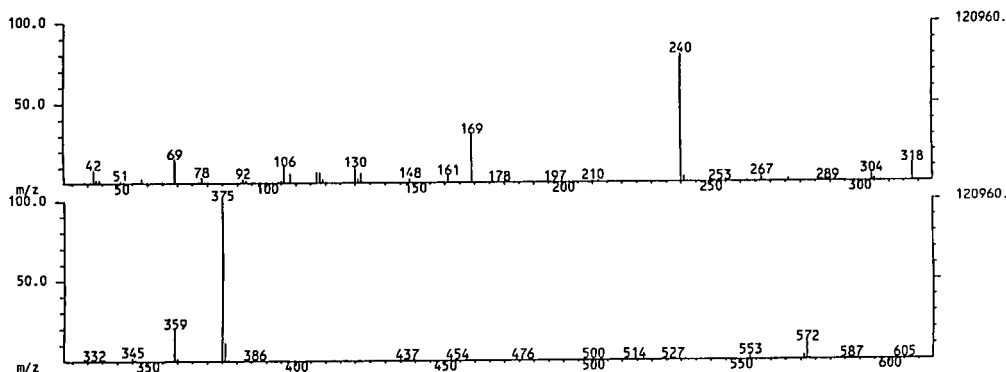
Fig. 2. Electron ionization mass spectrum of N,O-di-HFB-nicotine. Column: 15 m × 0.25 mm I.D. Rt$_x$-200.

$m/z = 180$ for this derivative supported an assignment of the HFB(O) group at C2'. This ion probably arises from cleavage of C2'–C3' bond with charge retention on the pyridinyl-CH$_2$-OTMS moiety. As expected, the ion at $m/z = 180$ is shifted 9 u for the [^{2}H$_9$]TMS derivative.

^{1}H and ^{13}C NMR. One- and two-dimensional NMR analyses, confirmed the ring-opened structure of **2**, as seen in Table I. The ^{1}H and ^{13}C resonances of the pyridinyl ring substituent were only slightly perturbed from **1** [40]. In the aliphatic chain, the protons displayed complex multiplets at 6.0(1H), 3.5(2H), 1.9(2H), and 1.7(2H) ppm, assigned as C$_{2'}$–H$_1$, C$_{5'}$–H$_2$, C$_{3'}$–H$_2$ and C$_{4'}$–H$_2$, respectively, on the basis of ^{1}H–^{1}H COSY. The N-methyl group displayed 2 singlets (3.1 and 2.9 ppm) in a 3:1 ratio, due to

amide resonance [41]. The aliphatic chain and N-methyl carbons were assigned on the basis of ^{1}H–^{13}C HETEROCOSY. The perfluorinated carbons were grouped as a highly complex series of multiplets from 100 to 120 ppm. The amidic carbonyl showed a triplet at 157.5 ppm and the ester carbonyl a triplet at 171.0 ppm.

IR. **2** was subjected to IR analysis as an oil between KBr salt plates. The spectrum was dominated by 2 carbonyl bands, at 1780 cm^{-1} [HFB(0) ester] and 1680 cm^{-1} (N-HFB amide). This data compares favorably with the N-HFB derivative of pyrrolidine and the N,O-di-HFB derivative of ring-opened N-methylpyrrolidine.

Nicotine derivatization yield

The yield of **2** at the μg level was >85%. This

TABLE I

^{1}H AND ^{13}C NUCLEAR MAGNETIC RESONANCE DATA FOR N,O-DI-HFB-NICOTINE

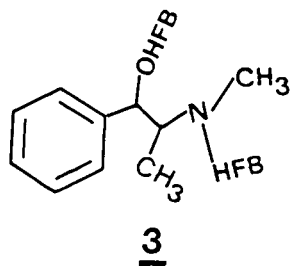| Proton	δ	Multiplicity	Carbon	δ	Multiplicity
C2-H	8.6	br m	C2	149.8	d
			C3	134.2(?)	s
C4-H	7.7	d	C4	134.5	d
C5-H	7.2	dd	C5	123.9	d
C6-H	8.6	br m	C6	147.5	d
C2'-H$_2$	6.0	m	C2'	78.1	d
C3'-H$_2$	1.9	m	C3'	32.4	t
C4'-H$_2$	1.7	m	C4'	22.0	t
C5'-H$_2$	3.5	m	C5'	48.8	t
CH$_3$	3.1/ 2.9	d-s	CH$_3$	34.6	q

Fig. 3. Perfluorinated derivative of ephedrine.

was verified against an internal standard prepared by the derivatization of an equal amount of ephedrine, which also yielded an N,O-di-HFB derivative, 3, seen in Fig. 3. Fig. 4 illustrates the cGC–ECD chromatogram of N-HFB-methamphetamine, 3, 2, aldrin internal standard and N-HFB-tetracaine on the 15-m DB-5 + column. The comparable responses for 2 and 3 at the 1-ng

level on-column is apparent. The reduced response for the methamphetamine and tetracaine derivatives is due to the fact that both contain only a single HFB group.

Derivative yield versus reaction temperature and time variables

The reaction yield of 2 was studied at 25, 75 and 95°C and at times from 1 min to 2 h. Significant yields were realized at 25°C after as little as 1 min (at the 100 μg level). Modest improvements in yields were noted after 15 min at 75 or 95°C. The results at 75 and 95°C were comparable and no further improvement was noted at 75°C even after extending the reaction from 15 min to 2 h.

Reaction by-products or GC injection port artifacts

During cGC–ECD analyses of 1 on the 15-m DB-5 + column, two later-eluting minor peaks (A and B) were observed. In order to improve their resolution, the 15-m DB-5 + column was replaced with a 30-m DB-5 column. When 1 was derivatized at 75°C for only 5 min, the intensity of A was quite significant, whereas B was undetectable. When the reaction was extended to 75 min, A was markedly diminished and B appeared, as illustrated in Fig. 5. Under either conditions, the yield of 2 was high and virtually unvaried.
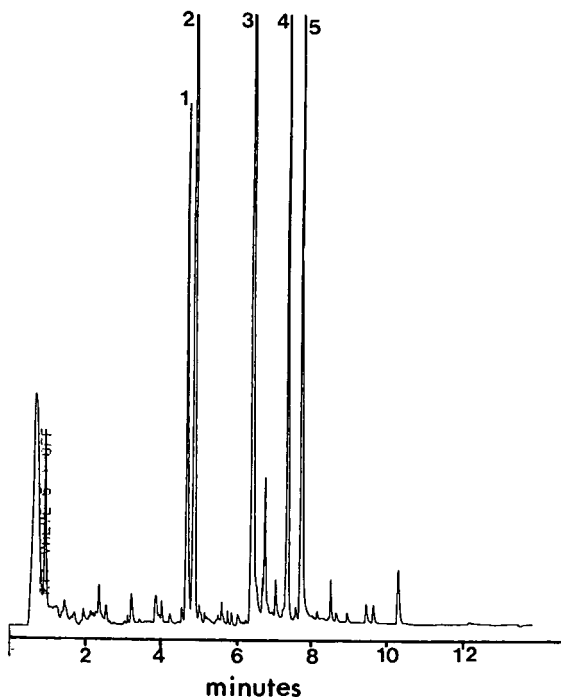

Fig. 4. Capillary gas chromatographic–electron capture detection chromatogram of perfluorinated nicotine and other drug derivatives. Column: 15 m × 0.25 mm DB-5 + ; splitless injection; attenuation: 2^8. Peaks: 1 = N-HFB-methamphetamine, 2 ng; 2 = N,O-di-HFB-ephedrine, 1 ng; 3 = N,O-di-HFB-nicotine, 1 ng; 4 = Aldrin internal standard, 200 pg; 5 = HFB-tetracaine, 2 ng.
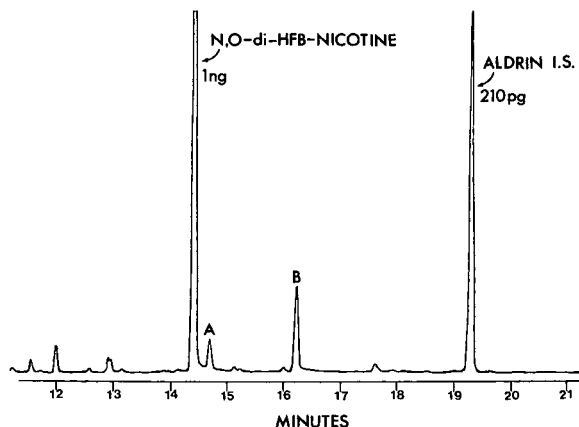

Fig. 5. Capillary gas chromatographic–electron capture detection chromatogram of perfluorinated nicotine and splitless injection port artifacts A and B. Column: 30 m × 0.25 mm DB-5; attenuation 2^8.
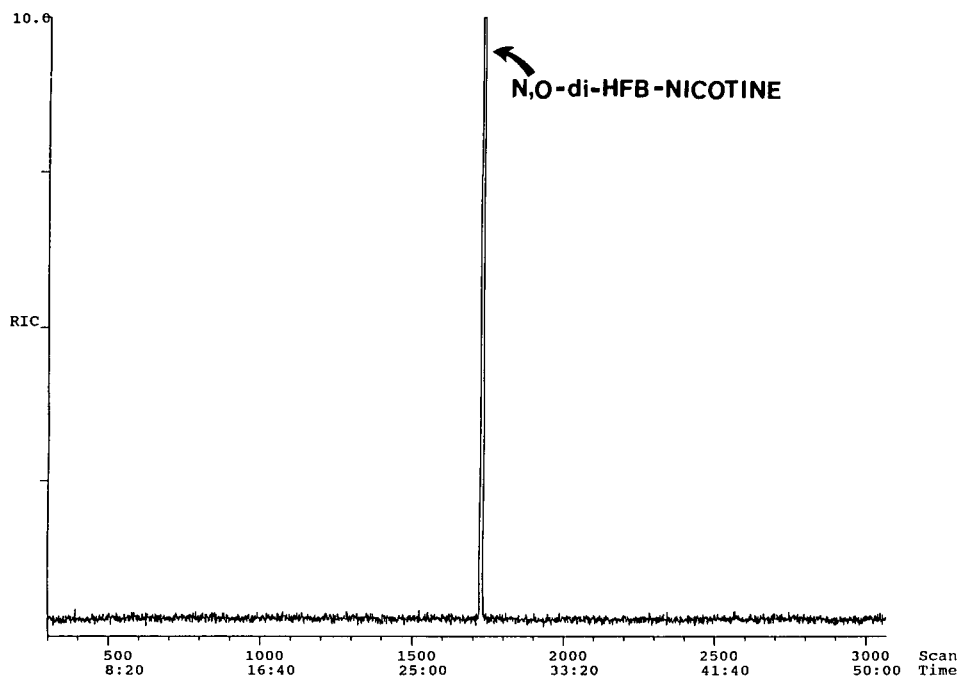
Fig. 6. Capillary gas chromatographic–mass spectrometric chromatogram of perfluorinated nicotine derivative. Column: 25 m × 0.25 mm RT$_x$-200; on-column injection, 90°C.

The appearance of A and B was also measured as a function of the splitless injection port temperature. It was observed that in going from an injection port temperature of 225 to 300°C, the response for **2** and B decreased, whereas A increased. Furthermore, as seen in Fig. 6, when **2** was injected on-column at 90°C and under pristine conditions into the 15-m Rt$_x$-200 column, A and B were not detected. These results suggested that A and B were artifacts, a consequence of the splitless injection at elevated temperatures. To maximize response for **2** and minimize artifacts, a splitless injection port temperature range of 200–250°C is recommended.

Derivatization in the presence and absence of added base

The reaction was studied in the presence of pyridine, 4-dimethylaminopyridine (PDAP) and without added base. Maximum yield was realized in the presence of pyridine. When PDAP (a hypernucleophilic acylation catalyst) was used, the yield was substantially reduced. This was surprising, as previous use of PDAP had consistently resulted in high-yield heptafluoro-

butyrylation at N, O and C sites in a variety of similar compounds [36–38]. It appears that, in the presence of PDAP, the C2' carbon exists as a carbanion stabilized by the close proximity of the electron withdrawing pyridinyl moiety, thereby inhibiting nucleophilic attack by the [HFB(O)] anion.

Finally, the reaction proceeded without any added base. However, this variant required extended heating times and resulted in substantially reduced yields. The positive reaction in the absence of base was probably due to **1** acting as a self-catalyst, since **1** contains a pyridinyl group.

Chromatography of nicotine derivative

The GC characteristics of **2** were evaluated on all three 30-m columns, i.e., DB-1, DB-5 and DB-1701, and the 15-m Rt$_x$-200 column. Of the DB columns investigated, optimum chromatography for **2** and highest resolution of A and B were best achieved on the DB-5 column. Perhaps ideal chromatographic behavior was realized on the Rt$_x$-200 column (Fig. 6). The retention data for **2**, A, B and the aldrin internal

TABLE II

CAPILLARY GAS CHROMATOGRAPHY–ELECTRON CAPTURE DETECTION RETENTION TIME DATA FOR N,O-DI-HFB-NICOTINE, INJECTION PORT ARTIFACTS A AND B, AND ALDRIN INTERNAL STANDARD USING 30 m × 0.25 mm DB-5, DB-1701, AND DB-1 CAPILLARY COLUMNS

Column	Retention times (min)			
	N,O-di-HFB-Nicotine	Peak A	Peak B	Aldrin I.S.
DB-5	14.36	14.66	16.15	19.18
DB-1701	14.80	[a]	17.19	15.89
DB-1[b]	9.96	9.85	10.95	13.59

[a] Artifact peak A coelutes with N,O-di-HFB-nicotine peak.
[b] Initial oven temperature hold time was 4.0 min as compared to 5.0 min for the DB-5 and DB-1701 columns.

standard on the three 30-m columns are summarized in Table II.

On-column and method minimum detectable quantities

The OC-MDQ of 1 (as the di-HFB derivative 2) was determined on the 30-m DB-5 column. About 100 μg of 1 was derivatized as previously described, except at 25°C for 75 min. After isooctane extraction, serial dilutions with additional isooctane were made to achieve a concentration for 1 of about 2.5 pg/μl. After a method blank was run, it was determined that the OC-MDQ of 1 was below 5 pg. Under optimized conditions, such as a shorter column and thinner film (e.g., 0.10 μm), on-column detection at the femtogram level may be within reach.

The procedure for MTH-MDQ has been previously described. About 5 ng of 1 was derivatized using reduced amounts of acetonitrile, HFBA and pyridine in order to reduce artifact contribution. Petroleum ether was used as a replacement extraction solvent, in order to facilitate the subsequent evaporation step. Ethyl acetate was the choice as a reconstitution solvent because of its polarity, moderate boiling point and compatibility with the cGC–ECD system. It was observed that for the 30-m DB-5 column, 5 ng of 1 was easily detected at a nominal instrumental attenuation of 2^7.

Environmental contamination

A frequently encountered problem in ultratrace level analyses of 1 is environmental con-

tamination, i.e., detection of 1 in methodology blanks. Typical contamination sources include air, water and glassware. These problems usually occur in those methods that do not employ ChD (which includes most methods). Environmental contamination is significantly diminished when using the present ChD methodology, because once the ChD reaction has been completed and the excess reagent quenched, any subsequent environmental contamination is undetectable, as the ECD detector responds only to 2 and not 1. The absence of 1 in a method blank was established using this method.

CONCLUSIONS

The derivatization of nicotine with HFBA in the presence of pyridine yields a di-HFB substituted product that exhibits good chromatography and excellent sensitivity when using capillary gas chromatography–electron-capture detection. With an on-column MDQ level of below 5 pg, the method described herein provides one of the most sensitive determinative steps for the detection of nicotine.

REFERENCES

1 I.E. Burrows, P.J. Corp, G.C. Jackson and B.F.J. Page, Analyst, 96 (1971) 81.
2 L. Neelakantan and H.B. Kostenbauder, Anal. Chem., 46 (1974) 452.
3 S.E. Falkman, I.E. Burrows, R.A. Lundgren and B.F.J. Page, Analyst, 100 (1975) 99.

4 C. Feyerabend, T. Levitt and M.A.H. Russell, *J. Pharm. Pharmacol.*, 27 (1975) 434.

5 I.D. Watson, *J. Chromatogr.*, 143 (1977) 203.

6 J. Dow and K. Hall, *J. Chromatogr.*, 153 (1978) 521.

7 C. Feyerabend and M.A.H. Russell, *J. Pharm. Pharmacol.*, 31 (1979) 73.

8 P. Hartvig, N-O. Ahnfelt, M. Hammarlund and J. Vessman, *J. Chromatogr.*, 173 (1979) 127.

9 O. Grubner, M.W. First and G.L. Huber, *Anal. Chem.*, 52 (1980) 1755.

10 C. Feyerabend and M.A.H. Russell, *J. Pharm. Pharmacol.*, 32 (1980) 178.

11 C. Feyerabend and M.A.H. Russell, *Analyst.*, 105 (1980) 998.

12 M.J. Kogan, K. Verebey, J.H. Jaffee and S.J. Mule, *J. Forensic Sci.*, 26 (1981) 6.

13 P. Jacob, III, M. Wilson and N.L. Benowitz, *J. Chromatogr.*, 222 (1981) 61.

14 J.A. Saunders and D.E. Blume, *J. Chromatogr.*, 205 (1981) 147.

15 J.A. Thompson, M-S. Ho and D.R. Petersen, *J. Chromatogr.*, 231 (1982) 53.

16 G. Stehlik, J. Kainzbauer, H. Tausch and O. Richter, *J. Chromatogr.*, 232 (1982) 295.

17 M. Curvall, E. Kazemi-Vala and C.R. Enzell, *J. Chromatogr.*, 232 (1982) 283.

18 B.J.L. Sudan, C. Brouillard, C. Strehler, H. Strub, J. Sterboul and J. Sainte-Laudy, *J. Chromatogr.*, 288 (1984) 415.

19 K.C. Cundy and P.A. Crooks, *J. Chromatogr.*, 306 (1984) 291.

20 P. Daenens, L. Laruelle, K. Callewaert, P. de Schepper, R. Galeazzi and J. van Rossum, *J. Chromatogr.*, 342 (1985) 79.

21 M.J. Horstmann, *J. Chromatogr.*, 344 (1985) 391.

22 S. Mousa, G.R. van Loon, A.A. Houdi and P.A. Crooks, *J. Chromatogr.*, 347 (1985) 405.

23 R.A. Davis, *J. Chromatogr. Sci.*, 24 (1986) 134.

24 G.B. Neurath and F.G. Pein, *J. Chromatogr.*, 415 (1987) 400.

25 C.L. Smith and M. Cooke, *Analyst.*, 112 (1987) 1515.

26 G.A. Kyerematen, L.H. Taylor, J.D. deBethizy and E.S. Vesell, *J. Chromatogr.*, 419 (1987) 191.

27 R.D. Barlow, P.A. Thompson and R.B. Stone, *J. Chromatogr.*, 419 (1987) 375.

28 C-Y. Chien, J.N. Diana and P.A. Crooks, *LC-GC.*, 6 (1988) 53.

29 M.T. Parviainen and R.D. Barlow, *J. Chromatogr.*, 431 (1988) 216.

30 P. Voncken, G. Schepers and K-H. Schäfer, *J. Chromatogr.*, 479 (1989) 410.

31 M.W. Ogden, *J. Assoc. Off. Anal. Chem.*, 72 (1989) 1002.

32 S. O'Doherty, M. Cooke and D.J. Roberts, *J. High Resolut. Chromatogr.*, 13 (1990) 74.

33 L.J. Lewis, J.D. Lamb, D.J. Eatough, L.D. Hansen and E.A. Lewis, *J. Chromatogr. Sci.*, 28 (1990) 200.

34 K.T. McManus, J.D. deBethizy, D.A. Garteiz, G.A. Kyerematen and E.S. Vesell, *J. Chromatogr. Sci.*, 28 (1990) 510.

35 P. Jacob, III, L. Yu, M. Wilson and N.L. Benowitz, *Bio. Mass Spectr.*, 20 (1991) 247.

36 D. Jones, M. Curvall, L. Abrahamsson, E. Kazemi-Vala and C. Enzell, *Biomed. Mass Spectrom.*, 9 (1982) 539.

37 J.M. Moore, A.C. Allen, D.A. Cooper and S. Carr, *Anal. Chem.*, 58 (1986) 1656.

38 J.M. Moore, A.C. Allen and D.A. Cooper, *Anal. Chem.*, 56 (1984) 642.

39 J.M. Moore, D.A. Cooper and R.F.X. Klein, unpublished results.

40 M. Shamma and D.M. Hindenlang, *Carbon-13 NMR Shift Assignments of Amines and Alkaloids*, Plenum Press, New York, 1979, p. 24.

41 R.M. Silverstein, G.C. Bassler and T.C. Marill, *Spectrometric Identification of Organic Compounds*, Wiley, New York, 4th ed., 1981, p. 197.

CHROM. 25 288

Capillary column electron impact and ammonia chemical ionization gas chromatographic–mass spectrometric and gas chromatographic–tandem mass spectrometric analysis of mustard hydrolysis products

P.A. D'Agostino* and L.R. Provost

Defence Research Establishment Suffield, P.O. Box 4000, Medicine Hat, Alberta T1A 8K6 (Canada)

ABSTRACT

Capillary column GC–MS and GC–MS–MS, under electron impact (EI) and ammonia chemical ionization (CI) conditions, were used to detect and identify longer-chain sulfur vesicant hydrolysis products. Interpretation of the MS data enabled the characterization of the partial and fully hydrolysed products of 2-chloroethyl (2-chloroethoxy)ethyl sulfide, bis(2-chloroethylthio)ethane (sesquimustard) and bis[(2-chloroethylthio)ethyl] ether before and after trimethylsilyl derivatization. EI data were generally lacking in significant molecular ion information while those obtained during ammonia CI contained valuable $(M + H)^+$ and/or $(M + NH_4)^+$ molecular ion information. The usefulness of this approach to degradation product analysis was demonstrated during the *3rd United Nations Conference on Disarmament Technical Group on Instrumentation Round Robin Analytical Exercise* held in 1991. Both thiodiglycol and thiodiglycol sulfone, the mustard degradation compounds spiked onto concrete samples circulated to fifteen international laboratories, were confirmed during capillary column GC–MS and GC–MS–MS analysis of the samples.

INTRODUCTION

The use of the chemical warfare agent bis(2-chloroethyl)sulfide (mustard) in the Iran/Iraq war [1,2], and threat of chemical weapons use in the recent Persian Gulf war emphasize the need for specific methods to detect and identify sulfur vesicants and their degradation products. Retrospective analysis of samples contaminated with chemical warfare agents remains an important means for the verification of allegations of use claims and will be a critical component of the United Nations Chemical Weapons Convention. Analyses of this type have been performed on Iranian victims of an alleged attack with mustard gas [3] and considerable effort has been expended on the development of analytical methods for the detection of mustard and a hydrolysis product of mustard, thiodiglycol, in biological media [3–7].

Gas chromatography (GC) [8,9] and mass spectrometry (MS) [10–17] have been used for the identification of mustard and mustard-related compounds with capillary column GC–MS being the most commonly employed technique for the detection of these compounds in environmental and biological samples. Destruction of mustard by hydrolysis or natural weathering in the environment results in the formation of thiodiglycol [18,19], a non-toxic compound that may be easily handled. However, munitions-grade mustard formulations typically contain only 50 to 80% mustard with most of the remaining content

---

* Corresponding author.

being other sulfur vesicants [14] which would decompose to other products. The characterization and identification of these degradation products would be valuable during chemical weapons destruction monitoring in support of the proposed Chemical Weapons Convention and for the verification of claims of allegations of chemical agent use.

Electron impact (EI) ionization has been used to characterize derivatives of mustard including thiodiglycol and the di-trimethylsilyl derivative of thiodiglycol [13]. The MS characterization of the hydrolysis products of longer-chain sulfur vesicants, commonly found in munitions-grade mustard [14], has not been previously investigated. During this study, two munitions-grade mustard samples, containing longer-chain sulfur vesicants were hydrolysed and analysed by capillary column GC–MS and GC–MS–MS in an attempt to obtain the MS data required for the verification of these compounds. Samples of the hydrolysed munitions-grade mustard were analysed by capillary column GC–MS under EI conditions before and after trimethylsilyl (TMS) derivatization. Molecular ion information, critical for the confirmation of the observed hydrolysis products, was generally absent during EI analyses. Chemical ionization (CI) [20] using ammonia [21] was evaluated as a complementary technique for the acquisition of molecular ion information, as this technique has proven its value during the analysis of organophosphorus nerve agents [22–26] and longer-chain sulfur vesicants [27].

Interpretation of the acquired MS data resulted in the characterization of both the partial and fully hydrolysed products of mustard and the longer-chain sulfur vesicants, 2-chloroethyl (2-chloroethoxy)ethyl sulfide, bis(2-chloroethyl-thio)ethane (sesquimustard) and bis[(2-chloro-ethylthio)ethyl] ether before and after TMS derivatization. In all cases complementary molecular ion information was obtained by the use of ammonia CI-MS. Tandem MS was particularly useful for the confirmation of the partial hydrolysis product of 2-chloroethyl (2-chloro-ethoxy)ethyl sulfide. This approach to mustard degradation product analysis was successfully applied during the analysis of spiked concrete

samples during the *3rd United Nations Conference on Disarmament Technical Group on Instrumentation Round Robin Analytical Exercise* in 1991.

EXPERIMENTAL

Hydrolysis samples

Samples of HT and HQ munitions-grade mustard formulations (2 ml) were hydrolysed in a 125-ml erlenmeyer flask with 50 ml water at 50°C overnight. Acetone was added to each sample to solubilize the remaining oil and each sample was stirred overnight at 50°C. Both hydrolysed samples cleared and the excess water was removed leaving a pale yellow oil for each sample. The oils were then distilled in a Kugelrohr oven at 220°C at 0.1 Torr (1 Torr = 133.322 Pa). Hydrolysed HT and HQ samples were dissolved in dichloromethane and a standard containing both hydrolysed HT and HQ at 1 mg/ml was prepared in dichloromethane.

Trimethylsilyl derivatization of this sample was performed by combining 100 μl of the hydrolysis products of HT and HQ (1 mg/ml) with 50 μl pyridine and 50 μl bis(trimethylsilyl)trifluoroacetamide (BSTFA) (containing 1% trimethylchlorosilane) for 20 min at 60°C [28]. Analysis of derivatized samples was performed within 24 h to minimize degradation. All hydrolysed munitions-grade mustard samples and derivatives of these samples were stored in polytetrafluoroethylene (PTFE)-lined 1.8-ml glass vials at 4°C prior to analysis.

Round robin concrete samples

Spiked concrete samples, typical of those expected during inspection of a military facility, were prepared by the Prins Maurits Laboratory TNO (Netherlands) and distributed to evaluate laboratory procedures as part of the *3rd United Nations Conference on Disarmament Technical Group on Instrumentation Round Robin Analytical Exercise*. The concrete round robin samples were extracted in their glass shipment bottles by ultrasonic vibration for 5 min with 15 ml of acetonitrile. The acetonitrile extract was removed and concentrated by nitrogen blowdown to 0.5 ml. Dichloromethane (4.5 ml) was added

to the acetonitrile extract (final volume of 5 ml) prior to analysis to improve chromatographic performance.

A 2-ml volume of the 5-ml volume (above) was concentrated by nitrogen blowdown to 300 μl and this concentrate was used for trimethylsilylation. Trimethylsilylation was performed by combining 100 μl BSTFA, 100 μl pyridine and the 300 μl extract in a 1.8-ml screw-capped (PTFE-lined) glass vial. This sample was heated for 20 min at 60°C prior to analysis [28]. Analysis was performed immediately after cooling to minimize degradation.

Instrumental

Capillary column GC–MS and GC–MS–MS analyses were performed with a VG AUTO-SPEC-Q hybrid tandem mass spectrometer equipped with a Hewlett-Packard Model 5890 gas chromatograph. A 15 m × 0.32 mm I.D. DB-1701 J&W capillary column (0.25 μm film thickness) was used for all analyses with the following temperature program: 40°C (2 min) 10°C/min 280°C (5 min). All GC injections were cool on-column using an injector of our own design [29]. The EI operating conditions were as follows: source pressure, $3 \cdot 10^{-6}$ Torr; source temperature, 200°C; electron energy, 70 eV; and electron emission, 100 μA. Ammonia (99.99%, Anhydrous grade, Liquid Carbonic) CI operating conditions were as follows: source pressure, $8 \cdot 10^{-5}$ Torr (NH_3^+:NH_4^+ approximately 15:1); source temperature, 120–130°C, electron energy, 50 eV; and electron emission, 300 μA. Source pressure readings were taken near the source and CI source temperatures increased slightly during each GC–MS analysis due to filament heating. All EI and CI mass spectra were obtained using a VG EI/CI source at a resolution of 1000 to 2000 (10% valley definition) and an accelerating voltage of 8 kV. Mass spectral data were collected from 400 to 40 u at a scan rate of 0.5 s/decade. Deuterated ammonia (99%, MDS Isotopes) CI-MS analysis of the TMS derivatives of the hydrolysis products of HT and HQ was performed under conditions similar to the ammonia CI-MS conditions described above.

The daughter spectrum of m/z 167 for the TMS derivative of 2-chloroethyl (2-hydroxyethyl-

thio)ethyl ether was obtained under ammonia CI conditions (above) with a collisional associated dissociation (CAD) cell energy of 13 eV and an argon pressure of 10^{-6} Torr (near CAD cell). Daughter spectra for thiodiglycol (m/z 122) and thiodiglycol sulfone (m/z 111) were obtained under EI conditions (above) with a CAD cell energy of 17 eV and an argon pressure of 10^{-6} Torr (near the CAD cell). The quadrupole was operated at unit resolution and scanned from 250 to 50 u at 0.5 s/scan during all capillary column GC–MS–MS analyses.

RESULTS AND DISCUSSION

HQ and HT, two munitions-grade mustard formulations, containing predominately mustard (H) and sesquimustard (Q), and mustard (H) and bis[(2-chloroethylthio)ethyl] ether (T), respectively [14], were hydrolysed in an attempt to characterize the principal hydrolysis products of these munitions samples. Fig. 1 illustrates the total-ion-current chromatogram for the principal hydrolysis products of mustard and the longer-chain sulfur vesicants, 2-chloroethyl (2-chloro-
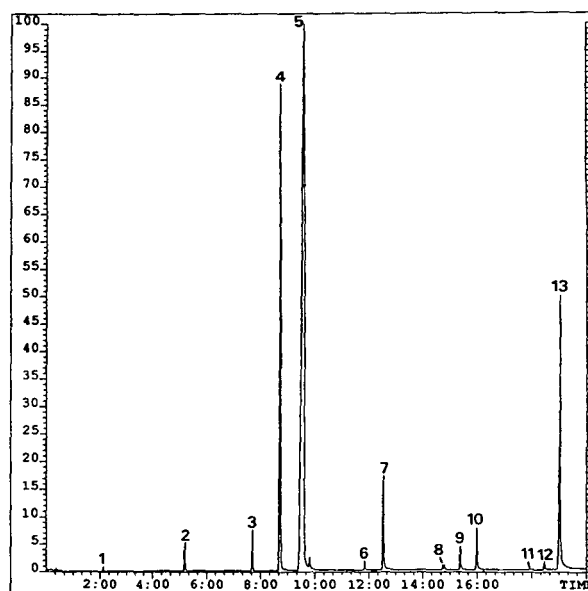

Fig. 1. Capillary column GC–EI-MS total-ion-current (400 to 40 u) chromatogram of the hydrolysis products of approximately 300 ng of HT and HQ. Compounds are identified in Table I. Time scale in min.

TABLE I

COMPOUNDS IDENTIFIED AFTER GC–MS AND GC–MS–MS ANALYSIS OF SAMPLES

Peak No.[a]	Molecular mass	Compound
1	104	1,4-Thioxane
2	120	1,4-Dithiane
3	158	Mustard
4	140	Hemisulfur mustard
5	122	Thiodiglycol
6	202	2-Chloroethyl (2-chloroethoxy)ethyl sulfide
7	184	2-Chloroethyl (2-hydroxyethylthio)ethyl ether
8	218	Sesquimustard
9	200	2-Chloroethyl (2-hydroxyethylthio)ethyl sulfide
10	182	Bis(2-hydroxyethylthio)ethane
11	262	Bis[(2-chloroethylthio)ethyl] ether
12	244	(2-Chloroethylthio)ethyl (2-hydroxyethylthio)ethyl ether
13	226	Bis[(2-hydroxyethylthio)ethyl] ether
14	212	TMS derivative of hemisulfur mustard
15	266	Di-TMS derivative of thiodiglycol
16	256	TMS derivative of 2-chloroethyl (2-hydroxyethylthio)ethyl ether
17	272	TMS derivative of 2-chloroethyl (2-hydroxyethylthio)ethyl sulfide
18	326	Di-TMS derivative of bis(2-hydroxyethylthio)ethane
19	316	TMS derivative of (2-chloroethylthio)ethyl (2-hydroxyethylthio)ethyl ether
20	370	Di-TMS derivative of bis[(2-hydroxyethylthio)ethyl] ether
21	298	Di-TMS derivative of thiodiglycol sulfone

[a] Refer to Figs. 1, 2 and 5.

ethoxy)ethyl sulfide, sesquimustard and bis[(2-chloroethylthio)ethyl] ether. The partial (*e.g.*, HO–CH$_2$CH$_2$–S–CH$_2$CH$_2$–Cl) and/or full (*e.g.*, HO–CH$_2$CH$_2$–S–CH$_2$CH$_2$–OH) hydrolysis products for mustard and the three other longer-chain sulfur vesicants were the predominate sample components, with a lesser contribution coming from intact sulfur vesicants and the commonly observed mustard impurities 1,4-thioxane and 1,4-dithiane [14].

Chromatography of partial hydrolysis products was excellent and equivalent to the gaussian peak shape routinely observed for the sulfur vesicants. However, the chromatographic quality deteriorates somewhat for the full hydrolysis products due to the polarity of two hydroxyl substituents. A small amount of tailing was typically observed (Fig. 1) during capillary column GC–MS of these compounds (peak numbers 5, 10 and 13). With more active or poorly conditioned capillary columns the quality of chromatography deteriorates significantly and

low nanogram detection of full hydrolysis products, such as thiodiglycol, cannot be reliably made. Analysis of authentic reference standards (*e.g.*, thiodiglycol) prior to the analysis of unknown samples is recommended to ensure good quality control for this reason.

The activity of capillary columns becomes less critical during the analysis of the TMS derivatives of the hydrolysis products, as these compounds are much less polar than the underivatized compounds. Gaussian peak shape was observed (Fig. 2) during chromatography of the TMS derivatives of the full hydrolysis products (peak numbers 15, 18 and 20). Improved chromatographic performance and the fact that direct trimethylsilylation of samples, such as soil, enables extraction of chemical warfare agent hydrolysis products [17] makes derivatization an attractive complementary confirmation technique.

The EI mass spectra of the partial and full hydrolysis products of mustard and the longer-
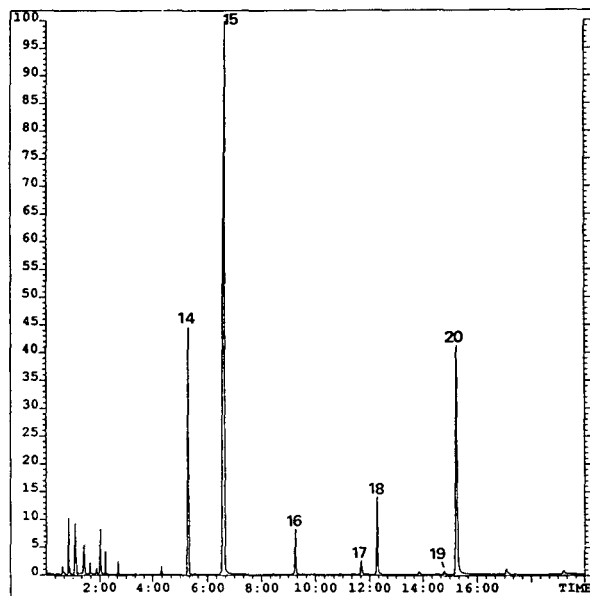
Fig. 2. Capillary column GC–EI-MS total-ion-current (400 to 40 u) chromatogram of the hydrolysis products of approximately 300 ng of HT and HQ after trimethylsilylation. Compounds are identified in Table I (minor sample components, with retention times near 2 min, were due to the TMS derivatizing reagent). Time scale in min.

chain sulfur vesicants generally provide little or no molecular ion information (Figs. 3 and 4). This fact, coupled with the lack of higher-mass structurally significant EI ions for several compounds, prompted the evaluation of ammonia CI as a complementary confirmation technique. Ammonia CI-MS, a technique recently reported for longer-chain sulfur vesicants [27], provided $(M + H)^+$ and/or $(M + NH_4)^+$ pseudo-molecular ions for all the hydrolysis products along with structurally significant CI fragmentation ions.

Mustard hydrolysis

Mustard hydrolysis results in the production of the partial hydrolysis product, hemisulfur mustard, and the full hydrolysis product, thiodiglycol. The EI mass spectra of hemisulfur mustard (Fig. 3a), thiodiglycol (Fig. 3e) and the di-TMS derivative of thiodiglycol (Fig. 3g), included for completeness, were similar to those reported by Wils and Hulst [13]. The EI mass spectrum of the TMS derivative of hemisulfur mustard (Fig. 3c) exhibited higher-mass ions at m/z 197 and

m/z 176 due to $(M - CH_3)^+$ and $(M - HCl)^+$ but did not exhibit a molecular ion.

$(M + H)^+$ and/or $(M + NH_4)^+$ pseudo-molecular ions were observed for hemisulfur mustard (Fig. 3b), the TMS derivative of hemisulfur mustard (Fig. 3d), thiodiglycol (Fig. 3f) and the di-TMS derivative of thiodiglycol (Fig. 3h). Hemisulfur mustard exhibited an intense CI fragmentation ion at m/z 105 due to protonated 1,4-thioxane and the TMS derivative was characterized by ions at m/z 177 and m/z 123 due to $(M + H - HCl)^+$ and $(C_2H_4-S-C_2H_4Cl)^+$. Thiodiglycol exhibited a weak CI fragmentation ion at m/z 105 due to protonated 1,4-thioxane and the di-TMS derivative of thiodiglycol was characterized by an intense CI ion at m/z 177 due to $[M + H - (CH_3)_3Si(OH)]^+$. CI ions characteristic of TMS derivatization at m/z 73, $(CH_3)_3Si^+$, and m/z 90, $[(CH_3)_3SiNH_3]^+$ were observed for the TMS derivatives of hemisulfur mustard, thiodiglycol and the other longer-chain sulfur vesicant hydrolysis products. The structure of the ammonia CI ion at m/z 90, observed for all TMS derivatives, was confirmed by the observation of an ion at m/z 93, due to $[(CH_3)_3N^2H_3]^+$, during deuterated ammonia CI-MS analysis.

2-Chloroethyl (2-chloroethoxy)ethyl sulfide hydrolysis

Only the partial hydrolysis product of 2-chloroethyl (2-chloroethoxy)ethyl sulfide was detected during EI and CI analysis of the hydrolysed sample. Under EI conditions 2-chloroethyl (2-hydroxyethylthio)ethyl ether exhibited an intense protonated 1,4-thioxane ion (Fig. 3i) and the TMS derivative of this hydrolysis product contained a weak ion at m/z 241 due to $(M - CH_3)^+$ (Fig. 3k). Under ammonia CI conditions molecular ion information was obtained for both 2-chloroethyl (2-hydroxyethylthio)ethyl ether (Fig. 3j) and its TMS derivative (Fig. 3l). An ion at m/z 167 due to $(C_2H_4-S-C_2H_4-O-C_2H_4-Cl)^+$ was observed during both ammonia CI analyses.

It was not obvious after interpretation of the EI and CI data as to whether the hydroxyl substituent was nearer the sulfur or oxygen position and only the following general structure was initially assumed: $ClC_2H_4-X-C_2H_4-X-C_2H_4OH$ (where one X was an oxygen and the
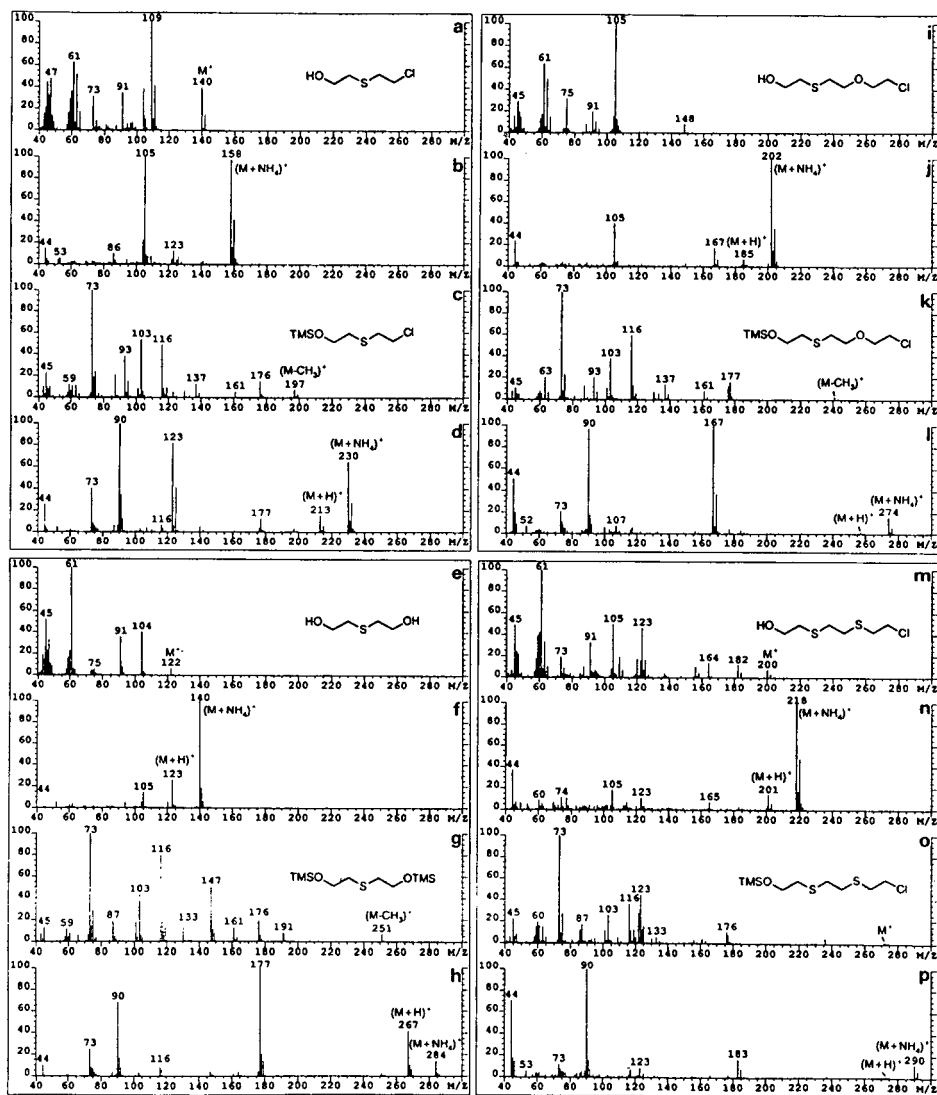
Fig. 3. (a) EI and (b) ammonia CI mass spectra of hemisulfur mustard and (c) EI and (d) ammonia CI mass spectra of TMS derivative of hemisulfur mustard. (e) EI and (f) ammonia CI mass spectra of thiodiglycol and (g) EI and (h) ammonia CI mass spectra of the di-TMS derivative of thiodiglycol. (i) EI and (j) ammonia CI mass spectra of 2-chloroethyl (2-hydroxy-ethylthio)ethyl ether and (k) EI and (l) ammonia CI mass spectra of TMS derivative of 2-chloroethyl (2-hydroxyethylthio)ethyl ether. (m) EI and (n) ammonia CI mass spectra of 2-chloroethyl (2-hydroxyethylthio)ethyl sulfide and (o) EI and (p) ammonia CI mass spectra of TMS derivative of 2-chloroethyl (2-hydroxyethylthio)ethyl sulfide.

second X was a sulfur). However under ammonia CI the TMS derivative of this compound exhibits an intense m/z 167 ion and GC–MS–MS analysis of this ion was performed as the daughters might provide the required structural data. The daughters of m/z 167 (Fig. 4m) for this compound at m/z 63, m/z 87 and m/z 107 were due to $(ClC_2H_4)^+$, $(C_2H_3-S-C_2H_4)^+$ and $(ClC_2H_4-O-C_2H_4)^+$, respectively, which strong-

ly suggested the presence of the partial hydrolysis product, 2-chloroethyl (2-hydroxyethylthio)ethyl ether or $ClC_2H_4-O-C_2H_4-S-C_2H_4OH$.

Sesquimustard hydrolysis

Both the partial hydrolysis product, 2-chloroethyl (2-hydroxyethylthio)ethyl sulfide, and the full hydrolysis product, bis(2-hydroxyethyl-
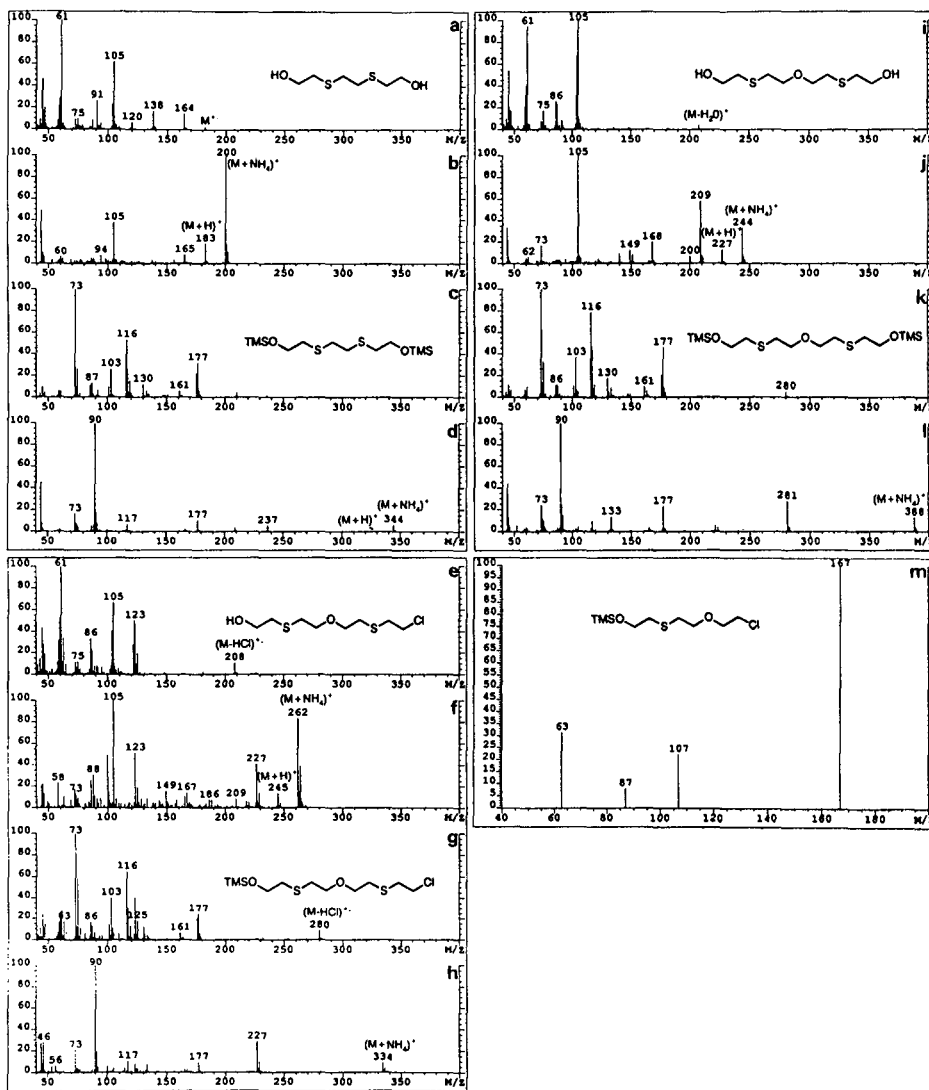
Fig. 4. (a) EI and (b) ammonia CI mass spectra of bis(2-hydroxyethylthio)ethane and (c) EI and (d) ammonia CI mass spectra of the di-TMS derivative of bis(2-hydroxyethylthio)ethane. (e) EI and (f) ammonia CI mass spectra of (2-chloroethylthio)ethyl (2-hydroxyethylthio)ethyl ether and (g) EI and (h) ammonia CI mass spectra of TMS derivative of (2-chloroethylthio)ethyl (2-hydroxyethylthio)ethyl ether. (i) EI and (j) ammonia CI mass spectra of bis[(2-hydroxyethylthio)ethyl] ether and (k) EI and (l) ammonia CI mass spectra of the di-TMS derivative of bis[(2-hydroxyethylthio)ethyl] ether. (m) Daughter spectrum (m/z 167) for TMS derivative of 2-chloroethyl (2-hydroxyethylthio)ethyl ether acquired during ammonia CI.

thio)ethane, of sesquimustard were detected during analysis. 2-Chloroethyl (2-hydroxyethyl-thio)ethyl sulfide exhibited a molecular ion at m/z 200 and higher mass ions due to $(M - H_2O)^{+\cdot}$ and $(M - HCl)^{+\cdot}$ at m/z 182 and m/z 164 under EI conditions (Fig. 3m). Lower-mass ions at m/z 61, $(C_2H_5S)^+$, m/z 105, protonated 1,4-thioxane, and m/z 123, $(C_2H_4-S-C_2H_4Cl)^+$, were typical of those observed for other partial

or full hydrolysis products. The EI mass spectrum after TMS derivatization yielded a very weak molecular ion (Fig. 3o). However, under ammonia CI conditions 2-chloroethyl (2-hy-droxyethylthio)ethyl sulfide provided both $(M + H)^+$ and $(M + NH_4)^+$ pseudo-molecular ions (Fig. 3n). Following TMS derivatization of 2-chloroethyl (2-hydroxyethylthio)ethyl sulfide the ammonia CI mass spectrum exhibited a reason-

able $(M + NH_4)^+$ pseudo-molecular ion and ions due to $[M + H - (CH_3)_3Si(OH)]^+$ and $[(CH_3)_3SiNH_3]^+$ at m/z 183 and m/z 90, respectively (Fig. 3p).

Bis(2-hydroxyethylthio)ethane was characterized by a weak EI molecular ion and ions at m/z 164 and m/z 138, due to $(M - H_2O)^{+\cdot}$ and $(M - OC_2H_4)^{+\cdot}$, respectively (Fig. 4a). The EI mass spectrum of the TMS derivative was void of molecular ion information and exhibited ions characteristic of TMS substitution (e.g., m/z 73). Ammonia CI was particularly useful as molecular ion information in the form of $(M + H)^+$ and $(M + NH_4)^+$ pseudo-molecular ions were observed before (Fig. 4b) and after TMS derivatization (Fig. 4d). As in the case of the partial hydrolysis product, 2-chloroethyl (2-hydroxyethylthio)ethyl sulfide, the most intense pseudo-molecular ions were obtained prior to TMS derivatization.

Bis[(2-chloroethylthio)ethyl] ether hydrolysis

Both the partial hydrolysis product, (2-chloroethylthio)ethyl (2-hydroxyethylthio)ethyl ether, and the full hydrolysis product, bis[(2-hydroxyethylthio)ethyl] ether, of bis[(2-chloroethylthio)ethyl] ether were detected in the hydrolysis sample. The EI mass spectra of the hydrolysis products prior to derivatization (Fig. 4e and i) and after trimethylsilylation (Fig. 4g and k) were void of molecular ion information and were characterized by higher-mass ions due to $(M - H_2O)^{+\cdot}$ or $(M - HCl)^{+\cdot}$. Ammonia CI was used to obtain molecular ion information for both hydrolysis products. Prior to derivatization both (2-chloroethylthio)ethyl (2-hydroxyethylthio)ethyl ether (Fig. 4f) and bis[(2-hydroxyethylthio)ethyl] ether (Fig. 4j) exhibited ions due to $(M + NH_4)^+$, $(M + H)^+$ and $(M + H - H_2O)^+$. After TMS derivatization ammonia CI ions due to $(M + NH_4)^+$, $[M + H - (CH_3)_3Si(OH)]^+$ and $[(CH_3)_3SiNH_3]^+$ at m/z 334, m/z 227 and m/z 90 (Fig. 4h) and m/z 388, m/z 281 and m/z 90 (Fig. 4l) were detected for the partial and full hydrolysis products of bis[(2-chloroethylthio)ethyl] ether, respectively.

Round robin concrete samples

Concrete samples, typical of those taken during inspection of a military facility, were received

by Defence Research Establishment Suffield as part of a multinational Round Robin Analytical Exercise organized by the United Nations Conference on Disarmament Technical Group on Instrumentation. The participating national laboratories in Canada, Australia, the Russian Federation (two laboratories), Finland, France, Germany, Netherlands, Norway, Sweden, China, Switzerland, Czech and Slovak Federal Republic, UK and the USA (two laboratories) were given the concrete samples with no prior knowledge of their content and were asked to report in a semi-quantitative manner the presence of any chemical warfare-relevant compounds.

Prior to TMS derivatization, only thiodiglycol could be detected during capillary column GC–MS under EI conditions. The second compound spiked onto the concrete, thiodiglycol sulfone, was not discernable above the hydrocarbon chemical background during EI-MS analysis. The molecular mass and presence of each of the compounds was confirmed by the presence of $(M + H)^+$ and/or $(M + NH_4)^+$ ions during GC–MS (ammonia CI) analysis. The high hydrocarbon content on the concrete samples, visible as an envelope of compounds in Fig. 5, was not ionized during ammonia CI-MS and highly specific detection of these two chemical warfare relevant compounds was possible. Fig. 6a illustrates the ammonia CI mass spectra for thiodiglycol sulfone obtained during analysis of the concrete extract.

Both thiodiglycol sulfone and thiodiglycol were characterized by tandem MS prior to derivatization of the concrete extract. Capillary column GC–MS–MS data were obtained by acquiring the daughter spectrum of m/z 122 (molecular ion) for thiodiglycol and the daughter spectrum of m/z 111, $[(HO)_2SC_2H_4OH]^+$, for thiodiglycol sulfone (Fig. 6b). The thiodiglycol sulfone EI fragmentation ion at m/z 111 was used for the MS–MS study as this was the highest mass ion (above 5% relative abundance) observed during MS analysis of a standard (refer to reference 30 for EI mass spectrum). For both compounds the principal daughter was due to loss of H_2O. The use of moderate resolution (1800 with 10% valley) in the sector significantly reduced the chemical background due to hydro-
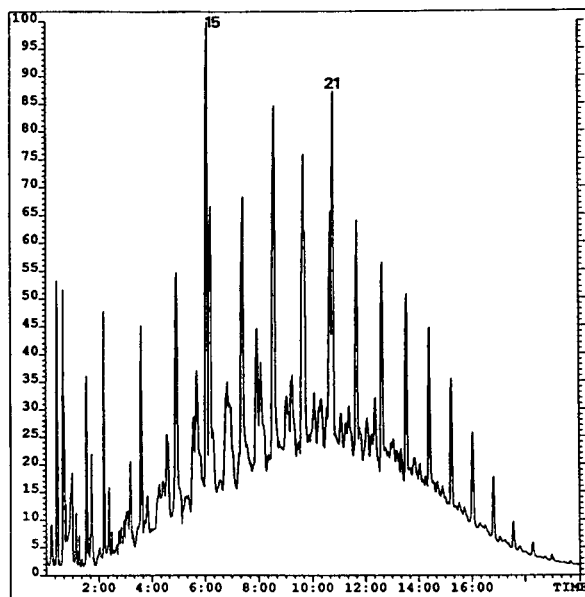
Fig. 5. Capillary column GC–EI-MS total-ion-current (400 to 40 u) chromatogram of the acetonitrile extract of an United Nations round robin concrete sample after tri-methylsilylation. Compounds are identified in Table I. Time scale in min.
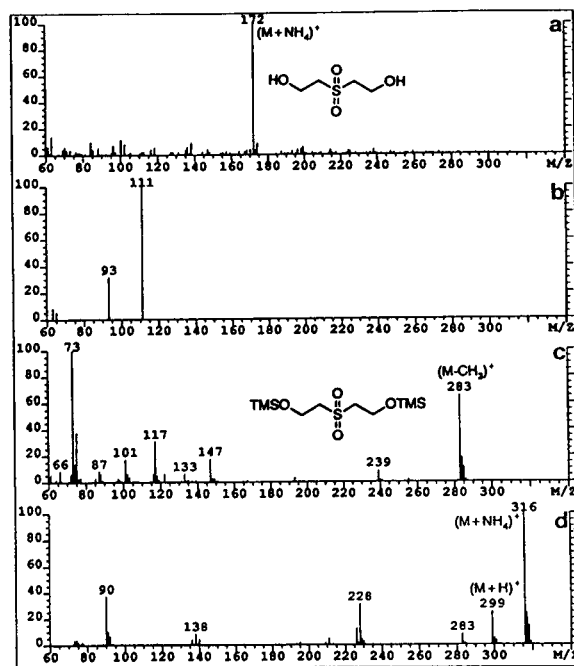

Fig. 6. (a) Ammonia CI and (b) daughter (m/z 111) spectra of thiodiglycol sulfone acquired during EI-MS and (c) EI and (d) ammonia CI mass spectra of di-TMS derivative of thiodiglycol sulfone.

carbons and resulted in chromatograms that did not contain the envelope of hydrocarbons observed during EI-MS.

Fig. 5 illustrates the capillary column GC–MS (EI) chromatogram obtained during analysis of the TMS derivative of the acetonitrile extract of the concrete sample. The EI mass spectra for the di-TMS derivatives of thiodiglycol and thiodiglycol sulfone (Fig. 6c), found in the acetonitrile extracts, were similar to previously published data [13]. The molecular mass of each of the derivatives was confirmed by the presence of $(M + H)^+$ and $(M + NH_4)^+$ ions during ammonia CI-MS analysis. Fig. 6d illustrates the ammonia CI mass spectrum for the di-TMS derivative of thiodiglycol sulfone.

Defence Research Establishment Suffield, the only participating Canadian laboratory, positively confirmed the two spiked chemical warfare-relevant compounds in the round robin concrete samples and did not detect any artifacts or false positives in the samples. During each analysis of thiodiglycol, thiodiglycol sulfone and their di-TMS derivatives the chromatographic/spectrometric data were confirmed with available authentic standards. A full summary of the

round robin results and a comparison of laboratory results has been recently published in a Finnish report [30].

CONCLUSIONS

Capillary column GC–MS and GC–MS–MS, under EI and ammonia CI conditions, were used to detect and identify longer-chain sulfur vesicant hydrolysis products. Interpretation of the MS data enabled the characterization of the partial and fully hydrolysed products of 2-chloroethyl (2-chloroethoxy)ethyl sulfide, bis(2-chloroethylthio)ethane (sesquimustard) and bis[(2-chloroethylthio)ethyl] ether before and after TMS derivatization. The usefulness of this approach to degradation product analysis was demonstrated during the *3rd United Nations Conference on Disarmament Technical Group on Instrumentation Round Robin Analytical Exercise* held in 1991. Both thiodiglycol and thiodiglycol sulfone, the mustard degradation compounds spiked onto concrete samples circulated to fifteen international laboratories, were confirmed

by capillary column GC–MS and GC–MS–MS analysis of the samples. The EI and CI data acquired for the hydrolysis products of munitions-grade mustard and their trimethylsilyl derivatives should prove valuable to researchers confronted with the analysis of samples containing mustard or other sulfur vesicants. Application of this approach, and the MS data presented, is anticipated during GC–MS analysis of these or similar hydrolysis compounds in weathered environmental samples, where the original sulfur vesicants have undergone extensive degradation, or for reaction progress monitoring during the destruction of chemical weapons stockpiles.

REFERENCES

1 G. Andersson, *NBC Defence and Technology International*, April 1986, p. 62.
2 *Report S/20060, Report of the Mission Dispatched by the Secretary-General to Investigate Allegations of the Use of Chemical Weapons in the Conflict Between the Islamic Republic of Iran and Iraq*, United Nations, New York, July 20, 1988.
3 E.R.G. Wils, A.G. Hulst, A.L. de Jong, A. Verweij and H.L. Boter, *J. Anal. Toxicol.*, 9 (1985) 254.
4 W. Vycudilik, *Forensic Sci. Int.*, 35 (1987) 67.
5 E.R.J. Wils, A.G. Hulst and J. van Laar, *J. Anal Toxicol.*, 12 (1988) 15.
6 R.M. Black and R.W. Read, *J. Chromatogr.*, 449 (1988) 261.
7 E.M. Jakubowski, C.L. Woodard, M.M. Mershon and T.W. Dolzine, *J. Chromatogr.*, 528 (1990) 184.
8 P.A. D'Agostino and L.R. Provost, *J. Chromatogr.*, 436 (1988) 399.
9 Z. Witkiewicz, M. Mazurek and J. Szulc, *J. Chromatogr.*, 503 (1990) 293.
10 *Systematic Identification of Chemical Warfare Agents, B.3, Identification of Non-Phosphorus Warfare Agents*, Ministry of Foreign Affairs of Finland, Helsinki, 1982.
11 E. Ali-Mattila, K. Siivinen, H. Kenttamaa and P. Savolahti, *Int. J. Mass Spectrom. Ion Phys.*, 47 (1983) 371.
12 D.N. Tripathi, A. Bhattacharya and R. Vaidyanathaswamy, *Can. Soc. Forens. Sci. J.*, 17 (1984) 55.
13 E.R.J. Wils and A.G. Hulst, *Fresenius' Z. Anal. Chem.*, 321 (1985) 471.
14 P.A. D'Agostino and L.R. Provost, *Biomed. Environ. Mass Spectrom.*, 15 (1988) 553.
15 P.A. D'Agostino and L.R. Provost, *Biomed. Environ. Mass Spectrom.*, 18 (1989) 484.
16 E.R.J. Wils, *Fresenius' J. Anal. Chem.*, 338 (1990) 22.
17 P.A. D'Agostino and L.R. Provost, *J. Chromatogr.*, 589 (1992) 287.
18 W.H. Stein, S. Moore and M. Bergmann, *J. Org. Chem.*, XI (1946) 664.
19 R. Trapp, *The Detoxification and Natural Degradation of Chemical Warfare Agents*, Stockholm International Peace Research Institute, Taylor & Francis, London, Philadelphia, PA, 1985.
20 L. Field and C.H. Foster, *J. Org. Chem.*, 35 (1970) 749.
21 J.B. Westmore and M.M. Alauddin, *Mass Spectrom. Rev.*, 5 (1986) 381.
22 P.A. D'Agostino, A.S. Hansen, P.A. Lockwood and L.R. Provost, *J. Chromatogr.*, 347 (1985) 257.
23 P.A. D'Agostino and L.R. Provost, *Biomed. Environ. Mass Spectrom.*, 13 (1986) 231.
24 A. Hesso and R. Kostiainen, *Proc. 2nd. Int. Symp. Protection Against Chemical Warfare, Stockholm, June 15–19, 1986*, National Defence Research Institute, Umeå, 1986, pp. 257–260.
25 P.A. D'Agostino, L.R. Provost and J. Visentini, *J. Chromatogr.*, 402 (1987) 221.
26 P.A. D'Agostino, L.R. Provost and K.M. Looye, *J. Chromatogr.*, 465 (1989) 271.
27 P.A. D'Agostino and L.R. Provost, *J. Chromatogr.*, 600 (1992) 267.
28 W.C. Butts, *Anal. Biochem.*, 46 (1972) 187.
29 P.A. D'Agostino and L.R. Provost, *J. Chromatogr.*, 331 (1985) 47.
30 *International Interlaboratory Comparison (Round Robin) Test for the Verification of Chemical Disarmament, F.3, Testing of Procedures on Simulated Military Facility Samples*, Ministry of Foreign Affairs of Finland, Helsinki, 1992.

Gas chromatographic–mass spectrometric study of the reductive silylation of hydroxyquinones

M.N. Bakola-Christianopoulou*, V.P. Papageorgiou and K.K. Apazidou

Department of Chemical Engineering, College of Engineering, Aristotle University of Thessaloniki, GR-540 06 Thessaloniki (Greece)

ABSTRACT

Reductive trimethylsilylation was carried out with N-methyl-N-trimethylsilyltrifluoroacetamide under optimized conditions to afford quantitatively the all-silylated products of several hydroxynaphthoquinones and -anthraquinones. The silylated products were investigated by GC–MS. The fragmentation patterns of the compounds provided valuable information about their structure and consequently about the structure of the initial hydroxyquinones. The silylation and GC–MS separation scheme was applied to mixtures of hydroxyquinones, leading to effective separation of all the ingredients, which included several hydroxyquinone isomers.

INTRODUCTION

Hydroxyquinones, their substituted derivatives and their transition metal chelates have long been known to possess numerous chemically and biologically significant properties [1–5]. For instance, several of the best known and widely used anthracycline and tetracycline antibiotics possess the hydroxyquinone structure, which is thought to be responsible for their biological activity [6,7]. The silylation of hydroxyquinones has attracted much attention in the last few years, because it offers the possibility of protecting the functional carbonyl and hydroxyl groups against destructive reaction conditions in a synthetic process, thus providing suitable intermediates. The products may be used as prodrugs, as their lipophilicity coupled with the facile hydrolysis of the Si–O bond would allow them to penetrate easily through lipophilic membranes and liberate the parent drug by gradual hydroly-

sis [8]. The conversion into their less polar and more volatile and thermally stable silyl ethers improves their GC–MS analysis and identification. Hence the GC–MS study of hydroxyquinones, both naturally occurring and synthetic, is of importance.

Despite the extensive studies of hydroxyquinones and their derivatives, little information is available about their silylation [9–12], which concerns mainly partial silylation of the hydroxyl groups of hydroxyanthraquinones for GC analysis. Henriksen and Kjøsen [13] dealt with the reductive silylation of some hydroxyanthraquinones for GC–MS analysis. Their approach suggests prolonged reaction periods and complex reaction conditions, involving both bases and solvents.

This work is a part of a programme to develop a better understanding of silylation reactions of quinones for synthetic, analytical and biological purposes [14,15]. We report here a simple and very efficient method for the quantitative reductive silylation of both hydroxynaphtho- and hydroxyanthraquinones with N-methyl-N-tri-

---

* Corresponding author.

methylsilyltrifluoroacetamide (MSTFA), along with a detailed discussion of the mass spectra of the products and a proposal for a fragmentation mechanism. The silylation scheme was applied also to synthetic mixtures of hydroxyquinones resulting in successful GC–MS separation of the silylated derivatives, which is particularly important for the isomers of dihydroxyanthraquinones.

EXPERIMENTAL

Materials

The hydroxyquinones employed were purchased from Fluka and were of analytical-reagent grade. Their purity was checked by TLC (one spot with a 20-μg sample). MSTFA was also obtained from Fluka and was of GC quality.

Reductive trimethylsilylation

Trimethylsilyl derivatives were prepared by treating of the hydroxyquinone with MSTFA. Although many silylating agents with different and specific activities are currently available, MSTFA was chosen as the most suitable among the four active silylamides [16] the others being bistrimethylsilyltrifluoroacetamide (BSTFA), bistrimethylsilylacetamide (BSA) and N-methyl-N-trimethylsilylacetamide (MSA), because of its greatly reduced retention time (t_R) (b.p. 132°C) and its volatile by-product N-methyltrifluoroacetamide (MTFA) and it was used as the reaction solvent. MTFA appears as a symmetrical peak before that of MSTFA and does not influence the chromatogram. Further, it can be easily removed by blowing a stream of dry nitrogen on to the surface of the reaction mixture at room temperature.

The extent of silylation was controlled by varying the MSTFA to hydroxyquinone ratio. The appropriate amount of NH_4I was added at the beginning (Table I). The reaction was carried out at 60°C and was completed in 20–60 min. The samples were then injected directly into the GC–MS system.

During the process of optimizing the reaction conditions (hydroxyquinone-to-MSTFA ratio, amount of NH_4I, reaction time, temperature), occasionally more than one peak was obtained in

the gas chromatogram, owing to the insufficient amount of the silylating agent used. The additional peaks were due to unsilylated compound and mono-, di-, etc., silylated derivatives.

In order to avoid the formation of siloxane by-products, particular care was taken to protect the reactants and products from moisture, even in trace amounts, by thorough drying of all starting materials and apparatus.

Instrumentation

GC–MS analysis was carried out on a Hewlett-Packard Model HP 5890 gas chromatograph coupled with a VG TS-250 mass spectrometer. The GC system was fitted with a 25 m × 0.2 mm I.D. OV-1 column and the end of the column was introduced directly into the mass spectrometer analyser chamber. The system was operated under the following conditions: helium pressure, 5 psi; injector temperature, 280°C; and GC column temperature, 80°C for 3 min, increased at 25°C/min from 80 to 280°C, held at 280°C for 10 min. The mass spectrometer was set to scan from 40 to 700 u per nominal second with an ionizing voltage of 70 eV.

RESULTS AND DISCUSSION

Optimization of reaction conditions

The reductive silylation reaction was applied to ten different hydroxyquinones, namely 5-hydroxy-1,4-naphthalenedione [5-HNQ (1)], 2-hydroxy-1,4-naphthalenedione [2-HNQ (2)], 5,8-dihydroxy-1,4-naphthalenedione [5,8-DHNQ (3)], 1-hydroxy-9,10-anthracenedione [1-HAQ
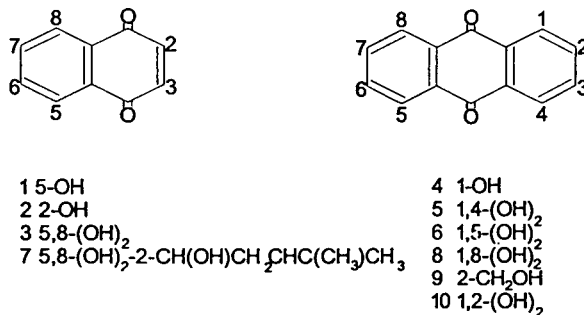

1 5-OH
2 2-OH
3 5,8-(OH)$_2$
7 5,8-(OH)$_2$-2-CH(OH)CH$_2$CHC(CH$_3$)CH$_3$

4 1-OH
5 1,4-(OH)$_2$
6 1,5-(OH)$_2$
8 1,8-(OH)$_2$
9 2-CH$_2$OH
10 1,2-(OH)$_2$

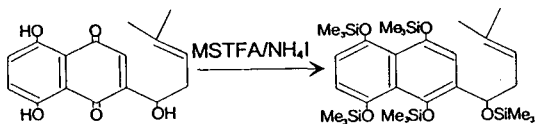Fig. 1. Structures of hydroxynaphtho- and hydroxyanthraquinones.

Fig. 2. Reaction scheme of the reductive silylation of hy-droxyquinones **1–10**.

(**4**)], 1,4-dihydroxy-9,10-anthracenedione [1,4-DHAQ (**5**)], 1,5-dihydroxy-9,10-anthracene-dione [1,5-DHAQ (**6**)], 5,8-dihydroxy-2(1-hy-droxy - 4 - methyl - 3 - pentenyl) - 1,4 - naphthalene-dione [5,8-DHHMPNQ (**7**)], 1,8-dihydroxy-9,10-anthracenedione [1,8-DHAQ (**8**)], 2-hydroxy-methyl-9,10-anthracenedione [2-HMAQ (**9**)] and 1,2-dihydroxy-9,10-anthracenedione [1,2-DHAQ

(**10**)] (Fig. 1) and to a mixture of the entire series.

The reductive silylation reaction may be ex-pressed as in the reaction scheme shown in Fig. 2 for [5,8-DHHMPNQ (**7**)].

The reductive silylation reaction was applied using gradually increasing amounts of the silylat-ing agent (MSTFA), in order to reach the optimum ratio of hydroxyquinone/silylating agent (Fig. 3). The completion of the reaction was checked by GC (one peak).

Table I presents the optimum conditions and yields of the reductive silylation reaction of the hydroxyquinones.

The longer reaction periods and the increased amounts of silylating agent required for the *ortho*
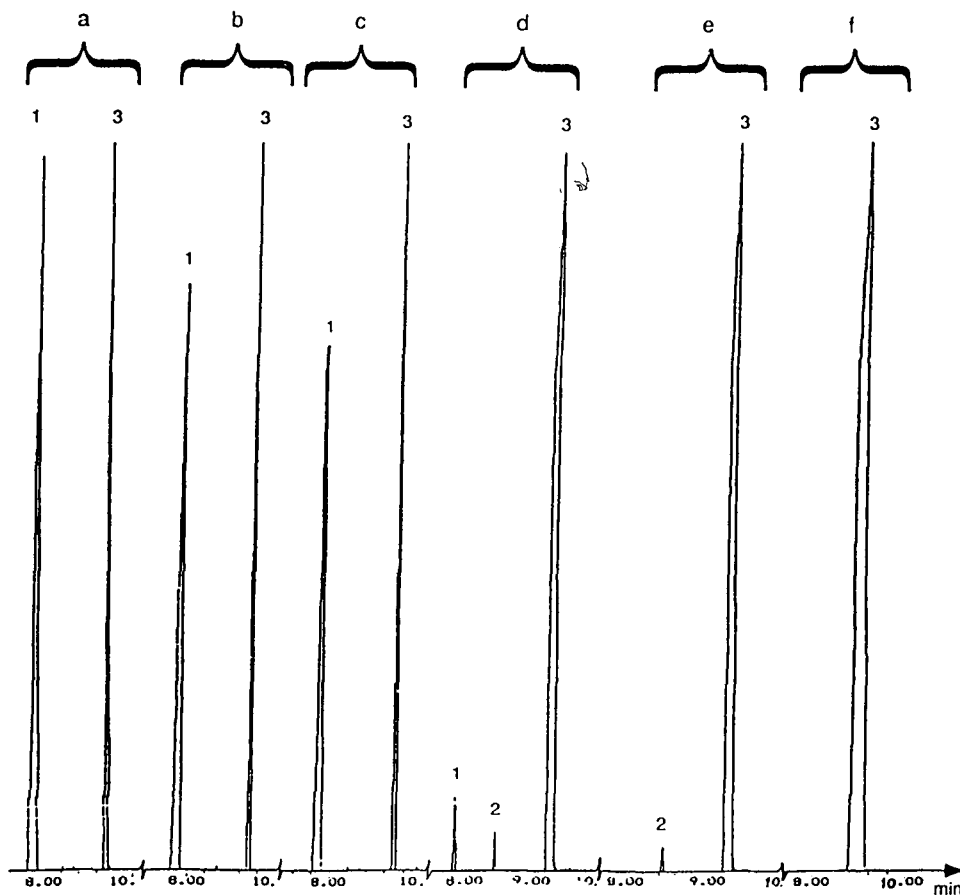
Fig. 3. 5-HNQ (**1**) as an example of optimization process of the hydroxyquinone-to-MSTFA ratio. Moles of hydroxyquinone to moles of MSTFA = (a) 1:14, (b) 1:21, (c) 1:28, (d) 1:35, (e) 1:40, and (f) 1:42. For conditions, see Experimental. Peaks: 1 = 5-HNQ-TMS; 2 = 5-HNQ-2-TMS; 3 = 5-HNQ-3-TMS.

TABLE I

REDUCTIVE SILYLATION OF VARIOUS HYDROXYQUINONES WITH MSTFA IN THE PRESENCE OF NH_4I

Substrate		Conditions				Product[a,b]		Yield[c]
No.	Compound	Temperature (°C)	Time (min)	Quinone/MSTFA (mmol)	MSTFA/NH_4I (ml/mg)	No.	Compound (%)	
1	5-HNQ	60	20	1:42	1:4	1a	5-HNQ-3-TMS	100
2	2-HNQ	60	20	1:42	1:4	2a	2-HNQ-3-TMS	100
13	5,8-DHNQ	60	30	1:56	1:4	3a	5,8-DHNQ-4-TMS	100
14	1-HAQ	60	25	1:42	1:12	4a	1-HAQ-3-TMS	100
15	1,4-DHAQ	60	60	1:80	1:12	5a	1,4-DHAQ-4-TMS	100
6	1,5-DHAQ	60	60	1:94	1:12	6a	1,5-DHAQ-4-TMS	100
7	5,8-DHHPMNQ	60	60	1:80	1:4	7a	5,8-DHHPMNQ-5-TMS	100
8	1,8-DHAQ	60	30	1:56	1:12	8a	1,8-DHAQ-4-TMS	100
9	2-HMAQ	60	25	1:56	1:4	9a	2-HMAQ-3-TMS	100
10	1,2-DHAQ	60	30	1:56	1:12	10a	1,2-DHAQ-4-TMS	100

[a] All products showed the expected spectra for the structures assigned.
[b] The silyl ether corresponding to substrate *n* is denoted as *n*a.
[c] Determined by GC.

2, 10 and *peri* (1, 3–8), hydroxy-substituted naphtho- and anthraquinones should be attributed to the strong hydrogen bonds between the hydroxyl groups and the quinonoid oxygens [17].

GC separation of silylated products

GC retention and MS data for the trimethylsilylated hydroxyquinones are presented in Table II.

In contrast to the free polyhydroxyquinones [10] and in spite of the relatively high molecular masses resulting from the reductive silylation, all compounds were eluted as symmetrical peaks without tailing.

As shown in Table II, the GC elution order largely follows the molecular masses, with the exception of compounds 4a, 7a and 9a in which more or less masking of the polar aromatic system resulted to reduced or increased t_R [9, 12].

MS fragmentation of trimethylsilylated products of hydroxyquinones

Few mass spectra of the trimethylsilylated hydroxyquinones have been discussed in detail before [13].

In this study of the mass spectra of TMS derivatives of the hydroxyquinones 1–10, the ions of m/z 73, 45 and 147 are common to all of them. The ion of m/z 73 corresponds to the trimethylsilyl cation, $[SiMe_3]^+$, and a mechanism for its production has been proposed by Henriksen and Kjøsen [13]. The ion of m/z 45 has also been observed in the mass spectra of di-TMS derivatives of dihydroxy-, diamino-, etc., naphthalenes [18] and corresponds to the $[CH_5Si]^+$ cation. Finally, the ion of m/z 147 is frequently observed in the mass spectra of di-TMS derivatives and is attributed to $(CH_3)_3Si-O^+ = Si(CH_3)_2$, produced upon rearrangements [19–21].

The compounds under study may be classified in two categories with respect to their fragmentation pattern; one possessing *peri* (Fig. 4) and the other *ortho* silylated groups (Fig. 5).

The presence of the $[M-88]^+$ ion in abundance in all the studied mass spectra except that of 9a, could be explained by the extreme local steric crowding leading to extensive fragmentation. Thus, elimination of a methyl group in the first step and subsequently of a trimethylsilyl radical from the molecular ion give rise to the $[M-88]^+$ ion. This fragmentation pattern is repeated for every existing pair of trimethylsilyl groups in *ortho* and *peri* positions in the molecule. The driving force for the expulsion of the trimethylsilyl radical, in the second step, is the

TABLE II

GAS CHROMATOGRAPHIC AND MASS SPECTROMETRIC DATA FOR THE REDUCTIVELY SILYLATED HYDROXYQUINONES 1–10

No.	Hydroxyquinone	Product		t_R (min)	$M^{+\cdot}$: m/z, relative intensity (%)	Principal ions: m/z, relative intensity (%)[a,b]
		No.	Compound			
1	5-HNQ	1a	5-HNQ-3-TMS	8:16	392(100)	394(18), 395(28), *392(100)*, 377(8), 304(12), 289(30), 273(12), 229(5), 147(1), 73(62), 45(18)
2	2-HNQ	2a	2-HNQ-3-TMS	8:20	392(100)	394(16), 393(30), *392(100)*, 377(5), 304(20), 289(15), 229(10), 147(5), 73(63), 45(20)
3	5,8-DHNQ	3a	5,8-DHNQ-4-TMS	8:36	480(95)	482(25), 481(31), 480(95), 392(10), 304(12), 274(8), 244(1), 229(5), 147(1), *73(100)*, 45(20)
4	1-HAQ	4a	1-HAQ-3-TMS	9:38	442(50)	444(8), 443(19), 442(50), 354(12), 339(6), 324(3), 281(9), 279(3), 235(3), 147(1), 74(9), *73(100)*, 45(18)
5	1,4-DHAQ	5a	1,4-DHAQ-4-TMS	9:45	530(7)	530(7), 442(2), 354(5), 324(2), 294(1), 279(2), 147(2), *73(100)*, 45(20),
6	1,5-DHAQ	6a	1,5-DHAQ-4-TMS	9:58	530(11)	530(11), 442(1), 354(6), 324(1), 294(1), 279(1), 147(1), *73(100)*, 45(20)
7	5,8-DHHMPNQ	7a	5,8-DHHMPNQ-5-TMS	10:07	650(5)	650(5), 583(10), 582(17), 581(40), 493(10), 421(5), 405(3), 229(1), 147(2), *73(100)*, 45(10)
8	1,8-DHAQ	8a	1,8-DHAQ-4-TMS	10:25	530(10)	531(5), 530(10), 442(5), 369(5), 412(1), 297(1), 279(1), *73(100)*, 45(20)
9	2-HAQ	9a	2-HAQ-3-TMS	10:35	456(47)	458(7), 457(20), 456(47), 367(5), 294(2), 279(7), 147(5), 75(6), 74(8), *73(100)*, 45(25)
10	1,2-DHAQ	10a	1,2-DHAQ-4-TMS	10:50	530(75)	532(18), 531(30), 530(75), 515(5), 442(18), 412(1), 369(6), 297(4), 279(1), 147(3), 74(8), *73(100)*, 45(20)

[a] Relative to the base peak.
[b] The base peak is italicized.
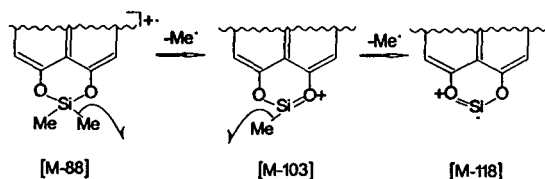
Fig. 4. Main fragmentation path of the *peri*-silylated hydroxyquinones.
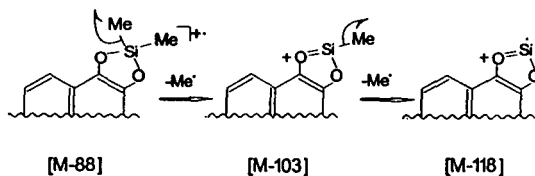
Fig. 5. Main fragmentation path of the *ortho*-silylated hydroxyquinones.
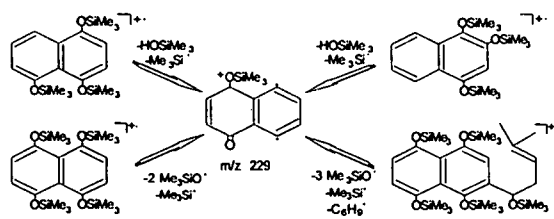
Fig. 6. Proposed fragmentation mechanism for the reductively silylated hydroxynaphthoquinones 1, 2, 3 and 7.

stability of the silicon–oxygen bond, which leads to the formation of a stable cyclic radical cation. The structure of the $[M - 88]^+$ ion, for both *peri* and *ortho* isomers, has been proposed [13].

According to Smith *et al.* [18], the ions $[M - 103]^+$ and $[M - 118]^+$, which are also observed in the mass spectra, are characteristic of the silyl ethers of *peri*-disilylated naphthalenes produced by elimination of a second and, in sequence, a third methyl radical and correspond to six-membered cationic chelate rings, of the type 2-methyl-1,3-dioxa-2-silanan and 1,3-dioxa-2-silanen, respectively (Fig. 4).

Ortho-disilylated naphthalenes also show these $[M - 103]^+$ and $[M - 118]^+$ ions, but to a lesser

extent, owing to the reduced stability of their five-membered radical cationic ring (Fig. 5). Further, the absence or the low intensity of the previously mentioned ions, and also $[M - 88]^+$ for the di-TMS derivatives of *meta-* and *para-*isomers, demonstrate that such positional isomerism *per se* is not responsible for the production of these ions in the disilylated naphthalenes.

These results are in agreement with ours (Table II). Consequently, this pronounced *ortho* and *peri* effect is valuable in the interpretation and identification of unknown hydroxyquinones in complicated mixtures or in natural products.

Two more ions of great importance are those of *m/z* 229 and 279. The former is characteristic of all the silylated hydroxynaphthoquinones studied and the latter characterizes all the silylated hydroxyanthraquinones. These two ions correspond to the cationic diradical of 1,4-naphthoquinone and 9,10-anthraquinone, respectively (Figs. 6 and 7).

The mass spectra of the tri-TMS ethers of 1, 2 and 4, exhibit a common fragmentation pattern and so do the tetra-TMS ethers 3a, 5a, 6a, 8a
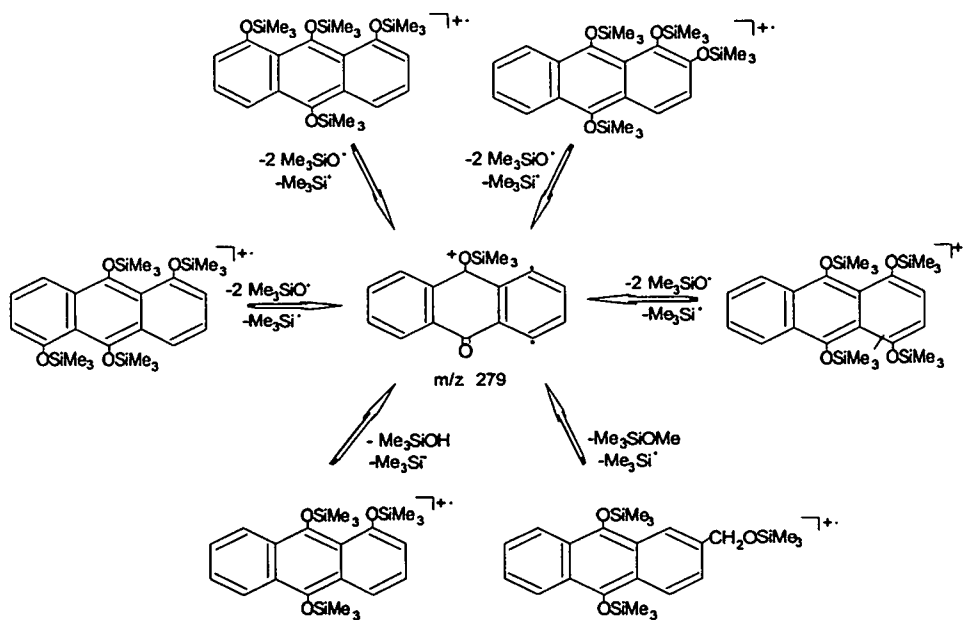
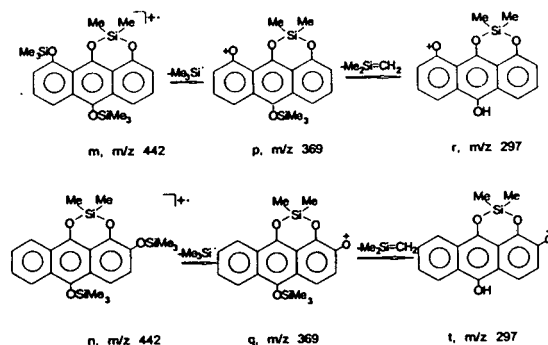Fig. 7. Proposed fragmentation mechanism for the reductively silylated hydroxynaphthoquinones 4, 5, 6, 8, 9 and 10.
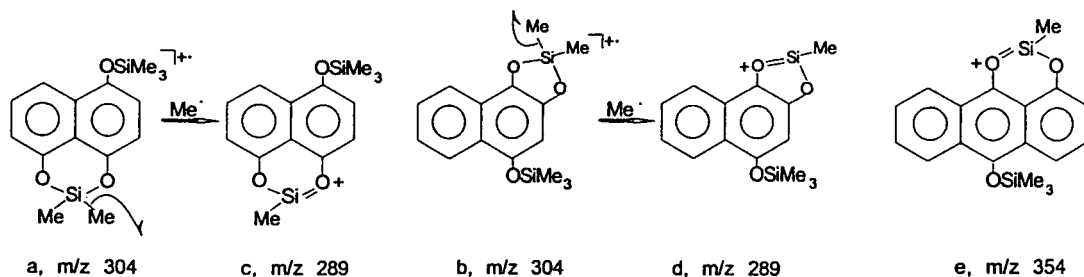
Fig. 8. Principal ions formed by the fragmentation of the reductively silylated hydroxyquinones **1** (**a, c**), **2** (**b, d**) and **4** (**e**).

and **10a**. Compounds **7a** and **9a** follow their own fragmentation pathway due mainly to the existence of an aliphatic side-chain in each of them.

Mass spectra of 5-HNQ-3-TMS (1a), 2-HNQ-3-TMS (2a) and 1-HAQ-3-TMS (4a)

Both **1a** and **2a** show the molecular ion $M^{+\cdot}$ of m/z 392 as the base peak and the $[M - 88]^+$ ion, **a, b**, of m/z 304 in significant abundance (12% and 20%, respectively) (Fig. 8). However, owing to the *ortho* effect, the ion **c**, $[M - 103]^{+\cdot}$, of m/z 289, is of lesser abundance (15%) in **2a** than in its isomer **1a** (**d**, 30%). In the mass spectrum of **4a** the ion $[M - 103]^+$ of m/z 339, **e**, is of lesser abundance (6%) than the $[M - 88]^+$ ion of m/z 354, suggesting the greater stability of the former ion, **e**.

Mass spectra of 5,8-DHNQ-4-TMS (3a), 1,4-DHAQ-4-TMS (5a), 1,5-DHAQ-4-TMS (6a), 1,8-DHAQ-4-TMS (8a) and 1,2-DHAQ-4-TMS (10a)

In the mass spectra of all these trimethylsilyl ethers the base peak is due to a fragment of m/z 73, through the gradual loss of two trimethylsilyl radicals for the first three or only one for the last two. Therefore, two peaks are observed at m/z 392 and 304 for **3a** and m/z 442 and 354 for the others, corresponding to the $[M - 88]^+$ and $[M - 176]^+$ ions, respectively.

For the last two ethers elimination occurs first of a tetramethylsilane molecule followed by the loss of a trimethylsilyl radical and finally of a $(CH_3)_2Si{=}CH_2$ molecule. Consequently, three ions are formed, of m/z 442 (**m** and **n**, respec-

tively, for **8a** and **10a**), m/z 369, (**p, q**) and m/z 297 (**r, t**), the last one being of very low abundance (0.1% and 2%, respectively) (Fig. 9).

Mass spectra of 5,8-DHHPMNQ-5-TMS (7a) and 2-HMAQ-3-TMS (9a)

The fragmentation pattern of **7a** begins by the elimination of the side-chain followed by two successive losses of tetramethylsilane molecules. Three ions of m/z 581, 493 and 405 are formed, corresponding to $[M - C_5H_9]$ (**u**), $[M - C_5H_9 - 88]$ (**v**) and $[M - C_5H_9 - 2 \times 88]$ (**w**) ions, respectively (Fig. 10).

Elimination of a trimethylsilyloxy radical from the molecular ion of **9a**, followed by the loss of a trimethylsilyl radical, forms two ions of m/z 367 (**x**) and 294 (**y**) (Fig. 11).

Fig. 9. Principal ions formed by the fragmentation of the reductively silylated hydroxyquinones **8** (**m, p, r**) and **10** (**n, q, t**).
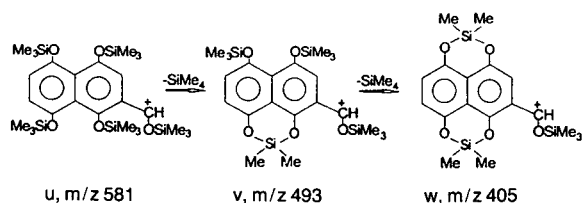
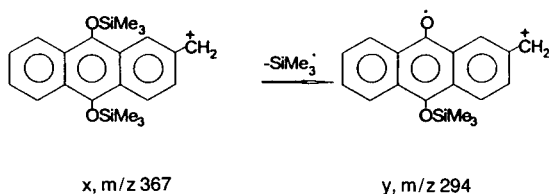Fig. 10. Proposed fragmentation mechanism for **7a**.

Fig. 11. Principal ions formed by the fragmentation of **9a**.

GC separation of a synthetic mixture of the hydroxyquinones studied

A typical GC separation of a synthetic mixture of all hydroxynaphtho- and hydroxyanthraquinones silyl ethers studied is presented in Fig. 12. The components were identified by co-injection with each component alone coupled by a computerized library search in the GC–MS system.
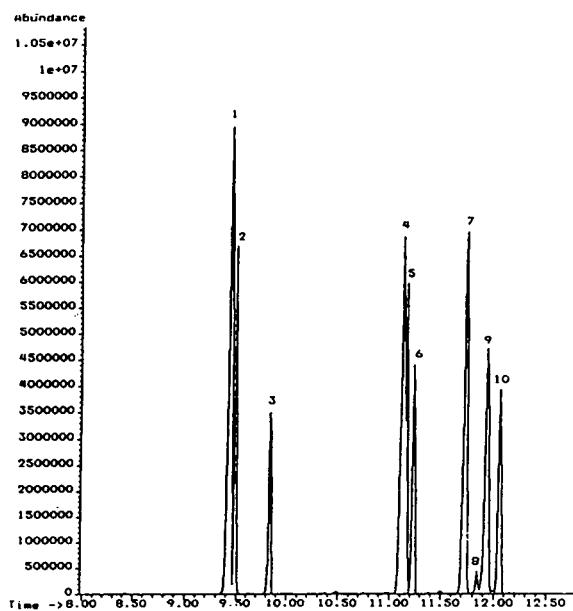

Fig. 12. Separation of a mixture of the trimethylsilylated hydroxyquinones **1–10**. For conditions, see Experimental. For peak identification, see Table II. Time in min.

In addition to the well formed peak shapes obtained and the complete separation of the mixture, especially that of the isomeric anthraquinones **5**, **6**, **8** and **10**, the retention times for the constituents of the mixture closely follow the order of the net trimethylsilylated compounds.

CONCLUSIONS

A straightforward and clear reductive trimethylsilylation reaction was applied to several hydroxyquinones, resulting in the quantitative protection of all functional groups. GC–MS proved to be a very effective method for the optimization of the silylation reaction conditions. The MS study of all silylated compounds provided some useful rules for the interpretation of the O-trimethylsilylated products. The reductive trimethylsilylation procedure is also applicable to the GC–MS separation and characterization of hydroxyquinones, even isomeric compounds, in mixtures.

REFERENCES

1 F. Arcamone, G. Cassinelli, G. Fautini, A. Grein, P. Orezzi, C. Pol and C. Spalla, *Biotechnol. Bioeng.*, 11 (1969) 1101.
2 A.J. Lin and A.C. Sartorelli, *J. Org. Chem.*, 38 (1973) 813.
3 C.A. Tsipis, E.G. Bakalbassis, V.P. Papageorgiou and M.N. Bakola-Christianopoulou, *Can. J. Chem.*, 60 (1982) 2477
4 V.P. Papageorgiou, M.N. Bakola-Christianopoulou and C.A. Tsipis, *Eur. Pat. Appl.*, No. 831116, 1983.
5 V.P. Papageorgiou, *J. Med. Plant Res.*, 38 (1980) 193.
6 H.S. Kadem (Editor), *Anthracycline Antibiotics*, Academic Press, New York, 1982.
7 D.E. Williamson and G.W. Eyerett, Jr., *J. Am. Chem. Soc.*, 97 (1975) 2397.
8 A.J. Crowe, *Chem. Ind. (London)*, (1983) 304.
9 T. Furuya, S. Shibata and H. Iizuka, *J. Chromatogr.*, 21 (1966) 116.
10 J.B. Terril and E.S. Jacobs, *J. Chromatogr. Sci.*, 8 (1970) 604.
11 G.W. Eijk and H.J. Roeijmans, *J. Chromatogr.*, 295 (1984) 497.
12 G.W. Eijk and H.J. Roeijmans, *J. Chromatogr.*, 124 (1976) 66.
13 L.M. Henriksen and H. Kjøsen, *J. Chromatogr.*, 258 (1983) 252.
14 M.N. Bakola-Christianopoulou, *J. Organomet. Chem.*, 308 (1986) C24.

15 M.N. Bakola-Christianopoulou, *J. Mol. Catal.*, 65 (1991) 307.
16 M. Donike, *J. Chromatogr.*, 42 (1969) 103.
17 S. Patai and Z. Rappoport (Editors), *The Chemistry of the Quinonoid Compounds*, Wiley, Chichester, 1988.
18 J.L. Smith, J.L. Beck and W.J.A. VandenHeuvel, *Org. Mass Spectrom.*, 5 (1971) 473.
19 W.J.A. VandenHeuvel, J.L. Smith, P. Haug and J.L. Beck, *J. Heterocycl. Chem.*, 9 (1972) 451.
20 J. Dickman, J.B. Thompson and C. Djerassi, *J. Org. Chem.*, 33 (1968) 2271.
21 E. White, V.S. Tsuboyama and J.A. McCloskey, *J. Am. Chem. Soc.*, 93 (1971) 6340.

Capillary gas chromatographic separation of some diastereomeric amides from carbonyldiimidazole-mediated microgram-scale derivatizations of the acid moiety of permethrin insecticide ☆

W.G. Taylor*, D.D. Vedres and J.L. Elder

Agriculture Canada Research Station, P.O. Box 3000 Main, Lethbridge, Alberta T1J 4B1 (Canada)

ABSTRACT

Mixtures from microgram-scale derivatizations of reference samples of (1*R*,3*S*)-*cis*-, (1*S*,3*R*)-*cis*-, (1*R*,3*R*)-*trans*- and (1*S*,3*S*)-*trans*-3-(2,2-dichloroethenyl)-2,2-dimethylcyclopropane carboxylic acid with carbonyldiimidazole and seven chiral amines were investigated by achiral phase capillary gas chromatography (GC) with a flame ionization detector. The desired diastereomeric amides were identified by GC–mass spectrometry. Several combinations of derivatives and GC liquid phases were useful for resolving either pair of enantiomeric acids. Baseline separation of the four acids was achieved with (*R*)(−)- or (*S*)(+)-amphetamine derivatives and with a polar GC column of DB-WAX. The enantiomeric composition of the permethrin amides determined by GC was in agreement with the enantiomeric composition of the permethrin acids determined by polarimetry.

INTRODUCTION

Permethrin, a synthetic pyrethroid insecticide possessing asymmetric centers at C-1 and C-3 of the cyclopropane ring, is a mixture of four stereoisomeric esters (**1a–4a**, Fig. 1). It is well known that the insecticidal activity is primarily associated with the (1*R*,3*S*)-*cis* and (1*R*,3*R*)-*trans* isomers, **1a** and **3a**. Metabolic studies have shown that ester hydrolysis occurs to various extents in plant and animal species [1]. Thus, the chiral carboxylic acids (**1b–4b**) and their water-soluble conjugates are important metabolites of permethrin.

To study stereoselective processes involved in the synthesis and degradation of permethrin, isomer-specific approaches are needed to sepa-

rate trace amounts of **1b–4b**. Separations by achiral phase gas chromatography (GC) with diastereomeric esters derived from (+)-2-octanol [2] and (−)-menthol [3] and by chiral phase GC with esters of achiral alcohols [4] have previously been reported. Diastereomeric amide derivatives, prepared from the acid chlorides of **1b–4b** and optically active α-methylbenzenemethaneamine [α-methylbenzylamine or 1-(1-phenyl)ethylamine], have also been resolved by high-performance liquid chromatography (HPLC) [5].

In analytical derivatizations of antiinflammatory 2-arylpropionic acids with the chiral amines leucinamide [6,7], α-methylbenzylamine [8–12] and α-methylbenzeneethanamine (amphetamine) [13,14], a popular amide bond-forming strategy has involved the use of carbonyldiimidazole (CDI). Some of these procedures were applied to the stereospecific HPLC [6,7,9–11] and GC [8,12–14] determination of the *R* and *S* enantio-

---

* Corresponding author.
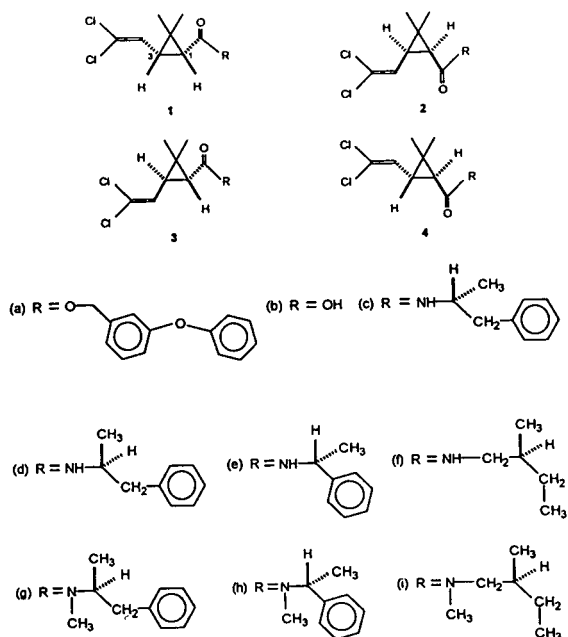☆ L.R.S. Contribution No. 3879265.

Fig. 1. Structures of the isomers of permethrin and of the derivatives under investigation.

mers of the carboxylic acids in biological samples. The capillary GC separation of other chiral carboxylic acids as their diastereomeric α-methylbenzylamides has also been reported [15]. Furthermore, CDI has previously been utilized in pyrethroid chemistry, for example in the preparative-scale coupling of (1R,3R)-*trans*-chrysanthemic acid with (R)(+)-1-(α-naphthyl)ethylamine [16].

Using CDI as the coupling reagent and reference samples of **1b–4b**, which were previously employed for preparing the stereoisomers of permethrin [17], we have investigated the microgram-scale derivatization of these carboxylic acids with (R)(−)-amphetamine, (S)(+)-amphetamine, (R)(+)-α-methylbenzylamine, (S)-(−)-2-methylbutylamine, N-methyl (S)(+)-amphetamine (methamphetamine), N-methyl (R)(+)-α-methylbenzylamine and N-methyl (S)(−)-2-methylbutylamine. The capillary GC properties of the 28 diastereomeric amides (**1–4**, **c–i**; Fig. 1) have been examined on three common achiral liquid phases with a flame ionization detector. The novel 1-methyl-2-phenylethylamides derived from amphetamine were found

to be the most useful derivatives for separating these four stereoisomeric carboxylic acids by capillary GC.

EXPERIMENTAL

Chemicals and reagents

Reference samples of **1b–4b** were purchased from Raylo Chemicals Ltd. (Edmonton, Canada). Comparison of $[\alpha]_D$ values to those found in the literature [18] showed that **1b–3b** were approximately 100% optically pure. The sample of **4b** gave $[\alpha]_D = -22.3$ ($c = 2.1\%$, ethanol) whereas the literature [18] $[\alpha]_D = -34.6$ ($c = 1.9\%$, ethanol). This corresponds to 64.5% optical purity or 82% **4b** (18% **3b**).

(R)(−)-Amphetamine sulfate, (S)(+)-amphetamine sulfate and (S)(+)-methamphetamine hydrochloride were gifts from Health and Welfare Canada. (R)(+)-α-Methylbenzylamine and (S)(−)-2-methylbutylamine were purchased from Aldrich, whereas the N-methyl derivatives of these amines were prepared by a literature procedure [19] using ethyl chloroformate and lithium aluminum hydride and characterized by mass spectrometry (MS). CDI was purchased from Aldrich and Sigma and stored under vacuum in a desiccator. Organic solvents were OmniSolv glass-distilled grade (supplied by BDH, Edmonton, Canada). Water was distilled and further purified by a Barnstead NANOpure II system. All glassware was sonicated in methanol and oven-dried prior to use.

Stock solutions of CDI (1 mg/ml) and the chiral amines (0.7–1.2 mg/ml; equivalent to 800 nmol of the free base/ml) were prepared fresh daily in methylene chloride (water for amphetamine and methamphetamine salts). Test solutions of **1b–4b** (100 μg/ml) were prepared weekly in methylene chloride and stored at 4°C. Prior to derivatizations with amphetamine or methamphetamine, the free bases were formed (100 × 13 mm glass tube equipped with a PTFE-lined screw cap) by diluting 100 μl of the aqueous stock solution with water (900 μl) and adding 1 M sodium hydroxide (100 μl). After mixing for 10 min on an electronic tube shaker (Vibrax Model VXR with VX attachment), the mixture was extracted (Vibrax) four times with

methylene chloride (1 ml) and the solvent was removed with a Savant evaporator (Model SVC-100H). The residue was transferred to the reaction vial in methylene chloride (200 μl).

Derivatizations

CDI (100 μl of stock solution, 100 μg, 616 nmol) and one of **1b–4b** (100 μl of test solutions, 10 μg, 47.8 nmol) were added to a Pierce Reacti-Vial (45 × 13 mm) equipped with a PTFE-coated micro stir bar (10 × 3 mm) and a PTFE-lined screw cap (septum type). The mixture was magnetically stirred (Reacti-Therm III module) under argon gas for 15 min at room temperature (21–23°C), then the amine (800 nmol) in methylene chloride (100 or 200 μl) was added and stirring was continued at room temperature for 1 h. The reaction mixture was evaporated to dryness (Savant). Methyl *tert.*-butyl ether (500 μl) and 1 *M* hydrochloric acid (500 μl) were added followed by a 2-min shake (Vibrax) and a 2-min centrifugation. The organic phase was transferred to a glass tube (100 × 13 mm) and washed with 500 μl of a saturated solution of sodium borate (prepared from $Na_2B_4O_7 \cdot 10H_2O$, Fisher), then with water (500 μl), centrifuging after each wash. The organic phase in a glass tube (100 × 13 mm) was evaporated (Savant), the residue was dissolved in methylene chloride (100 μl), vortexed (VWR vortex mixer) and 1–4-μl portions were removed (Hamilton 701 syringe) for capillary GC and GC–MS analyses.

Instrumentation and chromatographic conditions

Hewlett-Packard 5830 and 5890 gas chromatographs equipped with flame ionization detectors were used. The injector and detector temperatures were 225 and 250°C, respectively. Helium was used as the carrier gas with inlet pressures adjusted to give linear flow velocities for hexane of 28–29 cm/s at 35°C. J&W fused-silica capillary columns of DB-1 (30 m × 0.25 mm I.D.; film thickness 0.25 μm), DB-5 (30 m × 0.32 mm I.D.) and DB-WAX (30 m × 0.24 mm I.D.) were used. Samples were injected splitless (30 s) with column temperature programming (DB-1, DB-5) from 50 to 140°C at 25°C/min, at 3°C/min to 215°C and at 15°C/min

to 265°C. With DB-WAX, the rate was 25°C/min from 50 to 140°C and 3°C/min to 250°C.

Mass spectra were obtained on a Hewlett-Packard 5985B GC–MS instrument under electron-impact (70 eV) and chemical-ionization conditions. Isobutane (0.5 Torr; 1 Torr = 133.322 Pa) served as the reagent gas for chemical-ionization mass spectrometry. The transfer lines were maintained at 250°C and the ion source at 200°C (electron impact) or 180°C (chemical ionization). Capillary columns of HP-1 (25 m × 0.2 mm I.D.) from Hewlett-Packard and SPB-1 (30 m × 0.32 mm I.D.) from Supelco were used. The samples were injected splitless (30 s) with helium as the carrier gas.

RESULTS AND DISCUSSION

Derivatization experiments were initially carried out with the (1*R*,3*S*)-*cis* enantiomer **1b** by reacting this optically active acid with excess CDI and (*R*)(−)-amphetamine. Our procedure is based, in part, on a publication of Singh *et al.* [13] who reported the derivatization of several 2-arylpropionic acids with these reagents in methylene chloride or chloroform. Although the reported conditions suggested a 2-h stir at 65–85°C [13,14], **1b** (and the other permethrin acids) could be derivatized in methylene chloride at room temperature (1 h).

Assuming that both chiral reagents were optically pure and that racemization did not occur during the reaction, the anticipated derivative 3-(2,2-dichloroethenyl)-2,2-dimethyl-N-(1-methyl-2-phenylethyl) cyclopropanecarboxamide (**1c**) will possess the *R*, *S* and *R* stereochemistry at C-1, C-3 and in the amine moiety, respectively. Therefore, **1c** is designated as the *RSR* diastereomer.

GC–MS analysis of a derivatized mixture gave a mass chromatogram shown in Fig. 2. Under electron-impact conditions, the component at 22.7 min showed a pair of weak ions at *m/z* 325 and 327 corresponding to the molecular ions for **1c** ($C_{17}H_{21}Cl_2NO^{+\cdot}$). Prominent fragment ions at *m/z* 91 (base peak), 119 and 162, originating from the amphetamine portion of the molecule, were observed. The chemical-ionization mass
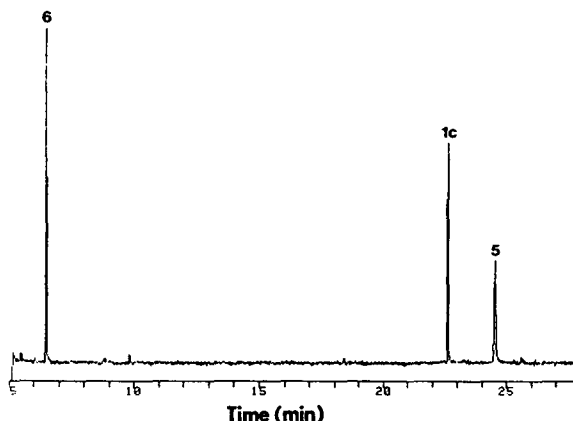
Fig. 2. Total ion mass chromatogram (70 eV) of a mixture obtained from derivatization of $(1R,3S)$-cis acid **1b** with CDI and $(R)(-)$-amphetamine. The HP-1 column was temperature programmed from 50 to 140°C at 25°C/min, at 5°C/min to 215°C, then at 15°C/min to 265°C. Peaks: **1c** = amide; **5** = urea; **6** = isocyanate.
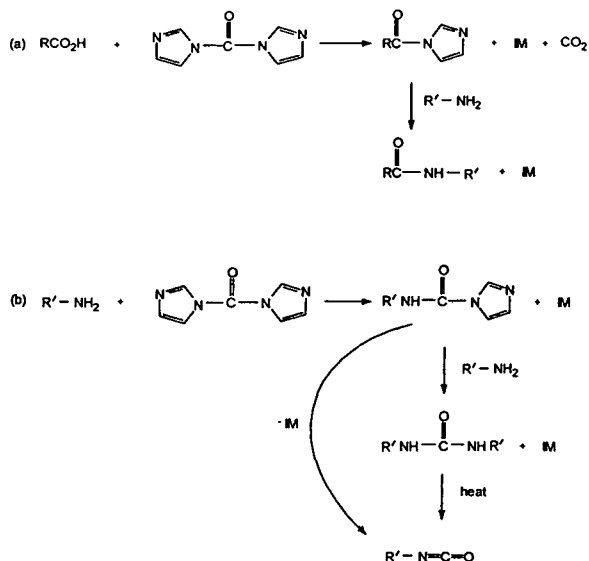

Fig. 3. Reactions of CDI with carboxylic acids and primary amines. (a) Amide formation; (b) urea and isocyanate formation. IM = Imidazole.

spectrum gave prominent quasimolecular ions for **1c**, at m/z 326 and 328.

Derivatization of **1b** with $(S)(+)$-amphetamine gave a mass chromatogram that was similar to Fig. 2 except that the desired **1d** (RSS) eluted before **1c**, at 22.4 min. The mass spectra of **1c** and **1d** were nearly identical.

Fig. 2 shows that a second major component of the derivatization reaction eluted from the capillary column at 24.5 min. The molecular mass (296) and fragment ions $(m/z$ 205, 91, 44) suggested that this product was the symmetrically disubstituted methylphenylethyl derivative of urea, $C_6H_5CH_2CH(CH_3)NHCONHCH(CH_3)$-$CH_2C_6H_5$ (**5**). Ureas are formed by the reaction of amines with CDI [20], and this pathway would be expected to compete with the desired amide bond-forming reaction (Fig. 3). Furthermore, intermediate imidazole-N-carboxamides can dissociate to an isocyanate and imidazole [20]. Indeed, a third major component eluting at 6.5 min (Fig. 2) gave a molecular ion at m/z 161 corresponding to $C_6H_5CH_2CH(CH_3)N = C = O$ (**6**) in addition to fragment ions at m/z 91 and 70. The urea (**5**) and isocyanate (**6**) were also found in control derivatizations without **1b**.

It is also possible that **6** represents a thermal degradation product since ureas are capable of

decomposing to isocyanates during gas chromatography [21].

GC analyses with DB-1 indicated that samples of **1c** (RSR) contained a small amount of a compound with the same retention time as **1d** (RSS). Naturally, **1d** would also be formed if $(S)(+)$-amphetamine was a contaminant in the sample of $(R)(-)$-amphetamine. This minor isomeric component (1–2% from GC peak area ratios) could also be **2c** (SRR) if **1b** was contaminated with **2b** because **1d** and **2c** are optical isomers and have identical retention times on achiral columns.

Samples of **1d**, prepared from **1b** and $(S)(+)$-amphetamine, were found by GC to contain **1c** (or possibly **2d**) but to the extent of 5%. This discrepancy could be attributed to small differences in the optical purities of the amine samples, $(R)(-)$-amphetamine being purer than $(S)(+)$-amphetamine. Indeed, derivatization of the $(1S,3R)$-cis acid **2b** with CDI and $(R)(-)$-amphetamine gave **2c** (SRR) and **2d** (or **1c**) in a ratio of 98 to 2 whereas experiments with $(S)(+)$-amphetamine gave a ratio of **2d** to **2c** (or **1d**) of 95 to 5. These results also indicated that the derivatizations proceeded without racemiza-

tion at C-1 or C-3 and that both of the *cis* acids were of high (98–100%) optical purity.

Derivatization of **1b** with CDI and ($\bar{S}$)(+)-amphetamine was studied in detail. Using the integrated peak areas of **1d** from capillary GC analysis of the samples with a DB-1 column, enhancements in derivatization yield could not be demonstrated by heating the reaction mixture, as suggested [13]. Furthermore, decreased amounts of CDI (15–30 μg) resulted in a 4–7-fold reduction in area counts compared with the standard 100 μg addition. Urea (**5**) was always found in the derivatized samples, regardless of conditions, but the relative amount detected by GC varied between experiments. Typically, a peak area ratio of **1d** to **5** of 0.3 was observed.

Two other chiral primary amines, (*R*)(+)-α-methylbenzylamine and (*S*)(−)-2-methyl-butylamine, were coupled to **1b** and **2b** using CDI. Under the standard derivatization conditions, these amines gave the expected amides as determined by GC–MS. On DB-1 and SPB-1 capillary columns, the urea from α-methylbenzylamine, $C_6H_5CH(CH_3)NHCONHCH(CH_3)$-$C_6H_5$ (**7**), eluted after **1e** and **2e** whereas the urea from 2-methylbutylamine, CH_3CH_2CH-$(CH_3)CH_2NHCONHCH_2CH(CH_3)CH_2CH_3$ (**8**), eluted before **1f** and **2f**. In the mixture from α-methylbenzylamine, an early-eluting component in the mass chromatogram corresponded to $C_6H_5CH(CH_3)N=C=O$ (**9**) but the isocyanate from 2-methylbutylamine was not found.

Derivatization of the (1*R*,3*R*)-*trans* acid **3b** with (*R*)(−)-amphetamine, (*S*)(+)-amphetamine, (*R*)(+)-α-methylbenzylamine and (*S*)-(−)-2-methylbutylamine gave the *trans* amides (**3c**, **3d**, **3e**, **3f**). Based on GC retention times with DB-1, the ureas (**5**, **7**, **8**) and isocyanates (**6**, **9**) were also formed. About 2% of **3d** (*RRS*) or **4c** (*SSR*) were detected in the reaction of **3b** with (*R*)(−)-amphetamine, which confirmed the high (98–100%) optical purity of **3b**. The impure (1*S*,3*S*)-*trans* acid **4b** on derivatization with (*R*)(−)-amphetamine gave **4c** and **3c** (*RRR*) in a ratio of 82 to 18, the same ratio calculated from the optical purity of **4b** determined by polarimetry.

Although the ureas encountered in these de-

rivatization reactions could be separated from the pyrethroid amides on non-polar liquid phases, it was of considerable interest to suppress their formation. Some interesting approaches to this problem have been described [22]. We rationalized (Fig. 3) that secondary amines might not react with CDI for steric reasons so the N-methylamines of (*S*)(+)-amphetamine, (*R*)(+)-α-methylbenzylamine and (*S*)(−)-2-methylbutylamine were investigated. Using the same stoichiometry and conditions as before, **1b**–**4b** were derivatized with these amines and the products were examined by capillary GC and GC–MS. These reactions gave the desired tertiary amides (**1–4, g–i**) but none of the N-methylureas were found as side products. A mass chromatogram from the derivatization of **1b** with (*S*)(+)-methamphetamine is shown (Fig. 4).

The identity of the diastereomeric amides was confirmed by chemical-ionization mass spectrometry. All of the derivatives gave prominent quasimolecular ions during GC–MS analysis. The (1*R*,3*S*)-*cis* derivatives **1c**–**1i** were selected for electron-impact mass spectrometry to illus-
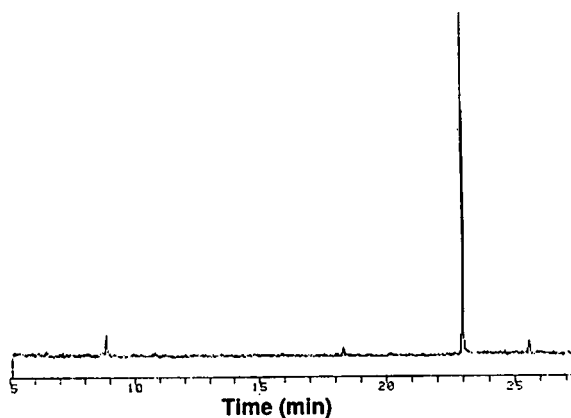

Fig. 4. Total ion mass chromatogram (70 eV) from the derivatization of (1*R*,3*S*)-*cis* acid **1b** with CDI and (*S*)(+)-methamphetamine. The HP-1 column was programmed as in Fig. 2. The peak at 23.0 min is amide **1g**. Minor peaks at 8.8, 18.3 and 25.6 min were present in control extracts without the derivatization reagents.

trate characteristic fragmentation patterns for these amides.

Besides weak molecular ions, **1c–1i** gave fragment ions (5–10% relative abundance) at m/z 163, which corresponded to the $C_7H_9Cl_2^{+\cdot}$ ion from bond cleavage α to the carbonyl group. Rupture of this same bond, but with charge retention on the amide fragment, resulted in

other diagnostic ions at m/z 176 (**1g**), 162 (**1c**, **1d**, **1h**), 128 (**1i**) and 114 (**1f**). The corresponding ion for **1e** at m/z 148 was very weak (1% of the base peak at m/z 105). Prominent ions were found that corresponded to N-alkyl bond cleavage and subsequent decomposition of the alkylaryl (or alkyl) portions. This resulted in strong ions (35–100% relative abundance) at

TABLE I

SEPARATION OF AMIDE DERIVATIVES OF PERMETHRIN ACIDS ON THREE CAPILLARY COLUMNS

Compound	Molecular mass[a]	Stereo- chemistry[b]	DB-1		DB-5		DB-WAX	
			Retention time (min)	α^c	Retention time (min)	α^c	Retention time (min)	α^c
1c (see Fig. 1)	325	*RSR*	30.92		30.10		49.66	
2c		*SRR*	30.34	1.019	29.50	1.020	48.81	1.017
3c		*RRR*	31.34		30.50		51.82	
4c		*SSR*	30.92	1.014	30.10	1.013	50.81	1.020
1d	325	*RSS*	30.34		29.52		48.82	
2d		*SRS*	30.92	1.019	30.10	1.020	49.67	1.017
3d		*RRS*	30.92		30.10		50.82	
4d		*SSS*	31.34	1.014	30.50	1.013	51.82	1.020
1e	311	*RSR*	32.44		28.22		49.03	
2e		*SRR*	32.18	1.008	27.84	1.014	48.43	1.012
3e		*RRR*	32.75		28.68		51.13	
4e		*SSR*	32.75	1.000	28.68	1.000	51.35	1.004
1f	277	*RSS*	23.16		18.64		32.64	
2f		*SRS*	23.12	1.002	18.65	1.001	32.63	1.000
3f		*RRS*	23.83		19.21		34.07	
4f		*SSS*	23.76	1.003	19.26	1.003	34.15	1.002
1g	339	*RSS*	34.37		30.97		45.45	
2g		*SRS*	34.42	1.001	31.03	1.002	45.65	1.004
3g		*RRS*	34.72		31.40		47.71	
4g		*SSS*	34.47	1.007	31.10	1.010	46.69	1.022
1h	325	*RSR*	33.65		29.99		44.09	
2h		*SRR*	33.52	1.004	29.76	1.008	43.82	1.006
3h		*RRR*	33.84		30.32		45.77	
4h		*SSR*	33.83	1.000	30.32	1.000	45.84	1.002
1i	291	*RSS*	23.96		19.18		26.85	
2i		*SRS*	24.06	1.004	19.21	1.002	26.89	1.001
3i		*RRS*	24.55		19.72		28.50	
4i		*SSS*	24.54	1.000	19.77	1.002	28.50	1.000

[a] Based on Cl = 35. M + 1 ions (100% relative abundance) were observed for each compound during isobutane chemical-ionization GC-MS analysis.

[b] The absolute stereochemistry at C-1, C-3 and in the amine moiety, respectively.

[c] α is the chromatographic separation factor, obtained from the indicated retention times.

m/z 119 and 91 (**1c**, **1d**, **1g**), at m/z 105 (**1e**, **1h**) and at m/z 71, 43 and 41 (**1f**, **1i**).

Samples of the derivatives were examined on capillary columns of differing polarities using the splitless injection technique (Table I). For the resolution of either pair of enantiomeric acids, the amphetamine derivatives showed the best chromatographic separation factors ($\alpha = 1.013$–1.020) on the three columns.

Only DB-WAX was adequate for the separation of the amphetamine derivatives because either **1c** and **4c** or **2d** and **3d** coeluted on DB-1 and DB-5. The separation achieved on DB-1 and DB-WAX is illustrated (Fig. 5).

The (R)(+)-α-methylbenzylamine derivatives showed relatively good separation of the cis isomers **1e** and **2e** ($\alpha = 1.008$–1.014) but the trans isomers **3e** and **4e**, which had longer retention times, were poorly separated on the three capillary columns. Derivatives prepared with 2-methylbutylamine (**1f**–**4f**) showed very small α values (1.000–1.003) although the cis and trans isomers were well separated.

In derivatizations with N-methylamines, the (S)(+)-methamphetamine derivatives were only separated on DB-WAX but the α value for separation of **1g** and **2g** was less than the corresponding derivatives from (R)(−)- and (S)(+)-amphetamine. The **2g** and **4g** stereoisomers nearly coeluted on DB-1 and DB-5. Use of N-methyl (R)(+)-α-methylbenzylamine resulted in

some separation of **1h** and **2h** ($\alpha = 1.004$–1.008) but **3h** and **4h**, like the trans isomers from (R)(+)-α-methylbenzylamine, were not completely resolved on these capillary columns. Derivatives from N-methyl (S)(−)-2-methylbutylamine (**1i**–**4i**) yielded very small α values also.

The techniques described here provide new approaches for derivatizing the permethrin acids with chiral amines and for estimating the enantiomeric composition of microgram quantities of these acids by achiral phase capillary GC. Although direct comparisons with previously reported separations of diastereomeric octyl and menthyl esters by packed column GC is difficult, the α values derived from the capillary column of DB-WAX appear to be smaller than those obtained with liquid phases of QF-1 [2] or OV-210 [3]. Samples of the diastereomeric amides described here were only studied on three common liquid phases. Other achiral capillary GC columns may give better separations. Introduction of a nitrogen atom raises interesting possibilities for the GC detection of these acids with a nitrogen-selective detector, which might be preferred by some laboratories to electron-capture or GC–MS techniques. We hope that this technology will be useful in the development of sensitive, enantiospecific assays for these metabolites, for example in the monitoring of **1b**–**4b** in urine samples following exposure to permethrin [23,24] or cypermethrin [25–27].
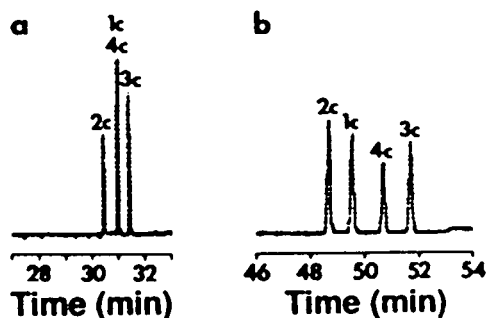
Fig. 5. Capillary gas chromatograms illustrating the separation of diastereomeric amides **1c**–**4c** on (a) DB-1 and (b) DB-WAX. The four permethrin acids (2.5 μg each of **1b**–**4b**) were derivatized with CDI and (R)(−)-amphetamine at room temperature. See the Experimental section for chromatographic conditions. HP 5890 chromatograph, HP 3396A integrator, attenuation 0.

REFERENCES

1 M. Elliott (Editor), Synthetic Pyrethroids (ACS Symposium Series, No. 42), American Chemical Society, Washington, DC, 1977.
2 M. Horiba, A. Kobayashi and A. Murano, Agr. Biol. Chem., 41 (1977) 581.
3 R.A. Chapman and C.R. Harris, J. Chromatogr., 174 (1979) 369.

4 N. Oi, H. Kitahara and T. Doi, *J. Chromatogr.*, 254 (1983) 282.

5 M. Jiang and D.M. Soderlund, *J. Chromatogr.*, 248 (1982) 143.

6 S. Björkman, *J. Chromatogr.*, 339 (1985) 339.

7 C. Volland, H. Sun and L.Z. Benet, *J. Chromatogr.*, 534 (1990) 127.

8 G.J. Vangiessen and D.G. Kaiser, *J. Pharm. Sci.*, 64 (1975) 798.

9 J.-M. Maitre, G. Boss and B. Testa, *J. Chromatogr.*, 299 (1984) 397.

10 M.P. Knadler and S.D. Hall, *J. Chromatogr.*, 494 (1989) 173.

11 A.C. Rudy, K.S. Anliker and S.D. Hall, *J. Chromatogr.*, 528 (1990) 395.

12 A. Carlson and O. Gyllenhaal, *J. Chromatogr.*, 508 (1990) 333.

13 N.N. Singh, F.M. Pasutto, R.T. Coutts and F. Jamali, *J. Chromatogr.*, 378 (1986) 125.

14 N.N. Singh, F. Jamali, F.M. Pasutto, A.S. Russell, R.T. Coutts and K.S. Drader, *J. Pharm. Sci.*, 75 (1986) 439.

15 M. Huffer and P. Schreier, *J. Chromatogr.*, 519 (1990) 263.

16 N. Oi, H. Kitahara, Y. Inda and T. Doi, *J. Chromatogr.*, 213 (1981) 137.

17 J.A. Shemanchuk and W.G. Taylor, *Pestic. Sci.*, 15 (1984) 557.

18 P.E. Burt, M. Elliott, A.W. Farnham, N.F. Janes, P.H. Needham and D.A. Pulman, *Pestic. Sci.*, 5 (1974) 791.

19 R.L. Fitzgerald, R.V. Blanke, R.A. Glennon, M.Y. Yousif, J.A. Rosecrans and A. Poklis, *J. Chromatogr.*, 490 (1989) 59.

20 H.A. Staab, *Angew. Chem., Int. Ed. Engl.*, 1 (1962) 351.

21 T. Tamiri and S. Zitrin, *Biomed. Environ. Mass Spectrom.*, 14 (1987) 39.

22 R.C. Morton, D. Mangroo and G.E. Gerber, *Can. J. Chem.*, 66 (1988) 1701.

23 H.J. van der Rhee, J.A. Farquhar and N.P.E. Vermeulen, *Acta Derm. Venereol. (Stockh.)*, 69 (1989) 170.

24 A. Anadón, M.R. Martinez-Larrañaga, M.J. Diaz and P. Bringas, *Toxicol. Appl. Pharmacol.*, 110 (1991) 1.

25 C.V. Eadsforth and M.K. Baldwin, *Xenobiotica*, 13 (1983) 67.

26 C.V. Eadsforth, P.C. Bragt and N.J. van Sittert, *Xenobiotica*, 18 (1988) 603.

27 B.H. Woollen, J.R. Marsh, W.J.D. Laird and J.E. Lesser, *Xenobiotica*, 22 (1992) 983.

Mobility of single-stranded DNA as a function of cross-linker concentration in polyacrylamide capillary gel electrophoresis

Daniel Figeys and Norman J. Dovichi*

Department of Chemistry, University of Alberta, Edmonton, Alberta T6G 2G2 (Canada)

ABSTRACT

Mobility, theoretical plate count, and resolution are reported for single-stranded DNA in polyacrylamide containing 0, 0.5, 2.5, and 5% cross-linker and 6% total acrylamide. An electric field of 300 V/cm was used with 50 μm I.D. capillaries. Mobility decreases with increasing cross-linker concentration. The transition from normal mobility to the limiting mobility of biased reptation with stretching occurs for longer fragments as the %C is decreased. Theoretical plate counts do not vary significantly between the different polyacrylamide compositions. Resolution is higher for 0%C polyacrylamide, due to the latter onset of biased reptation with stretching.

INTRODUCTION

Since 1989, there have been a number of reports of DNA sequencing by capillary gel electrophoresis [1–9]. The high surface-to-volume ratio of the capillary facilitates the use of high electric fields for fast separations. However, there have been few systematic studies of the effect of gel composition on separation parameters [10]. In this paper, we consider the effect of cross-linker concentration on mobility, plate count, and resolution in the separation of DNA sequencing fragments by polyacrylamide gel electrophoresis.

Bisacrylamide is the most common cross-linking agent used in polyacrylamide gels. The cross-linker concentration (%C) is usually expressed as a mass percentage of the total monomer concentration in the gel. The mass percent of monomer plus cross-linker is denoted as %T, the total acrylamide concentration. Most workers employ 5%C polyacrylamide gels, although there have been reports on the use of much lower %C gels.

Recently, attention has focused on the use of 0%C polyacrylamide in electrophoresis. These entangled polymer solutions have relatively low viscosity and they may be pumped from the capillary after use. There is hope that by refilling the capillary after every separation, it will not be necessary to realign optical systems in automated DNA sequencers. Bode [11,12] apparently performed the first work with non-cross-linked polyacrylamide in the mid-1970s; he combined 0%C polyacrylamide with agarose for separation of proteins and nucleic acids. Mobility was a function of polymer length. Crambach and co-workers [13–15] compared the performance of 0%C and 5%C gels at various total acrylamide concentrations. More recently, Heiger *et al.* [16] compared 0, 0.5 and 5%C gels for separation of

_____
* Corresponding author.

double-strand DNA; they also studied the effect of electric field on the resolution of fragments 4363 and 7253 bases in length. Sudor et al. [17] reported that 0%C polyacrylamide could be pumped from a capillary through use of a special high pressure syringe; the effect of the total acrylamide concentration was considered. Pentoney et al. [18] reported DNA sequencing in 10%T, 0%C polyacrylamide at an electric field of 300 V/cm; sequence could not be determined for fragments longer than 300 bases. Similar results have been reported by Huang et al. [19] with 9%T 0%C gels. Chiari et al. [20] argued that the high viscosity of 10%T, 0%C polyacrylamide eliminates any hope of refilling capillaries with that material; only low %T polyacrylamide has sufficiently low viscosity for replacement. These authors also pointed out that the polymerization reaction does not go to completion; at least 20% monomer remains after polymerization. Guttman et al. [21] reported the use of low total percent linear polyacrylamide for separation of double-strand DNA; they claimed that the capillary could be reused 100 times without replacement of the separation medium.

EXPERIMENTAL

Fluorescently labeled DNA sequencing samples were prepared using 1 μl M13mp18 single-stranded DNA (United States Biochemical, Cleveland, OH, USA), 1 μl of ROX primer (Applied Biosystems, Los Angeles, CA, USA) and 1 μl of Sequenase (United States Biochemical). Only ddATP was used as terminating nucleotide. The samples were ethanol precipitated, washed, and then re-suspended in 4 μl of a mixture of formamide–0.5 M EDTA (49:1) at pH 8.0.

Stock solution of 40% acrylamide–X%N,N'-methylenebisacrylamide (Bio-Rad, Toronto, Canada) were prepared monthly. Gels (6%T) were prepared daily in 5-ml aliquots by dilution of the stock acrylamide-bisacrylamide solution. The aliquots also contained 1 × TBE buffer (0.54 g Tris, 0.275 g boric acid, and 0.100 mmol disodium EDTA, diluted to 50 ml with deionized water) and 7 M urea. Before polymerization, the solution was carefully degassed for at least 20 min under vacuum provided by a water as-

pirator. Polymerization was initiated by addition of 2 μl of N,N,N',N'-tetramethylethylenediamine (TEMED) and 20 μl of 10% ammonium persulfate; polymerization was done at room temperature over night. The solutions were injected into a capillary using a modified syringe. The gels were covalently bound to the capillary wall through use of γ-methacryloxypropyltrimethoxysilane. 0%C polyacrylamide was covalently bound to the full length of the capillary; other gels were bound to the last 5 cm of the capillary. The polyimide-coated, fused-silica capillaries were typically 35 cm long × 50 μm I.D. × 190 μm O.D.

The one-spectral channel DNA sequencing capillary electrophoresis system has been described before [6,8]. In this system, the injection end of the capillary is kept in a Plexiglas box equipped with a safety interlock. The opposite end of the capillary is inserted into the flow chamber of a sheath flow cuvette; the cuvette is held at ground potential. Fluorescence is excited with the green (543 nm) line of a He–Ne laser. Fluorescence is collected at right angles with a microscope objective, imaged onto a pinhole, passed through a band pass filter and detected with a photomultiplier tube (PMT). A Macintosh computer digitizes the signal of the PMT. The samples were injected at 200 V/cm for 60 seconds and eluted at 300 V/cm with a fresh 1 × TBE buffer.

RESULTS AND DISCUSSION

Three to six electropherograms were obtained for each value of %C studied; in all cases, 6%T polyacrylamide was used. The order in which the gels were prepared was randomized, and fresh gels were used for each experiment. The results reported are average values. There were approximately a 5 to 10% variation in retention time for different gels of the same nominal composition. We believe that this variation arises during our vacuum degassing step; evaporation produces ca. 5% decrease in solution volume. Because the final volume is not precisely controlled, the concentration of polymer components will have a minor variation. It appears that the length of the polymer is a strong function of the concentration

of catalyst and initiator, which gives rise to the variation in viscosity and electrophoretic mobility.

As in our earlier work, there is a linear relationship between fragment length and retention time for relatively short sequencing fragments ranging from 60 to 240 bases [10]. The slope and intercept are summarized in Table I. The plots have a common intercept, which corresponds to a retention time of 11.7 min and a mobility of $1.43 \cdot 10^{-4}$ cm^2 V^{-1} s^{-1} for a vanishingly small fragment. This value is slightly less than observed in our %T study, and presumably results from differences in the fluorescent labeling scheme used in the two experiments.

The mobility (μ) of the DNA sequencing fragments is calculated from the retention time, t_r

$$\mu = \frac{L}{Et_r} = \frac{L^2}{Vt_r} \tag{1}$$

where L is the capillary length, E is electric field and V is the applied potential. Within experimental error, the mobility is identical for 2.5 and 5%C gels. The mobility increases with lower %C, and is maximum for 0%C.

The electrophoretic behaviour of long DNA fragments is described by the biased reptation model [22,23]. Fragments smaller than some threshold are in a random coil configuration; their mobility decreases inversely with fragment length. Fragments longer than that threshold are stretched into a linear configuration; their

mobility is independent of fragment length. The biased reptation model predicts that mobility is given by

$$\mu = a\left(\frac{1}{N} + \frac{1}{N^*}\right) = \frac{a}{N} + \mu_\infty \tag{2}$$

where a is the slope of the line, N^* is the fragment length for the onset of biased reptation with stretching and μ_∞ is the mobility of the longest fragments. A plot of μ versus N^{-1} is shown in Fig. 1. The biased reptation model seems to apply to all the fragments larger than 125 bases for 0.5, 2.5, and 5%C and 200 bases in the case of 0%C. Eqn. 2 was fit to the linear portion of the plot of mobility versus the inverse fragment length. The coefficients obtained are reported in Table II. The intercept, μ_∞, is the mobility of the longest fragments; lower %C gels generate higher mobility for the longest fragments. The slope decreases with %C. The ratio a/μ_∞ is N^*. Fragments with N^* bases have half the mobility compared to the absence of biased reptation with stretching. The 0%C polyacrylamide produces the highest values of N^*, which suggests that the non-crosslinked polymer suffers least from the effects of biased reptation with stretching.

According to the biased reptation model, the slope of eqn. 2 is proportional to the frictional coefficient for migration of an elongated fragment through the gel. The decrease in slope with increasing %C implies that the frictional force experienced by the fragment decreases with decreasing %C. The largest increase in slope between 5%C and 0%C should be related to the fact that 5%C is a gel and 0%C is an entangled polymer.

A Gaussian function was fit to peaks obtained for bases 85, 117, 184, 217, 258, 309, 350 and 396

$$I(t) = a_0 + a_1 \exp[-(t - a_2)^2/a_3^2] \tag{3}$$

where $I(t)$ is intensity as a function of time, a_0 is the baseline signal, a_1 is peak height, a_2 is the elution time for the peak center, and a_3 is the standard deviation of the peak. The number of theoretical plates, N_p, was estimated by

$$N_p = 2 \cdot \left(\frac{a_2}{a_3}\right)^2 \tag{4}$$

TABLE I

LEAST SQUARES SLOPE AND INTERCEPT FROM A PLOT OF RETENTION TIME (min) VERSUS THE FRAGMENT LENGTH IN BASES FOR FRAGMENTS RANGING IN SIZE FROM 60 TO 240 BASES IN LENGTH

| %C	Slope (min/base)	Intercept (min)	r
0	$1.02 \pm 0.04 \cdot 10^{-1}$	$1.1 \pm 0.1 \cdot 10^1$	0.9995
0.5	$1.17 \pm 0.08 \cdot 10^{-1}$	$1.2 \pm 0.1 \cdot 10^1$	0.9988
2.5	$1.75 \pm 0.03 \cdot 10^{-1}$	$1.1 \pm 0.5 \cdot 10^1$	0.9999
5.0	$1.61 \pm 0.09 \cdot 10^{-1}$	$1.2 \pm 0.2 \cdot 10^1$	0.9992
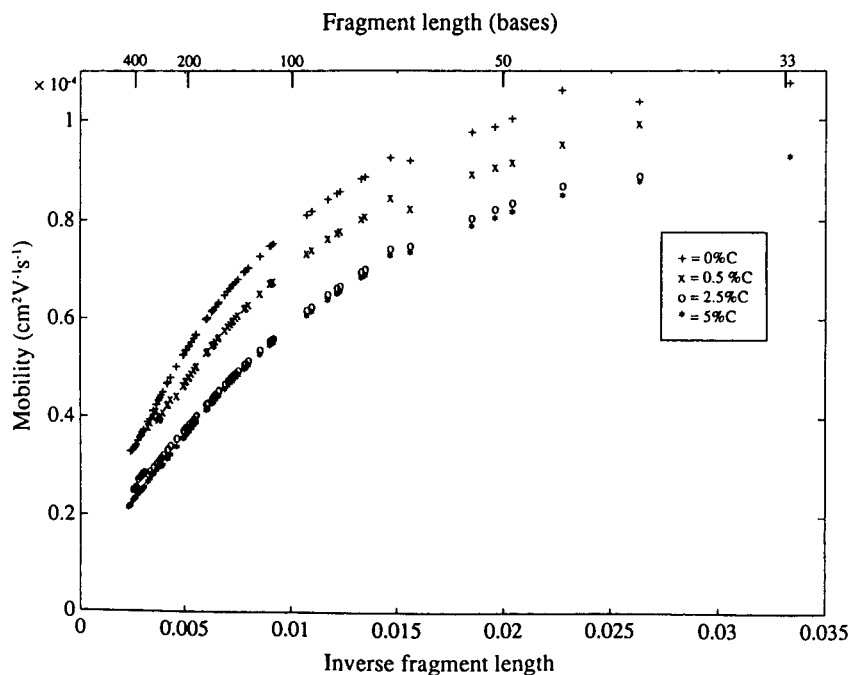
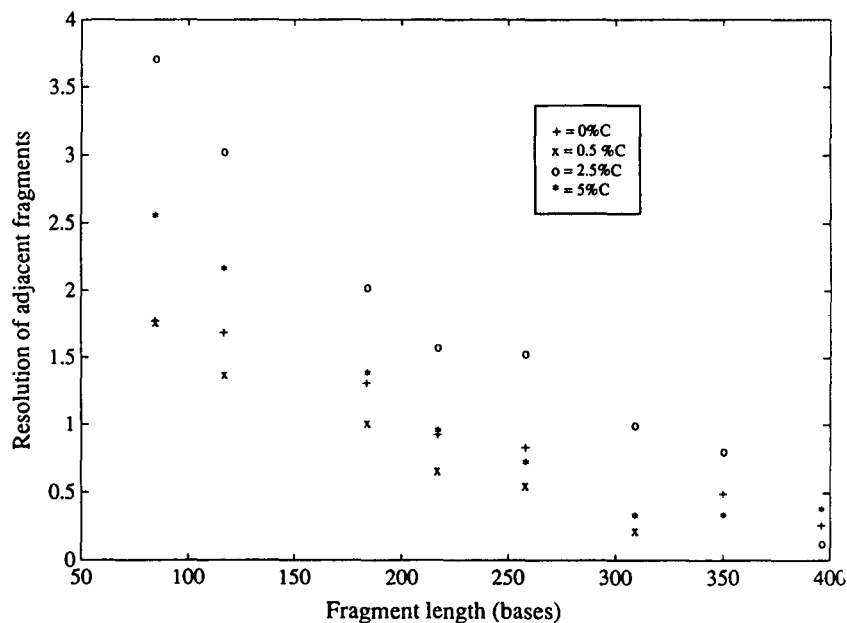Fig. 1. Mobility *versus* inverse fragment length. Data were obtained with 6%T polyacrylamide in 50 μm I.D. capillaries at 300 V/cm. The %C of the polyacrylamide is noted in the figure. Data were obtained at room temperature.

The plate count (Fig. 2) varied slightly with fragment length; the smallest fragments produced roughly a factor of two higher plate count compared with the longest fragments. Plate counts were lower for lower %C polyacrylamide; however, the correlation between plate counts and cross-linker concentration is poor, 0.62.

TABLE II

LEAST SQUARES SLOPE AND INTERCEPT FROM A PLOT OF MOBILITY *VERSUS* N^{-1}, WHERE N IS THE FRAGMENT LENGTH IN BASES

The least-squared fit was performed for fragments longer than 200 bases. N^* is found by dividing the slope by the intercept, and gives a measure of the fragment size for which biased reptation with stretching becomes significant.

%C	Slope	Intercept	N^*	r
0	$8.11 \pm 0.03 \cdot 10^{-3}$	$1.25 \pm 0.01 \cdot 10^{-5}$	650	0.9998
0.5	$5.77 \pm 0.04 \cdot 10^{-3}$	$1.78 \pm 0.02 \cdot 10^{-5}$	320	0.9994
2.5	$5.25 \pm 0.02 \cdot 10^{-3}$	$0.97 \pm 0.01 \cdot 10^{-5}$	540	0.9997
5	$4.97 \pm 0.02 \cdot 10^{-3}$	$1.23 \pm 0.01 \cdot 10^{-5}$	400	0.9997

In zone electrophoresis, the number of theoretical plates is given by

$$N_p = \frac{E\mu}{2D} \tag{5}$$

where D is the diffusion coefficient of the analyte. Both diffusion coefficient and mobility depend on the product of fragment size and viscosity; the ratio should be independent of those two parameters [24]. Variation in plate count with fragment length probably is associated with the change in the shape of the fragments as they undergo transition from a random coil conformation for small fragments to a linear configuration for longer fragments.

While plate count varies slowly with fragment length, the spacing between adjacent peaks decreases for longer fragments. This phenomenon is a result of biased reptation with stretching, and leads to a degradation in resolution with fragment length. Fig. 3 presents the resolution of adjacent fragments. We found that the resolution of adjacent peaks is inversely proportional to fragment length (Table III). In this case, res-
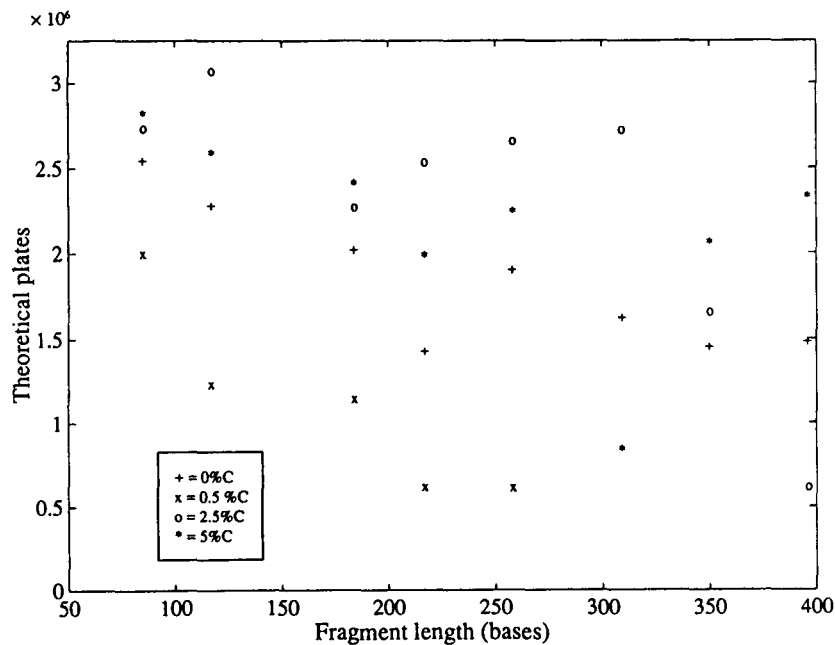
Fig. 2. Theoretical plates *versus* fragment length. Data were obtained with 6%T polyacrylamide in 50 μm I.D. capillaries at 300 V/cm. The %C of the polyacrylamide is noted in the figure. Data were obtained at room temperature. Plate count was estimated by use of a non-linear regression analysis of each peak with a Gaussian function.

Fig. 3. Resolution *versus* fragment length. Data were obtained with 6%T polyacrylamide in 50 μm I.D. capillaries at 300 V/cm. The %C of the polyacrylamide is noted in the figure. Data were obtained at room temperature. Resolution of adjacent peaks was estimated by peak width determined in Fig. 2 and by the peak spacing determined from mobility data of Fig. 1.

TABLE III

LEAST SQUARES SLOPE AND INTERCEPT FROM A PLOT OF RESOLUTION *VERSUS* N^{-1}, WHERE N IS THE FRAGMENT LENGTH IN BASES

Slope is given to two significant figures.

%C	Slope	Intercept	r
0	160 ± 30	0.1 ± 0.2	0.93
0.5	170 ± 20	-0.1 ± 0.2	0.97
2.5	350 ± 40	-0.2 ± 0.2	0.97
5.0	260 ± 20	-0.3 ± 0.1	0.98

olution asymptotically approaches zero for long fragments as peak spacing goes to zero for long fragments. Resolution may be written as

$$R = \frac{\beta}{N} \qquad (6)$$

where β is a proportionality constant. The proportionality constant increases with cross-linker concentration; there is a more rapid decrease in resolution with fragment length for high %C gels compared with low %C gels. This result reflects the earlier onset of biased reptation for higher %C gels.

Resolution drops below 1 for fragments longer than *ca.* 250 bases for low %C gels. As a result, it will be difficult to obtain sequence information for longer fragments. This observation is consistent with the data of both Pentoney *et al.* [18] and Huang *et al.* [19], who were unable to obtain sequence information for fragments longer than *ca.* 300 bases in 0%C gels.

We were unable to reproduce the long column life reported by Guttman *et al.* [21] for 0%C polyacrylamide gels. After two or three injections, our capillaries inevitably failed, producing very low resolution separations. This observation is not surprising. Early reports on capillary gel electrophoresis separations of oligonucleotide standards stated that at least a hundred separations could be performed without replacement of the gel. However, no group has been able to reuse gel filled capillaries for many separations when dealing with DNA sequencing samples. It appears that the high-molecular-mass template present in the sequencing sample leads to rapid

degradation of the gel performance [25]. 0%C polyacrylamide is not immune to this phenomenon. It might be argued that gel damage is produced by hot zones formed due to different ionic movement of buffer ions in the gel. However, we found that the polymer is quite stable if a blank solution is loaded onto the capillary; this blank solution contains all of the components used to prepare the sequencing sample, with the exception of the template.

CONCLUSIONS

Mobility decreases with increasing cross-linker concentration. It appears that addition of cross-linker increases the internal viscosity of the polymer, retarding the analyte. Similarly, the transition from normal mobility to the limiting mobility of biased reptation with stretching occurs for longer fragments as the %C is decreased. Both observations are explained by a decrease in pore size produced by higher concentration of cross-linker. This result is at odds with the classic Ogsten [26] sieving model of gels, which anticipates that pore size depends only on the total acrylamide concentration.

The later onset of the deleterious effects of biased reptation with stretching for low %C polyacrylamide implies that the material will be more useful for DNA sequencing applications; longer sequencing runs should be possible. However, it has been frustrating that fragments longer than *ca.* 320 bases can not be separated with high resolution in these polymers at an electric field of 300 V/cm. We anticipate that the use of lower electric fields will delay the onset of biased reptation with stretching, allowing the separation of longer fragments.

REFERENCES

1 H. Swerdlow and R. Gesteland, *Nucleic Acids Res.*, 18 (1990) 1415.
2 H. Drossman, J.A. Luckey, A.J. Kostichka, J. D'Cunha and L.M. Smith, *Anal. Chem.*, 62 (1990) 900.
3 A.S. Cohen, D.R. Najarian and B.L. Karger, *J. Chromatogr.*, 516 (1990) 49.
4 H. Swerdlow, S. Wu, H. Harke and N.J. Dovichi, *J. Chromatogr.*, 516 (1990) 61.
5 J.A. Luckey, H. Drossman, A.J. Kostichka, D.A. Mead, J. D'Cunha, T.B. Norris and L.M. Smith, *Nucleic Acid Res.*, 18 (1990) 4417.
6 D.Y. Chen, H.P. Swerdlow, H.R. Harke, J.Z. Zhang and N.J. Dovichi, *J. Chromatogr.*, (1991) 237.
7 A.E. Karger, J.M. Harris and R.F. Gesteland, *Nucleic Acids Res.*, 19 (1991) 4955.
8 H. Swerdlow, J.Z. Zhang, D.Y. Chen, H.R. Harke, R. Grey, S. Wu, N.J. Dovichi and C. Fuller, *Anal. Chem.*, 63 (1991) 2835.
9 D.Y. Chen, H.R. Harke and N.J. Dovichi, *Nucleic Acids Res.*, 20 (1992) 4873.
10 H.R. Harke, S. Bay, J.Z. Zhang, M.J. Rocheleau and N.J. Dovichi, *J. Chromatogr.*, 608 (1992) 143.
11 H.J. Bode, *Anal. Biochem.*, 83 (1977) 204.
12 H.J. Bode, *Anal. Biochem.*, 83 (1977) 364.
13 D. Tietz, M.H. Gottleib, J.S. Fawcett and A. Crambach, *Electrophoresis*, 7 (1986) 217.
14 H. Pulyaeva, D. Wheeler, M.M. Garner and A. Crambach, *Electrophoresis*, 13 (1992) 608.
15 D. Tietz, A. Aldroubi, H. Pulyaeva, T. Guszczynski, M.M. Garner and A. Crambach, *Electrophoresis*, 13 (1992) 614.
16 D.N. Heiger, A.S. Cohen and B.L. Karger, *J. Chromatogr.*, 516 (1990) 33.
17 J. Sudor, F. Foret and P. Boček, *Electrophoresis*, 12 (1991) 1056.
18 S.L. Pentoney, K.D. Konrad and W. Kaye, *Electrophoresis*, 13 (1992) 467.
19 X.C. Huang, M.A. Quesada and R.A. Mathies, *Anal. Chem.*, 64 (1992) 2149.
20 M. Chiari, M. Nesi, M. Fazio and P.G. Righetti, *Electrophoresis*, 13 (1992) 690.
21 A. Guttman, B. Wanders and N. Cooke, *Anal. Chem.*, 64 (1992) 2348.
22 O.J. Lumpkin, P. Déjardin and B.H. Zimm, *Biopolymers*, 24 (1985) 1573.
23 G.W. Slater and J. Noolandi, *Biopolymers*, 24 (1985) 2181.
24 Y.F. Cheng, S. Wu, D.Y. Chen and N.J. Dovichi, *Anal. Chem.*, 62 (1990) 496.
25 H. Swerdlow, K.E. Dew-Jager, K. Brady, R. Gesteland, R. Grey, and N.J. Dovichi, *Electrophoresis*, 13 (1992) 475.
26 A.G. Ogsten, *Trans. Faraday Soc.* 54 (1958) 1754.

β^+-Selective radiodetector for capillary electrophoresis

Göran Westerberg

Uppsala University PET Centre, Department of Organic Chemistry, Institute of Chemistry, UAS, S-751 85 Uppsala (Sweden)

Hans Lundqvist

Department of Radiation Sciences, Uppsala University, Box 535, S-751 21 Uppsala (Sweden)

Ferenc Kilár

Central Research Laboratory, University of Pécs, Medical School, Szigeti Út 12, H-7643 Pécs (Hungary)

Bengt Långström*

Uppsala University PET Centre, Department of Organic Chemistry, Institute of Chemistry, UAS, S-751 85 Uppsala (Sweden)

ABSTRACT

A compact and sensitive β^+-selective radiodetector for use with a high-performance capillary electrophoresis system for the analysis of compounds labelled with short-lived, positron-emitting radionuclides has been developed. The detector had a linear response in the range 0–600 kcps with a noise level of 0.2 cps and an efficiency of 85%. The detection limit was found to be in the Bequerel range. The capillary electrophoresis system was used in isoelectric focusing and capillary zone electrophoresis of ^{11}C-labelled iron-free transferrin.

INTRODUCTION

Macromolecules labelled with short-lived positron-emitting radionuclides such as ^{11}C and ^{18}F (half-lives of 20.3 and 110 min, respectively) are interesting as tracers in positron emission tomography (PET) [1] for the *in vivo* study of various physiological processes.

In the development of methods for labelling proteins with ^{11}C [2], we required a complement to analytical HPLC for analysis of labelled products. High sensitivity, short analysis times and small sample consumption are features that make capillary electrophoresis a suitable tool in the analysis of compounds labelled with short-lived radionuclides. Previously, radiodetection in capillary electrophoresis has been reported for both β- and γ-emitting radionuclides such as ^{32}P, ^{14}C and ^{99m}Tc [3–6]. In this paper, a positron radiodetector for use with a high-performance capillary electrophoresis system with simultaneous mass and radiodetection is described. The application of the electrophoresis system for the analysis of labelled proteins is illustrated by isoelectric focusing (IEF) and capillary zone electrophoresis (CZE) experiments.

MATERIALS AND METHODS

Radiodetector element

The radiodetector element was constructed

---

* Corresponding author.

from a small plastic scintillator ($2 \times 4 \times 4$ mm,
polyvinyltoluene, Nuclear Enterprise NE102A,
Nuclear Enterprise, Edinburgh, UK) mounted
onto a 3/8-in. (1 in. = 2.54 cm) photomultiplier
tube (Hamamatzu R 2055, Hamamatzu Photon-
ics, Japan). A slit (2 mm long, 0.5 mm wide and
2 mm deep) was made in the plastic scintillator
allowing the capillary to be placed centrally in
the detector, as shown in Fig. 1a. An amplifier
and low-energy discriminator, developed in-
house, was used for the amplification of the
photomultiplier tube signals and for minimiza-
tion of noise in the measurements. An equiva-
lent electronic system can be built from commer-
cial NIM modules (e.g. TC 242 amplifier and TC
451 single-channel analyser, Tennelec, USA).
The radiodetector was mounted adjacent to the
UV photodiode detector at a distance of 24 mm
in a cartridge sliding on guiding rods allowing the
simultaneous removal of both detectors (Fig.
1b). The distance between the detector cartridge
and the end of the capillary was 20 mm. The UV
detector compartment of a Bio-Rad HPE-100
microsampler capillary electrophoresis apparatus
(Bio-Rad, Richmond, CA, USA) was modified
to accommodate the two-detector assembly. The
incident light from the UV lamp was focused
through a 0.05×1 mm slit facing the capillary.
When operating the system, the entire capillary
compartment was closed by a removable housing
to prevent stray light from entering the detec-
tors. Both detectors were interfaced to a person-
al computer via a Beckman AI 406 interface,
adjusted to accept TTL (transistor-transistor-
logic) pulses from the photomultiplier tube and
the analogue signal from the UV photodiode.
Data were processed using a Beckman System
Gold Chromatography Software Package.

Labelled materials

[^{11}C]Carbon dioxide was prepared by the
^{14}N(p, α)^{11}C nuclear reaction using a nitrogen
gas target and the Scanditronix MC-17 cyclotron
at the Uppsala University PET Centre. Sodium
[^{11}C]carbonate for detector measurements was
obtained by trapping the [^{11}C]carbon dioxide in
5 M NaOH. [^{18}F]Fluoride$_{(aq)}$ was obtained by
the ^{18}O(p,n) ^{18}F nuclear reaction using ^{18}O-en-
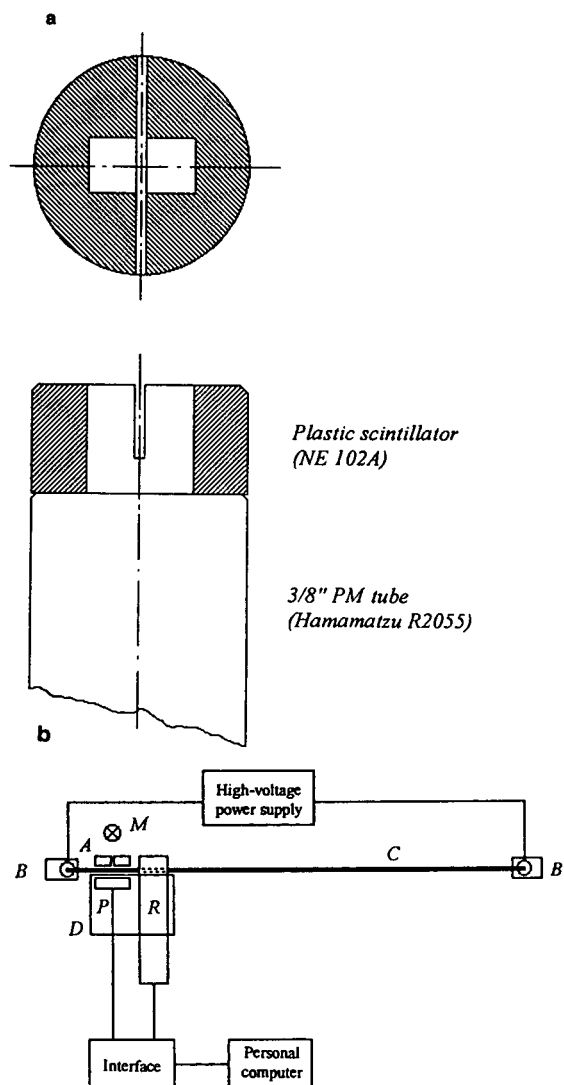
Fig. 1. (a) Scheme of the radiodetector element. The plastic
scintillator ($2 \times 4 \times 4$ mm) was connected to the photomulti-
plier (PM) tube using optical grease. (b) Scheme of the
detector assembly: B = buffer electrodes; M = UV lamp and
monochromator; A = aperture (0.05×1 mm); P = photo-
diode detector; R = radiodetector; D = removable detector
cartridge; C = capillary; " = inch.

riched water as target material. [^{11}C]Cyanogen
bromide was prepared from hydrogen
[^{11}C]cyanide according to a general procedure
described elsewhere [7]. ^{11}C-labelled iron-free
transferrin was obtained by treating iron-free
transferrin (Behring Werke, Marburg, Germany)
with [^{11}C]cyanogen bromide according to a
procedure described in detail elsewhere [2].

[^{11}C]Cyanogen bromide was transferred in a stream of nitrogen gas to a receiving vessel containing 300 μl of 50 mM borate buffer, pH 7.5. When the radioactivity had reached a maximum, the [^{11}C]cyanogen bromide solution was added to a solution of the protein (0.1–10 mg in 100 μl of 50 mM borate buffer, pH 7.5). The reaction mixture was incubated at 40°C for 5 min, and then diluted with sterile water (2.1 ml). The crude product was desalted on a Sephadex G25 cartridge (PD-10, bed volume 9 ml, Pharmacia LKB, Stockholm, Sweden) using sterile water as the eluent.

Detector performance tests

Radiodetector linearity was tested by placing the detector with the plastic scintillator end resting on a vessel (outside the modified Bio-Rad equipment) containing 11.2 GBq (304 mCi) of sodium [^{11}C]carbonate in a light-shielded lead pot. Data collection was started and the radioactivity was left to decay overnight (16 h).

The background noise level was evaluated by inserting a glass capillary (200 $\times$ 0.1 mm I.D. $\times$ 0.3 mm O.D.) filled with blank buffer (0.2 M phosphate buffer, pH 2.5) into the apparatus and then closing the detector compartment. Data were collected for 100 min using a scaler (Newport P6000, Newport Electronics, Santa Ana, CA, USA) connected to the discriminator.

The spatial resolution of the radiodetector was determined as the response to a step function. A glass capillary 200 $\times$ 0.1 mm I.D. $\times$ 0.3 mm O.D.) was partially filled with radioactivity (sodium [^{11}C]carbonate) acting as a line source. When inserting the filled part of the capillary into the detector, note was taken of the output from the detector (connected to a Newport P600 scaler). The capillary was moved 1 mm, detector output noted, etc. The capillary was taken out and the radioactivity distribution in the capillary measured by autoradiographic analysis using a PhosphorImager (Molecular Dynamics, Sunnyvale, CA, USA).

The efficiency of the detector was tested by placing a glass capillary (200 $\times$ 0.1 mm I.D. $\times$ 0.3 mm O.D.) filled with 278 MBq ml^{-1} (7.5 mCi ml^{-1}) sodium [^{11}C]carbonate in the radiodetec-

tor and collecting data with a scaler (Newport P6000). The capillary was taken out and the total radioactivity measured in a NaI(Tl) well counter.

Capillary electrophoretic analysis of labelled proteins

The performance of the capillary electrophoresis system was assessed by experiments with ^{11}C-labelled transferrin. The labelling procedure afforded the labelled protein as a 1–2 mg ml^{-1} solution in 10 mM potassium phosphate buffer, pH 7.4. This solution was used in capillary isoelectric focusing and zone electrophoresis analysis within 5–25 min after radiolabelling.

Glass capillaries (200 $\times$ 0.1 mm I.D. $\times$ 0.3 mm O.D.) or fused-silica capillaries (200 $\times$ 0.075 mm I.D. $\times$ 0.1 mm O.D.) were internally coated with non-cross-linked polyacrylamide to reduce electroendoosmosis according to a procedure published previously [8]. Before and after runs, the capillaries were rinsed with 0.2 M phosphate buffer, pH 2.5, or 20 mM phosphoric acid and dried by aspiration. All electrophoresis experiments were performed at room temperature with a procedure analogous to previous reports [8,9].

RESULTS AND DISCUSSION

The radionuclides of interest in PET decay by emission of a high-energy positron (β^+), as illustrated for ^{11}C in eqn. 1;

$$^{11}C \rightarrow ^{11}B + \beta^+ + \nu \tag{1}$$

where ν is a neutrino. The average energy of the positron emitted from ^{11}C is 385 keV. Thus, in principle, both the β- and γ-radiation emitted could be used for monitoring the radioactivity. In practice, β detection is preferable when considering the spatial resolution of the detector. The plastic scintillator has a high sensitivity for β detection (*i.e.* the full β energy of ^{11}C positrons is absorbed within 2 mm of scintillator plastic) and a low sensitivity for γ detection (hence a low background level).

Characterization of the radiodetector

The linearity of the radiodetector response was evaluated by placing the detector next to a

radioactive source which was left to decay while collecting data. The data obtained were plotted as the natural logarithm of the detector output as a function of time (Fig. 2). A regression line was fitted to the data to give a correlation coefficient (Pearson's r) of 0.9982, implying that a linear response can be expected in the interval 0–600 000 counts per second (cps).

The plastic scintillator has a very fast response to incident betas, i.e. the pulses are short (10–20 ns). The characteristics of the scintillator and the amplifier–discriminator (10–20 ns pulses, 100 ns TTL) sets an upper limit for the linearity of the order of 1 Mcps. In our application, low count rates can be expected (typically 0–10 kcps), while the limit of linearity is not considered to be a problem. Thus, a simple amplifier and a low-energy discriminator were developed, and found to give satisfactory results. If required, more sophisticated electronics can be used to increase the linear range to about 10 Mcps.

The detector background count rate was determined by collecting data from a blank sample buffer. Data were averaged over 100 min and the noise level found to be 0.2 cps. During operation, no interference from the UV lamp or the high-voltage power supply for the electrophoresis electrodes was observed.

The spatial resolution of the radiodetector was assessed by stepwise movement of a capillary partially filled with radioactivity through the detector (Fig. 3a). This required the detector compartment housing to be opened for each measurement. Removing the housing caused an increased background level but did not saturate the detector. Repositioning the housing quickly
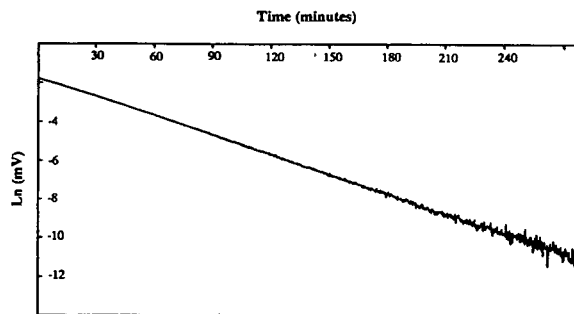
Fig. 2. The time course of the decay of sodium [^{11}C]carbonate as measured by the radiodetector.
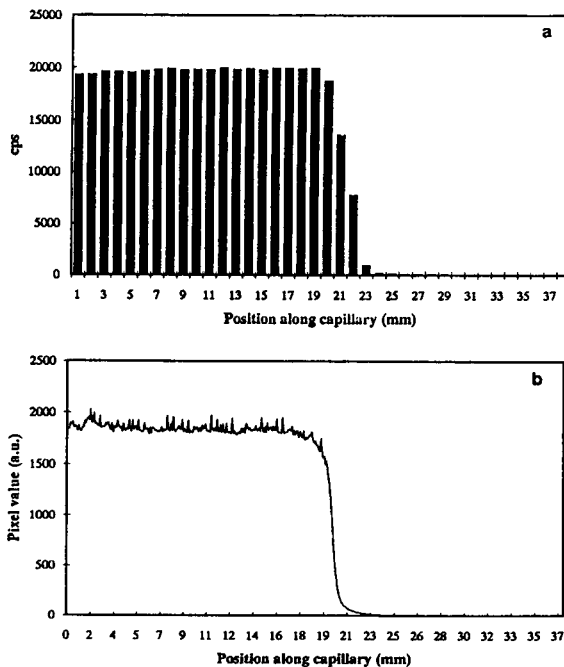
Fig. 3. (a) Plot of output from detector vs. relative position of radioactivity to detector. (b) Distribution of radioactivity in capillary obtained by autoradiography.

restored (within 5 s) the original background levels.

The detector response shown in Fig. 3a is thus a step function response (verified by autoradiography of the capillary source as shown in Fig. 3b). Assuming a Gaussian detector response to a point source, the measured data were fitted using the least-squares method. The standard deviation of the detector response function was 1.52 mm, corresponding to a full-width half-maximum value of 2.53 mm. The effective detector width using a line source was calculated to be 2.69 mm, corresponding to an effective detector cell volume of 21 nl when using a 0.1 mm I.D. capillary.

Using the value obtained above for the effective detector volume, the efficiency of the detector using a 0.1 mm I.D. capillary filled with sodium [^{11}C]carbonate 278 MBq ml^{-1} (7.5 mCi ml^{-1}) was approximately 85%. A similar value (87%) was obtained using ^{18}F$^-_{aq}$ (200 μCi ml^{-1}). The results are summarized in Table I.

The sensitivity of the radiodetector is best judged from the electropherograms in Figs. 4

TABLE I

DETERMINATION OF THE RADIODETECTOR EF-
FICIENCY FOR ^{11}C AND ^{18}F

After measuring the count rate using the radiodetector, the
capillary was taken out and the radioactivity measured in a
NaI(Tl) well counter.

Measurement number	^{11}C		^{18}F	
	cps[a]	dps[b]	cps[a]	dps[b]
1	4380	5378	162	186
2	4314	4967	162	192
3	4348	5002	177	201
4	4359	5043	149	169
Mean	4351	5098	163	187
Efficiency (%)	85.3		87.2	

[a] Radiodetector output, counts per second, decay corrected.
[b] Total radioactivity, disintegrations per second. Values were
corrected for dead-time and decay.

and 5. In the CZE experiments, a signal-to-
noise-ratio of >100 was obtained using a total
starting radioactivity of 5.05 kBq. The high
sensitivity results from the low noise level,
which, in turn, is attributable to the small size of
the scintillator. Assuming the least-detectable
signal to be twice the background noise count-
rate, the detection limit was 0.4 cps.

Least-detectable radioactivity =

$$e^{(\ln 2 + \text{ordinate value of intercept})} \qquad (2)$$

This was verified by extrapolating the linear
portion of the logarithm of a decay curve (^{11}C)
to the intercept with the background noise level.
The least-detectable amount of radioactivity was
then obtained by eqn. 2. This analysis gave as a
result a value of 0.5 cps, corresponding well to
the value above.

In a capillary of the size used in this work, the
self-absorption of the β-particles emitted from
^{11}C and ^{18}F is small (<10%). The plastic scin-
tillator volume is small (16 mm^3) and it has a low
sensitivity for absorption of high-energy photons.
No bulky lead shield is thus needed to keep the
background at very low levels. The resolution of
the radiodetector can fairly easily be improved
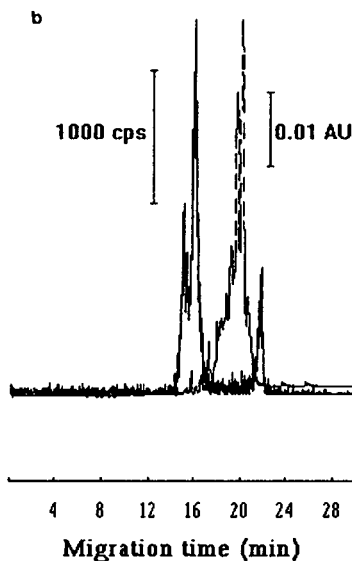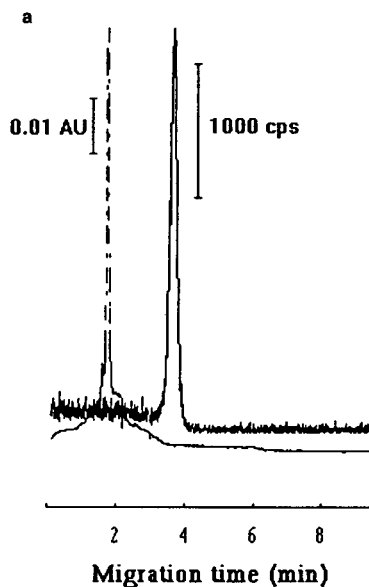
Fig. 4. isoelectric focusing of [^{11}C]transferrin. Radiochannel,
solid line; UV channel, dashed line. (a) Focusing step.
Applied voltage 5 kV, UV detection at 280 nm. (b) Mobiliza-
tion step; applied voltage 7 kV. The radiochannel electro-
pherograms are decay corrected. The amount of radioactivity
in the capillary was 1.01 MBq (27.2 μCi) at the start of the
experiment, specific radioactivity 45 GBq μmol^{-1} (1.2 Ci
μmol^{-1}), direction of migration $- \rightarrow +$. Experimental condi-
tions: 200-mm glass capillary, 0.1 mm I.D.; anolyte: (a) 20
mM phosphoric acid, (b) 20 mM NaOH; catholyte 20 mM
NaOH.
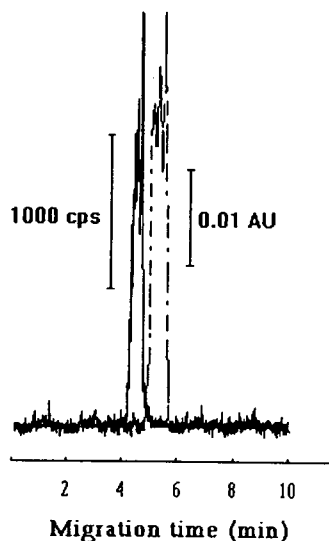
Fig. 5. Capillary zone electrophoresis of [^{11}C]transferrin. Radiochannel, solid line; UV channel, dashed line. Applied voltage 7 kV, UV detection at 280 nm. The sample was applied as 1-mm-long starting zone, with a total activity of 5.05 kBq (136 nCi), specific radioactivity 21 GBq μmol^{-1} (0.57 Ci μmol^{-1}). Experimental conditions: 200-mm glass capillary, 0.1 mm I.D.; electrophoresis buffer 18 mM Tris, 18 mM boric acid, 0.3 mM EDTA, pH 8.4; direction of migration $- \rightarrow +$.

by replacing the 2-mm-wide scintillator by a thinner one.

Electrophoresis experiments

Transferrin is a serum glycoprotein of molecular mass of 80 000 with the property of reversibly binding ferric ions, thus acting as a reservoir and transport protein for physiological iron. Human transferrin has an isoelectric point in the range 5.3–6.1, the variation in pI presumably caused by the varying carbohydrate content. Diferric transferrin has a higher pI than the apo-form [10]. Labelled transferrin was obtained by treating the protein at physiological pH with [^{11}C]cyanogen bromide according to a procedure under development in our laboratory [2]. Cyanation of protein SH groups using cyanogen bromide has been demonstrated previously [11–14]. Carbamylation of lysine residues in proteins using cyanate ion is a well-known reaction [15]. Whether the reaction of [^{11}C]cyanogen bromide with lysine residues proceeds directly to form cyanamides, or involves hydrolysis to

[^{11}C]cyanate ion with subsequent carbamylation, has not been evaluated. The ^{11}C-transferrin was obtained in 50–65% decay-corrected radiochemical yield in 5 min reaction time. The specific radioactivity of the ^{11}C-labelled transferrin used in this study was in the range 11–74 GBq μmol^{-1} (0.3–2 Ci μmol^{-1}).

An IEF experiment of a ^{11}C-labelled iron-free transferrin sample is shown in Fig. 4. The amount of radioactivity in the capillary at the start of the experiment was 1.01 MBq. In Fig. 4a, the focusing step, it can be seen that the amplitude of the noise and the baseline level of the radiochannel is higher before the peak than after. During the focusing step, the radioactivity, which was originally uniformly distributed along the capillary, is migrating towards the isoelectric point of the protein, thus giving rise to peak(s) in the radio- (and UV) detector. As the migrating components of the sample approach the isoelectric point, their migration speed decreases. Since the radiodetector is located closer to the isoelectric point, broader peak(s) results, as compared with the UV detector.

In the mobilization step (Fig. 4b), the labelled components enter the radiodetector before the UV detector, thus reversing the order of the radio and UV peaks. In Fig. 4b, the UV trace shows at least 5–7 peaks, possibly arising from the different transferrin isoforms. The radiotrace only shows two clearly resolved peaks. Whether this pattern reflects a lack of resolution in the radiodetector or a differential labelling of isoforms is not yet clear. An impurity can be seen at a migration time of 21 min. CZE of the same sample is illustrated in Fig. 5.

In conclusion, a capillary electrophoresis system with on-tube radiodetection of positron emitters has been developed. The high sensitivity and efficiency of the radiodetector allows the characterization of macromolecules labelled with short-lived, positron-emitting radionuclides. The resolving power of the instrument was illustrated by the partial resolution of transferrin isoforms.

ACKNOWLEDGEMENTS

REFERENCES

1 M. Phelps, J. Mazziotta and H. Schelbert (Editors), *PET and Autoradiography: Principles and Applications for the Brain and Heart*, Raven Press, New York, 1986.
2 G. Westerberg and B. Långström, in preparation.
3 R.E. Needham and M.F. Delaney, *Anal. Chem.*, 55 (1983) 148–150.
4 S.L. Pentoney, R.N. Zare and J.F. Quint, *Anal. Chem.*, 61 (1989) 1642–1647.
5 D. Kaniansky, P. Rajec, A. Svec, P. Havasi and F. Macásek, *J. Chromatogr.*, 258 (1983) 238–243.
6 K.D. Altria, C.F. Simpson, A.K. Bharij and A.E. Theobald, *Electrophoresis*, 11 (1990) 732–734.
7 G. Westerberg and B. Långström, *Acta Chem. Scand.*, in press.
8 F. Kilár and S. Hjertén, *Electrophoresis*, 10 (1989) 23–29.
9 F. Kilár and S. Hjertén, *J. Chromatogr.*, 480 (1989) 351–358.
10 F. Kilár, *J. Chromatogr.*, 545 (1991) 403–406.
11 K. Breddam and A. Kanstrup, *Carlsberg Res. Commun.*, 52 (1987) 65–71.
12 Y. Degani, H. Neumann and A. Patchornik, *J. Am. Chem. Soc.*, 92 (1970) 6969–6971.
13 Y. Degani and A. Patchornik, *J. Org. Chem.*, 36 (1971) 2727–2728.
14 H. Wiedner, R. Wetzel and F. Eckstein, *J. Biol. Chem.*, 253 (1977) 2763–2768.
15 G.R. Stark, W.H. Stein and S. Moore, *J. Biol. Chem.*, 235 (1960) 3177.

CHROM. 25 271

Optimized capillary zone electrophoretic separation of chlorinated phenols

M.F. Gonnord* and J. Collet

Laboratoire des Mécanismes Réactionnels, URA D 1307 CNRS, Ecole Polytechnique, F-91128 Palaiseau Cedex (France)

ABSTRACT

A mixture of thirteen chlorinated phenols was resolved within 16 min by using a 57 cm × 75 μm I.D. fused-silica tube with a 50 mM sodium phosphate buffer (pH 6.9) electrolyte, under an 18 kV potential. The electrophoretic behaviour of chlorophenol congeners was investigated in order to optimize their separation as a function of the running buffer pH, concentration and applied voltage. A migration order depending on both charge and size of the solutes was established. Selectivity is strongly affected by the electrolyte concentration, in a manner that cannot be easily predicted. Quantitative aspects of capillary zone electrophoresis are also discussed.

INTRODUCTION

Chlorinated phenols (CPs) in water can be degradation by-products of pesticides [1] or be formed from the chlorination of drinking water containing phenols originating from petroleum, steel or pulp and paper industry [2]. According to several workers, their toxicity and organoleptic properties are often manifested in the ppb range [3–5].

Chlorophenols are generally analysed by either GC [1] or HPLC [1–10]. Unfortunately, these separations are often time consuming or need derivatization of the solutes [5,9,10]. Moreover, the optimization of chromatographic methods, especially gradient HPLC [2,3,7,9], requires complex procedures or a large number of experiments.

The development of capillary zone electrophoresis (CZE) has permitted high-resolution separations of CPs faster than by conventional HPLC. Good results were achieved by Gaitonde

and Pathak [11], who determined eleven CPs in less than 24 min using phosphate–borate buffer (pH 8.0) in a fused-silica capillary (65 cm × 25 μm I.D.) with an applied potential of 20 kV. Detection was performed with an on-column electrochemical detector in the picomole range. Efficiencies of the order of 320 000 theoretical plates were reached.

The use of micellar electrokinetic chromatography (MEKC) for the separation of chlorinated phenols was first reported by Otsuka *et al.* [12] the nineteen isomers were separated within 18 min, by using a 65 cm × 50 μm I.D. fused-silica tube with a 0.07 M sodium dodecyl sulphate (SDS) solution (pH 7.0). Eleven substituted phenols, listed by the US Environmental Protection Agency (EPA) as priority pollutants, were resolved by Ong and co-workers [13–15].

MEKC techniques have been widely used for the study of these compounds, whereas comparatively little attention has been paid to CZE. However CZE has several advantages, as follows. (1) With MEKC, the theoretical plate numbers are not as high as those which can be achieved by CZE, because of the resistance to

---

* Corresponding author.

mass transfer introduced by the solute distribution between the conducting buffer and the micelles. Consequently, the sensitivity in MEKC is lower than in CZE [16]. (2) CZE is a simpler technique than MEKC, which often requires extensive studies for optimizing the resolution [16]. (3) CZE is reported to be compatible with electrospray ionization mass spectrometry [17,18], whereas no such data have yet been published concerning MEKC. (4) CZE allows separations between neutral interferents and CPs. (5) Detection in CZE is likely to be enhanced by on-column sample concentration using field amplification [19,20]. On the other hand, MEKC gives greater selectivity than CZE for the separation of ionic solutes, which is influenced by differential partitioning and differential migration mechanisms.

The objective of this work was to demonstrate the suitability of CZE for the separation of chlorinated phenols. For this purpose, we tried to achieve a satisfactory optimization to obtain good resolution, based on three parameters: pH, buffer concentration and applied voltage. Observations on the migration behaviour of the CPs under different conditions were related to their physico-chemical properties and were used to predict CP migration and resolution.

EXPERIMENTAL

Apparatus

Measurements were carried out on an HPCE P/ACE system 2000 (Beckman, Palo Alto, CA, USA), equipped with a UV absorbance detector, an automatic injector, a thermostated column cartridge and an autosampler. A 57.0 cm long (50.0 cm to the detector cell) 75 mm I.D. fused-silica capillary column (Beckman) was used. All experiments were performed at 22.0°C at constant voltage. Samples were introduced pneumatically by application of pressure during 5 s. Solutes were monitored at 214 nm. Peak areas and electrophoretic mobilities were measured using Beckman GOLD 6.01 software.

Chemicals

Phosphate running buffers (pH 6.9) were prepared by mixing equimolar solutions of

Na_2HPO_4 and NaH_2PO_4 (Sigma, St. Louis, MO, USA). HPLC-grade distilled water (Baker, Deventer, Netherlands) was used to prepare buffers and standard solutions. 2,3-, 2,4-, 2,5,-Di-,2,3,6-, 2,4,6-, 2,4,5-tri- and pentachlorophenol were obtained from Fluka (Buchs, Switzerland) and 2,6-, 3,5-di-, 2,3,4-, 2,3,5-tri-, and 2,3,5,6-tetra-chlorophenol from Janssen (Noisy Le Grand, France). Standard solutions were prepared at a concentration of about 1.0 mg/l, except for o-chlorophenol (10.0 mg/l). All solutions were filtered through a 0.22-μm Nalgene filter (Sybron, Rochester, USA). Buffers could be stored for 3 days at 4°C.

Procedure

The capillary column was first conditioned with the separation buffer (1 min) immediately prior to injection. The column was systematically washed with 0.1 M NaOH (1 min), then rinsed with water (1 min) between runs.

RESULTS AND DISCUSSION

Theoretical

According to Giddings [21], the resolution (R_s) of two zones in electrophoresis can be expressed as

$$R_s = \tfrac{1}{4} N^{1/2} \Delta v / \bar{v} \tag{1}$$

where N is the theoretical plates number, $\Delta v / \bar{v}$ is the relative velocity difference of the two ions to be separated and, $\bar{v}$ is the average velocity of these two ions.

Jorgenson and Lukacs [22] derived the following expression for resolution in CZE:

$$R_s = \tfrac{1}{4} \sqrt{2} (\mu_{ep,1} - \mu_{ep,2}) V^{1/2} D^{-1/2} (\bar{\mu}_{ep} + \mu_{eo})^{-1/2} \tag{2}$$

where V is the applied voltage, D the analyte average diffusion coefficient, $\mu_{ep,1}$ and $\mu_{ep,2}$ the electrophoretic mobilities of the two solutes, $\bar{\mu}_{ep}$ their average electrophoretic mobility and μ_{eo} the electroosmotic flow coefficient. Eqn. (2) suggests that optimization of resolution can be achieved by controlling either (1) the difference in the electrophoretic mobilities of the solutes,

$\Delta\mu_{ep} = \mu_{ep,1} - \mu_{ep,2}$, which represents the selectivity factor, or (2) the electroosmotic flow coefficient (μ_{eo}).

μ_{eo} and μ_{ep} are related through the relationships [23]

$$\mu_{eo} = -\epsilon\zeta_c/\eta \qquad (3)$$

$$\mu_{ep} = 2\epsilon\zeta_a f(\kappa r)/3\eta \qquad (4)$$

where ϵ is the permittivity of the bulk electrolyte, ζ_c and ζ_a are the zeta potentials of the capillary inner wall and of the analyte, respectively, η is the viscosity of the electrolyte and $f(\kappa r)$ is a function dependent on the analyte double layer thickness ($1/\kappa$) and the solute "radius" (r), assuming that CPs can be considered as spherical particles.

Whereas D is determined for each analyte, V can be selected by the operator and $\mu_{ep,1}$, $\mu_{ep,2}$ or μ_{eo} can be modified by using different running buffers, by varying the pH and electrolyte type or concentration.

Effect of buffer pH on resolution

Different buffer pH values have been used for the analysis of CPs [11–13], and the optimum pH for the separation of CPs has been reported to range from 6.6 to 8.0. Terabe and co-workers succeeded in resolving the nineteen isomers of CPs using phosphate–borate buffer (pH 7.0). In fact, in most instances, the buffer pH has been chosen in a very empirical manner. This is particularly true when performing MEKC, for which the elution order of the solutes is difficult to predict. On the other hand, in CZE, it is possible to estimate the migration order, based on the solute pK_a values, using the following model.

Hunter [24] defined the zeta potential of an analyte (ζ_a) as

$$\zeta_a = \frac{Q_a}{4\pi\epsilon r(1 + \kappa r)} \qquad (5)$$

where Q_a is the analyte charge. Q_a may be further defined as the product of the electron charge (e) and the degree of dissociation (α) of the CP in the medium

$$Q_a = e\alpha \qquad (6)$$

where

$$\alpha = 1/1 + 10^{pK_a - pH} \qquad (7)$$

Combining eqns. 4, 5 and 6 yields the following expression for the electrophoretic mobility:

$$\mu_{ep} = \frac{e\alpha f(\kappa r)}{6\pi\eta r(1 + \kappa r)} \qquad (8)$$

Therefore, as the ionic mobility of an analyte is dependent on its charge, manipulation of the buffer pH becomes one of the key strategies in optimizing a separation. As can be seen from Fig. 1, the optimum pH corresponds to larger values of α. In practice, this pH is obtained by calculating the mean value of the solute pK_a values. Consequently, the useful range of pK_a available for the separation is limited by the electrolyte buffer pH ± 2 units, leading to a degree of dissociation between 1% and 99%. Then, it can be assumed that compounds with a pK_a that is not included in this pratical interval of pH (4 units wide) will not be successfully resolved. This is exemplified in Table I, where the pK_a values of CPs range from 4.74 to 9.37. In that case, the wide distribution of pK_a values adds to the difficulty in resolving the nineteen isomers using a single buffer pH. Hence, different runs at different pH values could be performed in order to overcome such difficulties. The feasibility of this approach will be discussed later.

The thirteen CPs isomers tested in this work exhibit an average pK_a value of 6.82. Separa-
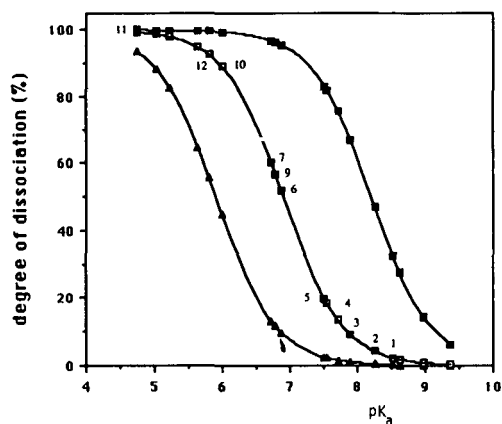
Fig. 1. Calculated degree of dissociation of CPs as a function of pK_a, at different constant pH values: (▲) 5.9; (□) 6.9; (■) 8.2. For solute numbers, see Table I.

TABLE I

pK$_a$ VALUES OF CHLOROPHENOL CONGENERS

Peak No.	Congener	pK$_a$ [2] (25°C)
1	2-Chlorophenol	8.52
a	3-Chlorophenol	8.97
a	4-Chlorophenol	9.37
4	2,3-Dichlorophenol	7.71
3	2,4-Dichlorophenol	7.90
5	2,5-Dichlorophenol	7.51
9	2,6-Dichlorophenol	6.78
a	3,4-Dichlorophenol	8.62
2	3,5-Dichlorophenol	8.25
6	2,3,4-Trichlorophenol	6.87
8	2,3,5-Trichlorophenol	?
12	2,3,6-Trichlorophenol	5.80
7	2,4,5-Trichlorophenol	6.72
10	2,4,6-Trichlorophenol	5.99
a	3,4,5-Trichlorophenol	7.55
a	2,3,4,5-Tetrachlorophenol	5.64
a	2,3,4,6-Tetrachlorophenol	5.22
13	2,3,5,6-Tetrachlorophenol	5.03
11	Pentachlorophenol	4.74
Average, monoCPs + diCPs		8.18
Average, triCPs + tetraCPs + pentaCP		5.95
Average, thirteen congeners tested		6.82

^{a} Not tested in this study.

tions were therefore performed using a phosphate buffer at pH 6.9 corresponding to the pK$_a$ of H$_2$PO$_4^-$–HPO$_4^{2-}$. Sodium salts were preferred to potassium salts, in agreement with Issaq et al. [25], who demonstrated that sodium phosphate buffers allow shorter migration times and better resolution and selectivity than potassium phosphate buffers of the same concentration and pH. Further, among commonly used buffer systems, phosphate buffer is the best known in capillary electrophoresis [11–13].

Fig. 2 illustrates the separation of thirteen CPs at pH 6.9. The reciprocals of the migration times of each ion were further plotted versus α for five different chlorophenols, at seven different buffer concentrations (Fig. 3). The experimental plots consist of straight lines with good correlation coefficients, as can be seen in Table II. The extrapolated values of 1/t$_m$ at α = 0 were used to calculate the migration times of a theoretical
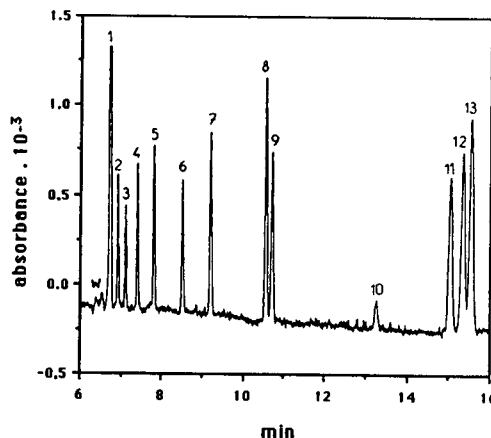
Fig. 2. Zone electrophoretic separation of thirteen CPs. Column, 57 cm × 75 μm I.D. fused-silica tube; buffer, [Na$_2$HPO$_4$] = [NaH$_2$PO$_4$] = 50 mM (pH 6.9); applied voltage, 18 kV; current 172 μA. For peak identification see Table I (w = water).

electroosmotic flow marker (t$_{eo}$). The extrapolated values of t$_{eo}$ are listed in Table II and experimental values of t$_{eo}$ are given for comparison. From these results, it is readily apparent that the experimental t$_{eo}$ has been systematically underestimated, the meaning of which is not clear. In this study, the electroosmotic flow marker was pure water, also contained in the samples: the water plug is detected by the UV cell as a result of local variation of the refractive
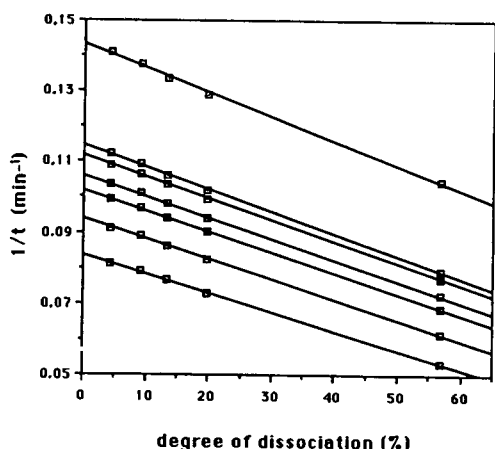
Fig. 3. Reciprocal of migration times as a function of the degree of dissociation of five different dichlorophenols at seven different buffer concentrations: [Na$_2$HPO$_4$] = [NaH$_2$PO$_4$] = (1) 10; (2) 25; (3) 30; (4) 35; (5) 40; (6) 50; (7) 75 mM. Constant pH, 6.9; constant applied voltage, 12 kV.

TABLE II

REGRESSION PARAMETERS FROM FIG. 3

Buffer concentration (mM)	r	Slope (10^{-4} min^{-1})	t_{eo} (min) (extrapolated value)	t_{eo} (min) (experimental)
10	−0.99901	−6.9242	6.980	7.002
25	−0.99955	−6.3169	8.719	8.537
30	−0.99968	−6.0860	8.957	8.697
35	−0.99966	−5.9710	9.421	9.197
40	−0.99972	−5.8627	9.810	9.477
50	−0.99976	−5.6780	10.655	10.293
75	−0.99964	−5.3243	11.968	11.330

index of the medium. Hence this water plug appears as a small peak on the electropherogram. Finally, the suitability of this marker is made questionable by these last results, and one should be cautious when using this method. Moreover, it must be remembered that a small error in t_{eo} determination may greatly influence the electrophoretic mobility (μ_{ep}) calculation. This is more critical when t_m is closed to t_{eo}

$$\mu_{ep} = \mu_{app} - \mu_{eo} = (1/t_m - 1/t_{eo})L'L/V \qquad (9)$$

where μ_{app} is the apparent mobility of the analyte, L' is the distance along the capillary between the sample introduction point and the detector and L is the total length of the capillary.

On the basis of eqn. 8 and 9, the linear plots observed in Fig. 3 should be interpreted as a linear relationship between μ_{ep} and α, as the radii (r) and $f(\kappa r)$ functions of the different diCPs are assumed to be nearly identical.

In addition, it is of interest to compare the behaviour of the diCPs and the triCPs. For example, it can be seen in Fig. 4 that 2,6-di-CP ($pK_a = 6.78$) has a larger migration time than 2,4,5-tri-CP ($pK_a = 6.72$). It is readily apparent that the two solutes are well resolved, despite a very minor discrepancy in their pK_a values. This can be explained by the fact that, in this case, the separation is primarily based on size rather than on charge.

Finally, it can be recognized from the results presented here that the migration order of CPs is based on both the solute pK_a value and size, that is, on the number of chlorine atoms on the aromatic ring.

Effect of buffer concentration on selectivity and resolution

Tsuda *et al.* [26] demonstrated ten years ago that the electrophoretic mobility and its complementary electroosmotic mobility should be inversely proportional to the square root of ionic strength. These results were later confirmed by Issaq *et al.* [27] and Atamna *et al.* [28]. Theoretical justifications for the dependence of μ_{ep} on buffer concentration can be summarized by the following equations.

According to Hunter [24], the reciprocal of the
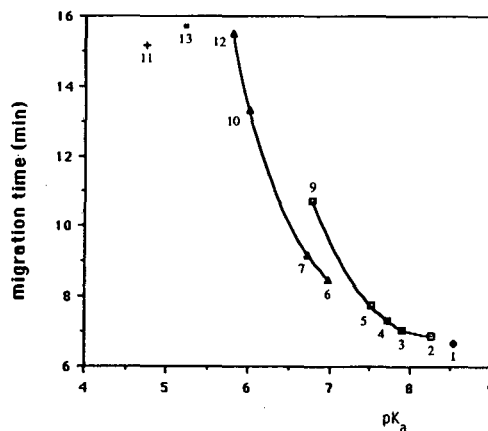
Fig. 4. Dependence of migration times of twelve CPs on their pK_a values. For solute numbers, see Table I. Conditions as in Fig. 2. $\diamond$ = 2-CP; $\square$ = diCPs; $\blacktriangle$ = triCPs; $\blacksquare$ = 2,3,5,6-tetraCP; + = pentaCP.

analyte double layer thickness (κ) may be given as

$$\kappa = (2000F^2/\epsilon RT)^{1/2}I^{1/2} \tag{10}$$

where F is the Faraday constant, R is the perfect gas constant, T is the temperature and I is the ionic strength, defined by

$$I = \tfrac{1}{2}\sum C_i Z_i^2 \tag{11}$$

where C_i is the concentration of ion i with a charge Z_i.

From eqns. 10 and 11, κ is proportional to the square root of the buffer concentration, if T and ϵ are kept constant: $\kappa = aC^{1/2}$, where a is a constant. As a result, eqn. 8 may be rewritten to express μ_{ep} as a function of C as

$$\mu_{ep} = \frac{e\alpha f(aC^{1/2}r)}{6\pi\eta r(1 + aC^{1/2}r)} \tag{12}$$

In practice, one could make the assumption that $f(\kappa r)$ is relatively unaffected by concentration changes [24]. It can then be expected that the plot of α/μ_{ep} ratio versus $C^{1/2}$ should be linear, assuming that r is constant for a given series of CPs, e.g., dichlorophenols:

$$\alpha/\mu_{ep} = m + nC^{1/2} \tag{13}$$

where m and n are constants.

In Fig. 5, the experimental plot consists of a straight line with a correlation coefficient of 0.99814, providing evidence that the previous assumptions were reasonable. Additionally, it can be shown that the five diCPs tested in this experiment show the same electrophoretic behaviour, that is, m and n are identical for these five congeners.

In contrast, it can be demonstrated that triCPs and tetraCPs or pentaCP exhibit different changes in electrophoretic mobilities with buffer concentration. The observed variations could not be accounted for solely by eqn. 12 as CP isomers are not influenced by C to the same extent.

The discrepancy in the behaviour of the different CPs results in a significant improvement of the separation selectivity, especially for the last three peaks (peaks 11, 12 and 13). Similar series of data, obtained at two different voltages, are
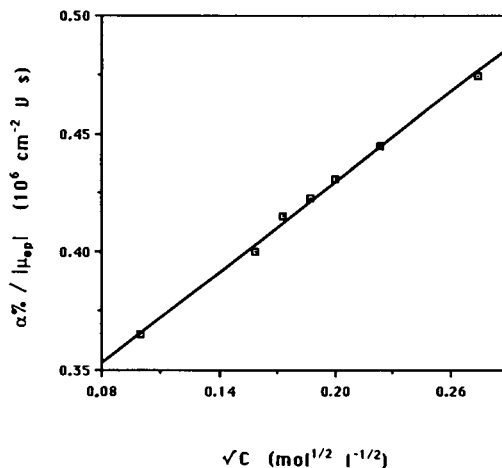
Fig. 5. $\alpha\%/|\mu_{ep}|$ ratio versus the square root of buffer concentration. The ratio values were obtained from the slopes of the experimental plots shown in Fig. 3. The extrapolated values of t_{eo} (listed in Table II) were used for calculations. Conditions as in Fig. 3.

illustrated in Figs. 6 and 7. Mobility differences $\Delta\mu$ have been calculated using the equation

$$\Delta\mu = \mu_{app,1} - \mu_{app,2}$$
$$= (\mu_{ep,1} + \mu_{eo}) - (\mu_{ep,2} + \mu_{eo})$$

Hence

$$\Delta\mu = \mu_{ep,1} - \mu_{ep,2}$$

which can be modified to
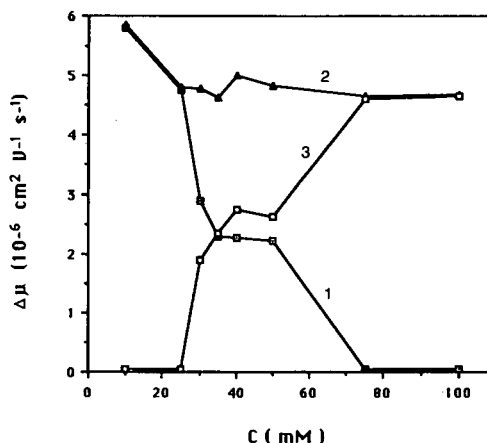
Fig. 6. Mobility difference versus buffer concentration. Constant applied voltage, $V = 12$ kV. Other conditions as in Fig. 2. $1 = \mu_{11} - \mu_{12}$; $2 = \mu_{11} - \mu_{13}$; $3 = \mu_{12} - \mu_{13}$ (subscript numbers refer to peak numbers in Table I).
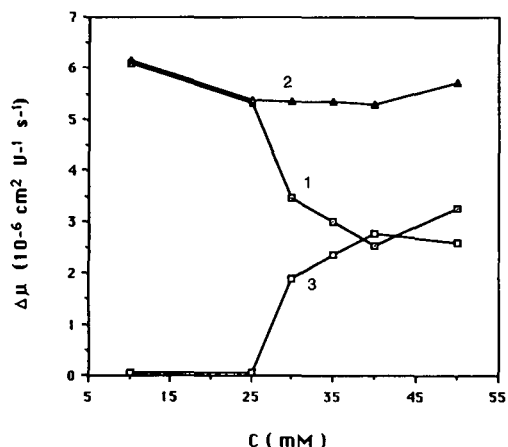
Fig. 7. Mobility difference *versus* buffer concentration. Constant applied voltage, $V = 18$ kV. Other conditions as in Fig. 2. Symbols as in Fig. 6.

$$\Delta\mu = (1/t_{m,1} - 1/t_{m,2})L'L/V \qquad (14)$$

It can be noted that $\Delta\mu$ is insensitive to t_{eo} determination.

As shown in Fig. 6 or 7, the $\mu_{11} - \mu_{13}$ difference is independent of the buffer concentration although the migration of solute 12 is greatly influenced. At low concentrations, solutes 12 and 13 co-migrate ($\Delta\mu = 0$) whereas, as the concentration increases, peak 12 moves towards peak 11. It can thus be demonstrated that the best separation can be achieved at an optimum buffer concentration 40 mM at $V = 12$ kV and 50 mM at $V = 18$ kV.

R_s is proportional to both $(\mu_{ep,1} - \mu_{ep,2})$ and $(\bar\mu_{ep} + \mu_{eo})^{-1/2}$ (eqn. 2). This is the reason why many workers [22,29,30] have predicted that maximum resolution is obtained when the the electroosmotic flow is opposite and equal to ion migration. This can be carried out by lowering electroosmosis, by increasing the buffer ionic strength. An improvement in resolution will be obtained, however, at the expense of a large increase in analysis time, as the migration time (t_m) is defined as

$$t_m = \frac{L'L}{(\mu_{ep} + \mu_{eo})V} \qquad (15)$$

Other workers [27,28] have recently pointed out that this argument cannot be taken as a systematic approach to improving resolution. In the present case, Fig. 6 clearly shows that an increase in buffer concentration results in co-migration of solutes 11 and 12. Hence the use of the more concentrated buffer does not systematically provide a significant improvement in resolution.

Applied voltage and heat dissipation

In most CZE separations, it can be observed that the ideal situation is obtained by applying as high a voltage as possible. This leads to the highest separation efficiency in the shortest time. However, the principal difficulty with this approach lies in the limited ability to dissipate the heat generated during the electrophoretic process. Indeed, numerous workers [22,26,27,31–33] have reported that μ_{app} (or V_{app} or $1/t_m$) deviates positively at high values of E. This effect is attributed to temperature-induced buffer viscosity changes, as a consequence of Joule heat dissipation. According to a generally accepted value of 2%/C for the decrease in water viscosity [22], in-column temperature increases (ΔT) have been estimated (Table III) from the non-linear dependence of the current on the applied voltage (Fig. 8). By analogy with the expression developped by Vindevogel and Sandra [33], ΔT can be calculated from the following expression

$$\Delta T(°C) = \frac{(I_m/I_{th}) - 1}{2\%} \qquad (16)$$

where I_m is the current measured for voltage V and I_{th} is the theoretical current, calculated from the assumption of a linear relationship between I and V. With a 50 mM phosphate buffer, I_{th} can be expressed as

$$I_{th} = I_{9\,kV}V_{kV}/9 \text{ kV} \qquad (17)$$

where $I_{9\,kV}$ is the experimental current corresponding to $V = 9$ kV, taken as a reference value (ΔT is there considered to be insignificant).

Estimated values of ΔT, calculated from data in Fig. 8, are listed in Table III. Results obtained with a borate buffer are given for comparison, but it should be remembered that the ionic strength is different in phosphate and borate buffers. Dissipated powers were calculated using the equation $P = VI/L$. As the upper power limit

TABLE III

ESTIMATED IN-COLUMN TEMPERATURE INCREASE AND DISSIPATED POWER AS A FUNCTION OF APPLIED VOLTAGE

Conditions as in Fig. 8.

V (kV)	Phosphate buffer		Borate buffer	
	ΔT (°C)	P (mW/cm)	ΔT (°C)	P (mW/cm)
9	0	11.5	0	1.4
12	2.6	21.5	–	–
15	5.3	35.3	0	3.9
18	9.2	54.4	–	–
20	13.9	72.6	0.51	6.9
22	18.9	94.7	–	–
25	–	–	1.2	11.0
30	–	–	2.2	16.2

recommended by the manufacturer is about 50 mW/cm [34], it can be concluded from the data in Table III that, using a 50 mM phosphate buffer, the applied voltage must be kept below 18 kV. Under extreme conditions, *i.e.*, at $I = 245$ μA, the temperature rise ($\Delta T = 18.9$°C) will become high enough to cause zone broadening, or affect the μ_{app} reproducibility. Another undesirable consequence of the increase in the running buffer temperature will be instabilities that can affect the baseline, probably due to solvent degassing. Finally, from these results, it can be

Fig. 8. Current as a function of applied voltage for two different buffers; □ = phosphate buffer (50 mM); ■ = borate buffer (100 mM). Column, 57 cm × 75 μm I.D. fused-silica tube.

suggested that the actual in-column temperature is likely to be enhanced with an increase in the buffer concentration. However, this temperature rise should not be responsible for the variations of selectivity that are observed in Figs. 6 or 7. As the phosphate buffer has a relatively small temperature coefficient (*ca.* −0.0028 pH/°C) [35], it can be concluded that the difference in pH of the buffers of various concentrations (10–100 mM) can be considered to be insignificant. Additionally, temperature-induced shifts in the solutes pK_a values is not a dominant factor for acting on the selectivity {*e.g.*, d(pK_a)/dT = −0.013°C^{-1} for the phenol [36]}. In fact, it can be seen from ref. 35 that changes in electromigration times of CPs with temperature should be predominantely due to temperature-induced viscosity changes of water. All the solutes being influenced to the same extent, resolution will not be modified by minor temperature shifts.

Key strategies of optimization

As discussed previously, combined effects of buffer concentration and applied voltage must be taken into consideration for optimizing a separation. Depending on the purpose of the study, a compromise between resolution, power consumption, speed and sensitivity must be achieved.

When coupling CZE with a mass spectrome-

ter, the objectives of the separation will be totally different. Indeed, the resolution of peaks 11, 12 and 13 will no longer be useful, as these three compounds have different molecular masses and will be easily discriminated by MS. In comparison with Fig. 1 ($C = 50$ mM; $V = 18$ kV), it can be deduced from Fig. 9 ($C = 10$ mM; $V = 30$ kV) that a decrease in buffer concentration permits a maximum voltage (the limit of the power supply) to be applied while the current drifts from 172 to 65 μA. This results in a loss of resolution between peaks 12 and 13, but a substantial improvement in both speed and efficiency is obtained. In addition, the baseline in Fig. 9 is more stable than that in Fig. 1.

Quantitative aspects

In Fig. 10, the standard deviations (σ) of corrected peak area, calculated as the average of five successive runs, are plotted versus the analyte concentration of various CPs. For $\sigma/\bar{x} = 33\%$ the detection limits are found to be between 60 and 100 μg/l, depending on the CPs tested; for $\sigma/\bar{x} = 10\%$, they are found between 80 and 340 μg/l. Therefore, it must be concluded that the sensitivity of the measurement is poor. This must be accounted for by the diameter of the capillary (75 μm) and the limited performance of the UV detector. Finally, the

Fig. 10. Standard deviation of corrected peak area versus sample concentration. Corrected peak areas (A_c) were calculated from electropherograms, using the Gold software, by the equation $A_c = A_m V_{app}$, where A_m is the measured area and V_{app} is the apparent velocity of the solute. Standard deviations were calculated on the basis of five succeeding runs. Experimental conditions as in Fig. 2. $\triangle$ = Peak 2; ■ = peak 3; $\square$ = peak 5; × = peak 7 (see Table I).

linearity of the calibration graphs is fairly good between 0 and 1 mg/l (Fig. 11).

CONCLUSIONS

The separation of thirteen chlorophenols has been satisfactorily optimized to obtain maximum peak separation in less than 16 min. By coupling CZE with electrospray ionization mass spec-

Fig. 9. Zone electrophoretic separation of thirteen CPs. Column, 57 cm × 75 μm I.D. fused-silica tube; buffer: [Na$_2$HPO$_4$] = [NaH$_2$PO$_4$] = 10 mM (pH 6.9); applied voltage, 30 kV; current, 65 μA. For peak identification, see Table I.
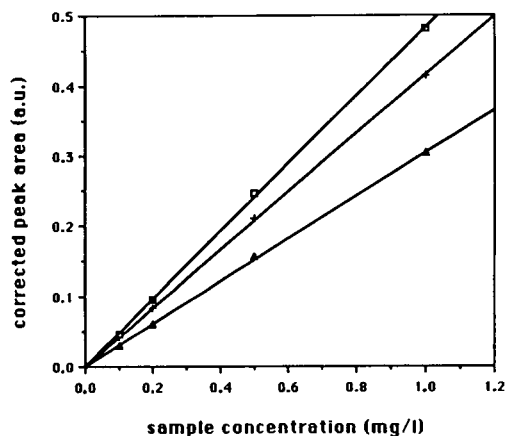
Fig. 11. Calibration graphs: corrected peak area (arbitrary units) versus sample concentration. $\triangle$ = Peak 2; + = peak 4; $\square$ = peak 5 (see Table I).

trometry, it can be expected that the analysis time could be reduced to 5 min. Although this approach seems to be promising, it should be remembered that 'the theory predicts that the nineteen congeners cannot be easily resolved using a single buffer pH. Therefore, an alternative method is to use two different buffer pH values, yielding two group separations penta-, tetra- and triCPs could be separated at pH 5.9 while mono- and diCPs could be conveniently resolved at pH 8.2. Further, the increase of selectivity due to the pH shift will allow two short and efficient separations, with extreme voltage (30 kV) and minimum buffer concentration (10 mM). Because the pH is a dominant factor that could be manipulated to control resolution, this last method should be applicable to complex samples, where inadequate separation is obtained at any single buffer pH.

REFERENCES

1 E.M. Lores, T.R. Edgerton and R.F. Moseman, J. Chromatogr. Sci., 19 (1981) 466.
2 K. Ugland, E. Lundanes, T. Greibrokk and A. Bjorseth, J. Chromatogr., 213 (1981) 83.
3 O. Busto, J.C. Olucha and F. Borrull, Chromatographia, 32 (1991) 423.
4 J. Czuczwa, C. Leuenberger, J. Tremp, W. Giger and M. Ahel, J. Chromatogr., 403 (1987) 233.
5 F. Dondi, A. Betti and C. Bighi, J. Chromatogr., 257 (1983) 69.
6 H. A. McLeod and G. Laver, J. Chromatogr., 244 (1982) 385.
7 E. Burtscher, H. Binder, R. Concin and O. Bobleter, J. Chromatogr., 252 (1982) 167.
8 N.G. Buckman, J.O. Hill, R.J. Magee and M.J. McCormick, J. Chromatogr., 284 (1984) 441.
9 F.P. Bigley and R.L. Grob, J. Chromatogr., 350 (1985) 407.
10 C. de Ruiter, J.F. Bohle, G.J. de Jong, U.A.Th. Brinkman and R.W. Frei, Anal. Chem., 60 (1988) 666.
11 C.D. Gaintonde and P.V. Pathak, J. Chromatogr., 514 (1990) 389.
12 K. Otsuka, S. Terabe and T. Ando, J. Chromatogr., 348 (1985) 39.
13 C.P. Ong, C.L. Ng, N.C. Chong, H.K. Lee and S.F.Y. Li, J. Chromatogr., 516 (1990) 263.
14 C.P. Ong, C.L. Ng, N.C. Chong, H.K. Lee and S.F.Y. Li, Environ. Monit. Assess., 19 (1991) 93.
15 Y.F.K. Yik, C.L. Ng, C.P. Ong, S.B. Khoo, H.K. Lee and S.F.Y. Li, Bull. Sing. N. I. Chem., 18 (1990) 91.
16 G.M. Janini and H.J. Issaq, J. Liq. Chromatogr., 15 (1992) 927.
17 F. Garcia and J.D. Henion, Anal. Chem., 64 (1992) 985.
18 M.A. Moseley, J.W. Jorgenson, J. Shabanowitz, D.F. Hunt and K.B. Tomer, J. Am. Soc. Mass Spectrom., 3 (1992) 289.
19 R.L. Chien and D.S. Burgi, Anal. Chem., 64 (1992) 489A.
20 R.L. Chien and D.S. Burgi, Anal. Chem., 64 (1992) 1046.
21 J.C. Giddings, Sep. Sci., 4 (1969) 181.
22 J.W. Jorgenson and K.D. Lukacs, Anal. Chem., 53 (1981) 1298.
23 T.T. Lee and E.S. Yeung, Anal. Chem., 63 (1991) 2842.
24 R.J. Hunter, Zeta Potential in Colloid Science—Principles and Applications, Academic Press, New York, 1981, pp. 27, 32 and 71.
25 H.J. Issaq, I.Z. Atamna, C.J. Metral and G.M. Muschik, J. Liq. Chromatogr., 13 (1990) 1247.
26 T. Tsuda, K. Nomura and G. Nakagawa, J. Chromatogr., 264 (1983) 385.
27 H.J. Issaq, I.Z. Atamna, G.M. Muschik and G.M. Janini, Chromatographia, 32 (1991) 155.
28 I.Z. Atamna, H.J. Issaq, G.M. Muschik and G.M. Janini, J. Chromatogr., 588 (1991) 315.
29 A.G. Ewing, R.A. Wallingford and T.M. Olefirowicz, Anal. Chem., 61 (1989) 292 A.
30 J.W. Jorgenson and K.D. Lukacs, Science, 222 (1983) 266.
31 H.T. Rasmussen and H.M. McNair, J. Chromatogr., 516 (1990) 223.
32 K.D. Altria and C.F. Simpson, Chromatographia, 24 (1987) 527.
33 J. Vindevogel and P. Sandra, J. High Resolut. Chromatogr., 14 (1991) 795.
34 P/ACE System 2000 Instrument Manual, Beckman Instruments, Palo Alto, CA, 1989.
35 C.W. Whang and E.S. Yeung, Anal. Chem., 64 (1992) 502.
36 D.D. Perrin, B. Dempsey and E.P. Serjeant, in pK$_a$ Prediction for Organic Acids and Bases, Chapman and Hall, London, 1981, p. 7.

Capillary zone electrophoresis of malto-oligosaccharides derivatized with 8-aminonaphthalene-1,3,6-trisulfonic acid

Claudia Chiesa and Csaba Horváth*

Department of Chemical Engineering, Yale University, New Haven, CT 06520 (USA)

ABSTRACT

Malto-oligosaccharides were derivatized via their reducing end with 8-aminonaphthalene-1,3,6-trisulfonic acid by reductive amination, and the separation and electrophoretic migration behavior of the labelled sugars were investigated by capillary zone electrophoresis. Series of linear malto-oligosaccharides were found particularly suitable for both the study of the effect of the operating conditions on the separation and the investigation of the relationship between the electrophoretic mobility and the molecular size of the homologues. The electrophoretic mobility of the malto-oligosaccharide conjugates was found to be a linear function of the molecular mass to the negative two-thirds power. The sugar derivatives employed here carry three negative charges due to the presence of the dissociated sulfonic acid groups even at strongly acidic pH. Therefore, the analytes can migrate in the electric field without interference by electroendosmotic flow and/or wall adsorption in uncoated silica capillaries at low pH. As a result, the separation of these carbohydrate conjugates can be carried out under such conditions with high speed and efficiency in free solution, *i.e.*, without an anticonvective medium such as a gel or a viscous polymer solution. Appropriate use of triethylammonium phosphate buffer, pH 2.5, as the background electrolyte improves not only the reproducibility, but also the efficiency and speed of the separation. The labelled sugars allow monitoring of the separation by UV detector or laser-induced fluorescence detector with concomitant enhancement of analytical sensitivity.

INTRODUCTION

The important role of complex carbohydrates in life processes is increasingly recognized. More and more therapeutic proteins produced by biotechnology entail glycan moieties that affect the biological activity, lifetime and specificity of the drug [1–3]. Consequently, there is a growing need for rapid analytical techniques of high resolution for oligosaccharides. However, the separation of carbohydrates is hampered by their similar chemical composition, as many oligosaccharides of biological interest consist of only a few kinds of residues and differ from each other mainly in their three-dimensional molecular structure. Moreover, the lack of chromophoric and/or fluorogenic functions in most sugar molecules impedes their high-sensitivity detection.

Traditionally, both chromatography and electrophoresis were employed for the analysis of carbohydrates. Most branches of chromatography such as size-exclusion, ion-exchange, ligand-exchange, reversed-phase and affinity chromatography as well as gas chromatography have found application in the quantitative and qualitative analysis of saccharides [4,5]. For complex oligosaccharides, the most popular HPLC method is anion-exchange chromatography at high pH with pulsed amperometric detection [6–8].

Electrophoresis of carbohydrates is encumbered by the absence of readily ionizable functions in most mono- and oligosaccharides. Whereas planar electrophoretic techniques have

---

* Corresponding author.

been widely used for the separation of naturally charged oligosaccharides and glycopeptides, the requirement of highly alkaline pH to ionize most carbohydrate molecules has impeded the use of electrophoresis for the separation of underivatized sugars. One approach to overcome this difficulty is the use of borate in the background electrolyte to form negatively charged borate complexes of neutral saccharides at moderately alkaline pH [9]. The borate complexes of carbohydrates are then separated by electrophoresis according to their differences in electric charge, molecular size and stability.

Polyacrylamide gel layers were preferentially employed for the electrophoretic separation of carbohydrate molecules. Since the diameter of the gel pores usually exceeded substantially the molecular dimensions of oligosaccharides and glycopeptides [10,11], their electrophoretic mobility in this matrix was largely determined by the charge-to-mass ratio, and molecular sieving did not contribute significantly to the separation. Despite its great merits, slab gel electrophoresis is a relatively slow process, and does not lend itself readily to automation or quantitative analysis with high precision.

In the past few years, capillary zone electrophoresis (CZE) has made great advances. This instrumental electrophoretic technique is particularly suitable for rapid analysis with high resolution as demonstrated by the analysis of peptide, protein and complex oligonucleotide mixtures [12–14]. A review of this technique can be found in the recent literature [15]. Moreover, CZE has been shown to also have promise for the analysis of mono- and oligosaccharides as well as glycoprotein fragments [16–20].

A promising approach in the CZE of carbohydrates entails their precolumn derivatization with reagents that contain ionogenic functions and suitable chromophoric or fluorogenic groups. Reductive amination at the reducing end of the saccharide with a reagent containing a primary amino group and allowing highly sensitive detection, offers a particularly convenient method for the preparation of these kinds of conjugates. Such a derivatization reaction of mono- and oligosaccharides with 2-aminopyridine was introduced originally for use in paper electrophoresis

and was later employed in HPLC [21]. It was recently modified for use in the CZE of monosaccharides and oligosaccharides as the borate complexes of their N-2-pyridylglycamine forms [22,23]. The separation by CZE of such malto-oligosaccharide conjugates was further improved by the addition of small amounts of tetrabutylammonium bromide to the background electrolyte at pH 5.0 [24]. In another example, reducing carbohydrates were derivatized with 3-(4-carboxybenzoyl)-2-quinolinecarboxaldehyde for the analysis by CZE with borate buffer in both free solution and highly concentrated polyacrylamide gel-filled capillaries [25–28]. With such derivatives, the use of polyacrylamide gel-filled capillaries was found to be essential for the CZE of carbohydrates at high resolution.

Most of the methods for the analysis of carbohydrates by CZE described so far in the literature are carried out at pH higher than 7.0, usually in order to form their borate complexes. Under such conditions, the silanol groups at the silica surface are dissociated and, as a result of the negatively charged capillary inner wall, considerable electroendosmotic flow is generated by the high electric field with possible untoward consequences for the separation. Furthermore, adsorption of positively charged analytes at the inner wall of the silica capillary significantly reduces the separation efficiency.

The goal of the present study was to investigate the potential of CZE in carbohydrate analysis under conditions where both electroendosmotic flow and adsorption at the capillary inner wall were negligible. This approach requires the use of derivatives which contain strongly acidic functions that dissociate even at low pH and facilitate UV and/or fluorescence detection. Derivatives of aromatic sulfonic acid can be particularly useful in this regard as they are ionized over a wide pH range. For this reason, reagents such as 7-aminonaphthalene-1,3-disulfonic acid and 8-amino-naphthalene-1,3,6-trisulfonic acid (ANTS), introduced for the derivatization of reducing saccharides prior to polyacrylamide slab gel electrophoresis, are potentially suitable also in CZE. Indeed, the reductive amination of N-acetylchitooligosaccharides with 7-amino-1,3-naphthalene disulfonic acid was recently de-

scribed for monitoring their chitinase-catalyzed hydrolysis by CZE analysis [16].

In our approach, we adapted the derivatization method with the fluorophore ANTS first described by Jackson and Williams [29,30] for use in polyacrylamide slab gel electrophoresis. The derivatization with ANTS imparts both electric charge and fluorescence to the saccharides. The three sulfonic acid groups in the ANTS moiety are negatively charged over a wide pH range and the concurrently high electrophoretic mobility of the derivatized carbohydrates facilitates their rapid separation. The ANTS derivatives can be used with UV detection and *a fortiori* with highly sensitive laser-induced fluorescence detection. Furthermore, ANTS, unlike other aminonaphthalene mono- and disulfonic acids, has adequate solubility in the reaction mixture [31] and is commercially available in a sufficiently pure form. Homologous malto-oligosaccharides of different provenance were selected as model substances because they span a wide molecular mass range. The mixtures were obtained from starch by acidic and/or enzymatic catalyzed hydrolysis and contained mainly linear homologues with up to approximately 40 glucose residues and a small amount of branched fragments.

EXPERIMENTAL

Equipment

A P/ACE Model 2100 capillary electrophoresis unit was used with System Gold Version 6.01 software (Beckman Instruments, Fullerton, CA, USA) and the 214-nm filter of the UV detector with a wavelength setting closest to the maximum absorbance wavelength for ANTS. Fused-silica capillary tubes of 365 μm O.D. with polyimide outer coating were obtained from Quadrex (New Haven, CT, USA) and employed without any coating of the inner wall. The dimensions of the capillaries used in the experiments were 270 mm × 50 μm, 370 mm × 50 μm and 670 mm × 20 μm. The pertinent migration distance from the inlet to the light beam of the detector, which passed through a narrow segment of the tube where the polyimide coating

was removed, was 70 mm shorter than the actual tube length.

Chemicals

Glucose (G1), maltose (G2), maltotriose (G3), maltotetraose (G4), maltopentaose (G5), maltohexaose (G6) and maltoheptaose (G7) standards as well as starch hydrolysate Cat. No. M3639 were purchased from Sigma (St. Louis, MO, USA). The main components of the latter mixture, referred to as mixture A, were linear malto-oligosaccharides of up to 12 glucose residues with a significant amount of branched isomers. Fig. 1 illustrates the structure of linear malto-oligosaccharides in which glucose molecules are joined by α-D(1,4) linkages. The number of glucose residues is denoted by "n" throughout this paper. Dextrin 15 (maltodextrin) starch hydrolysate was purchased from Fluka (Ronkonkoma, NY, USA). This sample, referred to as mixture B, contains over 30 linear malto-oligosaccharide homologues and only a small quantity of branched isomers. MALTRIN M040 (Maltodextrin) starch hydrolysate was a gift from Grain Processing (Muscatine, IA, USA). This sample contains linear malto-oligosaccharide homologues of up to almost 40 glucose residues and is referred to as mixture C. Sodium cyanoborohydride and mesityl oxide were purchased from Aldrich (Milwaukee, WI, USA). ANTS was obtained from Molecular Probes (Eugene, OR, USA). Dimethyl sulfoxide (DMSO) was purchased from Mallinckrodt (St.Louis, MO, USA), acrylamide was from Bio-Rad (Melville, NY, USA), and Triton X-100 was obtained from Rohm and Haas (Philadelphia, PA, USA). The buffers were prepared from
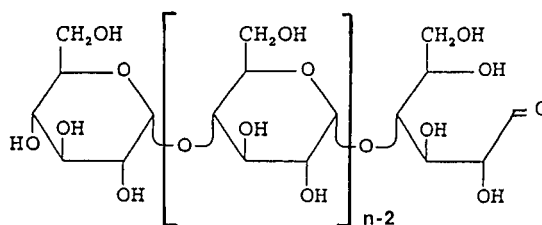
Fig. 1. General structure of linear malto-oligosaccharides: O - α - D - glucopyranosyl - (1 → 4) - [O - α - D - glucopyranosyl - (1 → 4)]$_{n-2}$-D-glucopyranose where n is the number of glucose residues in the molecule.

reagent grade phosphoric acid and sodium hydroxide supplied by Fisher Scientific (Pittsburgh, PA, USA) as well as triethylamine (TEA) purchased from Eastman Kodak (Rochester, NY, USA).

Derivatization with ANTS

The reductive amination of the saccharides with ANTS was adapted from the method described by Jackson [29]. In a typical procedure approximately 1 μmol of each authentic oligosaccharide standard with up to seven glucose units reacted in a microcentrifuge tube with 200 μl of 0.2 M ANTS solution in acetic acid–water (3:17, v/v) and 200 μl of 1 M NaCNBH$_3$ solution in dimethylsulfoxide. Furthermore, 20 μl of a 0.5 M aqueous solution of 1,3,5-benzene trisulfonic acid (BTA) were added to the reaction mixture to serve as a internal standard for the evaluation of the electropherograms. After mixing, the content of the tube was vortexed and then incubated for 15 h in a water bath at 40°C. Before the CZE injection, each sample was diluted twenty- to fortyfold with water and passed through 0.22-μm cellulose filters (Alltech, Deerfield, IL, USA). The average molecular mass of the starch hydrolysates was calculated for each mixture, and the conditions of the derivatization were optimized with regards to the amount of ANTS employed.

Electrophoresis

The samples were injected by applying 0.5 p.s.i. (1 p.s.i. = 6894.76 Pa) pressure for 3 to 7 s, and the approximate sample volumes were calculated according to the literature [32]. Electrokinetic injection was employed for the rapid separation depicted in Fig. 12. In most cases, the temperature was 25°C; only a few experiments were carried out at 50°C. Between runs, the capillary was flushed with approximately five tube-volumes of the background electrolyte. Some experiments were carried out with 30 and 50 mM phosphate buffers of pH 2.0 and 2.5, respectively, as the background electrolyte; the cathode was at the inlet end and the anode at the detector end of the capillary. In other experiments, 50 mM phosphate buffer, pH 9.0 or 9.4, was the background electrolyte, and the in-

strumental set up was configured so that sample introduction and detection took place at the anodic and cathodic ends, respectively. A mixture of 10 mM disodium phosphate and 10 mM trisodium borate, pH 9.4, was used in the study of the effect of borate on the electrophoretic mobility of the conjugated oligosaccharides. Electropherograms were obtained with a buffer prepared from a solution of 50 mM phosphoric acid and 10.8 mM TEA titrated with 1 M NaOH to pH 2.5. Major peaks in the electropherogram of the malto-oligosaccharides were identified by co-electrophoresis with ANTS derivatives of authentic standards containing up to seven glucose units.

Measurement of electroendosmotic flow

The magnitude of the electroendosmotic flow in capillaries filled with 50 mM phosphate buffer was determined from the migration times at 12 kV of three neutral tracers: acrylamide, mesityl oxide and Triton X-100. Subsequently, the electroendosmotic mobility was calculated and used to correct for the electrophoretic mobility when the ratio of the two mobilities was greater than 0.02.

In a particular set of experiments, the electroendosmotic flow velocity was measured by partially replacing sodium ions by TEA in the phosphate buffer, pH 2.5. Measurements were carried out using 50 mM phosphoric acid solutions containing 0, 3.6, 7.2, 10.8, 14.4, 21.6, 28.8 or 36 mM TEA that were titrated to pH 2.5 with 1 M NaOH. Before each measurement, the capillary was rinsed first with water and then with buffer each for 5 min. The electroendosmotic mobility was calculated with an average value from 3 measurements using phenol, DMSO and acrylamide as neutral markers.

Experiments with laser-induced fluorescence detector

A capillary electrophoresis unit (P/ACE 2100) in the reversed polarity mode with the UV detector at 214 nm was used for the separation of malto-oligosaccharide mixture A with a 270 mm × 20 μm uncoated fused-silica capillary and 50 mM phosphate buffer, pH 2.5, at 25°C. The same sample was also separated with an *ad hoc*

capillary electrophoresis system consisting of a high-voltage power supply (Glassmann High Voltage, Whitehouse Station, NJ, USA) and a 20 μm I.D. uncoated capillary of 470 mm (minimum length required for system) without temperature control. Fluorescence excitation was accomplished using the 325-nm line of a helium–cadmium laser (2.8 mW, Liconix, Santa Clara, CA, USA). The beam was focused into the separation channel of a 20 μm I.D. fused-silica capillary using a plano convex lens [0.5 in. diameter (1 in. = 2.54 cm), 5 cm focal length, Oriel, Stratford, CT, USA]. Fluorescence originating from the illuminated section of the capillary separation channel was collected and collimated by a parabolic reflector. The collimated light from the reflector was directed through a series of two bandpass filters (520 nm, 3-cavity, Oriel) and detected by an end-on photomultiplier tube (PMT) (R374, Hamamatsu, Japan). The PMT output was converted to voltage using socket-mounted pre-amp assemblies (C1053, Hamamatsu) and electronically filtered (risetime = 1.0 s) using a home-made filter unit. The analog signal was digitized at 4 Hz using System Gold Software and a Model 406 analog-to-digital converter (Beckman Instruments). All laser-induced fluorescence detection (LIF) separations were performed at room temperature and samples were injected electrokinetically at typical conditions of 10 kV for 5 s.

RESULTS AND DISCUSSION

Derivatization of carbohydrates with ANTS

The derivatization reaction scheme is shown in Fig. 2. First, the reducing end of the saccharides reacts with the primary amino group of ANTS to form a Schiff base that is subsequently reduced to a secondary amine by sodium cyanoborohydride. According to Jackson [29], complete derivatization by ANTS occurs under optimal reaction conditions in 15 h as determined by using [14C]glucose; more than 99% of the glucose reacted. As monitored using glucose and/or maltose as model substances, complete derivatization could be achieved in less than 2 h when sodium cyanoborohydride was added to the
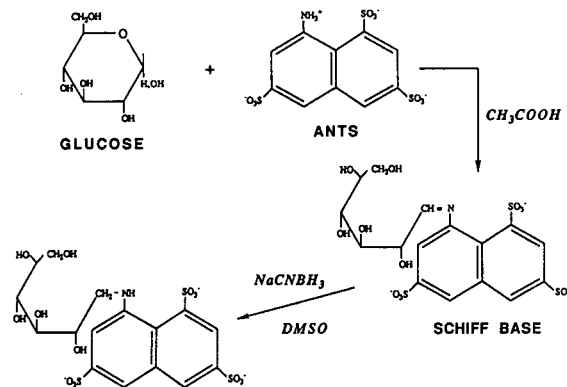
ANTS DERIVATIVE OF GLUCOSE

Fig. 2. Reaction scheme for the derivatization of carbohydrates with ANTS by reductive amination. The formula mass of the disodium salt of the ANTS–glucose conjugate (590) was used in the calculation of the molecular mass of the linear malto-oligosaccharide–ANTS conjugates with different number of glucose residues.

mixture at an advanced stage of the reaction and the temperature was increased from 40 to 80°C.

Another important aspect of the derivatization reaction is associated with the level of excess ANTS. Jackson routinely used approximately 200-fold excess of ANTS for the derivatization [29]. We have found that in the CZE of samples prepared with such a large excess of ANTS the peaks of the lower malto-oligosaccharides are masked by the large ANTS peak in the electropherogram. On the other hand, as suggested by Jackson [29], a fortyfold molar excess of ANTS sufficed for complete conversion, and under such conditions we observed no interference by excess ANTS in CZE.

The substantial advantage of ANTS as a labeling agent is that it is both a chromophore and a fluorophore which facilitates highly sensitive fluorescence detection of trace amounts under appropriate conditions. The UV spectrum of ANTS shows a maximum at approximately 220 nm followed by two other maxima at 270 and 360 nm; its molar adsorptivity in water is 5.700 cm^{-1} M^{-1} when measured at 360 nm. The spectrum of ANTS-derivatized maltose was found to be very similar except that the third maximum was shifted to 370 nm. With the UV detector, CZE analysis required relatively large amounts of sample with concomitant overload of

the system and reduced separation efficiency. When a 12-nl sample was subjected to CZE, approximately 15 fmol of ANTS-derivatized glucose could be detected at 214 nm (signal-to-noise ratio of 3) at the highest sensitivity setting.

As a fluorophore, ANTS has a maximum excitation wavelength at 360 nm in 50 mM phosphate buffer, pH 7.2, which shifts to 370 nm for the ANTS-derivatized maltose. The wavelength of maximum emission is at 515 nm. The fluorescent properties of ANTS facilitate LIF of its derivatives with a He–Cd laser with an output wavelength of 325 nm.

Fig. 3 depicts the results of some preliminary studies on the CZE of ANTS-derivatized malto-oligosaccharides from mixture A obtained by UV and LIF detection. The pattern is identical in both cases, but the sensitivity of LIF detection is about 3 orders of magnitude higher than that of the UV detection. As a result, a few attomoles can be analyzed by using an LIF detector. Moreover, as the capillary does not have to be overloaded, the potential of ANTS derivatization can be fully exploited without loss of efficiency. Precise values for the lower detection limit and for the efficiency of LIF detection are not available, but the preliminary results allow us to expect an efficiency of several hundred thousand theoretical plates per meter. In spite of the much higher sensitivity of LIF, the electropherogram depicted in Fig. 3B does not reveal
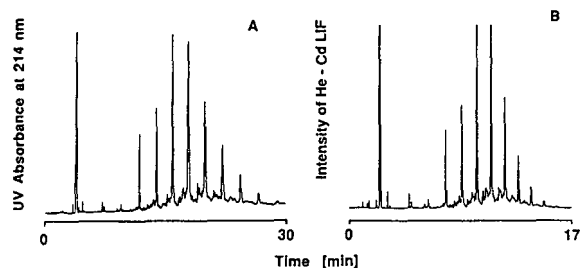
Fig. 3. Electropherograms of ANTS-derivatized malto-oligosaccharides (mixture A) obtained with UV and LIF detection. (A) 670 mm × 20 μm capillary; 200 mM phosphate buffer, pH 2.0; temperature, 25°C; voltage, 30 kV; UV detection at 214 nm; injected amount: 20 ng of ANTS-derivatized malto-oligosaccharide mixture. (B) 470 mm × 20 μm capillary; 200 mM phosphate buffer, pH 2.0; temperature, 25°C; voltage, 15 kV; He–Cd laser-induced fluorescence detector, emission wavelength 525 nm; injected amount: 70 pg of ANTS-derivatized malto-oligosaccharide mixture.

peaks that cannot be seen by UV detection at 214 nm. The derivatization reaction with ANTS appears to be a "clean" one not giving rise to minor side-products.

Theoretical aspects of CZE of carbohydrates derivatized with ANTS

Since the ANTS-derivatized saccharides are negatively charged over a wide pH range, they can be subjected to CZE at acidic pH where the electroendosmotic flow is usually negligible. Under such *arheic* (from the Greek *a* "without" and *rhéos* "flow") conditions, the sample components traverse the capillary in free solution solely by electrophoretic migration.

In the absence of electroendosmotic flow, the electrophoretic migration velocity u_{ep} is given by

$$u_{ep} = \mu_{ep}V/L \qquad (1)$$

where μ_{ep} is the electrophoretic mobility, and V is the potential across the capillary of length L [33,34].

Experimentally, the migration time t_m is measured and under arheic conditions given by

$$t_m = lL/\mu_{ep}V \qquad (2)$$

where L is the length of the capillary, and l is the pertinent migration distance, *i.e.* the tube length from the inlet to the detector's light beam.

In uncoated fused-silica capillaries of uniform surface properties at alkaline pH, the velocity of the electroendosmotic flow u_{eo} is expressed by

$$u_{eo} = \mu_{eo}V/L \qquad (3)$$

where μ_{eo} is the electroendosmotic mobility. Its magnitude depends [35] on the zeta potential, ζ, at the tube inner wall, the dielectric constant, ϵ, the viscosity of the fluid, η, and the permittivity of the vacuum, ϵ_0, as

$$\mu_{eo} = \epsilon_0 \epsilon \zeta/\eta \qquad (4)$$

By using eqns. 2 and 4, we can estimate the value of the zeta potential from the migration time of neutral markers.

In the presence of electroendosmotic flow, the migration rates of charged molecules are de-

termined by both the pertinent electrophoretic mobilities and the magnitude of the electroendosmotic flow. The net migration velocity of a charged substance u is given by

$$u = u_{ep} + u_{eo} = (\mu_{ep} + \mu_{eo})V/L \qquad (5)$$

The sign of the electrophoretic and electroendosmotic mobility can be positive or negative according to the signs of the charge on the analyte molecule and those of the fixed charges at the tube inner wall.

According to eqns. 2 and 5, the observed migration time t_m is expressed by

$$t_m = lL/(\mu_{ep} + \mu_{eo})V \qquad (6)$$

The electrophoretic mobility is evaluated by the relationship

$$\mu_{ep} = (lL/V)[(1/t_m) - (1/t_0)] \qquad (7)$$

where t_0 is the measured migration time of a neutral marker.

In our case, the ANTS-derivatized saccharides bear a strong negative charge over the whole pH range under investigation. Therefore, we shall examine the three situations that follow. (a) At alkaline pH, the inner wall of silica capillaries is negatively charged so that the direction of the electrophoretic migration of negatively charged analytes is opposite to that of the electroendosmotic flow. In this case, the negatively charged sample components reach the detector at the cathodic end only if the absolute value of the electroendosmotic mobility is higher than that of the electrophoretic mobility. When the convective velocity is lower than the opposite electrophoretic migration velocity, the polarity of the electrodes must be reversed in order to detect the negatively charged sample components. (b) At strongly acidic pH, when the electroendosmotic flow is negligible, arheic or near-arheic separation conditions can be reached without anticonvective gel filling or coating of the tube inner wall. (c) Certain positively charged buffer components and additives, such as TEA, may be absorbed at the capillary inner wall so that it becomes positively charged. In this case, electroendosmotic flow takes place toward the anodic end of the capillary, i.e. in the direction

of the electrophoretic migration of the ANTS-derivatized saccharides.

CZE at high pH

Fig. 4 shows the electropherogram of ANTS-derivatized saccharides obtained in a fused-silica capillary with phosphate buffer, pH 9.0, and cathodic detection. Under alkaline conditions, the convective transport is faster than the electrophoretic migration of the components and the analytes are carried toward the cathode by electroendosmotic flow. The sample components appear at the detector in the order of increasing electrophoretic mobility. The migration times of the lower homologues, which have higher electrophoretic mobilities, are longer than those with a higher degree of polymerization; the lower homologues also exhibit broad and tailing peaks. Under the conditions used in Fig. 4, the ANTS peak does not appear in the electropherogram. ANTS has the highest charge-to-mass ratio among the sample components, and its migration rate in the opposite direction is greater than the electroendosmotic flow velocity. Therefore, it can only be detected anodically by reversing the polarity of the instrument. Fig. 4 also clearly
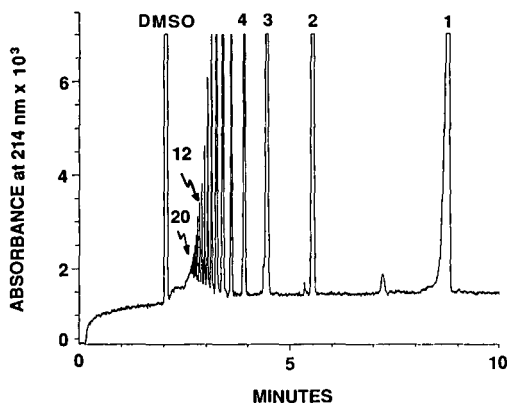
Fig. 4. Electropherogram of ANTS-derivatized malto-oligosaccharides obtained at alkaline pH in the presence of electroendosmotic flow with a fused-silica capillary, 370 mm × 50 μm. Conditions: 50 mM phosphate buffer, pH 9.0; temperature, 25°C; voltage, 17 kV; sample, 11 ng of mixture B derivatized with ANTS introduced at the anodic end. The number of glucose residues in the corresponding linear malto-oligosaccharide analytes, as determined by co-electrophoresis with authentic standards, is indicated for certain peaks.

illustrates that the electroendosmotic flow has an untoward effect on the separation; the migration times are not evenly spaced and the resolution decreases for homologues with increasing degree of polymerization. Therefore, for the resolution of the higher homologues it is desirable to carry out the separation of such samples with capillaries of commensurate dimensions in the absence of electroendosmotic flow.

CZE at low pH

As the magnitude of the electroendosmotic flow in silica capillaries depends on the pH of the medium, the appropriate pH for carrying out the separation under arheic conditions was experimentally determined over a wide pH range by measuring the migration time of neutral markers such as acrylamide, Triton X-100 and mesityl oxide, in 50 mM phosphate solutions as the background electrolyte. Upon plotting the electroendosmotic mobility against the pH (not shown), a kind of sigmoidal titration curve of the surface silanols is obtained with an inflection point around pH 5.3. As discussed in the literature [24,36–38], at low pH the ionization of the surface silanol groups is suppressed, and the electroendosmotic flow approaches zero. Indeed, at strongly acidic pH, the magnitude of the electroendosmotic mobility was often so low, i.e. less than $1.3 \cdot 10^{-9}$ m^{2}s^{-1}V^{-1}, that it did not affect the migration times of the ANTS conju-

gates. In contradistinction, under alkaline conditions the silanol groups are negatively charged and the electroendosmotic flow appears to reach a high plateau value. In such cases, the separation of ANTS derivatives could be carried out at or below pH 3.0 in the absence of appreciable electroendosmotic flow without treatment of the inner wall, use of an anticonvective medium or presence of additives in the background electrolyte. As a result, they could be separated rapidly by using a relatively simple electrophoretic system.

The electropherograms in Fig. 5 illustrate the separation of the ANTS-derivatized malto-oligosaccharides (mixture B) at pH 2.5 when the sample components traverse the tube solely by electrophoretic migration and can be detected anodically. The three sulfonic groups on the ANTS molecule impart strong negative charges and thus relatively high electrophoretic mobilities to the oligosaccharides. The use of phosphate buffer, pH 2.5, was appropriate because of its relatively high buffering power and low conductivity. Wall-adsorption of the highly negatively charged ANTS conjugates was negligible at pH 2.5, and the separation could be performed without such interference.

Since the net charge is the same for all derivatives, their migration velocity decreases with increasing number of glucose residues in the molecule. Indeed, short chain malto-oligosac-
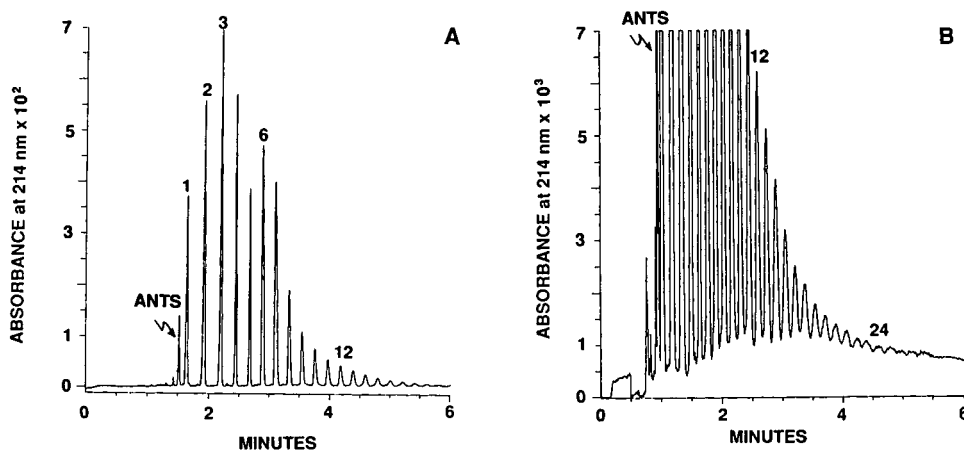
Fig. 5. Electropherograms of ANTS-derivatized malto-oligosaccharides (mixture B), obtained at acidic pH under arheic conditions at two different temperatures with a 270 mm × 50 μm capillary. (A) 50 mM phosphate buffer, pH 2.5; temperature, 25°C; voltage, 15 kV; 22 ng of sample. (B) 30 mM phosphate buffer, pH 2.5; temperature, 50°C; voltage, 17 kV; 31 ng of sample. In both cases, the samples were introduced at the cathodic end.

charides migrate faster than those containing a larger number of glucose residues as depicted in Fig. 5. The components of the mixture are very well resolved and baseline separation of more than 20 components was obtained contrary to the relatively poor separation of the higher homologues in the presence of electroendosmotic flow as shown in Fig. 4.

Comparison of Fig. 5A and B shows that separation of mixture B was improved and speed of analysis was increased by raising the temperature to 50°C. With increasing temperature, the viscosity of the liquid medium in the capillary decreases at a rate of approximately 2%/°C [39] leading to increased electrophoretic mobility. This enhancement of the transport properties accounts for the satisfactory separation of almost 30 homologues in 6 min.

The separation of the derivatized malto-oligosaccharide components of mixture A was also carried out under similar conditions, but a longer capillary tube of smaller inner diameter (670 mm × 20 μm) was needed for optimal resolution as illustrated by a typical electropherogram in Fig. 6. The main components were identified as the homologues of the linear malto-oligosaccharide series containing 4 to 12 glucose residues. The electropherogram shows a large number of small peaks that are attributed to branched isomers of the malto-oligosaccharides. This is further supported by the results of experiments in which mixture A was subjected to matrix-assisted laser desorption time-of-flight
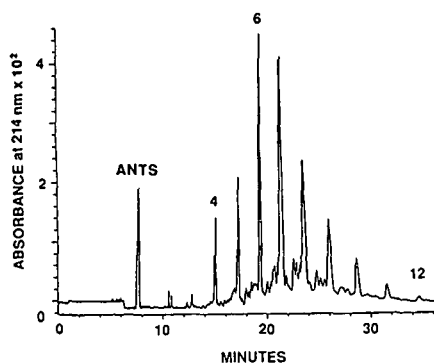
Fig. 6. Electropherogram of ANTS-derivatized malto-oligosaccharides (mixture A), obtained under arheic conditions. Capillary, 670 mm × 20 μm; 200 mM phosphate buffer, pH 2.0; temperature, 25°C; voltage, 30 kV; 100 ng of sample.

mass spectrometry (TOF-MS). The spectrum obtained by this highly sensitive technique revealed no components having molecular masses other than those of the linear malto-oligosaccharide homologues. The results in Fig. 6 confirm that oligosaccharide isomers can be separated with high resolution not only by reversed-phased HPLC [40,41], but also by CZE as ANTS conjugates. By using other derivatives, Nashabeh and El Rassi [18] have found that in the CZE of linear and branched oligosaccharides, the branched ones have longer migration times. Such a migration pattern is likely to apply in our case as well. In further investigations, samples of mixture B and C were used exclusively since they contain the highest number of readily identifiable linear homologues.

Relationship between electrophoretic mobility and molecular mass

The electrophoretic mobility of a molecule in free solution is, according to the simplest models [35,42], proportional to its electrical charge, q, and inversely proportional to the hydrodynamic radius, R. For small spherical ions in infinite conductive medium the electrophoretic mobility is expressed as

$$\mu_{ep} = q/6\pi\eta R \tag{8}$$

where η is the viscosity of the medium. If the model leading to eqn. 8 was applicable to our case involving linear malto-oligosaccharide–ANTS conjugates with molecular mass M_r, then $M_r^{1/3}$ could be substituted for R in eqn. 8, and plots of μ_{ep} against $M_r^{-1/3}$ would be linear. However, our experimental results do not show such linear dependence. Indeed, perusal of the literature on electrophoretic migration [35,42] reveals that the dependence of mobility on the molecular properties is quite complex and there is a lacuna for quantitative relationships between electrophoretic mobility, size and/or structure of large biological molecules despite considerable theoretical efforts over the last 30 years.

However, with the rapid development and growing applications of CZE, demand for such relationships is on the rise. For this reason, we investigated several approaches to correlate the electrophoretic mobilities of the ANTS-derivat-
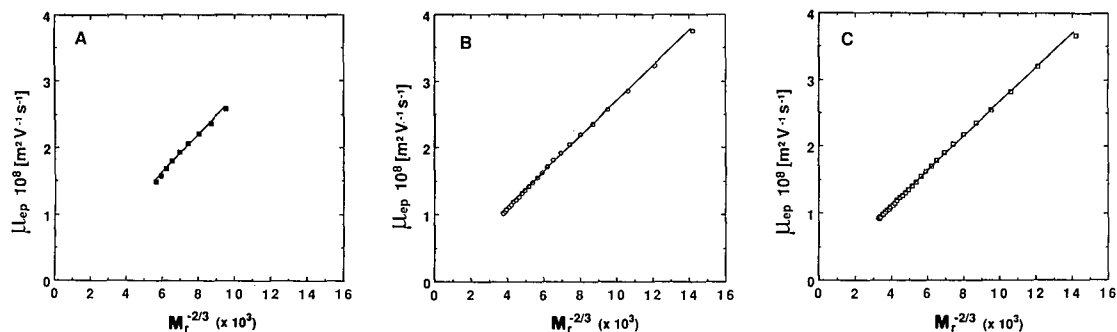
Fig. 7. Plot of the electrophoretic mobility of ANTS-derivatized malto-oligosaccharide homologues against their molecular mass to the −2/3 power. (A), (B) and (C) show data obtained with mixtures A, B and C, respectively. Capillary, 270 mm × 50 μm; 50 mM phosphate buffer, pH 2.5; temperature, 25°C; voltage, 17 kV.

ized malto-oligosaccharides with their molecular size. Such homologues carry the same electric charge and differ only in the number of glucose residues, and therefore they should represent a simpler system than other biopolymers such as peptides and nucleic acids. Peptide mobilities in paper electrophoresis have been successfully correlated to the molecular mass by Offord [43] using the relationship

$$\mu_{ep} = Cq(M_r)^{-2/3} \qquad (9)$$

where C is a constant. Eqn. 9 has some theoretical support for rodlike molecules whose mobility depends on molecular surface area rather than on radius.

We have evaluated the electrophoretic mobilities of ANTS–malto-oligosaccharides under conditions given in Fig. 5A at three different voltage settings (15, 17 and 20 kV). The highly reproducible results showed that the mobilities were independent of the electric field strength in agreement with theoretical prediction, indicating that the system was well behaving and electroendosmotic flow was indeed negligible. The data were plotted against $M_r^{-2/3}$ and the results are illustrated in Fig. 7. As seen, the plots show excellent linearity for all three malto-oligosaccharide mixtures. The mobility–molecular mass relationship represented by eqn. 9 was also successfully used by Wenn [44] for dansyl-glycopeptides with glycan moieties having different numbers of monosaccharide residues. Both series are composed of rather uniform monosaccharide residues, and magnitude and terminal

location of the charges carried by each member of the series are the same. It appears that in such relatively simple cases, eqn. 9 offers useful mobility–molecular size relationships also in the electrophoresis of ANTS derivatives of various oligosaccharides with biological significance. This possibility may further expand the usefulness of ANTS as a fluorescent marker which facilitates high sensitivity detection.

Other linear relationships between the number of glucose residues in the malto-oligosaccharides and their migration time or electrophoretic mobilities have also been found; they are shown in Fig. 8. The migration time depends linearly on the number of glucose units as seen in Fig. 8A.
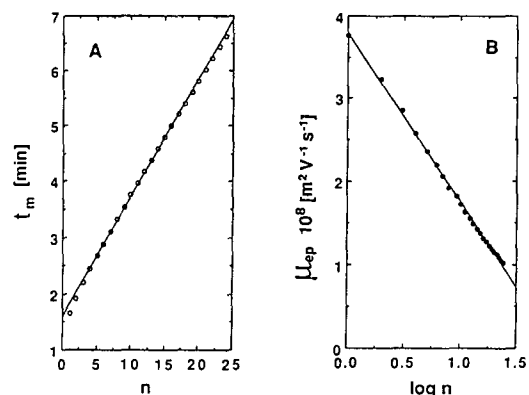
Fig. 8. Plots illustrating the dependence of electrophoretic properties of ANTS-derivatized malto-oligosaccharide homologues on the number of glucose residues. (A) Plot of the electrophoretic migration time against the number of glucose residues. (B) Plot of the electrophoretic mobility against the logarithmic number of glucose units in the molecule. Experimental conditions as in Fig. 5A.

Such linear relationships between t_m and the number of residues have been observed with oligomers in gel electrophoresis, *i.e.* under arheic conditions, in the following two cases: firstly, when the series of molecules under investigation have the same electrical charge and differ only in the number of neutral residues as with malto-oligosaccharide–ANTS conjugates, and secondly, when both the charge and molecular size increase in equal increments as is the case with oligonucleotides. Another empirical quasi-linear relationship is shown in Fig. 8B between the electrophoretic mobility of linear malto-oligosaccharide–ANTS conjugates and the logarithmic number of glucose residues. This correlation has been found convenient in this study among others for identification of the peaks in the electropherograms. The use of homologues offers a convenient means of testing the electrophoretic system in light of these linear relationships. However, further investigations are required to elucidate their basis at the molecular level.

The use of the linear relationships is further illustrated in Fig. 9 by plots of different sets of electrophoretic mobilities evaluated under diverse conditions. In one case, the electrophoretic mobility of the derivatized malto-oligosaccharide homologues was obtained directly from arheic migration times at pH 2.5 by eqn. 2. In the other, the electrophoretic mobility was calculated according to eqn. 5 from data measured in phosphate buffer at pH 9.4 with correction for the effect of the electroendosmotic flow on the overall migration rates. In the third case, the electrophoretic mobilities were evaluated from data measured at pH 9.4 in 10 mM phosphate buffers containing 10 mM borate. Measuring in the absence of electroendosmotic flow at pH 2.5 and calculating from the two sets of data obtained in the presence of strong electroendosmotic flow at pH 9.4, the electrophoretic mobilities show excellent linear correlation. The results are not unexpected since the three sulfonic acid functions are fully dissociated at either pH. Nevertheless, this finding also suggests that no significant changes occurred in the viscosity of the electrophoretic medium or in the relevant hydrodynamic size parameter of the sample molecules upon changing from pH 2.5 to 9.4. The higher electrophoretic mobility of the malto-oligosaccharides when borate is added to the buffer solution is readily explained by the formation of negatively charged complexes between borate and certain sugars at sufficiently high pH [38]. Such complexation augments the negative charge on the analytes and thus accounts for the relatively high electrophoretic mobility. The slope of the straight line for the mobilities measured in the presence of borate is steeper than for those obtained in its absence as seen in Fig. 9. Evidently, with increasing size of the carbohydrate moiety, the negative charge on the analyte molecules also increases due to borate complexation. The effect of the incremental charge on the electrophoretic mobility is greater than the opposing influence of the higher molecular mass of the borate complexes.

Effects of the addition of TEA to the background electrolyte

The electropherograms in Figs. 5A and 5B demonstrate that ANTS-derivatized malto-oligosaccharides can be efficiently and rapidly separated using untreated silica capillaries in free solution at low pH with a relatively simple electrophoretic system. Nonetheless, it is important to emphasize that when uncoated fused-silica capillaries are used, the reproducibility of the results usually depends on the uniformity and

Fig. 9. Correlation between electrophoretic mobilities directly observed at pH 2.5 and calculated from data measured at pH 9.4 with malto-oligosaccharide–ANTS conjugates in the presence (▲) and absence (△) of 10 mM borate buffer. Capillary, 370 mm × 50 μm; 50 mM phosphate buffer; temperature 25°C; voltage, 17 kV.

constancy of surface properties. In practice, the inner surface of silica capillaries varies even within the same batch of material; this, together with differences in the history of the capillary, give rise to variations in the magnitude of the electroendosmotic flow particularly in the pH range from 4.0–10. It is therefore essential to establish a rigorous washing protocol that allows one to equalize the different surface properties of importance and thus facilitate reproducible measurements as recommended by Schwer and Kenndler [36]. Considering the possibilities of a significant interaction between the phosphate ions and the silanol groups at the tube inner wall [45], we maintained the phosphate level constant in the solutions used in the washing procedure. We found that the respective use of 1 M trisodium phosphate and 1 M phosphoric acid solutions in the alkaline and acidic washing steps palpably enhanced the reproducibility of measurements.

In order to improve further the reproducibility and efficiency of the analytical procedure, TEA (widely employed in reversed-phase chromatography as a masking agent for the silanol groups at the stationary phase surface [46]), was added to the background electrolyte. Indeed, the use of the above washing protocol and of TEA in the sodium phosphate buffer resulted in satisfactory reproducibility; the relative standard deviation in the migration times of the ANTS conjugates of the malto-oligosaccharides in mixture B from 20 consecutive injections into two different capillaries was better than one percent. In general, higher efficiency also manifested itself in sharp and symmetrical peaks. Moreover, triethylammonium ions have relatively low mobility and therefore allow the employment of high voltage in order to bring about high-speed separations without the untoward effects of high current.

Most striking was the observation that varying the relative concentration of triethylammonium and sodium ions in phosphate buffer at pH 2.5 we could modulate the zeta potential at the inner surface of the capillary in a reproducible fashion. Typical results are shown in Fig. 10. The value for the zeta potential was calculated from the observed electroendosmotic flow velocity according to eqn. 4. Increasing the TEA concentration in the phosphate buffer as the percentage of the
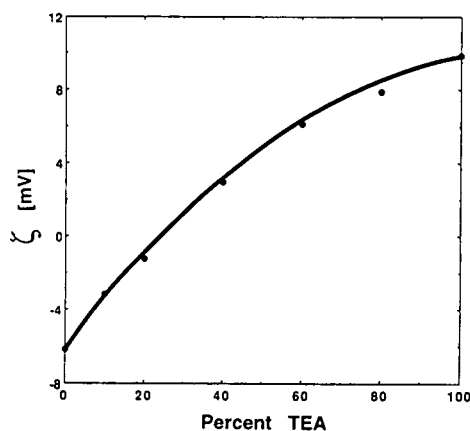
Fig. 10. Zeta potential titration curve of a 270 mm × 50 μm fused-silica capillary with triethylamine in 50 mM sodium phosphate buffer, pH 2.5, at 25°C. The abscissa is the triethylammonium ion (TEA$^+$) concentration as the percentage of the total cation (TEA$^+$ and Na$^+$) concentration. Electroendosmotic velocity was measured with phenol and acrylamide as indicators.

total cation concentration strengthens the interaction of the amine with the inner surface of the capillary and brings about a progressive decrease in the negative charge at the wall. In the case illustrated, when the fraction of TEA reaches about 25% of the total cationic concentration, the "point of zero zeta potential" is reached, and the electroendosmotic flow becomes negligibly small. Difficulties beset accurate determination of the point of zero charge because of the problems associated with the measurement of very low electroendosmotic flows. As inconsistencies in the inner surface of different capillaries were observed, different concentrations of TEA might be required in order to reach the zero point. Nevertheless, establishing a narrow range of TEA concentration that permits operation in the absence of appreciable electroendosmotic flow, i.e. under arheic conditions, is possible. This finding does not contradict the earlier observations that arheic conditions were also obtained without addition of TEA to the phosphate buffer at pH 2.5. It should be noted that with certain capillary tubes of different provenance and/or history arheic conditions were not always reached even by using phosphate buffer, pH 2.5, alone, and the reproducibility of those results was often not satisfactory. In contrast, the proper use of TEA additive with phosphate

buffer of pH 2.5–3.0 not only yields high speed and efficiency of the separation but also allows us to modulate the properties of the capillary inner wall to obtain a desired value of the electroendosmotic flow. Fig. 11A illustrates the separation of malto-oligosaccharide mixture C in free solution using sodium triethylammonium phosphate buffer, pH 2.5, under arheic conditions. Comparison of the results in Fig. 11A to those in Fig. 5A shows a significant increase in the speed of analysis without loss of separating efficiency for the higher members of the homologous series.

The effect of TEA is attributed to its interaction with the capillary inner wall rather than an interaction between the negatively charged ANTS derivatives and the triethylammonium ions. This is supported by the observation that at various TEA concentrations up to 36 mM in the phosphate buffer, the electrophoretic mobilities of the homologues were essentially constant; only a slight change in the electrophoretic mobilities of the lowest homologues was noted. On the other hand, in preliminary experiments with various alkyl diamines and triamines as buffer additives, a dramatic increase in the electrophoretic migration times was observed. This effect is likely to be associated with a strong interaction between such amines and the ANTS derivatives which alters the effective charge on the analyte molecules.

The zeta potential titration curve in Fig. 10 also shows that increasing the concentration of TEA in the buffer above approximately 25% of the total cationic concentration progressively imparts positive charge to the inner wall of the capillary in agreement with recent observations by others [47]. As a consequence, electroendosmotic flow toward the anodic end of the capillary is generated when the voltage is applied. Since the electrophoretic migration of the strongly negatively charged ANTS derivatives takes place in the same direction, the electroendosmotic flow at a sufficiently high TEA concentration has the beneficial effect of enhancing the speed of separation. Under such conditions, when both electroendosmotic flow and electrophoretic migration occur toward the detector end, the separation of more than 20 homologues can be carried out in less than 3 min, as shown in Fig. 11B. This approach permits a dramatic reduction of the analysis time for less complex samples; an example of ultrafast separations is illustrated in Fig. 12 where three short-chain malto-oligosaccharides are resolved in less than 10 s.

Electrophoretic behavior of derivatized saccharides in free solution and in polyacrylamide gels

As exemplified by the results in Figs. 5A, 11A, 11B, and 13, the derivatization of malto-
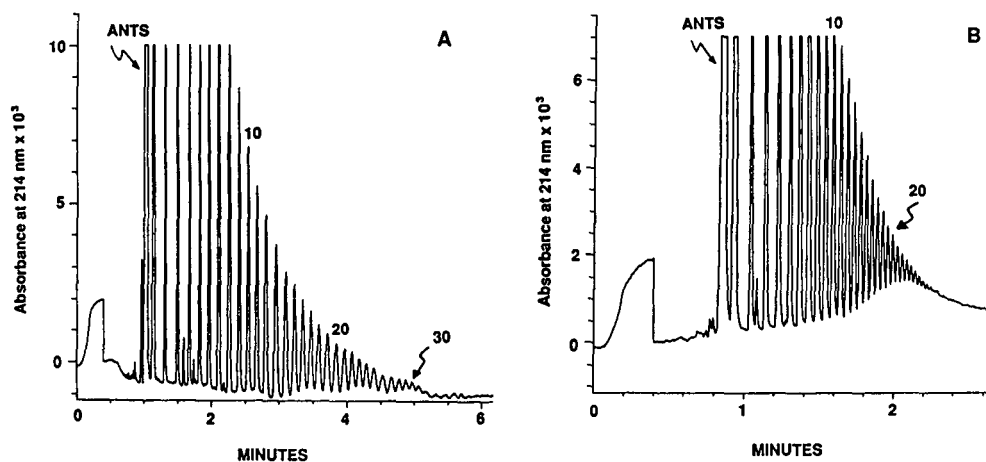
Fig. 11. Electropherogram of ANTS-derivatized malto-oligosaccharides (mixture C) obtained (A) with 50 mM sodium/triethylammonium phosphate buffer, pH 2.5, containing 10.8 mM TEA, (B) with 50 mM triethylammonium phosphate, pH 2.5. In both cases: capillary, 270 mm × 50 μm; temperature, 25°C; voltage, 22 kV; 80 ng of sample.
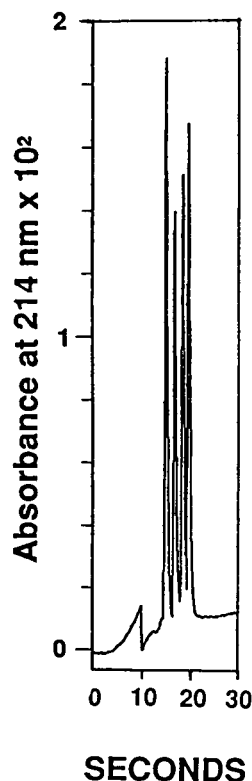
Fig. 12. Rapid separation of ANTS-derivatized malto-oligosaccharides. Conditions as in Fig. 11B, except for temperature of 50°C. Sample components in order of appearance: ANTS, ANTS-derivatized maltose, ANTS-derivatized maltotetraose, ANTS-derivatized maltohexaose.
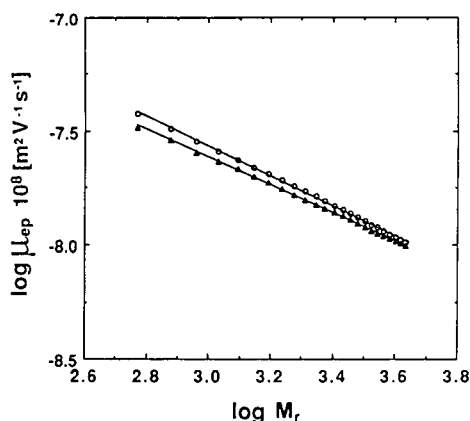
Fig. 13. Double logarithmic plots of the electrophoretic mobility of ANTS-derivatized malto-oligosaccharides against their molecular mass. Data were measured with 50 mM sodium phosphate buffer, pH 2.5 (O), and 50 mM tri-ethylammonium phosphate buffer, pH 2.5 (▲). Capillary, 270 mm × 50 μm; temperature, 25°C; voltage, 17 kV.

oligosaccharides with ANTS allows arheic separation of a very wide range of such homologues with excellent resolution in untreated fused-silica capillaries. According to the literature [25–28], however, the use of polyacrylamide gel-filled capillaries is essential for the CZE of complex mixtures of large oligosaccharides with fluorescent markers other than ANTS. This prompted us to investigate whether a sieving effect that may be associated with the use of a highly concentrated cross-linked polyacrylamide gel in the capillary or in the slab configuration would indeed provide higher selectivity for the separation.

We examined three different systems: (a) ANTS-derivatized saccharides, separated in polyacrylamide gel slab by Jackson [29], (b) ANTS-derivatized malto-oligosaccharides, separated in free solution at pH 2.5 in the present study and (c) 3-(4-carboxybenzoyl)-2-quinoline-carboxaldehyde (CBQCA)-derivatized malto-oligosaccharides, separated in capillaries filled with highly concentrated polyacrylamide gel by Liu et al. [25]. The selectivity of each of the three systems was evaluated by plotting the ratio of the electrophoretic mobilities of two neighboring homologues, μ_n/μ_{n+1}, against the number of glucose residues. As seen in Fig. 14A, the presence of the gel does not enhance the relative electrophoretic mobilities of oligosaccharide derivatives containing at least up to 20 glucose residues and the difference in the labels used in systems (b) and (c) also has no major effect on the selectivity. For comparison, the dependence of the relative electrophoretic mobility on the reciprocal of the corresponding molecular mass ratio to the 2/3 power is also shown in Fig. 14A. In agreement with the results illustrated in Fig. 7A and B, the change in the relative electrophoretic mobility of the malto-oligosaccharide conjugates with the molecular size over a wide molecular mass range is well represented by this relationship. Indeed, plots of log μ_{ep} against log M_r were linear with slopes of -0.63, -0.60, and -0.56 according to the data obtained in free solution, in gel-filled capillaries and in slab gel, respectively.

The electrophoretic mobilities of ANTS-derivatized malto-oligosaccharides in free solution
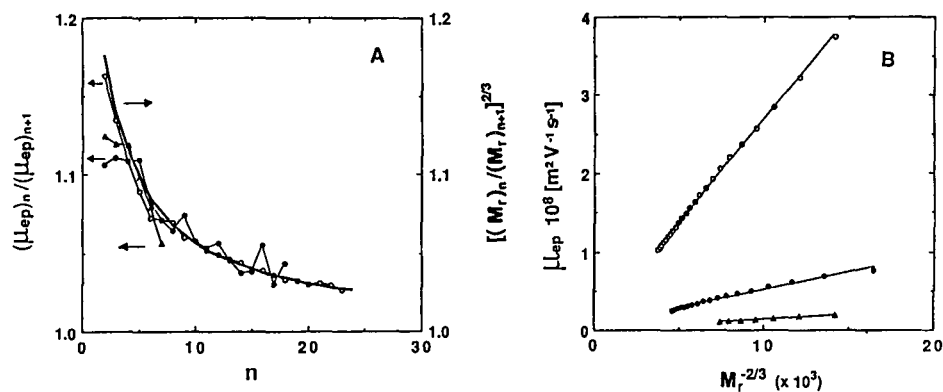
Fig. 14. Illustration of the electrophoretic behavior of malto-oligosaccharide conjugates in three different systems: ANTS derivatives in free solution CZE under arheic conditions (O) (see Fig. 5A), ANTS derivatives in slab gel electrophoresis (▲) [25], and CBQCA derivatives in polyacrylamide gel filled capillaries (●) [30]. The formula mass of the CBQCA–glucose conjugate (474) was used in the calculation of the molecular masses of the homologues. (A) Plots of the relative electrophoretic mobility of the conjugated oligosaccharides on the number of glucose residues. The solid line represents the plot of the molecular mass ratio to the two third power of the neighboring homologues as a function of the number of glucose residues. (B) Dependence of the electrophoretic mobility on the molecular mass to the $-2/3$ power.

at low pH can be compared to the electrophoretic mobilities of CBQCA-derivatized malto-oligosaccharides in gel-filled capillaries by the plots of μ_{ep} against $M_r^{-2/3}$ in Fig. 14B. The slopes of the two pertinent straight lines in Fig. 14B suggest that the electrophoretic mobilities of ANTS derivatives are higher by a factor of about 6 than those of the CBQCA derivatives. Much of this difference can be attributed to differences in the charges carried by the two label-moieties: ANTS and CBQCA. Whereas ANTS-derivatized saccharides have three negative charges, the dissociation of the carboxylic group in CBQCA derivatives results in only a single negative charge. However, the negative charge is believed to increase with the molecular size of the oligosaccharide moiety due to the formation of borate complexes under the operating conditions which results in higher electrophoretic mobilities [25]. From the comparison of the slopes, we can infer that the electrophoretic migration rates of derivatized malto-oligosaccharides ($n < 40$) are at least two times lower in the gel present in the capillary than in free solution. Fig. 14B also shows a plot of the electrophoretic mobilities of ANTS-derivatized oligosaccharides in polyacrylamide gel slab as estimated from the data by Jackson [29] against $M_r^{-2/3}$. This allows a direct

comparison, though limited to the first seven components of the homologous series, of the electrophoretic mobilities of ANTS derivatives in free solution and in the polyacrylamide gel slab. From the data shown in Fig. 14B, the mobility of the ANTS derivatives appears to be lower by a factor of 22 in the cross-linked gel than in free solution. The relatively high electrophoretic mobilities of the derivatized oligosaccharides under the conditions described in this study are mainly responsible for the high speed of analysis without the loss of resolution.

ACKNOWLEDGEMENTS

and Professor P.G. Righetti for their support and helpful discussions.

REFERENCES

1 N. Sharon, *Complex Carbohydrates: Their Chemistry, Biosynthesis and Functions*, Addison-Wesley, Reading, MA, 1975, pp. 33–47.
2 R. Montgomery, in W. Pigman and D. Horton (Editors), *The Carbohydrates*, Vol. 26, Academic Press, New York, 2nd ed., 1970, pp. 677–696.
3 N. Sharon, *Trends Biochem. Sci.*, 9 (1984) 198.
4 S.C. Churms, *J. Chromatogr.*, 500 (1990) 555.
5 M.F. Chaplin and J.F. Kennedy (Editors), *Carbohydrate Analysis: A Practical Approach*, IRL Press, Oxford, 1986, pp. 43–51.
6 S. Hughes and D.C. Johnson, *Anal. Chim. Acta*, 132 (1981) 11.
7 S. Hughes and D.C. Johnson, *J. Agric. Food Chem.*, 30 (1982) 712.
8 L.J. Basa and M.W. Spellman, *J. Chromatogr.*, 499 (1990) 205.
9 A.B. Foster, *Adv. Carbohydr. Chem.*, 12 (1957) 81.
10 O. Prem Das and E.J. Henderson, *Anal. Biochem.*, 158 (1986) 390.
11 S. Weitzman, V. Scott and K. Keegstra, *Anal. Biochem.*, 97 (1979) 438.
12 A.S. Cohen and B.L. Karger, *J. Chromatogr.*, 397 (1987) 409.
13 A.S. Cohen, D. Najarian, J.A. Smith and B.L. Karger, *J. Chromatogr.*, 458 (1988) 323.
14 A.S. Cohen, S. Terabe, J.A. Smith and B.L. Karger, *Anal. Chem.*, 59 (1987) 1021.
15 W.G. Kuhr and C.A. Monnig, *Anal. Chem.*, 64 (1992) 389R–407R.
16 K.B. Lee, A. Al-Hakim, D. Loganathan and R.J. Linhardt, *Carbohydr. Res.*, 214 (1991) 155.
17 P.J. Oefner, A.E. Vorndran, E. Grill, C. Huber and G.K. Bonn, *Chromotagraphia*, 23 (1992) 308.
18 W. Nashabeh and Z. El Rassi, *J. Chromatogr.*, 600 (1992) 279.
19 P.M. Rudd, I.G. Scragg, E. Coghill and R.A. Dwek, *Glycocong. J.*, 8 (1992) 86.
20 M. Taverne, A. Rainet, D. Biou, M. Sclüter, R. Werner and D. Ferrier, *Electrophoresis*, 13 (1992) 358.
21 N. Tomiya, J. Awaya, M. Kurono, S. Endo, Y. Arata and N. Takahashi, *Anal. Biochem.*, 171 (1988) 73.
22 S. Honda, A. Makino, S. Suzuki, and K. Kakeki, *Anal. Biochem.*, 191 (1990) 228.
23 S. Honda, S. Iwase, A. Makino and S. Fujiwara, *Anal. Biochem.*, 176 (1990) 72.

24 W. Nashabeh and Z. El Rassi, *J. Chromatogr.*, 514 (1990) 57.
25 J. Liu, O. Shirota and M.N. Novotny, *J. Chromatogr.*, 559 (1991) 223.
26 J. Liu, O. Shirota, D. Wiesler and M.N. Novotny, *Proc. Natl. Acad. Sci. U.S.A.*, 88 (1991) 2302.
27 J. Liu, Y.Z. Hsieh, D. Wiesler and M.N. Novotny, *Anal. Chem.*, 63 (1991) 408.
28 J. Liu, O. Shirota and M.V. Novotny, *Anal. Chem.*, 64 (1992) 973.
29 P. Jackson, *Biochem. J.*, 270 (1990) 705.
30 P. Jackson and G.R. Williams, *Electrophoresis*, 12 (1991) 94.
31 R.J. Stack and M.T. Sullivan, *Glycobiology*, 2 (1992) 85.
32 R.S. Rush and B.L. Karger, *Sample injection with P/ACE System 200: Importance of Temperature Control with Respect to Quantitation*; Technical Bulletin TIBC-104, Beckman Instruments, Spinco Division, Palo Alto, CA, 1990.
33 F.E.P. Mikkers, F.M. Everaerts and Th.P.E.M. Verheggen, *J. Chromatogr.*, 169 (1979) 11.
34 J.W. Jorgenson and K.D. Lukacs, *J.Chromatogr.*, 218 (1981) 209.
35 P.C. Hiemenz, *Principles of Colloidal and Surface Chemistry*, Marcel Dekker, New York, 2nd ed., 1986, p. 751.
36 C. Schwer and E. Kenndler, *Anal. Chem.*, 63 (1991) 1801.
37 C. Schwer and E. Kenndler, *Chromatographia*, 30 (1990) 546.
38 S. Hoffstetter-Kuhn, A. Paulus, E. Gassmann and H.M. Widmer, *Anal. Chem.*, 63 (1991) 1541.
39 J. Harbaugh, M. Collette and H.E. Schwartz, *Determination of Injection Volumes with P/ACE System 200*; Technical Bulletin TIBC-103, Beckman Instruments, Spinco Division, Palo Alto, CA, 1990.
40 V.M.B. Cabalda, J.F. Kennedy and K. Jumel, in R.B. Friedman (Editor), *Biotechnology of Amylodextrin Oligosaccharides* (*ACS Symposium series*, No. 458), American Chemical Society, Washington, DC, 1991, pp 140–170.
41 R.N. Ammeraal, G.A. Delgado, F.L. Tenbarge and R.B. Friedman, *Carbohydr. Res.*, 215 (1991) 179.
42 H. Mueller, in E.J. Cohn and J.T. Edsall (Editors), *Proteins, Amino Acids and Peptides*, Reinhold, New York, 1943, Ch. 25, pp. 623–643.
43 R.E. Offord, *Nature*, 211 (1966) 591.
44 R.V. Wenn, *Biochem. J.*, 145 (1975) 281.
45 B.M. Mitsyuk, *Russ. J. Inorg. Chem.*, 17 (1972) 471.
46 K.E. Bij, Cs. Horváth, W.R. Melander and A. Nahum, *J. Chromatogr.*, 203 (1981) 65.
47 W.R. Jones, P. Jandik and M. Merion, *U.S. Pat.*, 5 104 506 (1992).

Separation of isoforms of *Serratia marcescens* nuclease by capillary electrophoresis

Jytte Pedersen and Mikael Pedersen

Department of Biotechnology, Building 223, Technical University of Denmark, DK-2800 Lyngby (Denmark)

Henrik Søeberg

Department of Chemical Engineering, Building 229, Technical University of Denmark, DK-2800 Lyngby (Denmark)

Kirsten Biedermann*

Department of Biotechnology, Building 223, Technical Univesity of Denmark, DK-2800 Lyngby (Denmark)

ABSTRACT

Three *S. marcescens* nuclease isoforms differing mainly in charge (native nuclease with p*I* 6.8 and two minor isoforms with p*I* 7.3 and 7.4) were separated using several different modes of high-performance capillary electrophoresis. Separation of the isoforms by free solution capillary electrophoresis was unsatisfactory. Separation by micellar electrokinetic capillary chromatography was therefore investigated in detail and the method optimized with respect to pH and sodium dodecyl sulphate concentration; in addition, the effect of adding various substances to control dispersion and avoid analyte adsorption at the capillary wall was examined. Under optimal conditions there was almost complete baseline separation of the two isoforms with basic p*I* whereas there was only partial separation of the native form and the isoform with p*I* 7.4. With capillary isoelectric focusing there was complete baseline separation of the native nuclease and the other two isoforms.

INTRODUCTION

The use of high-performance capillary electrophoresis (HPCE) for protein analysis in biotechnological production is gaining increasing interest. Since HPCE is rapid and separates molecules by virtue of differences in their charge and hydrodynamic properties, it provides an advantageous alternative to existing analytical techniques such as gel electrophoresis, which is rather time consuming, and reversed-phase HPLC, which separates according to solute hydrophobicity and is therefore often unsuitable for separating globular proteins. Although interest in HPCE particularly concerns *in process* analysis, the possibilities for applying HPCE to biotechnological processes are largely unexplored.

Serratia marcescens nuclease is an active globular molecule with a p*I* of 6.8 [1], and a molecular mass of 26 705.8 as calculated from the amino acid sequence [2]. The enzyme is stable within the pH range 6–8 for at least 1/2 h at temperatures from 2 to 37°C [3], but is thermally degradable above 40°C [4]. Two closely related isoforms of the enzyme having p*I* 7.3 and 7.4 have recently been isolated from *S.*

---

* Corresponding author.

marcescens fermentation broth; both are N-terminal split variants of the native enzyme encoded from the nucleotide sequence of the *nuc* gene. The p*I* 7.4 isoform lacks Asp–Thr–Leu while the p*I* 7.3 isoform only lacks Asp [1].

Hitherto isoelectric focusing has been used to detect these isoforms in the fermentation broth and during isolation and purification of the enzyme. In the present study we evaluated the efficacy of the following modes of HPCE in separating these closely related and enzymatically active nuclease isoforms: free solution capillary electrophoresis (FSCE), micellar electrokinetic capillary chromatography (MECC) using the surfactant sodium dodecyl sulphate (SDS), and capillary isoelectric focusing (cIEF) using ampholytes. MECC has previously been used mainly for analyzing small organic molecules, especially small neutral organic molecules that are difficult to separate by FSCE [5,6]. In this study the separation of macromolecules such as nuclease isoforms by MECC was optimized with respect to pH, buffer type, SDS concentration, and by manipulation of the micellar buffer by the addition of methanol, hydroxypropylmethylcellulose, and mono- and divalent ions. A recent modification of MECC in which microemulsions are used as the medium [7,8] was also examined. The results obtained using MECC were compared to those obtained using FSCE and cIEF.

EXPERIMENTAL

Preparation of nuclease

Nuclease was produced and purified from two *S. marcescens* B10M1 fermentations as previously described [9,10]. The isoforms were partially separated by DEAE-cellulose chromatography, elution being undertaken using a narrow pH gradient (pH 8.25–7.2). The first peak to elute contained in one case a major basic isoform with p*I* 7.3, and a minor basic isoform with p*I* 7.4, and in the other case only the isoform with p*I* 7.4. The main peak, which eluted last, contained the native nuclease with p*I* 6.8. Fractions collected from the two peaks from each of the

fermentations were dialysed against water and lyophilized prior to HPCE.

Preparation of reagents

All reagents were of analytical grade. The pH of the Tris buffer was adjusted using H_2SO_4 and that of citrate buffer using citric acid. SDS solutions were prepared by adding SDS (Pharmacia Biotechnology, Allerød, Denmark) to the buffers, usually at a concentration of 25 m*M*. Hydroxypropylmethylcellulose (HMC) (Merck, Darmstadt, Germany) was solubilized in 40 m*M* Tris buffer, pH 7.5, while stirring overnight and then filtered through a 45-μm membrane filter (Millipore, Guyancourt, France). HMC buffers containing 25 m*M* SDS were prepared with HMC concentrations from 0.05 to 0.25% (w/v).

Three microemulsions were investigated, their composition being as described by Watarai [8]: (A) water–SDS–1-butanol–heptane (89.3:3.3:6.6:0.8, v/w/w/w), (B) water–SDS–1-butanol–heptane (76.0:6.3:12.7:5.0, v/w/w/w); (C) water–SDS–1-butanol–heptane (65.1:9.3:18.6:7.0, v/w/w/w) (the water was 40 m*M* Tris–H_2SO_4, pH 7.5). These microemulsions were chosen according to a ternary phase diagram [11] of the system water–SDS–1-butanol–heptane such that each gave a single-phase microemulsion of oil in water. In addition, the composition of microemulsion A was modified with respect to SDS and water, that of A_1 being water–SDS (91.9:0.7) and that of A_2 being water–SDS (91.1:1.5).

The reagents used for cIEF were prepared according to the method described by the HPCE equipment manufacturer [12]. The ampholyte used was Servalyt 3–10 (Serva, Heidelberg, Germany).

High-performance capillary electrophoresis (HPCE)

HPCE was performed using an Applied Biosystems Model 270 A system (Applied Biosystems, Foster City, CA, USA) comprising an untreated capillary tube (52 cm × 50 μm I.D. × 300 μm O.D.), a high-voltage power supply (0–30 kV), an autosampler with hydrodynamic in-

jection, and a variable-wavelength UV–Vis absorbance detector located on the capillary tube, the whole system being coupled to an LKB 2220 integrator (LKB, Bromma, Sweden).

The polarity of the internal power supply was set such that the components of the sample would migrate towards the cathode, and hence the detector. At the start of each analysis the electrode reservoirs at the detector and inlet ends of the capillary were filled with running buffer and the capillary then flushed (by vacuum displacement at 67.6 kPa) with 0.1 M NaOH for 2 min followed by 0.1 M HCl for 2 min. Running buffer was then introduced for 3 min to replace the flush fluid and a small sample zone introduced for 1.0 s with 16.9 kPa vacuum. The two ends of the capillary were then immersed in the buffer reservoirs and a high voltage (typically 3–20 kV) applied along the capillary. Electropherograms were made by measuring absorbance at 214 nm, using a range of 0.02 absorbance units full scale and a rise time of 1.0 s.

Prior to HPCE the nuclease samples were solubilized in a solution of electrophoresis buffer and water (1:3, v/v) so as to obtain stacking conditions during electrophoresis. The total protein concentration in the samples was approximately 0.5 $\mu g/\mu l$ buffer.

It was attempted to separate the three nuclease isoforms by means of the following modes of HPCE: FSCE, MECC and cIEF.

Separation by free solution capillary electrophoresis

This is the most simple and common mode of HPCE, separation being based solely on differences in the electrophoretic mobility of the analytes. Since pH of the running buffer plays a crucial role in determining the selectivity of separation, different types of buffers [Tris, tricine, phosphate, citrate and 2-(N-cyclohexylamino)ethansulfonic acid (CHES)] with different pH and molarity were tested with respect to separation of the three nuclease isoforms. The electric field strength and the ionic strength of the buffer were chosen such that Joule heating would not cause thermal degradation of the nuclease [4].

Separation by micellar electrokinetic capillary chromatography

As separation by FSCE was unsatisfactory (see Results), an extensive investigation was undertaken of separation by MECC, a more sophisticated mode in which analyte separation is based on a combination of differences in electrophoretic mobility and degree of partitioning with negatively charged SDS micelles. The method was optimized with respect to pH, buffer type, SDS concentration, micelle composition, etc.

Capillary isoelectric focusing

Separation was carried out using the method developed by the HPCE equipment manufacturer [12]. Since effective focusing is prevented by the electroosmotic flow that characteristicly takes place when using uncoated fused-silica capillaries, focusing was performed using a coated capillary [72 cm (length to the detector 50 cm) × 50 μm I.D. × 375 μm O.D.]. After flushing as described earlier, the capillary was loaded (8.3 min) with an electrolyte solution comprised of 20 mM NaOH containing 0.4% methylcellulose (Sigma, St. Louis, MO, USA) that had been filtered through a 0.2-μm membrane filter and centrifuged prior to use. The capillary was then loaded with the same buffer containing 0.5% Servalyt 3–10 (Serva) to a distance about 40 cm from the inlet end. The wavelength was adjusted to 280 nm since ampholytes strongly absorb UV light between 200 and 250 nm. The sample was injected using 16.9 kPa vacuum for 17.2 s and then more ampholyte solution injected for 6 s such that the front of the first ampholyte solution was near the detector window. Focusing was undertaken using 100 mM H$_3$PO$_4$ containing 0.4% methylcellulose as the anode electrolyte and applying a voltage of 30 kV until the current had stabilized at 0–1 μA (5.8 min).

Detection/mobilization was performed by turning on the 16.9 kPa vacuum and high voltage (30 kV) for 28.8 min with the anode end of the capillary still immersed in the anode solution (100 mM H$_3$PO$_4$) and monitoring the detector signal (indicating protein peaks) with the integrator. The relative mobility of the separated components is linearly related to their pI [12].
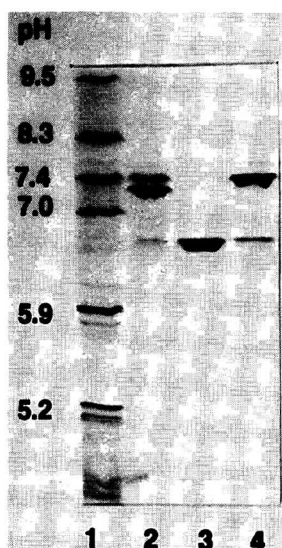
Fig. 1. Conventional isoelectric focusing of nuclease isoforms. Nuclease isolated from *S. marcescens* B10M1 was purified on a phosphocellulose column and the native nuclease, having p*I* 6.8, separated from the more basic isoforms by DEAE-cellulose chromatography. Lanes: 1 = p*I* marker; 2 = sample in which the p*I* 7.3 isoform is the major component and the p*I* 7.4 isoform the minor component; 3 = native nuclease with p*I* 6.8; 4 = sample in which the isoform p*I* 7.4 is the major component.

Conventional isoelectric focusing (IEF)

IEF was performed horizontally in 0.3 mm thick 1% IEF agarose (Pharmacia) on a LKB Multiphor 2117 (Pharmacia LKB Biotechnology) according to Biedermann and Nielsen [13]. Samples of the two peaks eluted by DEAE-cellulose chromatography were applied to the gel in a concentration of 1 μg/μl (10 μl) and the focused proteins stained with Coomassie Brilliant Blue G-250.

RESULTS AND DISCUSSION

Conventional isoelectric focusing in an agarose gel (Fig. 1) revealed that one sample of the purified nuclease contained the native nuclease with p*I* 6.8 (lane 2) and that two contained the isoforms with p*I* 7.3 and 7.4, albeit in different amounts (lane 1 and 3). These three samples were analyzed by HPCE, both separately and as a mixture of the samples shown in lanes 2 and 3. The difference in the primary structure of the isoforms is illustrated in Fig. 2.
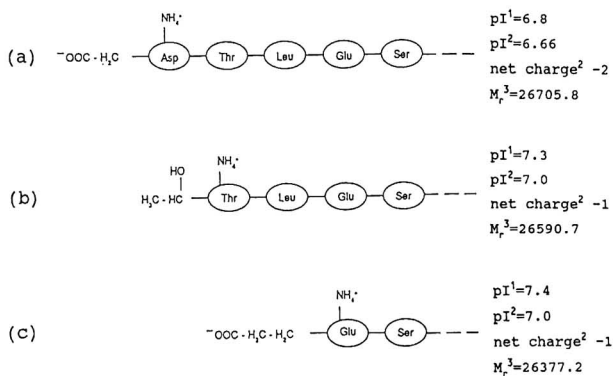
Fig. 2. Physico-chemical properties of the N-terminal amino acid residues of the three nuclease isoforms. (a) Native nuclease with p*I* 6.8 containing 245 amino acids residues; (b) isoform with p*I* 7.3 lacking the negatively charged amino acid aspartic acid; (c) isoform with p*I* 7.4 lacking both the aspartic acid and the two uncharged amino acids residues, threonine and leucine. [1]Isoelectric point determined by analytical IEF; [2]isoelectric point calculated from the amino acid sequence using the GCG-program (University of Wisconsin, USA); [3]molecular mass calculated from the amino acid sequence average value based on the natural abundance of isotopes [2].

Separation by FSCE

The separation efficiency obtained with Tris buffer at pH 7.5, 8.0 and 8.5 is shown in the electropherogram (Fig. 3). The best resolution was obtained at pH 8.0; however, isoform separation was poor, the sample resolving into only two partially separated peaks with the basic isoforms (p*I* 7.3 and 7.4) eluting together in the first peak. The elution order indicated on the figure was determined by analyzing each of the isoforms separately. Thus separation of the nuclease isoforms, all of which have a p*I* close to neutrality, was unsatisfactory with this mode of HPCE.

Separation by MECC

The effect of pH on isoform separation in 40 m*M* Tris buffer containing 25 m*M* SDS is illustrated in Fig. 4a–c. Separation was better than that obtained with FSCE, particularly at pH 7.1, which is between the p*I* of the isoforms, and at pH 7.5, which is just above the p*I* of the most basic of the isoforms. Similar separation was obtained using a citrate buffer at pH 7.1 instead of Tris–H$_2$SO$_4$ (Fig. 4d), and when using a tricine buffer.

With MECC the order of migration is the reverse of that seen with FSCE (Fig. 5). Because of electrostatic repulsion from the more slowly migrating micelle phase, native nuclease with p*I*

Fig. 4. Separation of nuclease isoforms by micellar electrokinetic capillary chromatography at different pH. The sample containing the three isoforms was introduced by applying a 16.9 kPa vacuum for 1.0 s at the detector end. 10 kV was applied during electrophoresis. (a–c) 40 m*M* Tris–H$_2$SO$_4$ electrophoresis buffer containing 25 m*M* SDS. (a) pH 7.1; (b) pH 7.5; (c) pH 8.5; (d) 40 m*M* citrate buffer, pH 7.1.

6.8, which has the most negative net charge, probably spends more time in the bulk phase than the more basic isoforms, thus explaining why it elutes first. The negatively charged side chain of glutamic acid at the N-terminal of the isoform with p*I* 7.4 (Fig. 2) may explain why it migrates faster than the isoform with p*I* 7.3; since the latter has uncharged Thr at the N-terminal, it probably has a greater affinity for the micelles and hence a slower migration velocity. Conditions other than electrostatic repulsion and attraction may also affect the elution order,

Fig. 3. Separation of nuclease isoforms by free solution capillary electrophoresis at different pH values. The electrophoresis buffer used was 40 m*M* Tris–H$_2$SO$_4$. The sample containing the three isoforms was introduced by applying a 16.9 kPa vacuum at the detector end for 1.0 s. A voltage of 5 kV was applied during electrophoresis. EO = electroosmotic flow.
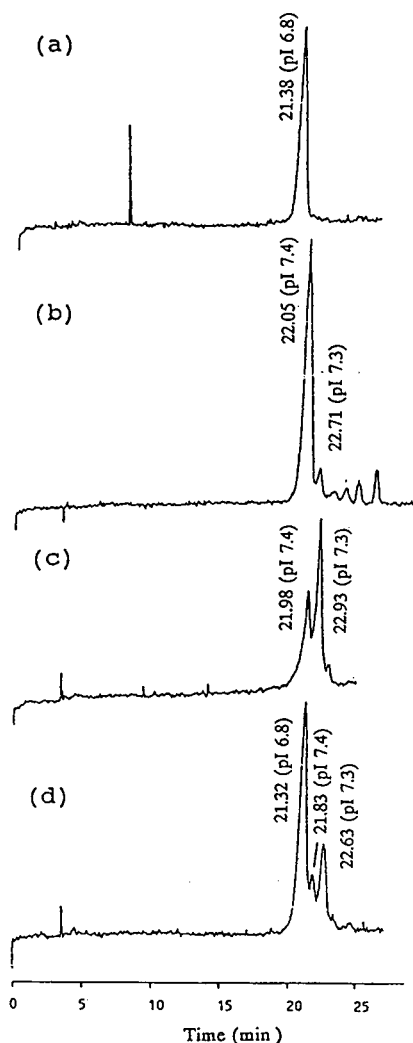
Fig. 5. Evaluation of the migration order of nuclease isoforms during separation by micellar electrokinetic capillary chromatography. The electrophoresis buffer was 40 mM Tris–H$_2$SO$_4$, pH 7.5, containing 25 mM SDS. Samples were introduced by applying a 16.9 kPa vacuum for 1.0 s at the detector end. 15 kV was applied during electrophoresis. (a) Native nuclease, pI 6.8; (b) sample in which the 7.4 isoform is the major component and the 7.3 isoform the minor component; (c) sample in which the 7.3 isoform is the major component and the 7.4 isoform the minor component; (d) mixture of (a) and (c).

Fig. 6. Influence of SDS concentration on electrophoretic migration time during micellar electrokinetic capillary chromatography with 40 mM Tris–H$_2$SO$_4$ buffer, pH 7.5, containing SDS. Voltage applied was 10 kV. O = Neutral components; □ = native nuclease with pI 6.8; * = isoform with pI 7.4; △ = isoform with pI 7.3.

optimal SDS concentration was between 25 and 50 mM, this being in agreement with the findings of Sepanik and Cole [5]. Fig. 6 shows that with increasing SDS concentration electroosmotic flow remains unchanged but there is a linear increase in electrophoretic migration time, a finding in concert with that of Terabe et al. [14]. The constancy of electroosmotic flow suggests that SDS has no effect on the zeta potential of the capillary/micelle phase. At the highest SDS concentration studied, 75 mM, the peaks began to broaden, possibly because of dispersion due to thermal effects.

Modification of the aqueous mobile phase by the addition of methanol has been reported to enhance MECC separation efficiency for small molecules such as aliphatic amines and aflatoxins [15]. Adding organic solvents both extends the elution range by reducing the electroosmotic flow velocity, and increases the solubility of hydrophobic compounds in the mobile phase, thereby reducing partititioning into the micelles. In the present study the addition of methanol in concentrations from 0 to 25% (v/v) actually reduced the electroosmotic flow and there was a small decrease in migration velocity relative to the electroosmotic flow. However, since the

however, e.g. hydrophobic interaction and electrophoretic migration of the analytes [14].

The influence of micelle concentration on separation was studied by using from 15 to 75 mM SDS in 40 mM Tris buffer, pH 7.5. The

extension of the elution range was inadequate to compensate for the reduction in isoform partitioning to the micelles, separation efficiency did not improve. That the degree of separation was lower and the peaks broader at higher methanol concentrations is probably attributable to methanol-induced polydispersion in the micelles [16].

Addition of hydroxypropylmethylcellulose to the SDS buffer was expected to increase the viscosity of the mobile phase and thereby lower the electroosmotic flow velocity; however, HMC did not enhance resolution of the isoforms at the concentrations used (0.05 to 0.25%). The expected enhancement should be due to reduced dispersion [17].

In order to reduce adsorption of the isoforms to negatively charged silanol groups on the capillary wall, NaCl was added to the buffer solution at concentrations from 10 to 100 mM; the theory was that Na^+ ions would compete with the analytes for the adsorption sites. However, although slightly better separation of the two basic isoforms was obtained when using 20 mM NaCl, separation of the isoforms with pI 6.8 and 7.4 was reduced; at higher NaCl concentrations the peaks broadened and migration velocity slowed.

The presence of divalent metals may enhance separation because divalent metals electrostatically attracted to the surface of negatively charged micelles could interact with the components to be separated [18,19]. However, although nuclease requires Mg^{2+} ions for its activity and hence might be expected to interact with metal sites on micelles, the addition of Mg^{2+} ions did not influence isoform separation and in fact the peaks actually broadened. The latter may be due to the additional adsorption of metal ions and consequently nuclease to the metal–fused silica surface.

One problem in applying MECC to large proteins is the rather small size of the SDS micelles (diameter 40 Å [5]) —only part of the protein molecule can interact with the hydrophobic tails of the SDS molecules. We therefore attempted to utilize an oil in water microemulsion which permits the formation of larger micelles [7,8,20]; this was comprised of Tris–H_2SO_4 buffer, pH 7.5, 1-butanol, SDS and

heptane. In such a pseudophase system the heptane oil droplet will be surrounded by both SDS molecules and butanol, thereby enhancing micellar diameter. Alcohol may loosen the micelle structure and thereby improve its mass transfer kinetics as compared with the more rigid micelles formed by SDS alone. The effect of varying microemulsion composition on the separation of the three nuclease isoforms was examined using 3 water–butanol–SDS–heptane systems, A, B and C, as described above (see Experimental). System A, which was characterized by a high percentage of water and a low percentage of the other components, provided the best separation although even then the three isoforms were found in one broad peak with a split in the top. Increasing the composition of SDS and reducing that of water only slightly improved in separation efficiency. It can thus be concluded that this microemulsion is unsuitable for the separation of large proteins such as nuclease isoforms.

Separation by cIEF

Separation of the three isoforms by cIEF, another means of achieving charge-based separation in HPCE, was also investigated. After the isoforms had been focused to a particular position according to their isoelectric points, the entire contents of the capillary were mobilized past the detector so as to yield an electropherogram in which time and pI are related. The anode electrolyte was acidic and the cathode electrolyte basic. In the cIEF electropherogram shown in Fig. 7, it can be seen that there is complete baseline separation of native nuclease and the two basic isoforms with pI 7.3 and 7.4, separation therefore being much more efficient than with FSCE and MECC. The elution order is that expected with cIEF, i.e. the basic isoforms eluted first. Full separation of the two basic isoforms was not achieved however, the difference in pI and primary structure being too small. Their separation probably requires further optimization of the conditions and the use of a narrower pH gradient. The separation of nuclease isoforms achieved with cIEF is virtually the same as that achieved with IEF in agarose gels (Fig. 1); however, cIEF is much easier and

(a)

11.78 (pI 6.8)

(b)

10.44 (pI 7.4)
11.00 (pI 7.3)

(c)

10.30 (pI 7.4)
10.80 (pI 7.3)
12.42 (pI 6.8)

```
4    6    8    10   12   14   16
```

Time (min)
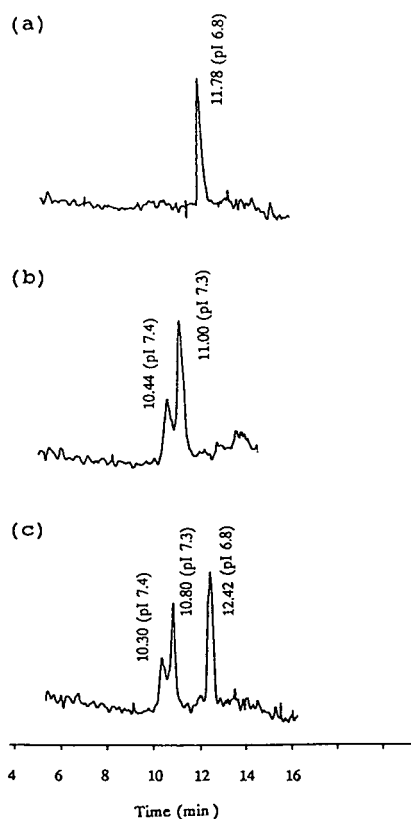
Fig. 7. Capillary isoelectric focusing of nuclease isoforms. The carrier ampholyte was Servalyte 3–10. (a) Native nuclease with pI 6.8; (b) sample in which the pI 7.3 isoform is the major component and the pI 7.4 isoform the minor component; (c) a mixture of (a) and (b) (1:1).

faster to perform, gel casting and lengthy staining procedures being obviated, and ampholyte consumption considerably reduced.

CONCLUSIONS

HPCE proved to be a promising new method for analyzing closely related proteins. However, optimization of separation is difficult compared to conventional electrophoresis because of the numerous factors involved. Separation of the nuclease isoforms by MECC was more efficient than with FSCE, the best results being obtained with a 40 mM Tris buffer, pH 7.5, containing 25 mM SDS but lacking any viscosity-increasing or complexing agents. Best separation was obtained using cIEF, which enabled complete baseline separation of the native nuclease with pI 6.8 and the isoform with pI 7.3, and nearly complete baseline separation of the pI 7.3 and 7.4 isoforms.

The main potential use of HPCE in biotechnology could be for the on-line monitoring of product formation and product quality during fermentation and downstream processing. Another potential use is for the separation of proteins under conditions that preclude using other techniques, in order to enable their further analysis. In this case fractionated proteins would have to be collected and if SDS and ampholytes have been used for the separation, they would have to be removed.

REFERENCES

1 J. Pedersen, M.N. Filimonova, P. Roepstorff and K. Biedermann, Biochim. Biophys. Acta, (1993) in press.
2 P. Højrup, in A. Hedin, B.U.R. Sundqvist and A. Benninghoven (Editors), Ion Formation from Organic Solids (IFOS V): General Protein Mass Analysis (GPMA), a Convenient Program in Studies of Proteins by Mass Spectrometry, Wiley, Chichester, 1990, p. 61.
3 K. Biedermann, P.K. Jepsen, E. Riise and I. Svendsen, Carlsberg Res. Commun., 54 (1989) 17.
4 A. Vinther, H. Søeberg, L. Nielsen, J. Pedersen and K. Biedermann, Anal. Chem., 64 (1992) 187.
5 M.J. Sepaniak and R.O. Cole, Anal. Chem., 59 (1987) 472.
6 S. Terabe, K. Otsuka and T. Ando, Anal. Chem. 61 (1989) 251.
7 H. Watarai, Chem. Lett., (1991) 391.
8 H. Watarai, Anal. Sci., 7, Suppl. (1991) 245.
9 M.N. Filimonova, A.A. Dementyev, I.B. Leshchinskaya, G. Yu Bakulina and S.V. Schlyapnikov, Biokhimiya (Russia), 56 (1991) 508.
10 Z.I. Panfilova and R.I. Salganik, Microbiologiya (Russia), 52 (1983) 974.

11 J. van Nieuwkoop, and G. Snoei, *J. Colloid Interface Sci.*, 103 (1984) 417.

12 *User Bulletin No. 5, Isoelectric Focusing on the 270A-HT*, Applied Biosystems, Foster City, 1992.

13 K. Biedermann and B.N. Nielsen, *Pharm. Technol. Int.*, 2 (1990) 37.

14 S. Terabe, K. Otsuka and T. Ando, *Anal. Chem.* 57 (1985) 834.

15 A.T. Balchunas, D.F. Swaile, A.C. Powell and M.J. Sepaniak, *Sep. Sci. Technol.*, 23 (1988) 1891.

16 J. Cai and Z. El Rassi, *J. Chromatogr.*, 608 (1992) 31.

17 A. Vinther, *Thesis*, Technical University of Denmark, Lyngby and Novo Nordisk, Novo Allé, Bagsværd, 1991.

18 A.S. Cohen, S. Terabe, J.A. Smith and B.L. Karger, *Anal. Chem.*, 59 (1987) 1021.

19 H. Kajiwara, *J. Chromatogr.*, 559 (1991) 345.

20 S. Terabe, N. Matsubara, Y. Ishihama and Y. Okada, *J. Chromatogr.* 608 (1992) 23.

Short Communication

Determination of ascorbyl dipalmitate in cosmetic whitening powders by liquid chromatography

Mei-Hwa Lien, Bin-Chung Huang and Mei-Chich Hsu*

National Laboratories of Foods and Drugs, Department of Health, Executive Yuan, 161-2, Kuen-Yang St., Nankang, Taipei 11513 (Taiwan)

ABSTRACT

A reversed-phase column liquid chromatograpic method was developed for the assay of ascorbyl dipalmitate in whitening powders. The linear calibration range was 0.1–0.7 mg/ml ($r = 0.9999$), and recoveries were generally greater than 98.8%. The coefficient of variation was less than 0.64%. The method has been applied to whitening powders produced by four different cosmetics companies. The assay results were compared with those obtained from a sodium hydroxide titration assay of ascorbyl ⸜dipalmitate in commercial whitening powders. The method can be successfully used for routine quality control and offers advantages in speed, simplicity and reliability.

INTRODUCTION

Ascorbyl dipalmitate is a more stable form of ascorbic acid and is found in nail lacquers [1], lotions [2,3], skin powders [4–6], skin conditioners [7], sunscreen [8], freckle formulations [9], creams [10,11] and dentifrices [12]. It has also been shown to extend the stability of adhesive transdermal pharmaceuticals [13]. Ascorbic acid and ascorbic acid derivatives are thought to be produced by the inactivation of tyrosinase, an enzyme that mediates the early steps of the melanin biosynthetic pathway [14]. Owing to its skin-whitening action, ascorbyl dipalmitate has been used widely in skin-whitening preparations [15–23].

In order to ensure effectiveness, safety and quality, the manufacture and import of medicated cosmetics are strictly controlled. In Taiwan no-one can operate such a business without obtaining approval and a license from the Department of Health, Taiwan. Requirements for approval and license applications for medicated cosmetics are almost the same as those for drugs. Hence, it is imperative to be able to determine accurately the amount of ascorbyl dipalmitate in cosmetic whitening powders.

Few methods have been reported in the literature for the analysis of ascorbyl dipalmitate. Luckewicz and Saccro [24] reported a differential scanning colorimetric method for the determination of ascorbyl dipalmitate and Matsumoto and Shinozaki [25] and Yamaoka *et al.* [26] described LC procedures for the determination of ascorbyl dipalmitate in vitamin preparations and ointments. The present official assay method for the analysis of ascorbyl dipalmitate in whitening

---

* Corresponding author.

powder is a titration method [27]. The purpose of this investigation was to develop an HPLC method that would permit the accurate determination of ascorbyl dipalmitate in cosmetic whitening powders.

EXPERIMENTAL

Apparatus

A Waters Model 510 liquid chromatography pump (Waters Chromatography Division, Millipore, Milford, MA, USA), a Shimadzu SPD-6A UV detector and a Waters 745 data module were employed during the study. The mobile phase was pumped through a reversed-phase column (Spherisorb S5 ODS2, 15 cm × 4.6 mm I.D., 5 μm; Phase Separation) with an isocratic flow-rate of 1.0 ml/min. The detector was set at 240 nm. Chromatography was performed at room temperature. Injections of 20 μl of all solutions to be analysed were made.

Reagents and materials

Methanol (liquid chromatography grade) was obtained from ALPS Chemical, Taipei, Taiwan. Glacial acetic acid, sodium hydroxide solution (0.1 mol/l) and ethanol (reagent grade) were obtained from E. Merck, Darmstadt, Germany. Octyl dimethyl p-aminobenzoic acid, ascorbyl dipalmitate and phenolphthalein were obtained from Tokyo Kasei Kogyo, Tokyo, Japan.

Mobile phase

The mobile phase was methanol–40% glacial acetic acid (97:3, v/v). The mobile phase was filtered (0.45 μm pore size Millipore filter) and degassed with an ultrasonic bath prior to use.

Internal standard solutions

Internal standard octyl dimethyl p-aminobenzoic acid (100.0 mg) was dissolved in 1.0 l of ethanol and shielded from light.

Ascorbyl dipalmitate standard solutions

To form ascorbyl dipalmitate standard solution, internal standard solution was added to an accurately weighed amount of ascorbyl dipalmitate standard equivalent to 40.0 mg and the

volume was brought up to 100.0 ml. The solution should be shielded from light.

Sample preparations

To form sample preparations, internal standard solution was added to an accurately weighed amount of whitening powder equivalent to 40.0 mg of ascorbyl dipalmitate and the volume was brought up to 100.0 ml. The solution should be shielded from light.

Solution for linearity response

Seven concentrations of ascorbyl dipalmitate, which ranged from 0.1 to 0.7 mg/ml, were prepared. Each concentration was chromatographed six times.

Solution for recovery studies

To an accurately weighed 40.0 mg of ascorbyl dipalmitate of sample composites of commercial preparations were added different amounts of ascorbyl dipalmitate standard. Each solution was made up to 100.0 ml with internal standard solution and was chromatographed in triplicate.

Sodium hydroxide titration

Whitening powder equivalent to ca. 300.0 mg of ascorbyl dipalmitate, accurately weighed, was transferred to a glass-stoppered, 50.0-ml conical flask, 30 ml of ethanol added, and the solution mixed. The solution was filtered and the flask and the filter were washed with small portions of ethanol. The washings were added to the filtrate. Two drops of phenolphthalein TS were added. The solution was titrated with 0.02 M sodium hydroxide until the entire mixture changed to a red colour. The red colour should persist for 30 s. Each millilitre of 0.02 M sodium hydroxide is equivalent to 13.06 mg of ascorbyl dipalmitate ($C_{18}H_{68}O_8$).

RESULTS AND DISCUSSION

Reproducibilities were determined by chromatographing seven standard solutions of ascorbyl dipalmitate ranging in concentration from 0.1 to 0.7 mg/ml in the presence of the internal standard octyl dimethyl p-aminobenzoic acid. Standard curves were obtained by plotting peak-area

ratios *versus* concentrations. The linear correlation coefficient was 0.9999 ($y = 0.1252x - 0.0027$). The coefficients of variation in the within-day assay were between 0.15 and 0.64% at the concentration of 0.4 mg/ml. The coefficient of variation in the between-day assay ($n = 5$) was 0.59% at the same concentration.

Standard addition recovery studies of ascorbyl dipalmitate from sample composites of commercial whitening powder were performed. The average recovery was 98.8–100.4% for four commercial compositions. These data indicate that the proposed HPLC method is relatively unaffected by the sample matrix.

Typical chromatograms of the ascorbyl dipalmitate in commercial whitening powder are shown in Fig. 1. The retention time was about 3 min for the internal standard and 8 min for ascorbyl dipalmitate. Excipients from commercial cosmetic formulations did not interfere. Furthermore, the HPLC method can separate compounds related to ascorbyl dipalmitate, *i.e.*, ascorbic acid and ascorbyl palmitate, which were eluted prior to ascorbyl dipalmitate (Fig. 1).

A study was initiated to ascertain the suitability of the proposed method for stability studies. Sample solutions of ascorbyl dipalmitate were stored in a cabinet at ambient temperature. Samples were taken from the cabinet periodically for LC assay. The resulting mixtures yielded chromatograms containing an additional
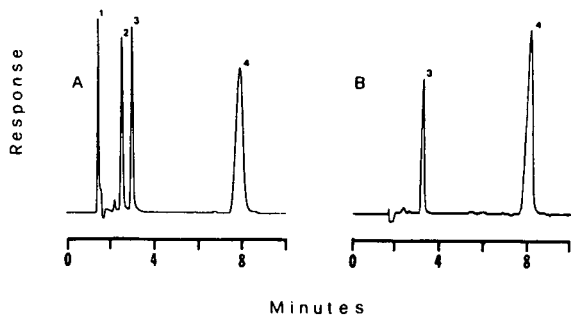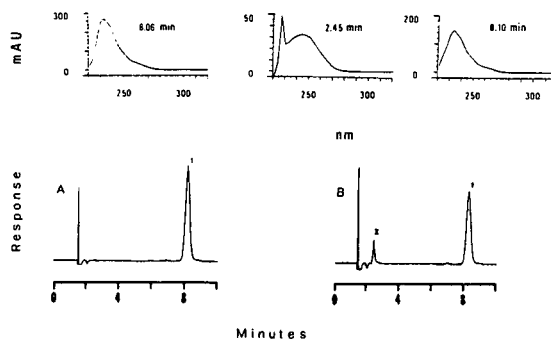
Fig. 2. Chromatograms and UV spectra. (A) Ascorbyl dipalmitate; (B) degradation of ascorbyl dipalmitate solution at ambient temperature for 5 days. Peaks: 1 = ascorbyl dipalmitate; x = degradation product.

peak, which did not interfere with the interpretation and measurement of the chromatographic peaks for ascorbyl dipalmitate and octyl dimethyl *p*-aminobenzoic acid, as shown in Fig. 2. In addition, ascorbyl dipalmitate disappeared and degradation product accumulated with increasing storage time. To examine the purity of the ascorbyl dipalmitate peak and identify the degradation product in the time-degraded samples, a UV photodiode array detector was used. The evaluation of chromatographic peak homogeneity was performed by absorbance ratios and a three-dimensional spectrochromatogram. The results presented good confirmation of the ascorbyl dipalmitate peak identity (data not shown). The peak obtained from the degradation of ascorbyl dipalmitate solution indicated that it may be ascorbyl palmitate, since its UV spectrum corresponds to the spectrum of ascorbyl palmitate (Fig. 2).

Four cosmetic whitening powders were analysed for ascorbyl dipalmitate content by HPLC. These samples were also assayed by the titration method. The results are shown in Table I. A *t*-test was applied to the data. The assay results obtained by the titration method were statistically significantly higher than those obtained by the proposed chromatographic method. These higher results are not unexpected, since the titration method is non-selective, and the end point of the titration is affected by other variables [28,29]. The skin-whitening powders contain ascorbyl dipalmitate, pyridoxine hydrochloride, mannitol,

Fig. 1. Chromatograms of ascorbyl dipalmitate preparations. (A) A mixture of ascorbic acid, ascorbyl palmitate, octyl dimethyl *p*-aminobenzoic acid and ascorbyl dipalmitate. (B) A sample of cosmetic whitening powder. Peaks: 1 = ascorbic acid; 2 = ascorbyl palmitate; 3 = octyl dimethyl *p*-aminobenzoic acid; 4 = ascorbyl dipalmitate.

TABLE I

COMPARISON OF TITRATION AND HPLC ASSAYS FOR ASCORBYL DIPALMITATE

Manufacturer	Declared (mg/ml)	Found (% of declared)	
		Titration[a]	HPLC[b]
A	250	113.1	98.0
B	250	110.0	98.5
C	250	112.6	97.6
D	250	120.1	92.6

[a] Average of two determinations.
[b] Average of triplicate determinations.

starch, etc. It is possible that the pyridoxine hydrochloride may be responsible for the bias of the titrimetic method described.

This study demonstrates the applicability of the proposed HPLC method for the determination of ascorbyl dipalmitate in cosmetic whitening powders. The method can be successfully used for routine quality control and offers advantages in speed, simplicity and reliability.

ACKNOWLEDGEMENTS

REFERENCES

1 N. Ito, Jpn. Kokai Tokkyo Koho JP 02235805 A2, Heisei, September 18 (1990).
2 Jpn. Kokai Tokkyo Koho JP 60116618 A2, Showa, June 24 (1985).
3 A. Noda, M. Yamaguchi, M. Aizawa and Y. Kumano, Eur. Pat. Appl. EP 316054 A1, May 17 (1989).
4 G. Okuyama, S. Shinho and J. Shimoyama, Jpn. Kokai Tokkyo Koho JP 61130206 A2, Showa, June 18 (1986).
5 A. Imamura and T. Kondo, Jpn. Kokai Tokkyo Koho JP 63280005 A2, November 17 (1988).
6 A. Munakata, Jpn. Kokai Tokkyo Koho JP 02169508 A2, Heisei, June 29 (1990).
7 I. Koiso, N. Kanbe, M. Oyama, Y. Okaya and K. Kinoshita, Jpn. Kokai Tokkyo Koho JP 62129212 A2, Showa, June 11 (1987).
8 S. Tobe and K. Shimizu, Jpn. Kokai Tokkyo Koho JP 61078715 A2, Showa, April 22 (1986).
9 A. Yokozuka, T. Takayabu, Jpn. Kokai Tokkyo Koho JP 61263906 A2, Showa, November 21 (1986).
10 Jpn. Kokai Tokkyo Koho JP 59073508 A2, Showa, April 25 (1984).
11 H. Tamabuchi, US Pat., 4 818 521 A, April 4 (1989).
12 T. Shino, Jpn. Kokai Tokkyo Koho JP 62273910 A2, Showa, November 28 (1987).
13 Jpn. Kokai Tokkyo Koho JP 59059616 A2, Showa, April 5 (1984).
14 Y. Tomita, A. Hariu, C. Mizuno and M. Seiji, J. Invest. Dermatol., 75 (1980) 379.
15 K. Masamoto, Y. Murakami and H. Tamabuchi, Jpn. Kokai Tokkyo Koho JP 52079032 A2, Showa, July 2 (1977).
16 Jpn. Kokai Tokkyo Koho JP 59010505 A2, Showa, January 20 (1984).
17 Jpn. Kokai Tokkyo Koho JP 59065007 A2, Showa, April 13 (1984).
18 Jpn. Kokai Tokkyo Koho JP 59104308 A2, Showa, June 16 (1984).
19 Jpn. Kokai Tokkyo Koho JP 60078912 A2, Showa, May 4 (1985).
20 R. Oomi and A. Matsumoto, Jpn. Kokai Tokkyo Koho JP 61100509 A2, Showa, May 19 (1986).
21 S. Yoshikawa, Y. Hiraki and T. Koyama, Jpn. Kokai Tokkyo Koho JP 02304012 A2, Heisei, December 17 (1990).
22 K. Omae and K. Ito, Jpn. Kokai Tokkyo Koho JP 04077409 A2, Heisei, March 11 (1992).
23 T. Hikima and M. Kondo, Jpn. Kokai Tokkyo Koho JP 04091009 A2, Heisei, March 24 (1992).
24 W. Luckewicz and R. Saccaro, J. Soc. Cosmet. Chem., 41 (1990) 359.
25 K. Matsumoto and K. Shinozaki, Jpn. Kokai Tokkyo Koho JP 61183217 A2, Showa, August 15 (1986).
26 K. Yamaoka, M. Matsui, Y. Saito and T. Sato, Byoin Yakugaku 7 (1982) 355.
27 Cosmetic Regulations for Raw Materials of Taiwan, Department of Health, Executive Yuan, Taipei, 1988, p. 57.
28 G. Hoogewijs and D.L. Massart, J. Chromatogr., 309 (1984) 329.
29 J.C. Kraak and J.P. Crombeen, J. Liq. Chromatogr., 5 (Suppl. 2) (1982) 273.

Short Communication

Separation of codeine and its by-products by capillary zone electrophoresis as a quality control tool in the pharmaceutical industry

Milos Korman, Johan Vindevogel* and Pat Sandra

Department of Organic Chemistry, University of Ghent, Krijgslaan 281 S4, B-9000 Ghent (Belgium)

ABSTRACT

Capillary zone electrophoresis can be used for the detection of by-products in purified codeine. Separation of the by-products thebaine and 6-methylcodeine illustrates that small geometrical differences can be exploited to achieve effective separation. Examples of the capillary zone electrophoresis and micellar electrokinetic chromatography of codeine-containing drug formulations are presented.

INTRODUCTION

Codeine (Fig. 1), an antitussive and mild analgesic, can be obtained from Indian opium or poppy straw and is additionally produced by methylation of morphine from the same sources [1]. To obtain pure codeine, various impurities, ranging from naturally occurring alkaloids (such as thebaine) to reaction side-products such as 6-methylcodeine and 3-O-(1,2-dichlorovinylmorphine) [2] must be removed. The purity of the codeine must then be ascertained.

Basic drugs can be analysed by HPLC [3] or TLC [4,5], but interactions with the stationary phases [3] can lead to tailed peaks. In electroosmotically driven chromatography, with the stationary phase still present, tailing still occurs, as can be inferred from data presented by Verheij *et al.* [6]. As was demonstrated with another class of compounds, the hop acids [7], only the complete elimination of the stationary phase solves this kind of adsorption problem.
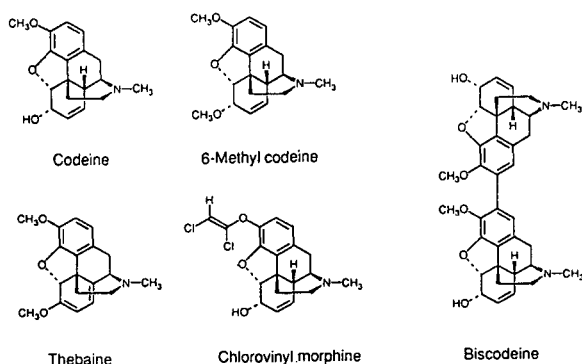
Fig. 1. Codeine and its by-products.

---

* Corresponding author.

Therefore, capillary zone electrophoresis (CZE) is a convenient alternative.

Several groups have reported the capillary electrophoretic separation of basic drugs [8–11] and alkaloids [12–14]. All of the work on codeine [8–10] has focused on its determination for forensic drug screening. This contribution deals with codeine in its pharmaceutical dosage form.

EXPERIMENTAL

Codeine was obtained from Sigma (St. Louis, MO, USA). The purified by-products of codeine and drug formulations were obtained from Slovakofarma (Hlohovec, Slovak Republic). The pure compounds were dissolved in separation buffer at the required concentration, except for the trace impurity analysis of codeine, for which 0.01 M hydrochloric acid was used as the sample solvent. The tablets (Kodynal, Spasmoveralgin, Alnagon) were crushed in a mortar and 65–150 mg of powder, equivalent to one-tenth of a tablet, were sonicated in 100 ml of separation buffer and filtrated through a 0.45-μm membrane filter (Schleicher & Schüll, Dassel, Germany). The Ipecarin drops were simply diluted 100 times with separation buffer. The actual concentrations of the substances are listed in the figure legends.

CZE was performed on a Quanta 4000 system (Millipore, Bedford, MA, USA). Fused-silica capillaries were 50 μm or 75 μm I.D., 375 μm O.D., 60 cm long, with the detection window at 53 cm.

Electropherograms were obtained with various buffers, all prepared with deionized water (Milli-Q, Millipore). Samples were introduced hydrodynamically with an elevation of 10 cm and an injection time of 5 or 10 s, analysed with an applied voltage of 17 or 20 kV and detected at 214 nm. After each run the column was rinsed with 0.05 M sodium hydroxide (1–3 min) and separation buffer for 3 min.

Molecular modelling calculations were performed on a MicroVAX II (Digital Equipment, Shrewsbury, MA, USA) with the MM2(85) Force Field program (MacroModel v3.0, W.C. Still, Columbia University, 1990).
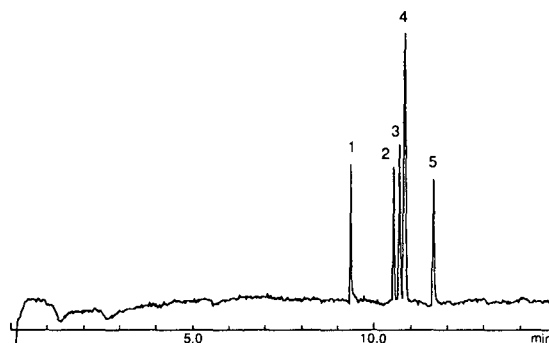
Fig. 2. CZE analysis of a synthetic mixture of codeine and its by-products. Buffer: 25 mM citrate, pH 4.2. Column: 60 cm (53 cm to detector) × 75 μm I.D. Applied voltage: 20 kV. Detection: 214 nm. Injection time: 5 s. 1 = Biscodeine; 2 = codeine; 3 = thebaine; 4 = 6-methylcodeine; 5 = 3-O-1,2-dichlorovinylmorphine.

RESULTS AND DISCUSSION

Fig. 2 shows an electropherogram of an artificial mixture of codeine and its by-products. The excellent separation of thebaine and 6-methylcodeine is remarkable as these compounds differ by only two hydrogen radicals. As the pK_a of thebaine is 6.05, charge effects are not expected to have a strong influence at pH 4.2. This is confirmed by examining the separation in the range pH 2.5–6.0 (Fig. 3). To avoid interferences from different ionic strengths in the pH scale, the buffers contained a large excess of sodium chloride. We did not attempt to measure electroosmotic flow at these low pH values, but by selecting a reference compound, in this case thebaine, and considering differences in observed mobility, the effect of electroosmosis is effectively neutralized (μ_{ep} = electrophoretic mobility, μ_{eo} = electroosmotic mobility)

$$\Delta\mu = (\mu_{ep,1} + \mu_{eo}) - (\mu_{ep,2} + \mu_{eo}) = \mu_{ep,1} - \mu_{ep,2}$$

$$(1)$$

No pH-related difference in electrophoretic mobility could be found between thebaine and 6-methylcodeine. The changes for bis-codeine are very likely related to the transition from the mono- to the diprotonated form. The small changes for codeine and 3-O-(1,2-dichlorovinylmorphine) are less well understood but
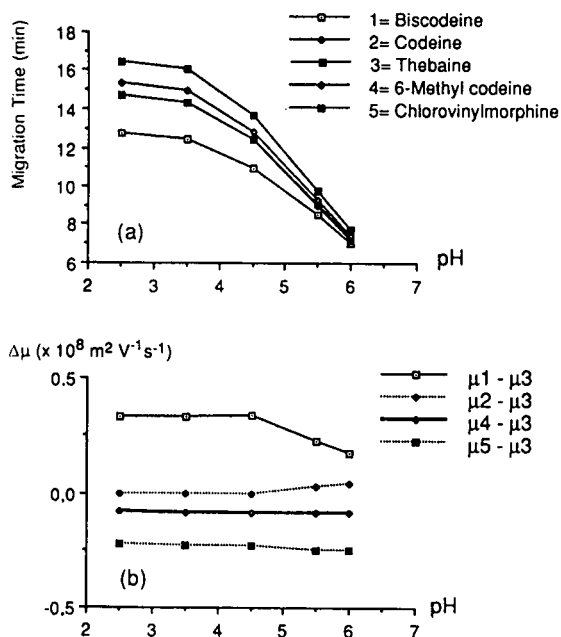
Fig. 3. Migration times (a) and mobility differences (b) in the pH range 2.5–6.0. Buffer: 100 mM NaCl with 10 mM phosphate (pH 2.5) or citrate (pH ⩾ 3.5). Column: 60 cm (53 cm to detector) × 50 μm I.D. Applied voltage: 17 kV. (Codeine and thebaine are not well separated under these high-ionic-strength conditions.)

could be related to the presence of the allylic alcohol function, a common and distinctive feature of these structures.

From molecular modelling calculations, it follows that there is a geometric difference between thebaine and 6-methylcodeine (Fig. 4), related to the position of the double bonds. As the electrophoretic mobility is determined not only by the charge but also by friction in the aqueous medium, a property determined by the effective

radius, geometric differences can lead to separation. Generally, such geometric differences are amplified through selective complexation with, for example, cyclodextrins [15], but this example shows that they can lead to separation by their own virtue. This type of geometry-controlled separations has also recently been reported for *cis–trans* isomers by Chadwick and Hsieh [16].

Up to 1% impurities are allowed in codeine [5]. However, for the determination of codeine in pharmaceutical formulations [17], we require that the level of by-products in the standard be less than 0.05%. Fig. 5 illustrates that these levels can effectively be detected in a codeine sample. Although satisfactory for our purpose, this is very likely not the ultimate limit. Altria [18] demonstrated better signal-to-noise ratios at the 0.02% impurity level by using wide-bore (180 μm) capillaries, but at the expense of an increased analysis time. The recently introduced capillaries with bubble cells [19], having a three-fold increase in capillary internal diameter at the detection location, could provide better sensitivity without the need to reduce the separation voltage.

This type of analysis, CZE in acid medium, can also be used for the determination of codeine in drug formulations (Fig. 6a and b), but, depending upon the nature of the accompanying drugs, other separation conditions may be necessary. The presence of neutral compounds necessitates the use of micellar electrokinetic chromatography (Fig. 6b and c).

Fig. 4. Geometrical difference between 6-methylcodeine (left) and thebaine (right) according to MM2 calculations (for clarity, H atoms have been omitted).
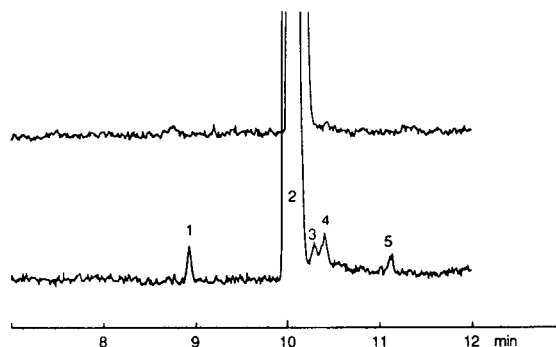
Fig. 5. CZE analysis of codeine (a) and codeine spiked with 0.05% by-products (b). Conditions and compounds as in Fig. 2, except for the injection time, which is 10 s. The codeine concentration is 10 000 ppm.
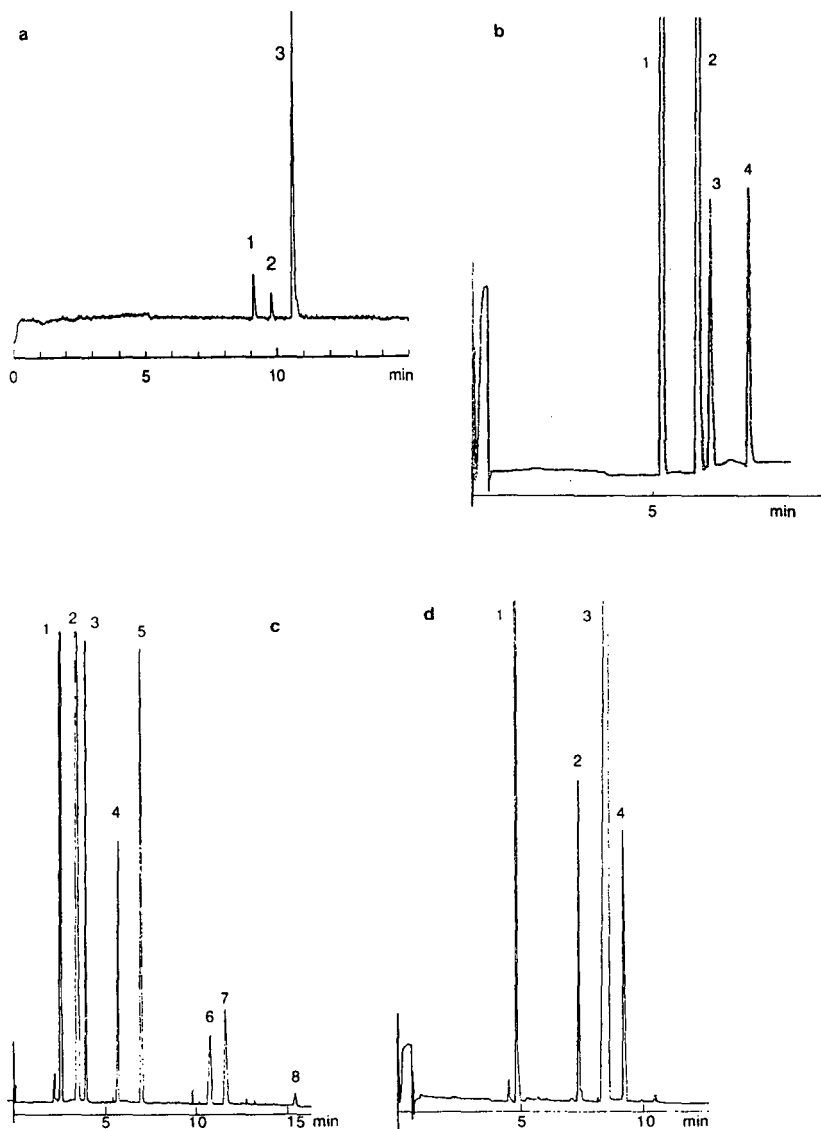
Fig. 6. Examples of the analysis of codeine-containing drug formulations. The concentrations reflect the relative amounts in the formulation. (a) Kodynal. Same conditions as in Fig. 2. 1 = Emetine (1 ppm); 2 = ephedrine (20 ppm); 3 = codeine (40 ppm). (b) Ipecarin. Buffer: 12.5 mM citrate, pH 6.5. Other conditions as in Fig. 2. 1 = Ephedrine (130 ppm); 2 = codeine (93 ppm); 3 = emetine (1 ppm); 4 = pilocarpine (15 ppm). (c) Spasmoveralgin. Buffer: 40 mM SDS in 10 mM phosphate, pH 8.5. Other conditions as in Fig. 2. 1 = Caffeine (50 ppm); 2 = aminophenazone (150 ppm); 3 = bromoisovalum (250 ppm); 4 = phenobarbital (20 ppm); 5 = codeine (15 ppm); 6 = ephedrine (5 ppm); 7 = papaverine (30 ppm); 8 = antropine methylbromide (0.5 ppm). (d) Alnagon. Same conditions as in (c), except for the addition of 15% acetonitrile to the buffer. 1 = Caffeine (80 ppm); 2 = phenobarbital (20 ppm); 3 = aspirin (380 ppm); 4 = codeine (20 ppm).

work at the University of Ghent and the European Community for a study grant (JEP 0379-92/3).

REFERENCES

1 R.J. Bryant, *Chem. Ind. (London)* (1988) 146.
2 B. Proksa and J. Cerny, *Chem. Zvesti*, 37 (1983) 837.
3 R.M. Smith, J.P. Westlake, R. Gill and M.D. Osselton, *J. Chromatogr.*, 514 (1990) 97.
4 P.M.J. Coenegracht, M. Dijkman, C.A.A. Duineveld, H.J. Metting, E.T. Elema and Th.M. Malingré, *J. Liq. Chromatogr.*, 14 (1991) 3213.
5 K. Hartke and E. Mutschler (Editors), *Deutsches Arzneibuch, Band 2*, Wissenschaftliche Verlagsgesellschaft, Stuttgart, 9th ed., 1986, p. 1300.
6 E.R. Verheij, U.R. Tjaden, W.M.A. Niessen and J. van der Greef, *J. Chromatogr.*, 554 (1991) 339.
7 J. Vindevogel, P. Sandra and L.C. Verhagen, *J. High Resolut. Chromatogr.*, 13 (1990) 295.
8 R. Weinberger and I.S. Lurie, *Anal. Chem.*, 63 (1991) 823.
9 P. Wernly and W. Thormann, *Anal. Chem.*, 63 (1991) 2878.
10 P. Wernly and W. Thormann, *Anal. Chem.*, 64 (1992) 2155.
11 G.L. Chee and T.S.M. Wan, *J. Chromatogr.*, 612 (1993) 172.
12 Y.M. Liu and S.J. Sheu, *J. Chromatogr.*, 600 (1992) 370.
13 Y.M. Liu and S.J. Sheu, *J. Chromatogr.*, 623 (1992) 196.
14 H. Stuppner, S. Sturm and G. Konwalinka, *J. Chromatogr.*, 609 (1992) 375.
15 C.L. Ng, H.K. Lee and S.F.Y. Li, *J. Chromatogr.*, 632 (1993) 165.
16 R.R. Chadwick and J.C. Hsieh, *Anal. Chem.*, 63 (1991) 2377.
17 M. Korman, J. Vindevogel and P. Sandra, in preparation.
18 K.D. Altria, *LC · GC Int.*, 6(3) (1993) 164.
19 D.N. Heiger, lecture presented at the *5th International Symposium on High Performance Capillary Electrophoresis, Orlando, FL, January 25–28, 1993*.

Book Review

High speed narrow bore capillary gas chromatography, by A. van Es, Hüthig, Heidelberg, 1992, IX + 158 pp., price DM 88.00, ISBN 3-7785-2027-X.

This is an interesting text that reviews recent advances in capillary gas chromatography, which calls upon the expertise of an author who is clearly an authority in the field. The book consists of six well written chapters, each supported by a concise up-to-date bibliography and refreshingly illustrated by original chromatograms that help the reader to follow the theoretical arguments.

After a short introduction to the topic in Chapter 1, the theoretical basis of capillary GC is discussed in Chapter 2. Here, particular attention is paid to the various factors that affect efficiency and analysis times together with strategies available to gain in analysis speed. This chapter could be regarded as essential reading for the busy analyst required to increase sample throughput.

The introduction of samples into narrow-bore columns is treated in Chapter 3. A discussion of the requirements of sample introduction systems is followed by description and evaluation of currently available injectors and injection techniques, including preconcentration and cryogenic focusing. Emphasis is placed upon micro-scale instrumentation and the use of silicon micro-machining to fabricate a miniature capillary gas chromatograph. Helpful tips on the selection of injectors are included.

The relationship between the sample capacity of narrow bore capillaries and detector characteristics is considered in Chapter 4. Theoretically it is shown that column and detector performance affect minimum detectable concentrations and this is confirmed experimentally. The advantages and limitations of a range of detectors are reviewed. Micro volume thermal conductivity and photoionization detectors are described and evaluated using 50 μm I.D. columns. Aspects of data handling, in particular fast acquisition and processing, are discussed.

Correlation or multiplex chromatography, which employs cross-correlation statistical techniques to improve limits of detection, is briefly described in Chapter 5. The final chapter deals with the potential use of turbulent flow capillary GC as a means of increasing analysis speeds.

This is not a book for the absolute beginner, however, practising analysts may find it helpful in extending their understanding of the theory of narrow-bore GC. Some readers may find the format of theory, experimental, results and discussion adopted for some chapters somewhat disconcerting.

Hatfield (UK)   M.B. Evans

Author Index